University of Southern Queensland

STELLAR CHROMOSPHERIC ACTIVITY IN MAIN-SEQUENCE STARS

A thesis submitted by

Howard Isaacson

For the award of

Doctor of Philosophy

2024

ABSTRACT

The research presented here presents a narrow slice of several large-scale, ground-based astronomy surveys focused on chromospheric activity measurements of stars from the Keck Observatory. We conducted a comprehensive study analyzing chromospheric activity and its relationship with stellar properties in exoplanet host stars and solar neighborhood stars. By extracting chromospheric activity measurements from the California-Kepler Survey and the California Legacy Survey, we explored connections between stellar activity, rotation periods, and magnetic dynamos across a large sample of stars. Our analysis includes 879 planet-hosting stars and 710 solar neighborhood stars, providing insights into stellar rotation, magnetic braking, and activity cycles. We observed discrepancies between photometrically and activity-derived rotation periods, supporting the theory of weakened magnetic braking. Our study also identified potential Maunder Minimum-like states in some stars and suggested that stellar activity cycles are strongly correlated with effective temperature in younger stars but not in older, low-activity stars. Additionally, we found that average chromospheric activity remains nearly constant while variations in activity decrease significantly with age, indicating measurable changes in stellar dynamos that are not strongly correlated with average activity. These findings have implications for the age-dating of mature solar-type stars and the understanding of the impact of stellar activity on exoplanet detection.

CERTIFICATION OF THESIS

I, Howard Isaacson, declare that the Ph. D. thesis entitled *Stellar Chromospheric Activity in Main Sequence Stars* is not more than 100000 words in length including quotes and exclusive of tables, figures, appendices, bibliography, references, and footnotes. This thesis is the work of Howard Isaacson except where otherwise acknowledged, with the majority of the contribution to the papers presented as a thesis by publication undertaken by the student. The work is original and has not previously been submitted for any other award, except where acknowledged.

Signed: Date: 5 September 2024

Endorsed by:

Dr. Brad Carter
Principal Supervisor

Dr. Stephen Kane
Associate Supervisor

Student and supervisors' signatures of endorsement are held at UniSQ.

This section details contributions by the various authors for each of the papers presented in this thesis by publication.

Chapter 3: Isaacson, Howard; Kane, Stephen R.; Carter, Brad; Howard, Andrew W.; Weiss, Lauren; Petigura, Erik A.; Fulton, Benjamin. ”The California-Kepler Survey. XI. A Survey of Chromospheric Activity Through the Lens of Precise Stellar Properties”.

Author	Percent Contribution	Tasks Performed
Isaacson, Howard	70	Extracted the raw data into high-level data products, helped to collect the data, wrote the paper, conducted the analysis, created the graphics.
Kane, Stephen R.	8	Provided scientific guidance, suggested edits to manuscript.
Carter, Brad	8	Provided scientific guidance, suggested edits to manuscript.
Howard, Andrew W.	8	Helped to conceive of original ideas, helped to collect the data, provided scientific guidance, suggested edits to manuscript.
Weiss, Lauren	2	Helped to collect the data, suggested edits to manuscript.
Petigura, Erik	2	Helped to collect the data, suggested edits to manuscript.
Fulton, Benjamin	2	Helped to collect the data, suggested edits to manuscript.

Chapter 4: Isaacson, Howard; Howard, Andrew W.; Fulton, Benjamin; Petigura, Erik A.; Weiss, Lauren M.; Kane, Stephen R.; Carter, Brad; Beard, Corey; Giacalone, Steven; Van Zandt, Judah; Akana Murphy, Joseph M.; Dai, Fei; Chontos, Ashley; Polanski, Alex S.; Rice, Malena; Lubin, Jack; Brinkman, Casey; Rubenzahl, Ryan A.; Blunt, Sarah; Yee, Samuel W.; MacDougall, Mason G.; Dalba, Paul A.; Tyler, Dakotah; Behmard, Aida; Angelo, Isabel; Pidhorodetska, Daria; Mayo, Andrew W.; Holcomb, Rae; Turtelboom, Emma V.; Hill, Michelle L.; Bouma, Luke G.; Zhang, Jingwen; Crossfield, Ian J. M.; Saunders, Nicholas.
"The California Legacy Survey. V. Chromospheric Activity Cycles in Main Sequence Stars".

Author	Percent Contribution	Tasks Performed
Isaacson, Howard	75	Extracted the raw data into high-level data products, helped to collect the data, wrote the paper, conducted the analysis, created the graphics.
Howard, Andrew W.	5	Helped to conceive of original idea, helped to collect the data, provided scientific guidance, suggested edits to manuscript.
Fulton, Benjamin	2	Provided foundational survey work, helped to collect the data.
Petigura, Erik A.	2	Provided foundational survey work, helped to collect the data, suggested edits to manuscript.
Weiss, Lauren M.	2	Provided foundational survey work, helped to collect the data, suggested edits to manuscript.
Kane, Stephen R.	2	Provided scientific guidance, suggested edits to manuscript.
Carter, Brad	2	Provided scientific guidance, suggested edits to manuscript.

Chapter 4: CONTINUED

Author	Percent Contribution	Tasks Performed
Beard, Corey	10	review formattingCollected data, suggested edits to paper.
Giacalone, Steven		Collected data, suggested edits to paper.
Van Zandt, Judah		Collected data, suggested edits to paper.
Akana Murphy, Joseph M.		Collected data.
Dai, Fei		Collected data, suggested edits to paper.
Chontos, Ashley		Collected data.
Polanski, Alex S.		Collected data, suggested edits to paper.
Rice, Malena		Collected data, suggested edits to paper.
Lubin, Jack		Collected data.
Brinkman, Casey		Collected data.
Rubenzahl, Ryan A.		Collected data.
Blunt, Sarah		Collected data.
Yee, Samuel W.		Collected data.
MacDougall, Mason G.		Collected data.
Dalba, Paul A.		Collected data.
Tyler, Dakotah		Collected data.
Behmard, Aida		Collected data.
Angelo, Isabel		Collected data, suggested edits to paper.
Pidhorodetska, Daria		Collected data.
Mayo, Andrew W.		Collected data.
Holcomb, Rae		Collected data, suggested edits to paper.
Turtelboom, Emma V.		Collected data, suggested edits to paper.
Hill, Michelle L.		Collected data.
Bouma, Luke G.		Collected data, suggested edits to paper.
Zhang, Jingwen		Collected data
Crossfield, Ian J. M.		Collected data, suggested edits to paper.
Saunders, Nicholas		Collected data, suggested edits to paper.

Chapter 5: Isaacson, Howard; Kane, Stephen R.; Carter, Brad; Howard, Andrew W. ”The California Legacy Survey VI - The Fate of Activity Cycles in Sun-like Stars”.

Author	Percent Contribution	Tasks Performed
Isaacson, Howard	85	Extracted the raw data into high-level data products, helped to collect the data, wrote the paper, conducted the analysis, created the graphics.
Kane, Stephen R.	5	Provided scientific guidance, suggested edits to manuscript.
Carter, Brad	5	Provided scientific guidance, suggested edits to manuscript.
Howard, Andrew W.	5	Helped to conceive of original ideas, helped to collect the data, provided scientific guidance, suggested edits to manuscript.

ACKNOWLEDGEMENTS

I would like to thank Brad Carter and Stephen Kane who spent endless hours with me on telecons both in support of the research and my general well-being. Thank you to USQ colleagues Rob Wittenmyer, Chelsea Huang, George Zhou, and Simon Murphy for an incredible visit to USQ that inspired me to finish this project. Thank you to Travis Metcalfe for the many-many explanations of stellar magnetic phenomena. Thank you to the Keck Observatory community for creating the most dynamic astronomical observatory in the world. The quality and consistency of the data presented here are directly linked to the standards of the Observatory. It is an honor to be associated with such an amazing institution. Thank you to Andrew Howard, my longest collaborator, and for keeping me in the field for all of these years. Thank you to my California Planet Search Collaborators past and present, especially Lauren Weiss, Erik Petigura, and BJ Fulton. CPS has been the foundation of my scientific experience. Thank you to Lloyd Magnuson, my 8th grade science teacher, who helped me skip health class to work on science projects. Thank you to my wife Missy tolerating the extensive time required for this project and for her relentless encouragement. And a very broad nod of appreciation goes to everyone who encouraged me in small ways to embark on this journey.

This research has been supported by the Australian Government Research Training Program Scholarship.

TABLE OF CONTENTS

LIST OF FIGURES

(excluding figures included in Chapters 3–5)

LIST OF ABBREVIATIONS

TESS Transiting Exoplanet Survey Satellite 11

UniSQ University of Southern Queensland ii

WASP Wide Angle Search for Plaents 13

WMB Weakened Magnetic Braking 10

CHAPTER 1: INTRODUCTION

1.1 Foundational ground-based astronomy surveys

The following original research is based upon ground-based observing surveys that use the Keck I Telescope on Maunakea and High-Resolution Echelle Spectrograph (HIRES) instrument to survey solar-type stars in the solar neighborhood. With the first-light Keck observations in 1994 (Marcy and Butler 1996), and the identification of the first extra-solar planets from the ELODIE spectrograph of the Haute-Provence Observatory, France (Mayor and Queloz 1995), these surveys would establish the foundational methods for producing long-term, consistent data, with repeatable methods capable of reaching 3.0 meters per second RV precision (Butler et al. 1996). Simultaneous observations of stellar activity metrics are collected with each high-resolution spectrum and used to track variations on the stellar surface over a variety of timescales. These stellar activity metrics, specifically those used to monitor the chromospheres of main-sequence stars, are presented here to address three primary research questions.

1.2 The history of stellar chromospheric activity

The study of solar activity began with observations of sunspots by Galileo over 400 years ago (Galileo's "Letters on Sun Spots") were enabled by a novel astronomical instrument: the telescope! One hundred twenty years ago, further advancement in astronomy instrumentation, in the form of spectroscopy and photographic plates, led to the discovery of variable spectral features in stars (Eberhard and Schwarzschild 1913). This discovery was predicated on the rise of modern physics and knowledge of the presence of spectral features due to different elements in the Sun and other stars. One set of spectral features in particular, the Ca II H & K lines at 396.8 nm and 393.4 nm, probe the chromosphere. Situated above the photosphere, where the most spectral absorption features are formed in the Sun, the chromosphere is hotter, more diffuse and is a sensitive indicator of the magnetic fields that lie below the surface.

The Ca II H & K lines and their connection to the magnetic fields of stars led to the Mount Wilson H & K survey (Wilson 1968; Vaughan et al. 1978), which collected flux measurements of the H & K lines for a few hundred main-sequence stars in the solar neighborhood. The dedication to regular, consistent measurements for over three decades with the primary purpose of probing nearby stars for solar-like cycles proved foundational for the study of stellar magnetic fields and improved our understanding of stars' age, rotation period, and activity relationship (Noyes et al. 1984a,b).

The publication of the decades long time-series data (Duncan et al. 1991; Baliunas et al. 1995) which identified many stars with cycles similar to the solar-cycle also identified many variable and inactive stars. This dataset served as the foundation of convection, rotation, activity, and age analyses for the next 30 years (Barnes 2007; Mamajek and Hillenbrand 2008). The desire to put the Sun's solar cycle into context became a reality and the study of magnetic fields on stars, which are difficult to study with spectroscopy (Marcy 1982), blossomed into its own astronomical field of study.

As the understanding of time-domain stellar activity improved, the connection between activity, rotation and convection identified stellar rotation as a fundamental parameter of the stellar dynamo (Noyes et al. 1984a). The Rossby number, defined as the ratio of the stellar rotation period to the convective turnover time became a fundamental tool for describing stellar dynamos, even though the exact value of the convective turnover time was not well constrained. Combined with the powerful Mount Wilson H & K Project dataset, our understanding of stellar dynamos improved when computing allowed for complex modeling of stellar interiors (Belvedere 1985; Brandenburg et al. 1998). By monitoring stellar rotation timescales of days and stellar cycle timescales of years, observational surveys, with Mount Wilson data as the foundation, would continue to fuel development of models to explain the observed phenomena and motivate new observational surveys.

1.3 Stellar activity and exoplanets

Near the time of publication of the Mount Wilson S-value catalog, the first exoplanets around Sun-like stars were discovered (Mayor and Queloz 1995; Marcy and Butler 1996) using precise radial velocities (RVs). Only a few years before, the discovery of the first planets outside of the solar system, two planets around a pulsar with masses roughly three times that of Earth (Wolszczan and Frail 1992), opened the door for exoplanet discoveries on the horizon. This ground-breaking discovery required assessment of possible false-positive scenarios including the use of the Ca II H & K lines to determine if the RV signal could be due to star spot modulation. Fortunately, the Ca II H & K lines fall within the optical wavelength coverage of the spectrographs used for early exoplanet detection. Measurements of the S-value, defined as the ratio of the flux in the cores of the Ca II H & K lines normalized by the flux of nearby continuum regions, became the standard method for determining the effect of chromospheric activity on RV measurements (Santos et al. 2000; Wright et al. 2004). With simultaneous S-value measurements for every RV, the false-positive scenarios decreased, the confidence in exoplanet scenarios increased, and their discoveries around both Sun-like stars (Marcy and Butler 1996; Butler et al. 1996) and M-dwarfs (Marcy et al. 1998; Delfosse et al. 1998) multiplied.

As interest in exoplanets exploded, existing exoplanet surveys extended their observing baselines, and new surveys began. The first exoplanet discoveries were Hot Jupiters, planets near the mass of Jupiter with orbital periods of less than 10 days. Detecting such a planet requires only a single season of observations. To find Jupiter analogs, with orbital periods of 10 years or more, temporal observing baselines on the same instrument are required. Combination of long-baseline RVs from different instruments can be used to identify long-period planets, RV offsets and non-overlapping time frames can make definitively identifying a planet difficult. With longer baselines, the possibility of discovering a planet with an orbital period that overlaps with stellar rotation or stellar activity periodicity increases. The planet HD 154345b (Wright et al. 2008) has an orbital period of 9.2 years and a 9-year activity cycle. Disentangling the activity signal and the planet signal would be the first of many such scenarios (Kane et al. 2011; Fulton et al. 2015). In order to better understand the exoplanets, continued monitoring of the chromospheric activity metrics, and understanding stellar activity, became a necessity (Santos et al. 2010; Isaacson and Fischer 2010).

1.4 The discovery of transiting exoplanets

The probability that a Hot Jupiter transits its host star is roughly 10% and by chance, the 10th Hot Jupiter discovered was found to be transiting (Charbonneau et al. 2000; Henry et al. 2000). This discovery provided an important, independent, confirmation of the detection of exoplanets by RV. Along with the transit detection method, photometric monitoring of planet host stars could be used to further limit the astrophysical false-positives of RV surveys.

Proposals for studies of photometric surveys capable of detecting Earth analogs were already underway (Borucki et al. 1996; Koch et al. 1996) when the first transiting planets were detected, but ground-based transit surveys searching for exoplanets were limited by instrumental precision and detection limitations caused by the Earth's atmosphere and by the diurnal observing cycle caused by the Earth's rotation. Instrumentation was capable of detecting Earth-sized planets around small M-dwarfs (Charbonneau et al. 2009), but were limited to planets larger than Neptune around F-type, G-type, and K-type dwarfs. Hot Jupiters were prolifically discovered, despite their 1% occurrence rate (Wright et al. 2012) due to their relatively large, typically 1%, transit depth. Ground-based photometry and precise RV surveys had set the stage for the exciting exoplanet discoveries on the horizon but were limited by the technology of the time from finding planets smaller than the mass and radius of Neptune.

With the collection of ground-based photometric data to complement RV data, exoplanet detections were verified, and the photometric data could additionally be used to study stellar activity, rotation, and age (Barnes 2007; Mamajek and Hillenbrand 2008). Similar limitations applied to astrophysical studies as hindered the ground-based transit searches, sensitivity and shear number. But NASA's *Kepler* Mission would soon revolutionize exoplanet science, stellar activity studies, and much more.

1.5 The *Kepler* space telescope: finding planets, measuring activity

Conceived prior to the first exoplanet detection, *Kepler* pioneers pushed the threshold forward on CCD photometric precision, biding their time as the technology caught up with their aspirations. In 2009, *Kepler* launched into space from Cape Canaveral, Florida, USA, into an Earth-trailing orbit starting its four-year journey to search for exoplanets (Borucki et al. 2010). Desiring the capability of detecting an Earth-sized planet around a Sun-like star with orbital periods of one year, *Kepler* scientists and engineers used lessons from ground-based surveys and space-based predecessor missions such as Corot (Léger et al. 2009) to fulfill its technical specifications.

The scientific purpose of the *Kepler* mission was to discover transiting planets and the ultra-precise, continuous, stellar photometry went far beyond achieving the primary science goals. The astronomy sub-fields of asteroseismology (Gilliland et al. 2010), rotation in stellar cluster (Meibom et al. 2011), planetary dynamics (Ford et al. 2011), stellar rotation (McQuillan et al. 2014), and planetary formation were revolutionized by *Kepler*. The photometric data products used to discover exoplanets could also be used in complementary analyses of precise radial velocities enabling measurements of planets near in size and mass to the Earth (Howard et al. 2013; Pepe et al. 2013).

In the study of stellar activity, *Kepler* provided exquisite data on timescales of minutes to weeks to years. Stellar rotation period measurements for main-sequence stars increased from a few hundred to over 30,000 (McQuillan et al. 2014), and every star observed by *Kepler* had stellar variability metrics on timescales useful for detecting exoplanets (Jenkins et al. 2010b) and capable of measuring stellar pulsations (Chaplin et al. 2010). The uniformity and sensitivity of the data led to the achievement of the primary science goal of measuring eta-Earth, the frequency of Earth-sized planets around Sun-like stars (Petigura et al. 2013; Burke et al. 2015). The early science returns would be further refined in the years to come, but these estimates constrained eta-Earth to within a few orders of magnitude compared to unbridled speculation before *Kepler*.

1.6 The California Kepler Survey

A homogeneous set of high-resolution spectra with similar signal to noise ratio were collected to more precisely determine planet and stellar radii to uncertainties of ten percent. The high-quality, uniform spectra were used to identify the small-planet radius gap (Fulton et al. 2017, The Fulton Gap) beginning a long list of scientific uses. Multi-planet systems (Rowe et al. 2014) were used to identify the Peas-in-a-Pod like architecture that reveals how planets in a system tend to have similar sized planets (Weiss et al. 2018a). When the Gaia spacecraft's second data release (DR2) was made public, the parallax measurements of*Kepler* planet hosts improved the stellar and planet parameters below the level of model uncertainties (Fulton and Petigura 2018), making the*Kepler* photometry uncertainties the dominant source of error for planet radii measurements (Petigura 2020). Expansion of the survey to cooler stars resulted in the identification of the stellar mass function of the planet radius gap, with the average size of sub-Neptune-sized planets increasing with stellar mass, but super-Earths do not (Petigura et al. 2022). The richness of the data set is yet to be fully exploited. We perform additional analysis on CKS dataset, focusing on stellar chromospheric activity in Chapter 3.

1.7 RV and stellar activity surveys post-*Kepler*

With the plethora of discoveries from *Kepler* photometry such as the identification of new populations of planets dubbed Super-Earths and Sub-Neptunes (Petigura et al. 2013; Fressin et al. 2013), an extended network of ground-based astronomical resources were used to follow-up and enhance *Kepler* discoveries (Gautier et al. 2010). Adaptive optics imaging of planet-host stars was used to identify blended background eclipsing binary stars and hierarchical triple star systems masquerading as planets (Adams et al. 2012). Low-precision radial velocities were used to identify single or double-lined spectroscopic binaries, identifying false positives (Latham et al. 2011). And precise radial velocities were used to measure the masses of *Kepler*-identified transiting planets (Holman et al. 2010; Jenkins et al. 2010a; Batalha et al. 2011; Marcy et al. 2014). The ability to use ground-based resources to observe transiting exoplanet hosts instead of surveying nearby stars for exoplanets was a paradigm shift in exoplanet science.

This shift in resource allocation toward transiting planets resulted in many exciting discoveries, but in order to find the true Jupiter-analog systems and place the solar system planets in context with exoplanet discoveries, the time baselines of the original RV exoplanet surveys needed to be extended through the *Kepler* era. These surveys, with their complementary measurements of S-values, were indeed extended and came to fruition when the occurrence rates of Jupiter-mass planets in decades-long orbits were meaningfully quantified (Rosenthal et al. 2021; Fulton et al. 2021). The time-series RV was used to great effect for exoplanet demographics of distant, jovian-mass planets. We extend the use of the valuable spectroscopic time-series data in Chapters 4 and 5.

1.8 Data in hand

With twenty years of S-value time series from RV surveys, combined with four years of the *Kepler* space telescope's photometric time-series, the time for studying stellar and chromospheric activity is imminent. The most precise photometric data for 198,709 stars is publicly available (Twicken et al. 2016). There are 2,662 Kepler candidates dynamically confirmed or numerically validated as planets. Ground-based RV surveys have over 20 years of data available for nearby, Sun-like stars. Next, we lay out the scientific motivation for utilizing the data in hand to study stellar chromospheric activity in*Kepler* planet-hosts and nearby main-sequence stars.

1.9 Research questions

With an abundance of ground-based data from the HIRES instrument on Keck, we aim to address three research questions, all related to the California Planet Search's (CPS) spectroscopic catalog of nearby stars and the *Kepler* mission's photometry. We focus on stellar and chromospheric activity of stars that have been surveyed for, or are known to host, exoplanets.

- Research Question 1: Does chromospheric activity play a role in the planet-radius distribution determined by studies of *Kepler* Space Telescope data, and can *Kepler* data be used to support the theory of Weakened Magnetic Braking (WMB)?
- Research Question 2: For slowly rotating Sun-like stars surveyed for exoplanets, how common are stellar activity cycles, and are fundamental stellar parameters responsible for the periods of stellar activity cycle period?
- Research Question 3: Using the spectroscopic survey stars in the solar neighborhood, how can late stage main-sequence activity evolution inform the final activity state of stars?

CHAPTER 2: LITERATURE REVIEW

2.1 Observations of stellar activity

The study of stellar activity began over 400 years ago, with daily sunspot counting (Galileo's "Letters on SunSpots"). Monitoring of sunspots over time led to the discovery of solar cycles, the solar rotation period, the Maunder minimum (Maunder 1922), differential rotation and the connection between magnetic fields and sunspots (Hale 1908). These fundamental observations of the Sun would lead to the study of stellar rotation and activity cycles. Studies began with photographic plates and ever-larger telescopes (Eberhard and Schwarzschild 1913). Photographic plates would give way to photomultiplier tubes (Wilson 1968; Vaughan et al. 1978). Digital technology on computer-controlled telescopes (Schwarzschild 1993) eventually supplanted photomultiplier tubes due to their superior efficiency. In contrast to the serial observations of single stars in the Mount Wilson survey and spectroscopic surveys, the *Kepler* spacecraft simultaneously monitored hundreds of thousands of stars nearly continuously for four years (Twicken et al. 2016). The Transiting Exoplanet Survey Satellite (TESS) mission has observed 85% of the sky for periods lasting months to years, transforming the time-domain landscape of stellar activity (Ricker et al. 2015).

While the analysis of optical broadband photometry is valuable in large scale monitoring of stellar activity including flares, individual spectral features have been linked to chromospheric and coronal activity. Among the most well studied are the Ca II H & K emission features that originate in the chromospheres of Sun-like stars (Wilson 1968). Astronomers at the Mount Wilson Observatory are responsible for establishing the protocol for these measurements or S-values (Vaughan et al. 1978). The log($\mathrm{R}'_{\mathrm{HK}}$) would become a widely used metric that enabled combination and comparison across observational surveys, and across stellar types, requiring only a $B - V$ color and S-value measurement as inputs (Noyes et al. 1984a).

2.2 Chromospheric activity and precise radial velocities

The last three decades of astronomy have seen the emergence of the field of exoplanets from the discovery of the first extra-solar Jupiter mass planets (Mayor and Queloz 1995; Marcy and Butler 1996) to the compositional constraints of planets nearly the size of the Earth (Howard et al. 2013; Pepe et al. 2013; Barclay et al. 2013b,a; Marcy et al. 2014). The first discoveries in 1995-1996 were remarkable. Astronomers were confronted with a new paradigm for the types of planetary systems that exist beyond the solar system. When the first transiting planet was discovered, HD 209458b (Charbonneau et al. 2000; Henry et al. 2000), the paradigm would shift again. This discovery solidified the previous RV discoveries as exoplanets and set the stage for studies of exoplanet composition.

After the discovery of HD 209458b, the search for transiting exoplanets intensified. The highly successful Wide Angle Search for Planets (Pol-

Iacco et al. 2006, WASP) has successfully identified and confirmed 193 systems with transiting planets. With thirteen telescopes around the world, the Hungarian-made Automated Telescope Network (Bakos et al. 2004, HATNet) has discovered 70 confirmed planets. The Kilodegree Extremely Little Telescope (Pepper et al. 2007, KELT) focused on stars between eighth and tenth visual magnitude, much brighter than WASP and HATNet. The MEarth survey was dedicated to searching M-dwarf stars and was sensitive to smaller planets due to the smaller radii of its target stars. All of these surveys proved fundamental in developing the knowledge and experience that would be needed for the space-based exoplanet finding mission, *Kepler*.

As the individual discoveries increased they eventually led to population statistics and occurrence rates of Neptune to super-Jupiter mass planets (Howard et al. 2010b; Mayor et al. 2011). Planet formation theories that disagreed with the new observational results (Ida and Lin 2010) needed significant revision to enable replication of these systems from scratch.

A few short years later, when detector technology finally caught up to the ambitions of those searching for Earth-sized planets, the first planetary discoveries of NASA's *Kepler* spacecraft emerged (Borucki et al. 2010). The unprecedented and exquisitely precise photometry of 198,709 (Twicken et al. 2016) stars revealed an entirely new family of exoplanets, those ranging in size between the Earth and Neptune (Borucki et al. 2011; Batalha et al. 2013). Ambiguous in their gaseous or rocky composition, these planets suddenly became the most intriguing due to their abundance and lack of solar system analogs.

To support the *Kepler* Science Team, an RV survey of 30 *Kepler* planet-hosting stars was undertaken for 4 years using the HIRES instrument on Keck. The masses of the smallest planets yet-measured were combined with planet radii to provide bulk densities for dozens of super-Earths and sub-Neptunes (Marcy et al. 2014). RV measurements and *Kepler* photometry, combined with planet composition models, soon revealed that rocky planets are mostly limited to sizes smaller than 1.6 Earth radii (Rogers 2015) with larger planets requiring a significant gas component. The detection of non-transiting planets, beyond the inner transiting planets, added complexity and depth to the exoplanet systems (Gilliland et al. 2013; Weiss et al. 2013; Gettel et al. 2016). Transit-timing variations were observed for the first time, allowing planet masses to be measured with a novel method (Lissauer et al. 2011; Steffen et al. 2012). The observed diversity in planet density as a function of planet radius (Weiss and Marcy 2014) provided planet formation theories with challenges that have yet to be fully resolved. Every *Kepler* discovery included a detailed light curve analysis. The measurement of planet densities also required precise RV time series measurements to detect exceptionally small RV amplitudes of small planets (Howard et al. 2013; Pepe et al. 2013). Every RV follow-up campaign included measurements of S-value time series, building a valuable set of spectroscopic observations consistent with the high quality and consistency, if not yet the time baseline, of the original RV exoplanet surveys.

2.2.1 Stellar activity surveys and analysis

The primary source of S-value time series is the Mount Wilson H & K Survey (Baliunas et al. 1995). With its initial publication, Sun-like stars were identified as variable, cycling or inactive on decades-long timescales for the first time. Some stars were identified as having cycling activity similar to the Sun's and the study of the solar-stellar connection was advanced dramatically (Gilliland and Baliunas 1987). Many other observational surveys would contribute to our understanding of stellar and chromospheric activity (Henry et al. 1996; Wright et al. 2004; Hall et al. 2007), but the Mount Wilson survey and its extended time-series would bear the most scientific fruit even decades after its publication (Böhm-Vitense 2007; Oláh et al. 2016; Brun et al. 2017; Mittag et al. 2018, 2023).

As ground-based photometric surveys improved their techniques, stellar rotation period catalogs grew , and our understanding of the connection between stellar rotation and stellar cycles was deepened (Böhm-Vitense 2007). With more sophisticated signal detection techniques, sequences of co-existing activity cycles were identified (Brandenburg et al. 2017). Adding information about the ages of stars, and comparing those ages to stellar activity cycle properties showed that solar-type G and K-dwarfs with ages younger than 2 Gyr tend to have shorter and highly variable cycles. Solar age and older stars tend to have longer, regular cycles (Oláh et al. 2016). Further dissection of the Mount Wilson data, and the differentiation between active and inactive branches improved the understanding of stellar interiors and identified the layers at which the magnetic activity is generated (Mittag et al. 2023). Short cycle periods were linked to deeper layers of the convective zone compared to shallower zones that drive the longer period activity cycles.

Early releases of CPS chromospheric activity data (Wright et al. 2004; Isaacson and Fischer 2010) were useful in quantifying the impact of stellar activity on precise RV performance, but the time baseline of the data was not sufficiently long to identify stellar cycles. The scientific focus of those analyses remained on radial velocities. Long-baseline observations from the HARPS planet search provided summary statistics of chromospheric activity for their survey of southern hemisphere stars, but only the average values were made available (Lovis et al. 2011; Gomes da Silva et al. 2021). Occasional data showing the detection of chromospheric activity cycles and their time-series would be made available for single stars (Flores et al. 2016), but the lack of survey scale data releases of HARPS time-series data inhibited these studies from having the impact of the Mount Wilson dataset. However, with the summary statistics, the HARPS studies identified two ideas that we explore in Chapters 4 and 5: the idea that variability of the activity time-series is important and that this variability should be considered for precise RV surveys (Lovis et al. 2011; Brown et al. 2022).

2.3 Stellar activity metrics

The Mt. Wilson S-value is the most widely used chromospheric activity indicator due its simplicity and the ability to collect the measurements from ground-based observatories using either a photometer or pixelated detector (Vaughan et al. 1978; Baliunas et al. 1995; Wright et al. 2004). The measurement consists of four components, two from the cores of the Ca II H & K spectral features and two from the nearby continuum sections of spectrum, one redward, and one blueward of the line cores. Figure 2.1 breaks down the components of the Ca II K line core. It consists fo a photospheric component that can be calculated analytically and a photospheric

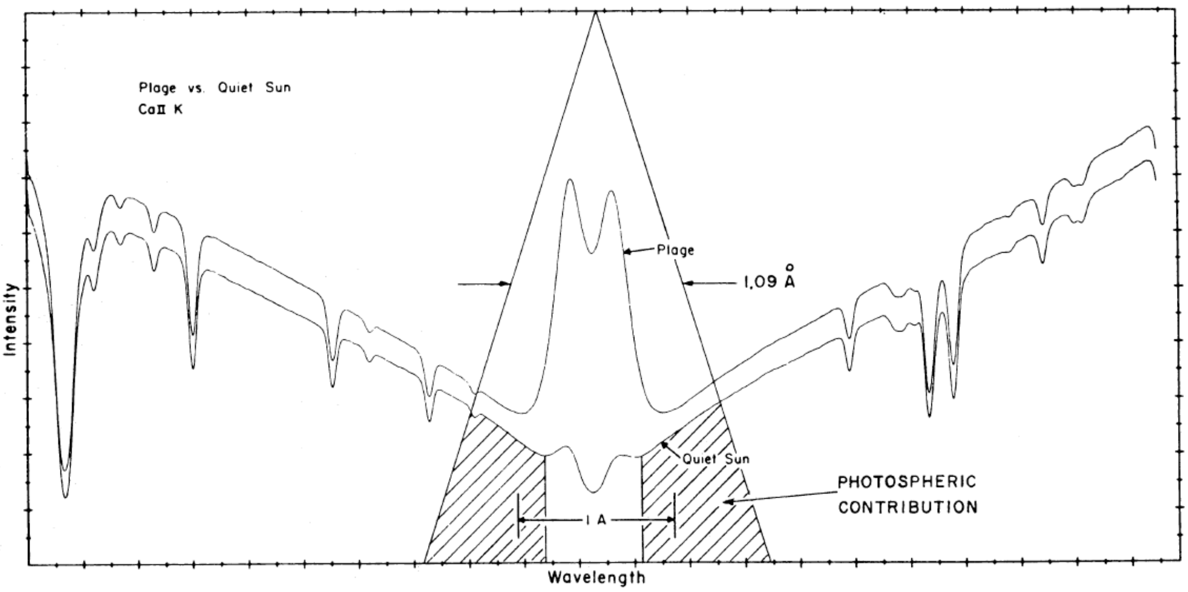

Figure 2.1: From Hartmann et al. (1984): "Fig 1. The central bandpass of the HK photometer is shown superposed on a spectrum of the quiet Sun taken from White and Livingston (1981) with the minimum photospheric contribution to the S index indicated." The identification of the 1.09 Angstrom triangular bandpass and the differentiation between the photospheric and chromospheric contribution provides the fundamental measurements for every chapter of this thesis.

component that is calculated by subtracting the photospheric component from the total flux. The line core measurements are 1.09 Angstroms each and weighted by a triangular bandpass. The sum of flux in the H and K line cores is normalized by the redward and blueward bandpass flux Figure. 2.2. Normalization factors on one or more of the flux values can be used to calibrate new datasets to the Mt. Wilson scale (Wright et al. 2004; Isaacson and Fischer 2010; Lovis et al. 2011) allowing for datasets to be easily merged.

The log($\mathrm{R}'_{\mathrm{HK}}$) activity metric was established in order to compare the activity stars across FGK spectral types (Noyes et al. 1984a). The simplicity and robustness of the metric, requiring only a $B-V$ color, and single measurement of the S-value led to its widespread use.

Log(R'_{HK}) is a derivative of the S-value and is proportional to the flux per square centimeter in the H & K bandpasses over $T_{eff}{}^{4}$. The original calibration was conducted on the Mt. Wilson H & K spectrometer itself. Two different sources of spectrophotometry were used to calibrate the H & K flux. Fay et al. (1974) produced spectrophotometry from four bright stars and O'Connell (1973) presented energy distributions for stars in 20 Angstrom bandpasses. The three methods were found to be in good agreement (Noyes et al. 1984a) and the result is a color correction factor. Broadly speaking, the Mt. Wilson H & K spectrometer was calibrated to an absolute photometric scale so that the relative flux measurements, S-values, could be put on an absolute scale, log(R'_{HK}), with the best calibration for stars between 6400 and 4800 K. log(R'_{HK}) is defined as the flux in the Ca II H & K lines relative to the bolometric flux of the star. More recent studies have recalibrated the color correction factor with modern tools (Mittag et al. 2013) as discussed in Chapter 5. Since this metric was linked to the Mount Wilson H & K Project, and the Rossby number was linked to the log(R'_{HK}) value, it has remained fundamental in stellar chromospheric activity studies, especially those involving Rossby number (Mamajek and Hillenbrand 2008; van Saders et al. 2016; Corsaro et al. 2021; David et al. 2022). Variations of log(R'_{HK}) have been identified as important variables in dedicated magnetic dynamo studies (Brown et al. 2022) and planet searches.

$B - V$ photometry is a proxy for stellar effective temperature, so calculating log(R'_{HK}) directly from T_{eff}, using contemporary models to calculate the photospheric contribution to the S-value, improves the precision of

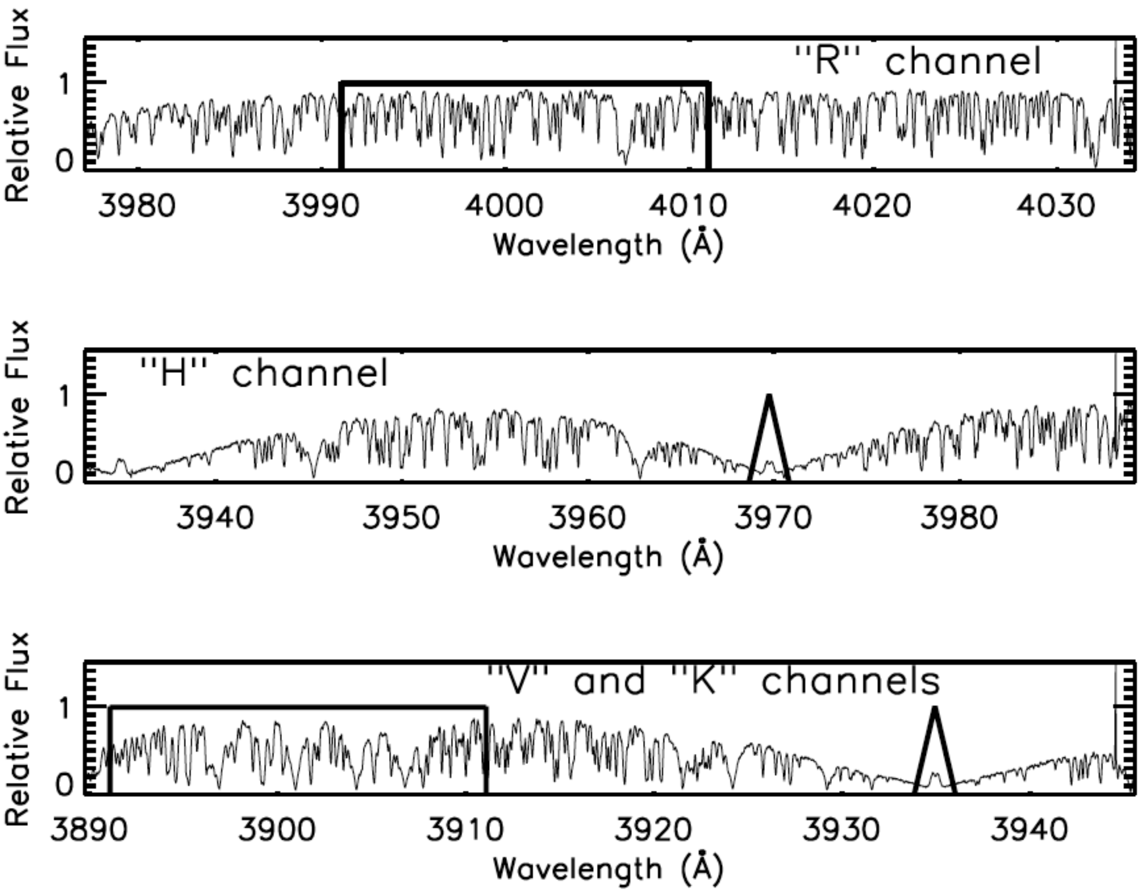

Figure 2.2: From Wright et al. (2004): "Fig. 1: R, H, K, and V channels in a representative Keck spectrum. The ordinate is relative photon flux in arbitrary units. Wavelength is in the rest frame of the star. The H and K channels are always centered on the line cores; the R and V channels are fixed in the observer's frame." In the blue portion of a typical high-resolution optical spectrograph the Ca II H & K line flux measurements contribute to understanding the chromosphere of a star and its magnetic field. They are collected simultaneously with a precise RV allowing for simultaneous monitoring of activity and RV.

the activity metric (Mittag et al. 2013). Extending the $\log(R'_{HK})$ metric to cooler stars (Marvin et al. 2023) is also useful when comparing a wide range of spectral types, but requiring an offset to relate to the traditional $\log(R'_{HK})$ value can prohibit its adoption in other studies. To dispense with the logarithms, the R_5 metric was used (Gomes da Silva et al. 2021). We find an empirically determined $\log(R'_{HK})$ value that is calibrated for solar-age and older stars is useful for our purposes. In Chapter 5 we use the reformulated $\log(R'_{HK})$ value from Lorenzo-Oliveira et al. (2018) to study extremely inactive stars. Using the original formulation of $\log(R'_{HK})$ to define our sample, we allow for comparison of our results to previous works.

Only the S-value itself is a more fundamental activity metric than $\log(R'_{HK})$, but the flux in the cores of the Ca II H & K lines contains both a photometric and chromospheric component. Properly calibrating the photometric component is the critical part of any metric that will be used across spectral types. Compared to the typical uncertainties in stellar mass when the $\log(R'_{HK})$ metric was formulated, we now have much smaller systematic uncertainties which are limited by our stellar models (Tayar et al. 2022). Since our ability to calculate the stellar mass has improved, we will revisit the S-value as a fundamental activity metric and use it for stars binned by mass. For small mass bins, the S-value does not involve the T_{eff} nor [Fe/H] values and so very small differences in mean activity can be measured.

2.4 Stellar activity, rotation, and age

The connection between magnetic activity, stellar rotation, convection and Ca II H & K flux is a critical and fundamental part of our research. Using data from the decades-long survey acquired to search for stellar activity cycles (Duncan et al. 1991; Baliunas et al. 1995) these astrophysical connections were described by Noyes et al. (1984a). Stellar age and chromospheric activity are connected through rotational braking (Skumanich 1972). The connection between stellar spin-down rate and stellar age, dubbed gyrochronology (Barnes 2007) led to detailed studies of stellar age using young clusters with ages up to 1 Gyr (Mamajek and Hillenbrand 2008). Older stars tend to be difficult to age beyond 3 Gyr with this technique (Pace 2013) and would require rotation data from older clusters for calibration (Curtis et al. 2020).

The variation in S-value or log($\mathrm{R}'_{\mathrm{HK}}$) enables measurements of stellar spot modulations to identify rotation periods and stellar activity cycles. Rotation periods are measured on timescales of days or weeks, and stellar activity cycles require years of observing baseline. With measurements that span only partial rotation periods or cycle periods, the mean activity is not precisely known. Even less accurate are single value activity measurements, though they can still be valuable for stars younger than about 4 Gyr, when less accuracy is needed.

The foundational results from the Mt. Wilson H & K Survey are worthy of summary. The primary Mt. Wilson Survey (Baliunas et al. 1995) observed 111 stars, eighteen of which were designated as standard stars and showed very small variation over time. Three of these were ultimately moved to the variable category. The standards were used to determine an empirical uncertainty of 1.2% over the 25 year baseline. With spectral types from M2-F2 28/111 (25%) stars were found to be variable, with large scatter and no identifiable period. Sixteen (16/111, 14.4%) stars were identified as having long-term trends in activity, indicating their periods were more than four times the observing baseline. Fifty-two of 111 (47 %) of stars were found to have cycles between 2.5 and 21 years. Uncertainties in the cycle period are found using the shape of the periodogram and reliability estimates were made using a false alarm probability calculation requiring a confidence level of 99.9% in order to be considered a cycle. The importance of measuring the variation in S-value or log(R'_{HK}) has been previously noted (Brown et al. 2022; Gomes da Silva et al. 2021), specifically in terms of their use choosing targets for precise RV surveys or in the choice of stellar activity mitigation in RV analysis. Those studies identify active and inactive populations of stars, noting that active stars can either have small or large activity variability (Figure 2.3). We counter this in Chapter 5, showing that only the least active stars show this type of variability, and we attribute this new conclusion to the homogeneous stellar parameters that we use. When stellar parameters are collected from multiple sources, the small differences in T_{eff} can lead to inconsistent calculations of log(R'_{HK}). Therefore studies of these intricacies in deciphering active from inactive populations should use homogeneous, precise stellar parameters, that include Gaia parallax measurements (Fulton and Petigura 2018).

2.4.1 Rossby number

The Rossby number, defined as the ratio of the stellar rotation period to the convective turnover time (Noyes et al. 1984a) is used to connect dynamo theories to the observables such as activity and rotation. The original conception of the Rossby number used ground-based stellar rotation periods

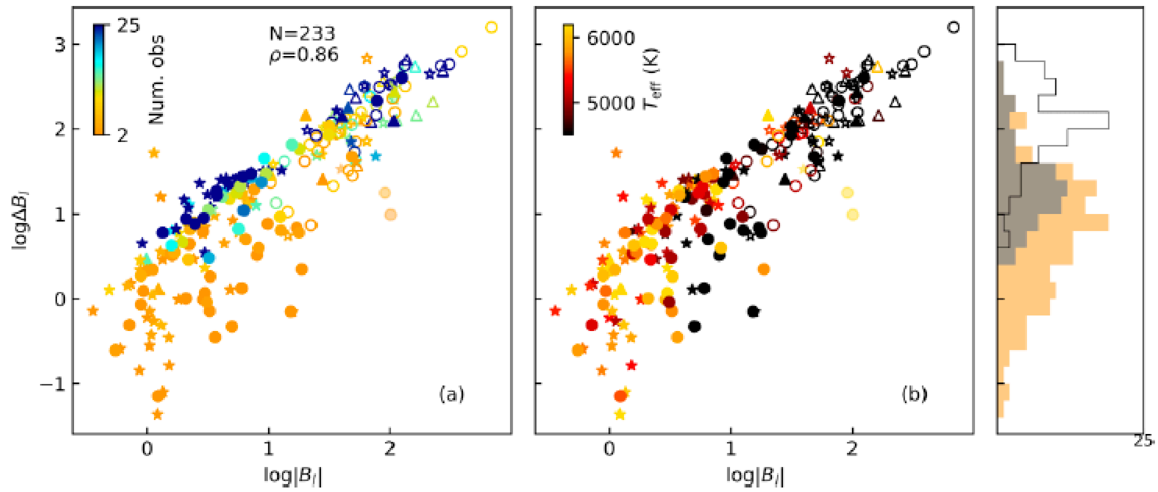

Figure 2.3: From Brown et al. (2022): "Magnetic field variability amplitude versus mean magnetic field strength... In (a) the marker colour scales with the number of observations, while in (b) marker colour scales with stellar effective temperature. The histograms to the right of the plots indicate the distributions of ΔB_l for the entire main-sequence sample (orange), main-sequence stars for which the variability amplitude is based on > 10 observations (grey), and young stars (black line)." The authors identify an important variable that contributes to our analysis in Chapter 5, the variation in magnetic field, which we probe as a variation in S-value. The variability is important for identifying activity trends in stars older than about 4.0 Gyr.

and a theoretical value of convective turnover time. A critical Rossby number was observationally identified using activity and rotation to understand when observed stellar spindown diverges from theoretical predictions (van Saders et al. 2016). Using space-based photometry from *Kepler* to determine the rotation periods and color index calibrated with asteroseismology, a 'calibrated' Rossby number (Corsaro et al. 2021) was defined, and made into a function of Gaia color.

2.4.2 Weakened magnetic braking

Prior to *Kepler* hundreds of stars had measured stellar rotation periods. With four years of space-based photometry, tens of thousands of rotation periods (McQuillan et al. 2014; Santos et al. 2021) including hundreds of rotation periods of transiting planet hosting stars (Angus et al. 2018) were measured. A host of other metrics calculated from *Kepler* data have been used to determine stellar gravity (Bastien et al. 2016), differential rotation (Reinhold and Gizon 2015), and spot patterns (Basri and Nguyen 2018).

The connection between rotation rate and age begins to weaken near the age of the Sun (Metcalfe and Egeland 2019) , requiring a diversion from traditional spin-down (Figure 2.4). The theory of WMB was constructed to explain the discrepancy between stellar age calculations from gyrochronology and those from chromospheric activity (van Saders et al. 2016). The observational question was posed using photometric rotation periods identified in *Kepler* data. Stellar rotation periods determined via asteroseismology were used to independently confirm the link between WMB and observations (Hall et al. 2021; Saunders et al. 2024). Using the precise stellar properties of the CKS survey, thoroughly vetted rotation periods identified the ”Rossby Ridge” (David et al. 2022), an observation consistent with the stalled spin-down explained by WMB. The addition of chromospheric activity metrics to the ”Rossby Ridge” interpretation can add support to WMB (Chapter 3).

Spectropolametric observations of a star’s magnetic field strength have also been used to test WMB. With observations of two stars that are cooler than the Sun, Tau Ceti and 61 UMa, the rate of angular momentum loss due to magnetic braking was shown to drop by a factor of 300 between ages of 1 – 9 Gyr (Metcalfe et al. 2023). Similar observations have been used to examine planet-host stars and their magnetic field states. 51 Peg was observed to lie in the WMB regime (Metcalfe et al. 2024) providing information on the magnetic field evolution that may be relevant for planet formation theories (Atkinson et al. 2024), and placing our Sun into context (Bhalotia et al. 2024).

2.4.3 Activity and stellar metallicity

One of the most basic stellar observables is the $B - V$ which can serve as a proxy for $\mathrm{T_{eff}}$. It is easily determined and known for almost every star, but it conflates the $\mathrm{T_{eff}}$ and the [Fe/H] (Ramírez and Meléndez 2005). To study the effects of metallicity on rotation and activity (Amard and Matt 2020), one must use temperature and metallicity independently. The disambiguation led to detailed modeling of the metallicity effect on rotation, likely due to the influence on stellar opacity. Before detailed models were available, observational studies suggested that metal-poor main sequence stars have a higher minimum activity value than solar-metallicity stars (Saar 2006). *Kepler* data contributes here, showing metal-rich stars

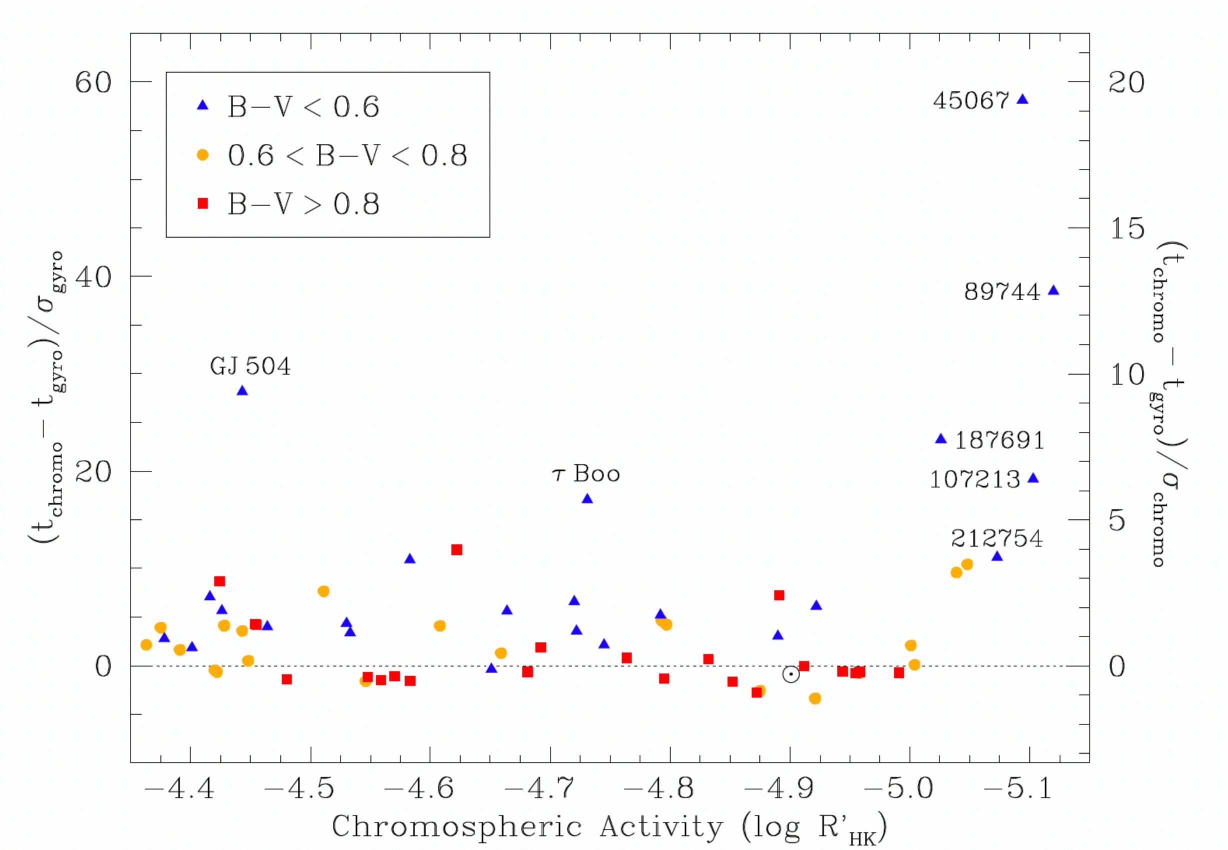

Figure 2.4: From Metcalfe and Egeland (2019): "Difference between the chromospheric age and the gyro age, in units of the uncertainties (σgyro and σchromo), for Mount Wilson stars at various activity levels. Data are taken directly from Table 3 of Barnes (2007)). Colored symbols indicate hotter stars with $B-V$ < 0.6 (blue triangles), solar-type stars with 0.6 < $B-V$ < 0.8 (yellow circles), and cooler stars with$B-V$ > 0.8 (red squares), while the Sun is shown with its usual symbol (e). With the exception of two Jovian exoplanet host stars (GJ 504 and Tau Boo), the two age estimates generally agree within 3 σ_{chromo} (9σ_{gyro}) until the lowest activity levels (log(R'_{HK}) < -5) where rotation appears to decouple from activity (see the text for details). Most of these F- and G-type stars are classified as "Flat" or "Long" by Baliunas et al. (1995) from 25 years of Ca II H & K observations, suggesting that their global dynamos may already be shutting down, eliminating the large-scale fields that dominate magnetic braking." The activity level at which the chromospoheric age and gyrochronology ages begin to diverge will be identified in Chapter 4 using long-term activity cycles, supporting the theories that explain the discrepancy in ages as related to an abrupt change in a star's magnetic field near log(R'_{HK}) of -5.0

spin-down more quickly (See et al. 2024) than metal poor stars.

2.5 The *Kepler* space telescope

The most influential result from *Kepler* was the determination of the occurrence rate of Earth-sized planets around Sun-like stars. With current estimates between 10-30% of Sun-like stars (Petigura et al. 2013; Fressin et al. 2013; Burke et al. 2015) and even higher for M-dwarfs (Dressing and Charbonneau 2015), we now know that exoplanets are prolific. Statistically speaking, the next generation space telescopes that will search for biosignatures will have an abundance of targets. Surveys that Search for Extra Terrestrial Intelligence (SETI) have become ever more hopeful and common (Isaacson et al. 2017; Czech et al. 2021), with the knowledge that small rocky planets are plentiful. The types and variety of planets found by *Kepler* have greatly expanded the field of exoplanets and taught astronomers, once again, to expect the unexpected.

Kepler's survey design was solely focused on providing precise photometry for finding exoplanets. This required allowing the spacecraft to make quarterly rotations in its on-sky orientation to face the solar panels toward the sun. A nearly symmetric layout of the *Kepler* detectors enabled continuous coverage for 95% of stars (Twicken et al. 2016). The quarterly spacecraft rolls resulted in a star's photons being collected on a different detector. These offsets, when searching for planets can be removed with a single offset variable, but connecting the quarters together to search for stellar activity cycles proved challenging because the astrophysical changes and systematic changes in amplitude were difficult to disentangle. When searching for stellar rotation periods, researchers were rarely able to use continuity across quarterly rolls resulting in the majority of *Kepler* identified stellar rotation periods having periods less than 90 days, the duration of one quarter of observing (McQuillan et al. 2014). In early 2010 *Kepler* lost two of its 42 CCDs and two shortly thereafter two more, but this did not dramatically impact the stellar rotation science pursuits because quarters were not typically stitched together for rotation analysis.

The *Kepler* spacecraft revolutionized time-domain astronomy not only with its exquisite precision but also with its incredibly high duty cycle of almost 90% (Caldwell et al. 2010). With four years of coverage on the *Kepler* field, stellar rotation curves in the photometry were ubiquitously discovered (McQuillan et al. 2014; Angus et al. 2018). The field of asteroseismology was revolutionized (Gilliland et al. 2010), but the advances in stellar astrophysics, would not outshine the discovery of new demographics of exoplanets (Petigura et al. 2013; Burke et al. 2015).

The early returns on the occurrence rates for planets with orbital periods less than 50 days were robust and their uncertainties improved with time and especially the addition of Gaia photometry (Fulton and Petigura 2018; Hsu et al. 2019). But measurements of eta-Earth diverged with time and the uncertainties in this long-awaited value grew. Kunimoto and Matthews (2020) claimed that G-type stars have less than 0.18 planets per star for those near in size to the Earth at similar orbital period compared to Hsu et al. (2019)'s 0.27 value. The Kepler Team produced varied results through time. From 2020 to 2021, eta-Earth values varied from 0.15 ± 0.01, Bryson et al. (2020) to 0.37 (+ 0.4, -0.2) for the conservative habitable zone and 0.58 (+0.7, -0.33, lower range quoted) for the optimistic habitable zone. This collection of uncertainties suggests that more work must be done before the launch of Habitable World Observatory (HWO).

2.6 The California-Kepler Survey

The CPS research group, with collaborators and telescope time pooled from the Keck Observatory partners at the University of California, California Institute of Technology and the University of Hawai'i have acquired high resolution spectra of ~ 1000 transiting planet host stars. The California Kepler Survey (CKS) was focused on improving the uncertainties on the stellar parameters of sun-like stars relative to the Kepler Input Catalog (Brown et al. 2011), specifically the stellar radii and, as a result, planet radii (Johnson et al. 2017). These results have led to numerous discoveries including the mass-radius gap or The Fulton Gap (Fulton et al. 2017; Fulton and Petigura 2018) shown in Figure 2.5.

The radius gap is defined by the bimodal distribution of planet radii for planets less than four times the radius of the Earth. The two peaks in the distribution are best described by planetary formation models (Lopez and Fortney 2014) that include photo-evaporation and result in either mostly solid planets or mostly gaseous planets, but few planets in between. The CKS collaboration has also explored stellar multiplicity (Weiss et al. 2018a,b), host-star metallicity (Petigura et al. 2018), and eccentricity (Mills et al. 2019).

With the extensive effort to collect the CKS spectra, it would be challenging to continuously monitor the entire sample for activity analysis. However, the follow-up observations to collect precise RV measurements to determine planet masses could provide an excellent dataset for such a

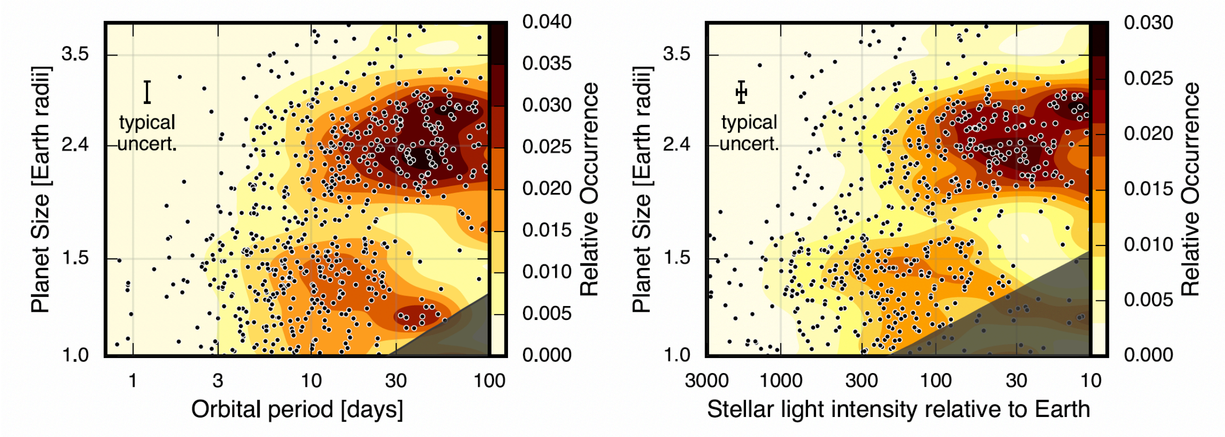

Figure 2.5: From Fulton and Petigura (2018): "Left: Two-dimensional distribution of planet size and orbital period. The median uncertainty is plotted in the upper left. Right: same as left but with insolation flux on the horizontal axis. In both plots, the two peaks in the population as observed by (Fulton and Petigura 2018) are clearly visible, but with greater fidelity." The subtle relationships that were revealed between orbital period and planet size from CKS exemplify the need for uniform measurements with the same instrument of the same quality. We use this philosophy to examine the CKS sample and its chromospheric activity in Chapter 3.

study. The Kepler Giant Planet Survey (Weiss et al. 2024, KGPS) is an observational campaign to measure the occurrence of Jovian planets in Jupiter-like orbits around systems of *Kepler*-identified transiting planets. Chapters 4 and 5 use precise RV in this way, but extended follow-up for stars observed by *Kepler* can provide additional value beyond what is possible for field stars.

2.7 Activity and extremely precise RVs

Our study of chromospheric activity goes hand-in-hand with the study of exoplanet masses due to the simiultaneous measurements of precise radial velocities and the Ca II H & K S-values. Initial surveys of exoplanets using precise RVs focused on slowly rotating F, G and K-type main-sequence stars. The next most-critical component is the addition of $\log(R'_{HK})$. For surveys probing eta-Earth, the frequency of Earth-sized planets around Sun-like stars, the cutoff of $\log(R'_{HK})$ < -4.70 was used (Howard et al. 2010a) to minimize the amount of stellar activity affecting the RV data. In order to isolate RV signals due to planets from those due to stellar activity, decorrelation with S-values can be used to remove activity signals (Fulton et al. 2015). Gaussian process analysis adds a level of complexity to decorrelating RVs and activity, allowing non-periodic signals from activity to be disentangled from Keplerian RV signals (Kosiarek et al. 2019; Lubin et al. 2021; Beard et al. 2022). When RVs from stabilized spectrographs such as HARPS are analyzed, methods of activity mitigation can be made on every spectral absorption line (Dumusque 2018; Siegel et al. 2022). Instead of using the Ca II H & K lines to assess a planet claim, the Ca II H & K spectral lines can be used to identify stars hosting evaporating planets by checking for anomalously low flux in the line cores that is due to planet outgassing absorption Staab et al. (2020).

Detecting RV amplitudes caused by Earth-analogs will require a combination of precise instrumentation and analysis. Understanding stellar activity and variability will be a crucial part of any analysis. While we do not analyze precise RVs in this work, each of our primary research questions is deeply intertwined with precise RVs and will be an essential element in interpreting and understanding the most exciting exoplanet discoveries in the future.

Drawing from our experience in exploring two astrophysical phenomena in Chapters 3 (stellar rotation) and 4 (stellar activity cycles), we will now focus on a narrow, but interesting fraction of the CLS sample to analyze the late stages of main-sequence stellar activity. Our sample, chosen to be older than the age of the Sun at 4.5 Gyr, has weak rotational modulation, as measured by S-values, making it difficult to study compared to a sample of younger stars. We explore the traditional activity metrics and use the time-series derived S-value variability to show that these old stars tend to have a large range of activity variability for a given mean activity level. We include the precise and homogeneously derived stellar properties to show that this variability only occurs for the oldest stars. While we present evidence that stars can have varying cycle amplitudes over short timescales (10–20 years), we identify the least active stars as the likely end-state of stellar activity. The activity floor appears to be at the limit of our spectral measurements and is identified in stars with masses ranging from 0.70 to 1.1 solar masses.

CHAPTER 3: THE CALIFORNIA-KEPLER SURVEY. XI. A SURVEY OF CHROMOSPHERIC ACTIVITY THROUGH THE LENS OF PRECISE STELLAR PROPERTIES

3.1 Introduction

The rich sequence of studies of*Kepler* planet hosts will be continued with the addition of chromospheric activity data in the form of Ca II H & K line flux measurements. The set of planet hosting*Kepler* stars is already well studied in their stellar properties (Petigura et al. 2017), the occurrence rate of planets (Fulton et al. 2017; Fulton and Petigura 2018), planet multiplicity (Weiss et al. 2018a), eccentricity (Mills et al. 2019), and more among others. We will add to this legacy with chromospheric measurements for 879 transiting planet hosts and use the data set to test the theory of weakened magnetic braking via stalled spin-down. In combination with previously published data of rotation periods, we analyze age-activity-rotation relations. Chapter 3 includes a catalog of*Kepler* stellar activity metrics and examination of chromospheric activity indices with fundamental stellar properties, and the search for relationships between planet hosts, stellar rotation periods and chromospheric activity in the CKS dataset.

3.2 Accepted paper

The Astrophysical Journal, 961:85 (22pp), 2024 January 20 https://doi.org/10.3847/1538-4357/ad077b

The California-Kepler Survey. XI. A Survey of Chromospheric Activity through the Lens of Precise Stellar Properties

Howard Isaacson[1,2], Stephen R. Kane[2,3], Brad Carter[2], Andrew W. Howard[4], Lauren Weiss[5], Erik A. Petigura[6], and Benjamin Fulton[7]
[1] 501 Campbell Hall, University of California at Berkeley, Berkeley, CA 94720, USA; hisaacson@berkeley.edu
[2] Centre for Astrophysics, University of Southern Queensland, Toowoomba, QLD, Australia
[3] Department of Earth and Planetary Sciences, University of California, Riverside, CA 92521, USA
[4] California Institute of Technology, Pasadena, CA 91125, USA
[5] Department of Physics, University of Notre Dame, Notre Dame, IN 46556, USA
[6] Department of Physics & Astronomy, University of California Los Angeles, Los Angeles, CA 90095, USA
[7] NASA Exoplanet Science Institute/Caltech-IPAC, MC 314-6, 1200 E. California Boulevard, Pasadena, CA 91125, USA
Received 2023 July 26; revised 2023 October 13; accepted 2023 October 25; published 2024 January 16

Abstract

Surveys of exoplanet host stars are valuable tools for assessing population level trends in exoplanets, and their outputs can include stellar ages, activity, and rotation periods. We extracted chromospheric activity measurements from the California-Kepler Survey Gaia survey spectra in order to probe connections between stellar activity and fundamental stellar properties. Building on the California Kepler Survey's legacy of 1189 planet host star stellar properties including temperature, surface gravity metallicity, and isochronal age, we add measurements of the Ca II H and K lines as a proxy for chromospheric activity for 879 planet hosting stars. We used these chromospheric activity measurements to derive stellar rotation periods. We find a discrepancy between photometrically derived and activity-derived rotation periods for stars on the Rossby Ridge. These results support the theory of weakened magnetic braking. We find no evidence for metallicity-dependent activity relations, within the metallicity range of −0.2 to +0.3 dex. With our single epoch spectra we identify stars that are potentially in Maunder minimum–like state using a combination of $\log(R'_{\rm HK})$ and position below the main sequence. We do not yet have the multiyear time series needed to verify stars in Maunder minimum–like states. These results can help inform future theoretical studies that explore the relationship between stellar activity, stellar rotation, and magnetic dynamos.

Unified Astronomy Thesaurus concepts: Stellar activity (1580); Exoplanet astronomy (486); Stellar chromospheres (230)

Supporting material: machine-readable table

1. Introduction

The study of stellar chromospheres was championed in the late 1960 s by the Mt. Wilson *S*-value project (Vaughan et al. 1978; Duncan et al. 1991). With a dedicated telescope for daily observations, the Mt Wilson team began a series of observations that would last decades culminating in the study of stellar activity cycles and comparison to the solar activity cycle. The legacy of the Mt. Wilson HK project was expanded from the photomultiplier era to the era of charge coupled devices by additional studies of stellar activity cycles including those conducted by Henry et al. (1996; 815 stars), Wright et al. (2004; 1200 stars), Hall et al. (2007; 143 stars), Isaacson & Fischer (2010; 2630 stars), and more recently Gomes da Silva et al. (2021; 1674 stars). These surveys were often secondary to the primary science objectives (Hall et al. 2007; excepted) of searching for exoplanets and measuring their masses via high-resolution spectroscopy and precise radial velocities (RVs). For example, the importance of understanding stellar activity as a possible false-positive scenario for RV planet mass detection was a primary concern since the first exoplanet discovery (Mayor & Queloz 1995). In addition to the search for direct correlations between RVs and stellar activity cycles over the timescale of decades (Wright et al. 2008; Fulton et al. 2015), sophisticated analyses such as the FF′ method, Gaussian processes, and other signal processing algorithms can be employed on data spanning shorter timescales to disentangle the complex relationships that planets have on stars gravitationally from stellar activity due to surface inhomogeneities (Aigrain et al. 2012; Howard et al. 2013; Pepe et al. 2013). However, sophisticated signal processing techniques can sometimes overfit the data, and their results should be interpreted with caution (Blunt et al. 2023). When additional information beyond stellar spectra are available, such as space-based photometry from Kepler, K2, or the Transiting Exoplanet Survey Satellite (TESS; Kosiarek & Crossfield 2020), ever smaller planets can be characterized with RVs from instruments such as the High Resolution Echelle Spectrometer (HIRES; Akana Murphy et al. 2021) or refuted with instruments such as Habitable Planet Finder (Lubin et al. 2021). Analysis of stellar flares in photometric data, along with activity metrics from spectra such as Hα can be used to study planetary habitability. Su et al. (2022) used Hα measurements from LAMOST's low-resolution (1026 stars) and medium-resolution spectra (158 stars) plus light curves from Kepler, K2, and TESS host stars, and assessed both atmospheric burn off and recovery.

The impact of stellar activity observations has led to a greater understanding the relationship of stellar activity, rotation periods, and age. Noyes et al. (1984) laid the foundation for studying connection between activity, convection and rotation, showing that rotation periods correspond to certain levels of activity and both are related to the convective action in solar-type main-sequence stars. Remarkably, the study used only 40 stars, with what would now be considered primitive determinations for stellar temperature and mass that were based on $B - V$ colors, without parallaxes or high-resolution spectra. Identification of the Rossby number, the ratio of the stellar rotation period to the convective turnover time, was a critical piece of the rotation-activity-age puzzle. This early work, focusing primarily on solar-like, main-sequence stars, was summarized by Duncan et al. (1991) who provided the activity catalog for a large number of stars, and Baliunas et al. (1995) who focused on 111 Sun-like stars. To extend the age–activity relations beyond solar-type stars, Mamajek & Hillenbrand (2008) determined ages by analyzing young star clusters with ages between 200 Myr and 7 Gyr open clusters using both X-rays and chromospheric activity measurements. As stars age, the stellar wind, and more generally magnetic activity, transports angular momentum away from the star, resulting in decreasing rotation periods and lower activity levels. By adding star clusters with various well-known ages, Mamajek & Hillenbrand (2008) quantified the relationship between stellar spindown and stellar age for stars much younger than the Sun. With the use of Gaia proper motion, new young clusters have been identified, adding to the collection of age and activity analyses. Curtis et al. (2020) used open clusters with ages between 0.7 and 1.4 Gyr to identify a pause in the spindown relationships that is especially prominent for lower-mass stars. The change in spindown can be accounted for tuning core-envelope models, but other explanations remain possible.

The Kepler era of space-based photometric surveys led to the detection of over 4000 transiting planet candidates (Borucki et al. 2011a, 2011b; Batalha et al. 2013; Thompson et al. 2018). While the first exoplanet systems detected by Kepler were confirmed by ground-based follow-up observations (Borucki et al. 2010; Batalha et al. 2011), it was the large-scale survey of ∼200,000 stars by Kepler that led to the most important results.

The California-Kepler Survey (CKS), a magnitude-limited spectroscopic survey of 1189 Kepler host stars was undertaken with the focus on improving the uncertainty in stellar radius, and the associated planetary radii. Analysis of high-resolution stellar spectroscopy using local thermodynamic equilibrium (Valenti & Fischer 2005) is capable of determining fundamental stellar properties and can be combined with stellar evolution models to determine stellar mass and radius to a typical precision of 10% and as low as 2% (Johnson et al. 2017; Berger et al. 2020b). The uniform, and homogeneous data set of high-resolution spectra from the Keck I telescope and HIRES instrument (Petigura et al. 2017) has allowed for detection of the detailed structure in the radius distribution for planet sizes between 1 and 4 R_{Earth} (Fulton et al. 2017). The CKS data set has allowed for a series of papers including beyond the planet radius gap including detailed analysis of systems with multiple transiting planets Weiss et al. (2018), refinement on the minimum mass extra-solar nebular (Dai et al. 2020), and analysis showing that the Kepler field has similar metallicity to the solar neighborhood (Petigura et al. 2018).

The eventual addition of Gaia parallaxes further refined the stellar properties of the full Kepler sample, their planets' radii, and more broadly planet occurrence (Fulton & Petigura 2018; Hsu et al. 2019). With precise Gaia distances, the dominant source of error on the planet radius, now on average 5%, becomes the photometry (Petigura 2020), a major transition compared to the first transiting planets measured with Kepler data. Theoretical studies have suggested that the substructure in the planet radius distribution is due to photoevaporation that occurs in the first 100 Myr of planet formation (Lopez & Fortney 2013; Owen & Wu 2013; Chen & Rogers 2016). Observational studies calculating precise ages reveal that planet radius changes may continue beyond 1 Gyr when considering the entire Kepler planet sample (Berger et al. 2020a) and well-defined subsamples (David et al. 2022). The radius gap is also reported observationally by Van Eylen et al. (2018) in an analysis of planet hosts studied with asteroseismology.

The paper is laid out as follows. Section 2.1 describes how we derived S values from the HIRES spectra, and Section 2.2 describes our star and planet sample. Section 3.1 shows how the planet properties of CKS-Gaia relate to new stellar activity metrics. Section 3.2 explores how the rotation periods determined from Kepler photometry relate to activity metrics from this sample. Activity measurements are correlated with fundamental stellar properties in Section 3.3. In Section 3.4 we discuss ages derived from $\log(R'_{\mathrm{HK}})$ values and we touch on the least active stars in our sample and discuss implications in Section 3.5. Finally, Section 3.6 explores activity and our Kepler planet sample.

2. Methods

2.1. S-value Extraction and Calibration

We follow the method of Isaacson & Fischer (2010) to extract the flux values in the cores of the Ca II H and K lines and continuum regions redward and blueward of the H and K absorption features (Equation (1); Vaughan et al. 1978). While this extraction method has been used to analyze post-upgrade HIRES data dating back to 2005, we modified the existing algorithm to optimize the signal-to-noise ratio (S/N) of single-epoch spectra that range from 6 to 10 per reduced pixel. Isaacson & Fischer (2010) used an S/N cutoff of 5, but only 2% of spectra were below S/N of 10, so the extraction routine was not well tested for S/N = 5–10. Examples of the Ca II H and K line cores for stars with the highest, median, and lowest S-values in our sample are shown in Figure 1. This is distinct from the most and least active stars, which are measured by $\log(R'_{\mathrm{HK}})$. Note that low S/N makes the extraction of the fluxes more challenging in spectra with S/Ns of 5–10 in the continuum sections. In this work, we spline the National Solar Observatory (NSO) solar atlas onto the HIRES rest-frame wavelength solution, and use it as the template to align all other spectra. The Isaacson & Fischer (2010) spectral extraction method was optimized for measuring differential S-values of the same star using a high-S/N template, the current analysis utilizes the NSO template for all stars in this sample to ensure the absolute scale is as accurate as possible for the single epochs of the CKS-Gaia sample.

$$S_{\mathrm{HK}} = \frac{H + K}{R + V} \tag{1}$$

S-values are calculated by summing the flux in the cores of the Ca II H and K lines and dividing by the flux in two continuum sections redward and blueward of the line cores (Figure 2). The value of an isolated S-value is difficult to interpret across different spectral types because the intensity of the neighboring regions varies with stellar type, which means

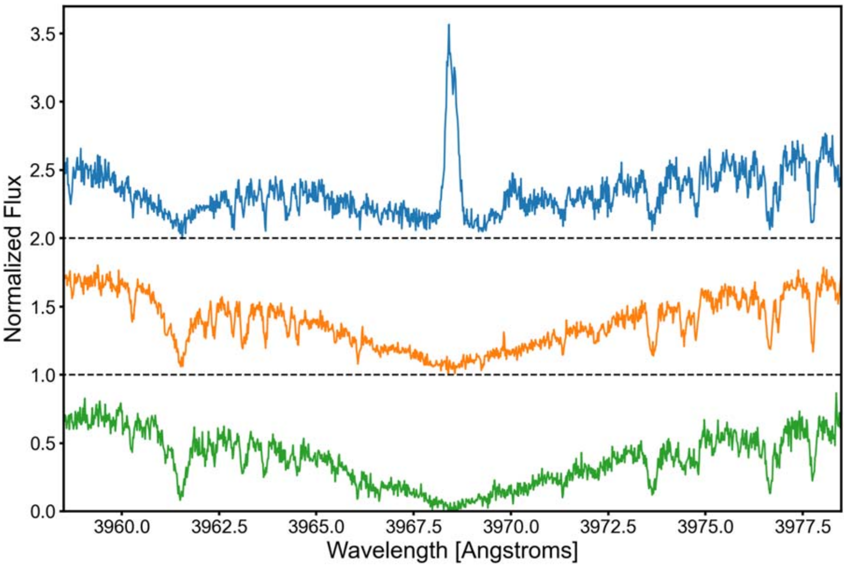

Figure 1. The Ca II H-line is shown for the stars with the highest, median, and lowest S-values from top to bottom. They are KOIs-3497, 700, and 629. The S/Ns of 5–10 per pixel in the continuum sections for these stellar spectra makes the spectral extraction challenging. For active stars, the reversal in the core of the Ca H-line is obvious and rises above the continuum. Small changes in the activity level of low-activity stars are challenging to detect due to the lower flux in the line cores.

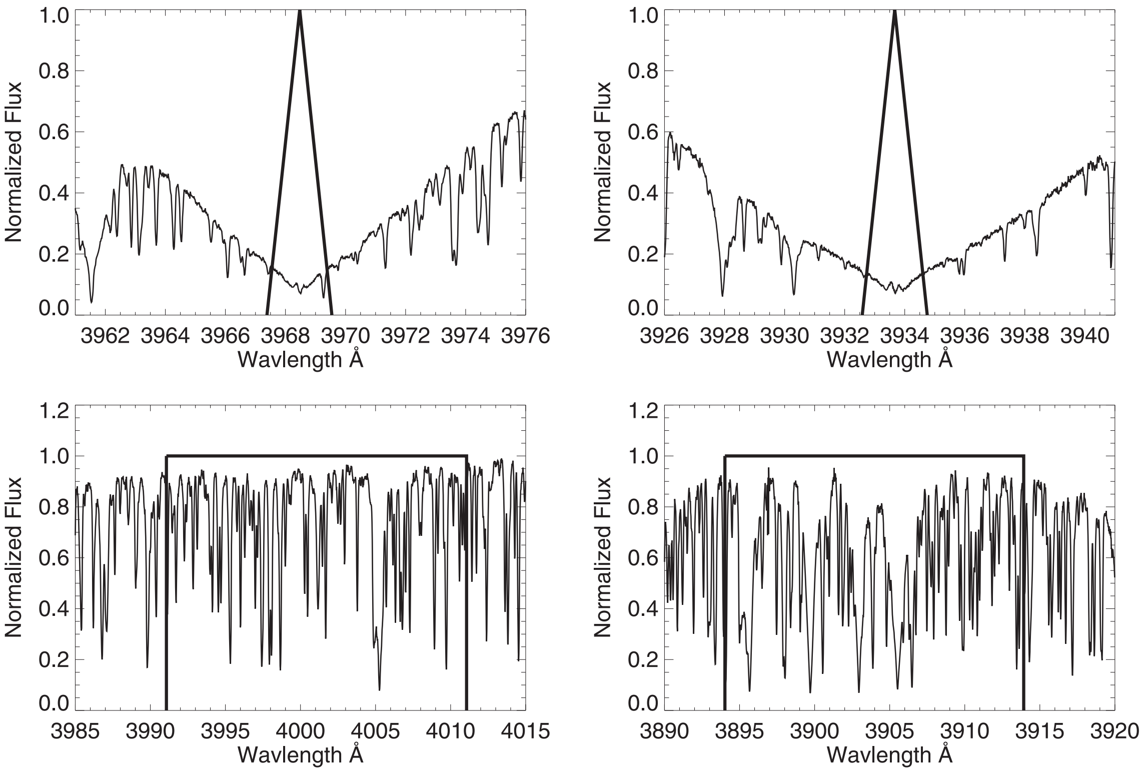

Figure 2. Clockwise from top left: the Ca II H and K lines, and the two continuum sections on either side of the H and K lines, dubbed V (centered at 4000 Å) and R (centered at 3905 Å) sections. The two 20 Å continuum sections are used to calibrate the variable flux in the 1 Å weighted sections in the line cores. Extracting the spectral segments in this way allows for calibration to the Mt. Wilson scale and comparison to other activity surveys.

the raw S-value index is sensitive to both chromospheric emission and overall SED. So we calculate $\log(R'_{\rm HK})$, a metric of chromospheric activity that is comparable across stars with different $T_{\rm eff}$. $\log(R'_{\rm HK})$ is defined as the base-10 logarithm of the chromospheric portion of the flux in the Ca II H and K line cores relative to the bolometric flux of the star (Noyes et al. 1984). We use the Ca II H and K line flux to measure the nonthermal heating that is related to magnetic activity in the star. By accurately accounting for and subtracting the photospheric contribution to the flux in the cores of the Ca II H and K line cores, we can compare activity across a range of effective temperatures.

With this new flux normalization and extraction method, we require a new calibration to the Mt. Wilson Scale to ensure we

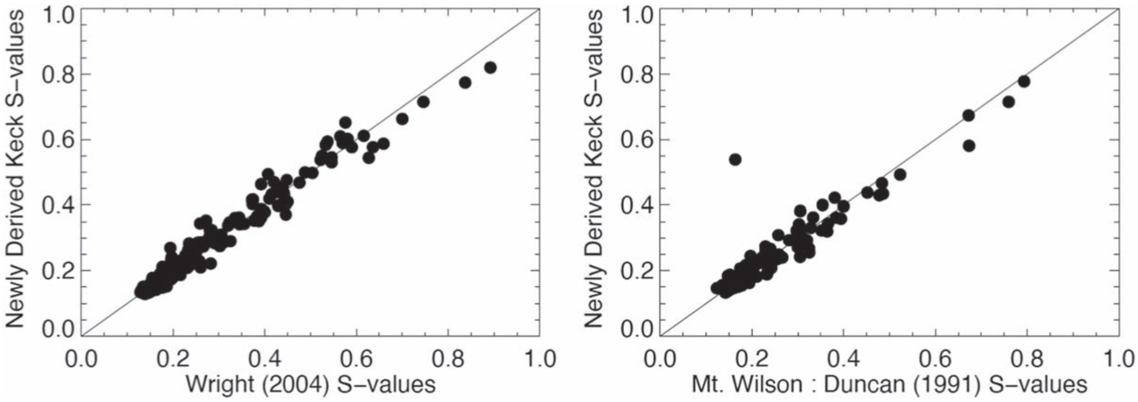

Figure 3. By selecting stars that have been observed with HIRES by CPS and by the Mt. Wilson survey, we can determine the coefficients needed to convert flux values to *S*-values. (Left) We assess our *S*-values for consistency by comparing our newly created values with those published in Wright et al. (2004), whose values were calculated from spectra collected on the previous HIRES detector, pre-2005. The *S*-values on the *y*-axis were created with the coefficients determined by fitting our newly extracted flux values to the Wright *S*-values. Four-hundred and forty-seven stars were used in this comparison. The standard deviation of the residuals 0.020. (Right) The Mt. Wilson values from Duncan et al. (1991) are plotted against our newly determined values for 154 overlapping stars. Scatter in the relation is due to observing stars at different points in their activity cycles as well as imperfect accounting of the blaze function. The star at [0.2, 0.6] is a known outlier, HD 137778, detailed in Wright et al. (2004). If we include HD 137778, the standard deviation of the residuals is 0.044. Removing the single outlier reduces the standard deviation to 0.024.

can compare our activity metrics on a standard scale. Using a procedure similar to Isaacson & Fischer (2010), we use four coefficients and perform a least-squares fit for two free parameters, C_1 and C_4 in Equation (2), with two of the coefficients, C_2 and C_3 determined by the ratios of the H to K line fluxes and R to V line fluxes. The final coefficients are shown in Equation (2) and were found using 154 stars that were observed on HIRES and Mt. Wilson. We restrict the calibration stars to $T_{\rm eff}$ between 4700 and 6500 K with $V\,\sin(i) < 10$ km s^{-1} and a log(g) greater than 4.0, matching the demographics of the majority of the CKS-Gaia sample.

$$S_{\rm HK} = C_1 * \frac{(H + C_2^* K)}{(R + C_3^* V)} + C_4 \tag{2}$$

$$S_{\rm HK} = 22.5 * \frac{(H + 1.01019 * K)}{(R + 1.26134 * V)} - 0.006 \tag{3}$$

The newly created HIRES *S*-values are plotted against the Duncan et al. (1991) *S*-values, showing a standard deviation of the residuals of 0.023 (Figure 3, right panel). This is comparable to the Isaacson & Fischer (2010) *S*-values, that showed a scatter of 11% when calibrated to the Mt. Wilson values. We attribute the larger scatter in the 2010 work to the broader range of stars in that sample, both in terms of activity and $T_{\rm eff}$, compared to this work. We verify our calibration by comparing our new *S*-values of 447 non-Kepler stars that also have *S*-values in the Wright et al. (2004) sample of planet search stars observed on HIRES prior from 1995–2004. The standard deviation of the residuals is 0.020 (Figure 3, left panel). We adopt 0.02 as the calibration uncertainty, similar to survey calibration uncertainty found by Mittag et al. (2013).

We verified continuity in the activity scale from the Isaacson & Fischer (2010) method to the new NSO method described in the paper by plotting both sets of *S*-values for two stellar activity standards, Tau Ceti and HD 60532 (Figure 4). Gomes da Silva et al. (2021) noted that the chromospheric standard star Tau Ceti varies by 0.83% or a dispersion of 0.0015, and recommended using HD 60532 as well, with a scatter of only 0.36%, and absolute dispersion of 0.0005. This tiny variation over time makes HD 60532 an excellent standard star for checking single instrument Ca II H and K*S*-value precision.

There is a small offset between the values from the Isaacson & Fischer (2010) method and our new HIRES-NSO method that is visible for both standard stars. With the HIRES-NSO method, Tau Ceti shows a median *S*-value of 0.1720 with a standard deviation of 0.0023. The HIRES-NSO derived *S*-values for HD 60532 show a median value 0.1197 with a dispersion of 0.0031. For Tau Ceti, the Isaacson & Fischer (2010) method yields a median of 0.1670, with a standard deviation of 0.0016. For HD 60532 the median is 0.1231 with a standard deviation of 0.0029. The new *S*-values for Tau Ceti and HD 60532 are offset by +0.005 and −0.004, respectively. The offsets are due to scatter in the calibration and the amplitude of the offset is similar to the amplitude of the scatter. Our uncertainties are consistent with previous works. For example, Tau Ceti shows very little long-term variation but calibration uncertainties result in published values of 0.168 from Wright et al. (2004) and 0.175 from Duncan et al. (1991). The performance of these standard stars gives us confidence in our extraction method and quantifies the error in our calibration.

Our distribution of *S*-values extends to lower values than previous surveys, with a tale toward very low activity that reaches $\log(R'_{\rm HK}) = -6.0$ (Figure 5). We choose a value of $\log(R'_{\rm HK}) = -5.50$ as the lowest value that should be considered reliable. In Section 3.5 we discuss very inactive stars, and WASP-12 is an example of a star with the exceptionally low value of $\log(R'_{\rm HK})$ of −5.50. The low value is thought to be due to absorption beyond the chromosphere of the star (Fossati et al. 2013). Stars in our sample with $\log(R'_{\rm HK})$ values below −5.50 should be considered very inactive, but these values likely underestimate their activity.

For the CKS-HK sample, most stars have a single observation, limiting our knowledge of the long-term behavior of these stars. For stars with two observations, we choose the one with higher S/N. For stars observed more than twice, such as those with multiple epochs for RV follow-up, we choose the median *S*-value. Time-series *S*-values for these stars are available in Weiss et al. (submitted). The coolest stars in our

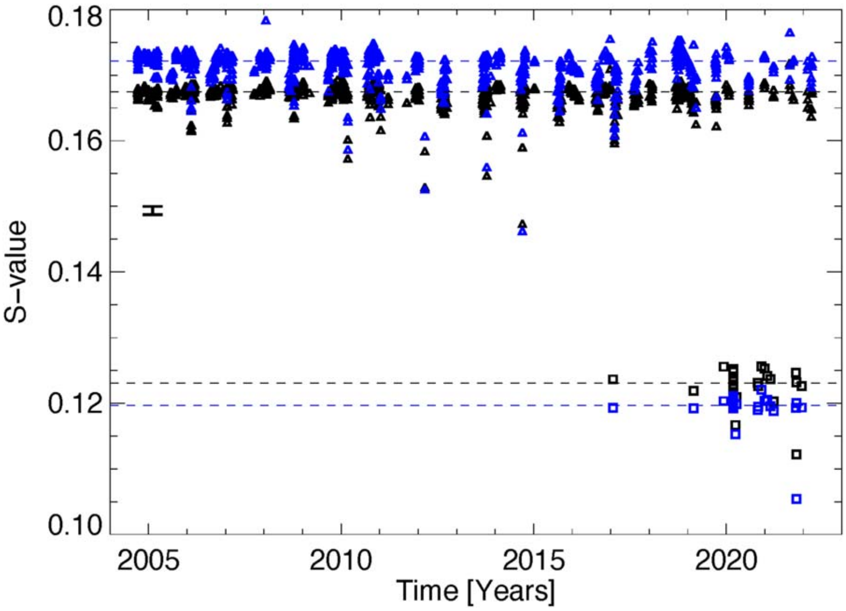

Figure 4. For the standard stars Tau Ceti (top set, triangles) and HD 60532 (bottom set, squares), S-values are calculated using the Isaacson & Fischer (2010) routine (black) and from the new HIRES-NSO routine (blue). The average values of 0.1670 ($\log(R'_{\rm HK}) = -4.980$) and 0.172 ($\log(R'_{\rm HK}) = -4.954$), respectively, are plotted as dashed lines. The offset of 0.005 or 3% is due to different methods for addressing the blaze function as well as calibration errors. (The Mt. Wilson average value for Mt. Wilson is 0.175, compared to our HIRES-NSO median value of 0.172.) The standard deviations of the Isaacson & Fischer (2010) values and the newly derived values for Tau Ceti are 0.0016 and 0.0024. For HD 60532, they are 0.0029 and 0.0031. The single-epoch uncertainty of 0.03 is depicted at [2005, 0.015]. We use 942 observations of Tau Ceti. A representative error bar 1% as determined by the scatter of Tau Ceti and HD 60532, two S-value standards, is shown at [2005, 0.15].

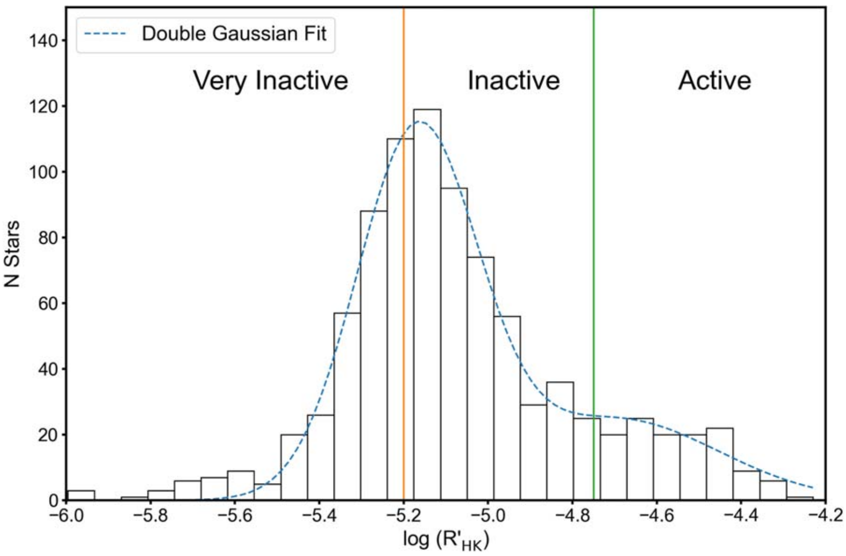

Figure 5. Double-Gaussian fit for the full CKS stellar sample of 893 stars.

sample have spectra that differ most significantly from the Sun, and we find that the S-values for these stars still meet our quality standards. Another limitation of using a single epoch in time to measure stellar activity is that we measure the activity at an unknown phase of the rotation period and activity cycle. This challenges our search for stars that are exceptionally inactive, in Maunder minimum or magnetic minima states (Section 3.5). We rely on the statistical power, rather than time series, of our sample for the analysis of fundamental stellar properties, activity, and rotation periods. Without time-series spectra to monitor long-term activity cycles, we are unable to make comparisons of years long cycles with rotation periods such as Brandenburg et al. (2017) and Metcalfe et al. (2016). Instead, our analysis is similar to Zhang et al. (2020), which also utilizes single-epoch spectroscopy to assess activity for 59,816 stars. Our smaller sample has a $T_{\rm eff}$ uncertainty of 60 versus 100 K for the Large Sky Area Multi-Object Fiber Spectroscopic Telescope (LAMOST) sample (Petigura et al. 2017), and we focus our attention on the rotation periods from David et al. (2021).

2.2. The CKS-HK Sample

The CKS sample has several components including a magnitude-limited sample, with a cutoff at a Kepler magnitude of 14.2, and a collection of fainter stellar host stars that includes habitable zone planets (Borucki et al. 2013), multiplanet systems (Lissauer et al. 2014; Rowe et al. 2014), and ultra-short-period planets (Sanchis-Ojeda et al. 2014). The habitable zone planets and the multis fainter than 14.2 tend to have lower S/Ns and are often omitted from our sample for having insufficient data quality in the bluer wavelengths where the Ca II H and K lines reside. To define the CKS-Gaia sample, Fulton & Petigura (2018) make a similar magnitude restriction because the primary sample selection for stars fainter than $V{\sim}14.2$ was nonuniform. We choose to begin with the sample of 1189 planet stars hosting 1896 total planets from Fulton & Petigura (2018) and make additional quality cuts for our analysis. We did not include the stars from the recent CKS-Cool project (Petigura et al. 2022) because the target S/N is too low at 4000 Å to precisely measure the Ca II H and K line fluxes.

In order to ensure sufficient quality of the S-value activity metric, we made restrictions on the S/N near the Ca II H and K lines and on the local seeing conditions for each observation. The CKS-Gaia S/N for HIRES spectra was chosen to be ~40 per pixel at 5000 Å. This choice impacts the S-values resulting for cooler stars that have lower S/N in the Ca II H and K region compared to hotter stars due to inherent differences in their blackbody spectra. Beginning with the CKS-Gaia results (Table 1 from Fulton & Petigura 2018), which has 1189 planet host stars, we remove 180 observations that have $S/N < 5$ pixel^{-1} in the continuum regions near the Ca II H and K lines. In most cases, we use the same spectra as the CKS-Gaia project; however, there were 25 stars with higher-S/N spectra, collected more recently, that were available. From the 2D echellogram, we measured the seeing value for each observation and removed observations with seeing greater than 1$''$.6, ensuring high-quality measurements (Baum et al. 2022). The HIRES spectrometer, a slit-fed spectrograph that uses an echelle grating as the cross-dispersing optic, results in a 2D echelle format in which the orders become closer together toward bluer wavelengths. (Spectrographs with cross-dispersing prisms have orders that are closer together in the red). Since we use the C2 decker (0$''$.87 × 14$''$.0) for observations of faint stars in order to remove background sky flux (Batalha et al. 2011), when a faint star ($V > 11$) is observed in poor seeing conditions, the bluest orders overlap, causing cross order contamination and a poor-quality S-value measurement. Removing 109 observations with poor seeing values and three stars that have no stellar mass or radius leaves 900 planet host stars with well-characterized stellar properties and S-values. Three stars have no log(g) value. Fourteen stars have an S-value lower than 0.10, chosen as a minimum value for calculating $\log(R'_{\rm HK})$, leaving 879 host stars. We define this as our CKS-HK stellar sample.

Binary star systems can challenge studies of stellar activity due to tidal interaction or spectral contamination, or with spectral contamination. To mitigate binary star contamination, stars with a detected secondary spectrum, with flux ratios as low as 1% of the primary, using the technique of Kolbl et al. (2015) were identified by Fulton et al. (2015) as planet false positives and are excluded as such.

The CKS-HK catalog of chromospheric activity is quite different compared to RV surveys of planet search stars. While most RV surveys focus on either M-dwarfs or FGK stars providing large catalogs of high-resolution spectra, the stars in these surveys typically have an unknown number of short-period planets with planet radii from 1–4 Earth-radii (Rosenthal et al. 2021). In comparison, every star in our sample has one or more known transiting planets, and the distance to the average Kepler field star is about a kiloparsec rather than a 1–200 pc for typical RV survey stars.

2.2.1. The CKS-HK Planet Sample

In addition to the quality metrics applied to the CKS-HK stellar sample, for analysis involving planet properties, we make further qualifications. The CKS-HK planet sample will be defined by the quality cuts that are described in Section 2.1 and further quality cuts that depend on the planet properties in these systems. Much of the analysis focuses on planets smaller than 4.0 $R_{\rm Earth}$. We define this as our CKS-HK planet sample.

2.3. Literature Data

2.3.1. Kepler Stellar Rotation Curves

The field of stellar rotation period analysis has richly benefited from the Kepler 30 minute cadence with near continuous data collection for 90 days of a typical Kepler quarter, up to 4 yr over the life of the mission. While ground-based photometric surveys had been critical in building our understanding of stellar rotation periods (Duncan et al. 1991; Henry et al. 1996), Kepler has grown the number of available stellar rotation periods into the tens of thousands (McQuillan et al. 2014).

Novel techniques applied to light curves can quickly analyze vast amounts of photometry. The auto-correlation function (ACF; McQuillan et al. 2014) was used to create a catalog of rotation periods for 30,000 stars ranging from 0.2–70 days across stellar masses from 0.1–1.3 $M_\odot$. Angus et al. (2018) used a machine-learning technique, trained on that catalog, to determine rotation periods for Kepler objects of interest (KOIs), which we use in Section 3.2. Santos et al. (2021) used a combination of wavelet analysis, ACFs, and machine learning to further study the rotation periods of Kepler stars.

Recently, David et al. (2022) examined Kepler rotation periods from Walkowicz & Basri (2013), McQuillan et al. (2014), Mazeh et al. (2015), and Angus et al. (2018) resulting in the identification of the "Rossby Ridge," a relationship between the $T_{\rm eff}$ and stellar rotation period. The Rossby Ridge results support the stellar spindown theory of weakened magnetic braking (WMB) as formulated in van Saders et al. (2016), which is a deviation from the spindown relationships that govern young stars until the ages of a few gigayears. We build upon vetted rotations periods of the CKS-Gaia sample from David et al. (2021), adding the chromospheric activity measurements from the Ca II H and K lines to explore $\log(R'_{\rm HK})$ and its relation to stellar rotation periods and stellar spin down in the Rossby Ridge in Section 3.2.

2.3.2. The CKS-HK Stellar Rotation Sample

The CKS-HK rotation sample begins with the CKS-HK stellar sample, and is refined based on the quality of the determination of the photometric rotation periods from Kepler. We use this sample to examine activity-rotation relations and stellar effective temperature, metallicity, and stellar surface gravity. The stellar rotation analysis will require dividing the sample by stellar type, evolution, and [Fe/H]. In order to utilize the most well-determined stellar rotation periods, we keep only the reliable stellar rotation periods from Kepler photometry compiled and vetted by David et al. (2021) to define the CKS-Gaia sample of rotation periods. The quality of rotation periods are labeled 0, 1, 2, and 3 as having no periodicity, an ambiguous period, a reliable period and a highly reliable period, respectively. We take the CKS-HK stellar sample of 879 stars, with valid chromospheric activity measurements and the vetted rotation periods, to finalize our CKS-HK rotation period sample with 168, 325, 216, and 184 stars and reliability ranks of 0, 1, 2, and 3, respectively.

3. Results and Discussion

We begin our analysis by examining the relationships between our new $\log(R'_{\rm HK})$ measurements of the chromospheric activity and the fundamental stellar properties from CKS-Gaia.

3.1. $T_{\rm eff}$, log(g), [Fe/H], and $\log(R'_{\rm HK})$

We examine the full distribution of $\log(R'_{\rm HK})$ for our stellar sample, and model it with a two-Gaussian fit (Figure 5). As a function of the stellar properties $T_{\rm eff}$, [Fe/H], and $R_\star$ in Figure 6. To allow for quantitative comparisons between surveys (such as Santos et al. 2021), we model three subsets of our sample as both single- and double-Gaussian distributions. The top panel of Figure 6 shows the distribution of $\log(R'_{\rm HK})$ divided at $T_{\rm eff}$ values of 6000 and 5400 K, with the hotter F-stars on the left and cooler K-dwarfs on the right. In the middle panel, we divide stars into bins of metallicity at +0.1 and −0.1 dex, with the most metal-rich stars of the left and solar metallicity stars in the middle. The $\log(R'_{\rm HK})$ distribution as a function of stellar radii is divided at 0.9 and 1.1 $R_\odot$ with solar radius-like stars in the bottom-middle panel. Gaussian fitting results for the full sample, and the subdivided sample are compiled in Table 1.

Sun-like stars are a common focus in activity analyses, and our study focuses on stars between 4800 and 6250 K. Stars with temperatures above the Kraft Break at $T_{\rm eff}$ of 6250 K have thinning convective zones, dividing fully radiative and partially convective stars (Kraft 1967). Fully radiative stars are magnetically different than those below the Kraft Break because they lack a tachocline that is thought to be the critical to the production of magnetic activity. The study of rotation and convection near the Kraft Break is an active field of study (Metcalfe & Egeland 2019) and is relevant in our rotation period analysis. The histogram of $\log(R'_{\rm HK})$ colorized via stellar radius (Figures 5, bottom right) complements the $\log(g)$ histogram (upper right) showing a more intuitive value than stellar surface gravity. Generally, the stars with the largest radii in our sample are evolved and are also the least active. We will discuss the relationship between [Fe/H] and stellar rotation periods in Section 3.3.2.

We examine the CKS-HK stellar sample broadly in Figure 7 by plotting the CKS-HK stellar properties sample as a function $\log(R'_{\rm HK})$. In the temperature plot, we see the most active stars are cooler than the Sun, and all of the inactive stars have super-solar temperature. The relationships between stellar surface gravity and stellar radius relations to $\log(R'_{\rm HK})$ reveal the most active stars in our sample are on the main sequence and near to 1.0 $R_\star$, consistent with Figure 8. Viewing the sample in $T_{\rm eff}$ versus $\log(g)$ space, the subgiant population rises above the main sequence as $\log(g)$ decreases (Figure 8). While the division between subgiant and main-sequence stars is ill-defined, we will use various cutoffs for $\log(g)$ in the next few Sections, including $\log(g) = 4.0$. The color scaling shows that most stars are in the "inactive" or "very inactive" categories. The most active stars exist along the lower envelope, with the highest $\log(g)$ values, as expected for stars that lie nearest to the zero-age main sequence. For the rotation period analysis in Section 3.2 and the study of the least active stars (Section 3.5), we will focus on main-sequence stars rather than subgiants.

When testing for a correlation between chromospheric activity and metallicity, we might expect to see metal-rich stars, which tend to be younger than metal-poor stars, and are also more active. This property is visible in the bottom-left panel of Figure 7, which shows a fairly smooth distribution around the average $\log(R'_{\rm HK})$ and [Fe/H], with a slight overabundance of active stars that are metal-rich.

The least active stars are examined in detail in Section 3.5, and we search for candidates for stars that are in Maunder minimum or magnetic minimum (MM) type states (Eddy 1976; Saar 2011). Metallicity is also thought to be a factor in the study of stellar rotation periods, as the metal content of the star can affect the depth of the convective zone, and therefore the convective turnover time and rotation period (see Section 3.3.2).

3.2. Activity and Stellar Rotation Period

Decades-long observations of chromspheric activity measurements have identified relationships between chromospheric activity and stellar rotation, especially for solar-like stars. Noyes et al. (1984) formalized conclusions into equations that can be used to predict the rotation period based upon the average chromospheric activity of a star. By focusing on main-sequence Sun-like stars, the Mt. Wilson studies were able to isolate variables such as stellar $\log(g)$, $T_{\rm eff}$ (using $B - V$ as a proxy), and to an unknown extent, [Fe/H]. Wright (2004) speculated that spectral synthesis and precise stellar abundances (Valenti & Fischer 2005) would assist in finding very inactive stars. Stellar activity in the least active stars revealed that changes in $\log(g)$ due to stellar evolution is an important variable when identifying very inactive stars. Saar (2011) showed that stellar metallicity has an impact on both the minimum activity of a star and on the stellar rotation period. Additional metal content in a star changes the opacity and is perhaps more important when the convective zone is thin, such as in stars near the Kraft Break. Amard & Matt (2020) used theoretical models with stellar masses of 0.8, 1.0, and 1.3 $M_\odot$ and [Fe/H] between −0.5, and +0.5 and show that, metallicity is indeed an important variable to consider when calculating rotation period. They confirm that the impact is more significant near the Kraft Break, where small changes in metallicity affect the convective turnover time and have a larger impact due to the thinner convective zone.

In an observational test of those theoretical models, Avallone et al. (2022) used Kepler rotation periods, APOGEE data, and Gaia parallaxes to analyze rotation periods for stars mostly hotter than 6250 K, the Kraft Break. They found no rotation dependence on metallicity but noted the difference in $T_{\rm eff}$ for the two samples. The CKS-HK sample is well populated between 0.7 and 1.3 $M_\odot$, and we analyze the metallicity in the range 0 + 0.2 to −0.2 as well as, $T_{\rm eff}$, $R_\star$, and Kepler rotation periods in Section 3.3.2. The metallicity dependence is explored along with other fundamental stellar parameters, and we consider the activity derived rotation periods in the same context.

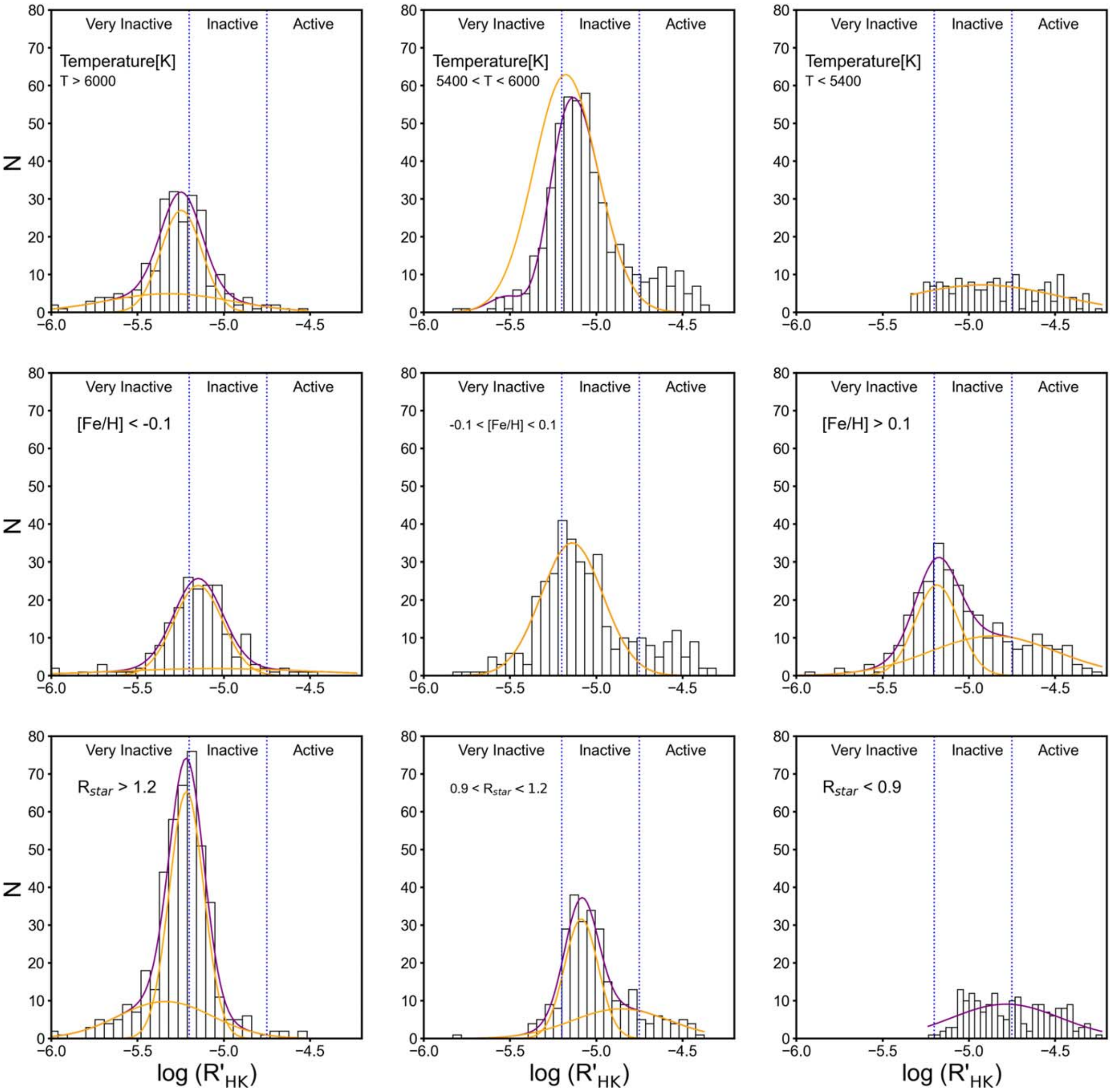

Figure 6. For each stellar property and property bin, the data are show in the histogram, and the two-model Gaussian fit is show in purple, with component Gaussians in yellow. A single-component Gaussian fit was preferred for the coolest bin of $T_{\rm eff}$, the middle bin of [Fe/H], and the bin of smallest $R_\star$. Top row: $T_{\rm eff}$ separates the three panels from left to right with break points at 6000 and 5400 K. Middle row: [Fe/H] separated from highest to lowest with break points at −0.1 and +0.1. Bottom row: $R_\star$ is plotted from the largest bin to the smallest with break points at 0.9 and 1.2 $R_\odot$. The values of the fitted Gaussians are shown in Table 1.

3.2.1. Rotation Periods for the CKS-HK Sample

Beginning with the CKS-HK rotation sample defined in Section 2.3.2, we compare how the Noyes et al. (1984) rotation-activity relations used to calculate a stellar rotation period from $\log(R'_{\rm HK})$ to stellar rotation periods recovered from Kepler photometry (David et al. 2021). We explore both methods of determining rotation periods and how they relate to the precise stellar properties from CKS-Gaia. Compared to the CKS techniques used to determine stellar properties to those used in Noyes et al. (1984), we have much more powerful tools in the form of high-resolution spectroscopy, to determine stellar surface gravity and metallicity. We also have a broader range of stellar temperatures, which will expose the bias of solar-like stars when using the rotation periods derived from activity.

To visually confirm the relationship between activity and rotation, we plot $\log(R'_{\rm HK})$ versus the Kepler rotation period in Figure 9. As a function of $\log(R'_{\rm HK})$, we plot 215 stars with grade 2, "reliable," stellar rotation periods from David et al. (2021) in the left panel and 185, grade 3, "highly reliable" rotation periods in the right panel. The color scale shows stellar effective temperature from 4800−6400 K, the full range of the CKS-HK sample. If a strong correlation between rotation

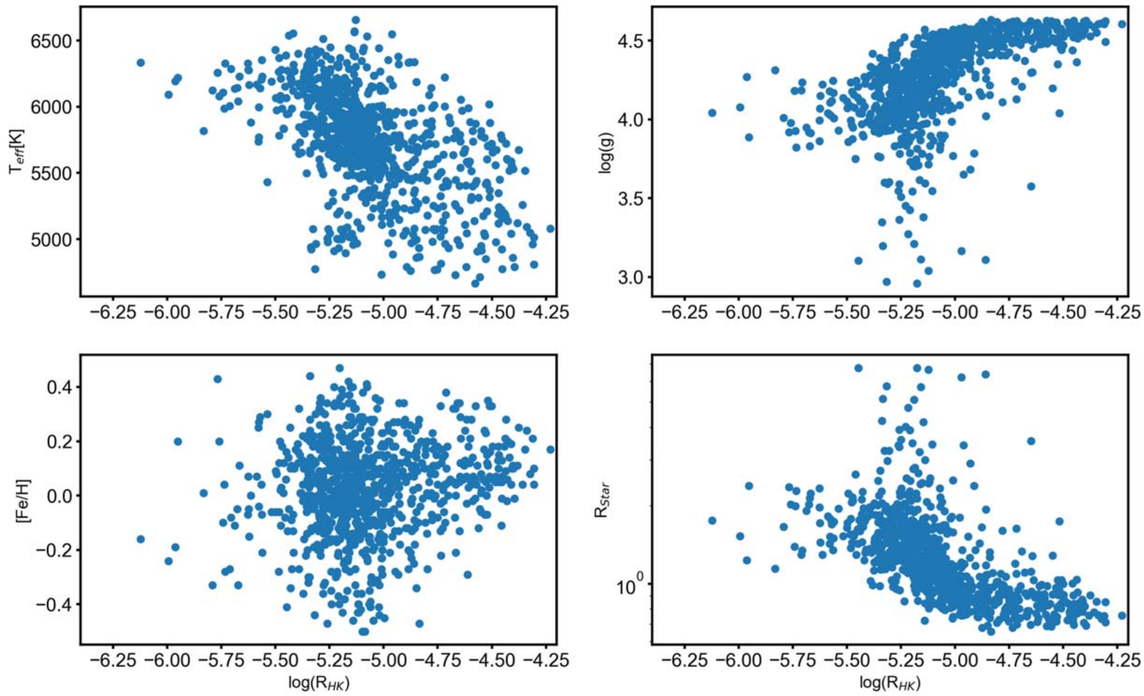

Figure 7. $\log(R'_{\mathrm{HK}})$ is plotted on the *x*-axis for all plots (more active stars are to the right), and fundamental stellar parameters are plotted on the *y*-axis. Top left: $\log(R'_{\mathrm{HK}})$ vs. T_{eff} shows that more active stars tend to be cooler. Top right: $\log(R'_{\mathrm{HK}})$ vs. $\log(g)$ reveals that subgiants are sparse and are inactive ($\log(R'_{\mathrm{HK}}) < -5.1$), which are lower on the plot. Most main-sequence stars have a range of activities. Bottom left: $\log(R'_{\mathrm{HK}})$ vs. [Fe/H] shows a balanced distribution with more active stars being more metal-rich. This is consistent with those stars being younger. Bottom right: $\log(R'_{\mathrm{HK}})$ vs. $R_\star$. This plot shows that as activity increases to the right, most stellar radii are near 1.0 $R_\odot$

Table 1
Gaussian Fit Parameters

Property Bin	Amplitude	Mean	Sigma	Amplitude	Mean	Sigma	Chi-squared	Reduced Chi-Squared
Full Sample (893)	111.5	−5.167	0.143	24.73	−4.691	0.242	500.19	20.84
$T_{\mathrm{eff}} > 6000$	30.75	−5.25	0.14	...	...	...	309.30	11.46
$5400 < T_{\mathrm{eff}} < 6000$	56.89	−5.12	0.14	...	...	...	825.83	30.59
$T_{\mathrm{eff}} < 5400$	7.26	−4.92	0.44	...	...	...	180.21	6.67
[Fe/H]< -0.1	25.18	−5.15	0.16	...	...	...	119.22	4.42
$-0.1 <$ [Fe/H]< 0.1	35.03	−5.14	0.18	...	...	...	796.18	29.49
[Fe/H]> 0.1	26.83	−5.13	0.22	...	...	...	507.50	18.80
$R_\star > 1.2$	72.28	−5.22	0.11	...	...	...	494.04	18.30
$0.9 < R_\star < 1.2$	35.02	−5.07	−0.13	...	...	...	436.10	16.15
$R_\star < 0.9$	9.08	−4.78	0.31	...	...	...	267.61	9.91
$T_{\mathrm{eff}} > 6000$	27.00	−5.25	0.12	4.94	−5.32	−0.37	248.36	10.35
$5400 < T_{\mathrm{eff}} < 6000$	62.91	−5.18	−0.18	−28.45	−5.34	0.11	697.72	29.07
$T_{\mathrm{eff}} < 5400$	7.26	−4.92	0.44	1.00	−5.70	0.03	180.21	7.51
[Fe/H]< -0.1	23.87	−5.15	−0.14	1.87	−5.06	−0.58	102.02	4.25
-0.1 < [Fe/H]< 0.1	14.38	−7.06	0.05	35.03	−5.14	−0.18	796.18	33.17
[Fe/H]> 0.1	10.48	−4.86	0.37	24.01	−5.18	0.13	92.77	3.87
$R_\star > 1.2$	65.36	−5.22	0.10	9.78	−5.34	0.27	294.67	12.28
$0.9 < R_\star < 1.2$	7.84	−4.86	0.28	31.62	−5.09	0.10	198.27	8.26
$R_\star < 0.9$	...	...	...	...	...	...	...	...

period and chromospheric activity is present, we expect stars with similar stellar temperature to have a smooth function with rotation period. Instead, in the left panel, we see a large amount of scatter at every temperature where stars are less active. By analyzing only stars that rank as (David et al. 2021) highly reliable from the CKS-HK rotation sample, the temperature, rotation, and activity relation are clarified (Figure 9, right panel). A correlation between stellar surface temperature, $\log(R'_{\mathrm{HK}})$ and rotation period is now visible. Metcalfe et al. (2016) showed a similar relationship (their Figure 1), noting the different slopes for different spectral types and lack of long rotation period stars for solar-type stars. We do not yet filter on stellar properties by removing subgiants, but few subgiants have definitive rotation periods because they have fewer surface inhomogeneities. By focusing solely on the most well-determined rotation periods, and validated $\log(R'_{\mathrm{HK}})$ values, we

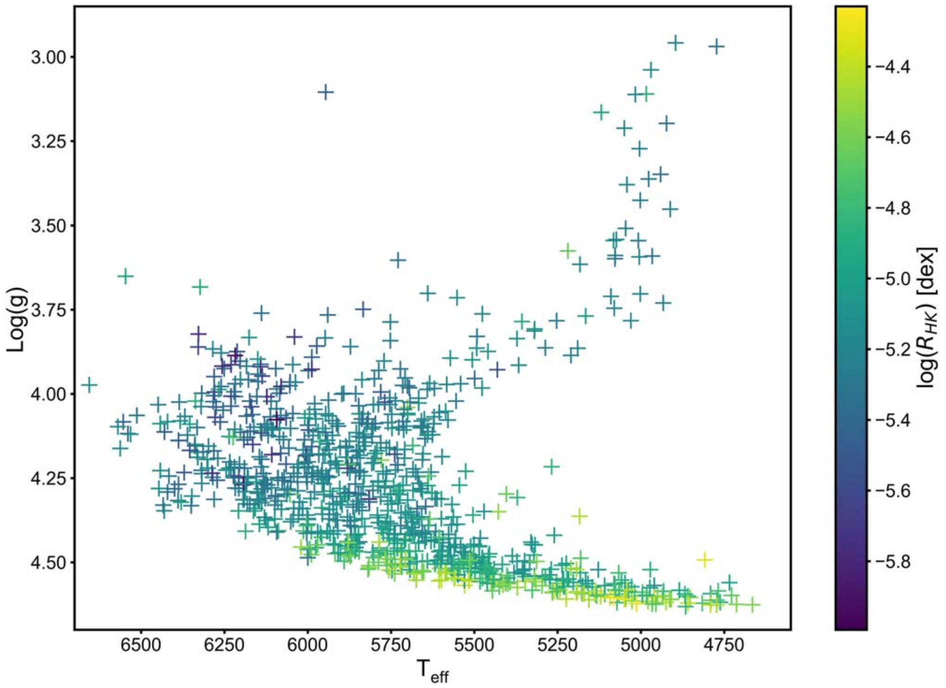

Figure 8. Stellar surface gravity is plotted as a function of stellar effective surface temperature for the CKS-HK stellar sample of 879 stars. The color bar indicates $\log(R'_{\rm HK})$ with yellow as more active and purple as less active. The giant branch moves from the center to the upper right of the plot. The most active stars (yellow) are cool dwarfs that make up the lower envelope of the main sequence. From CKS-Gaia (Fulton & Petigura 2018), the typical errors on $T_{\rm eff}$ and $\log(g)$ are 60 K and 0.01 dex, respectively. We use the calibration error of 0.02 as the uncertainty on $\log(R'_{\rm HK})$.

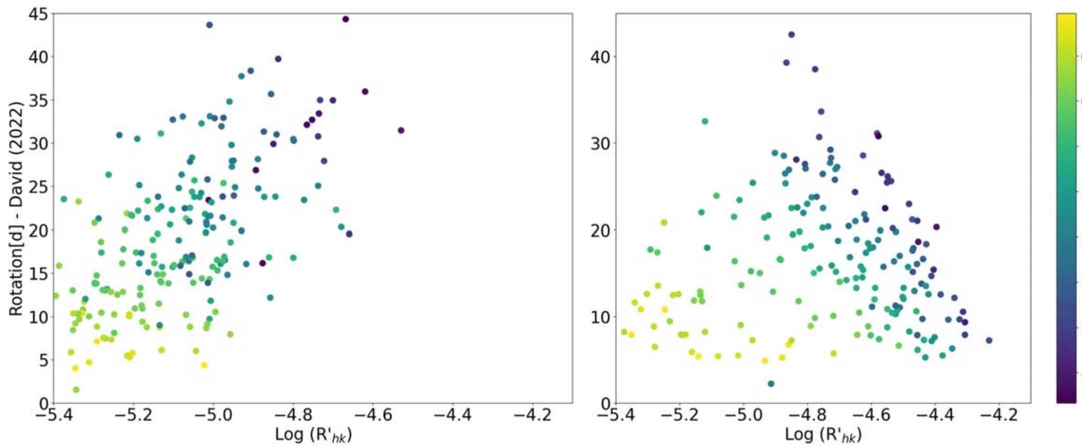

Figure 9. Left panel: Kepler rotation periods are plotted as a function of $\log(R'_{\rm HK})$ and all rotation periods from David et al. (2021) are included. Right: only grade 3 rotation periods from David et al. (2021) are plotted. In the left and right panel, 215 and 184 stars from the CKS-HK rotation sample are plotted, respectively. Recovering stellar rotation periods with single-epoch Ca II H and K measurements is challenging because $\log(R'_{\rm HK})$ values for a given star naturally vary. Our Sun's 11 yr stellar activity cycle, which changes the average $\log(R'_{\rm HK})$ value preserves the 27 day rotation period. The colors denote stellar surface temperature with cooler stars having darker shades. We expect rotation period to be related to activity within a given temperature bin.

can make further definitive statements about rotation periods and the stellar properties provided by the HIRES spectra in the CKS-HK rotation sample, which we do in Section 3.3.

3.2.2. Photometric versus Activity Derived Rotation Periods

Recovering stellar rotation periods with single-epoch Ca II H and K measurements is challenging because $\log(R'_{\rm HK})$ values for a given star naturally vary, similar to our Sun's 11 yr stellar activity cycle, changing the average $\log(R'_{\rm HK})$ value while preserving the 27 day rotation period. Noyes et al. (1984) used a few tens of stars to create relations between Rossby number, convective turnover time, and rotation period, but relied on average S-values of stars that had been collected over decades, which effectively averaged out the stellar activity cycles $\log(R'_{\rm HK})$ values. The long-term nature of that data set makes it very valuable for analyzing stellar activity cycles as producing accurate long-term averages. We will utilize a larger number of stars with single epochs of activity measurements, and rely upon the larger number offset the lack of time series when we calculate rotation periods using the Mamajek & Hillenbrand (2008) activity-period relations, which are very similar to Noyes et al. (1984), and compare them with photometric rotation periods from Kepler.

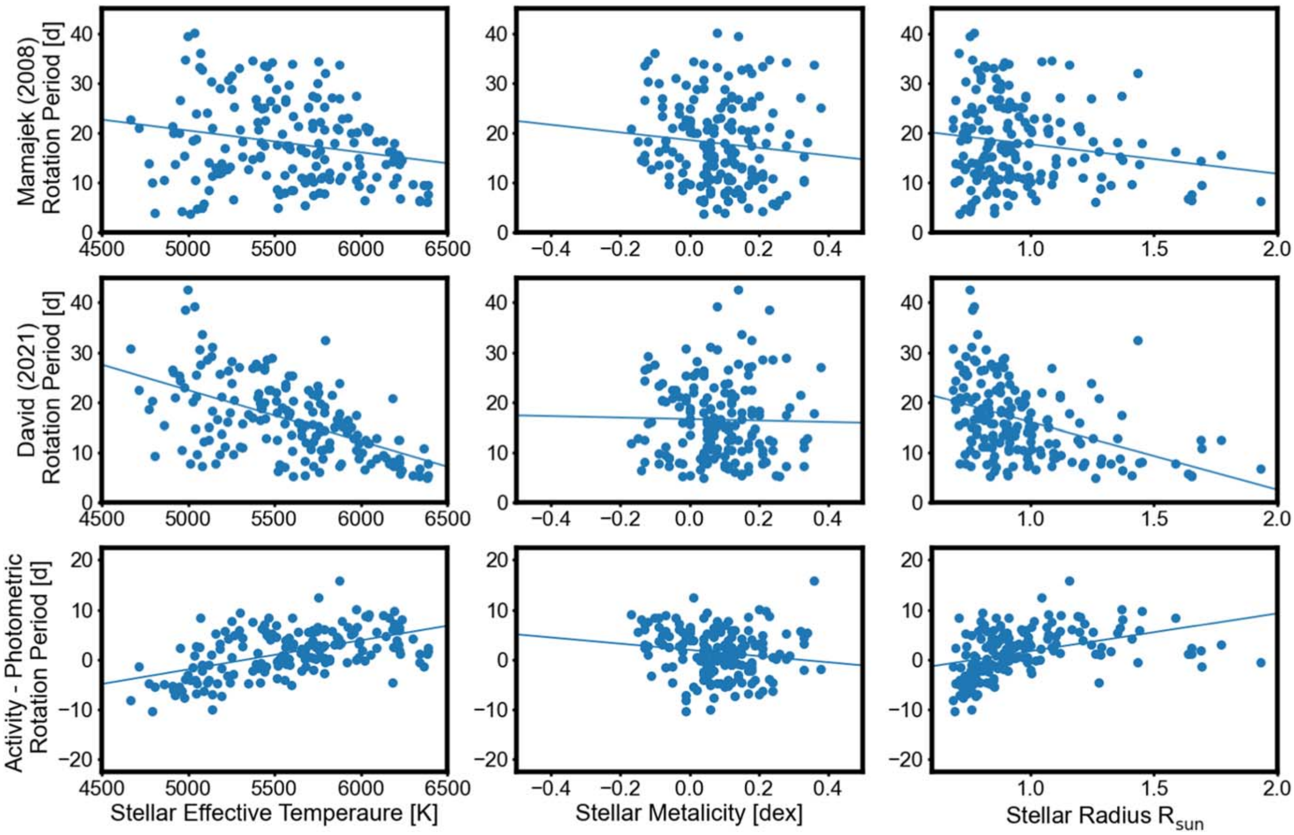

Figure 10. The top row shows the Mamajek & Hillenbrand (2008) rotation periods, derived from *S*-values as a function of $T_{\rm eff}$, [Fe/H] and stellar radius from left to right. Each vertical column is the same in all rows. The second column shows the David et al. (2021) rotation periods with very-reliable grade. The bottom row shows the difference between activity derived rotation periods and the photometric rotation periods as a function of each stellar property for of each plot for 173 stars from the CKS-HK rotation sample with log(g)> 4.0 and grade 3 rotation periods. The rotation period uncertainties are 10%.

3.3. Rotation Period and Fundamental Stellar Properties

3.3.1. Overview

To explain inconsistencies between stellar spindown models and observations of rotation periods for stars older than 1 Gyr, van Saders et al. (2016) developed theoretical relations that better describe spin down than empirical relations (Skumanich 1972). van Saders et al. (2016) showed that asteroseismically determined rotation periods (Hall et al. 2021) align with their theory of WMB and can reliably predict stellar rotation periods for stars older than 1 Gyr.

The Van Sanders conclusions are reinforced by the work of Metcalfe & Egeland (2019), who provide additional observational evidence that there exists a transition phase for stellar spindown that occurs in middle ages stars that leads to a breakdown of the previous spin−age relation for stars older than 1 Gyr. They show that the consistency between gyrochronology ages and ages determined with chromospheric activity break down near a value of log($R'_{\rm HK}$) of −4.95. In analyzing the rotation periods and $T_{\rm eff}$, David et al. (2022) used Kepler derived rotation periods to solidify the conclusions of van Saders et al. (2016) by showing that stars older than a few gigayears do not spin down beyond a certain point stalling to populate the Rossby Ridge.

3.3.2. Rotation Period, T_{eff}*, [Fe/H], and* $R_\star$

We use the CKS-Gaia precise stellar parameters, our log ($R'_{\rm HK}$) activity measurements, the activity-derived rotation periods, and photometric rotation periods to examine rotation-activity relationships. In Figure 10 we plot rotation periods derived from log($R'_{\rm HK}$) using the Mamajek & Hillenbrand (2008) equations, the Kepler photometric rotation periods from David et al. (2021), and the difference in those values versus stellar properties for each star. We select only the grade 3, highly reliable, rotation periods from David et al. (2021), and we remove subgiants by restricting the log(g) to be greater than 4.1 leaving 173 stars. Using this highly selective set of rotation periods, we calculate the difference between Kepler photometric rotation period and the activity derived rotation periods. For each panel in Figure 10, we fit a linear trend to the data to assess trends in each stellar property. We checked for evidence that the S/N of the *S*-value measurements affects the *S*-values themselves and found none, reducing the chance that a systematic error is occurring due to low S/N.

In the $T_{\rm eff}$ versus $P_{\rm rot}$ plots (Figure 10, left column), we see the expected trend, hotter stars rotate faster, but the slope between the two rotation determinations is quite strong. If the difference plot for activity-derived rotation periods and photometric rotation periods showed a flat slope, then both determination methods would agree. Instead, the activity-derived relation overpredicts rotation periods for cool stars and underpredicts rotation periods for hotter stars. The main result of the stellar property and rotation period analysis is that the relations for determining rotation period work very well for solar-type stars, but less well as stars diverge from solar $T_{\rm eff}$. This reflects the bias toward solar-type stars used in the

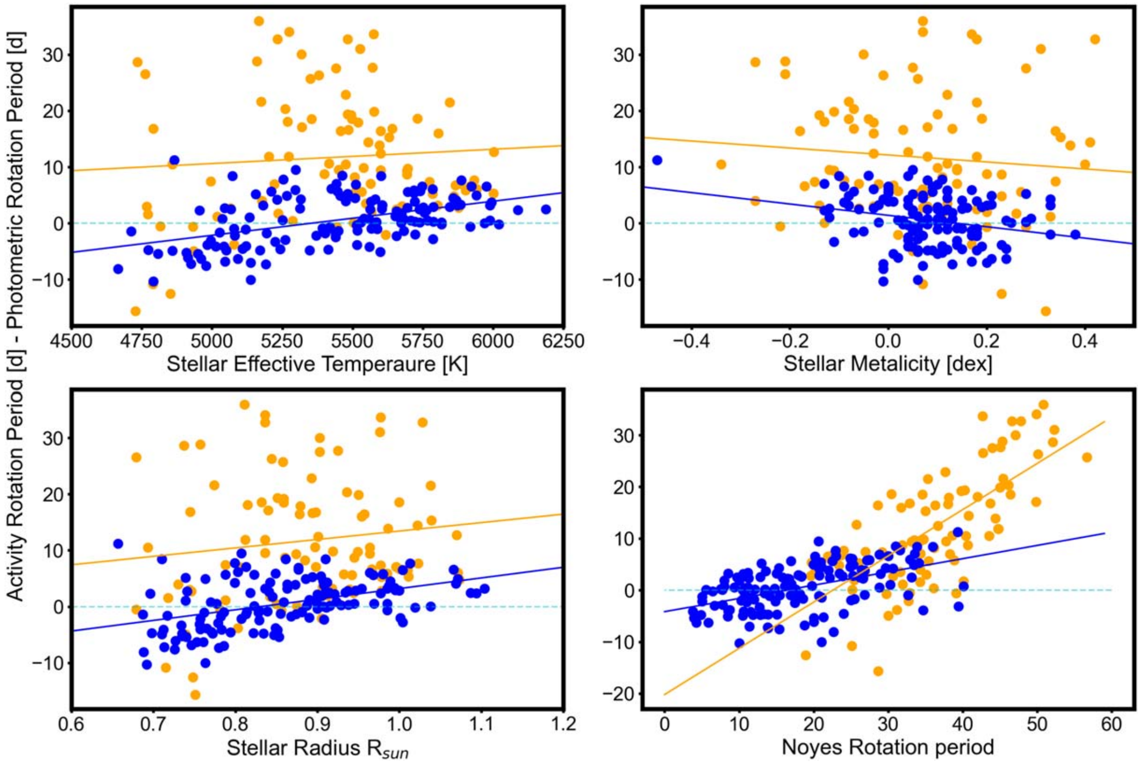

Figure 11. The difference between photometric and activity derived rotation periods are plotted on the *y*-axis of each plot for 130 stars from the CKS-HK rotation sample with log(g)> 4.4 and have rotation periods with grade 2, reliable (orange points) or grade 3, high reliable (blue points). The rotation period uncertainties are 10%. Top left: the grade 2 rotation periods are far more discrepant than the grade 3 rotation periods and both show the same modest correlation with $T_{\rm eff}$. Top right: the grade 2 rotation periods show a larger variation in metallicity than those with grade 3. Bottom right: the grade 2 rotation periods show a strong correlation when plotted against the activity derived periods. This shows that for stars with a clear but not strong photometric rotation period (grade 2), the discrepancy between the two methods of obtaining the rotation period is more than 30% for periods beyond 40 days. If the photometric rotation period is very clear, the agreement is much better, but the photometric rotation periods do not extend beyond 40 days. Bottom left: stellar radius shows a modest slope, meaning there is a systematic error in rotation period determinations from activity metrics that is linear with $R_\star$.

creation of past activity-period relationships, and motivates the development of the WMB theory of stellar spindown.

When considering [Fe/H] (Figure 10, center column), we see a linear correlation with metallicity for the activity derived periods, but no trend for the photometric periods. This disconnect may reveal the bias of Mt. Wilson survey toward solar metallicity stars. The negative trend with stellar metallicity shows that more metal-rich stars have rotation periods that are underpredicted by activity. Contrast this with metal-poor stars showing rotation periods that are over-predicted compared to the photometric rotation periods. Amard & Matt (2020) and Avallone et al. (2022) both studied the influence of metallicity on rotation periods. The former used theoretical models to conclude that stars of the same mass but with metal-poor versus solar metallicity rotate faster and have a higher Rossby number resulting from the change of the depth of the convective zone. The latter measured rotation periods in TESS and Kepler light curves that do not show a statistically significant relationship between metallicity and rotation period. These analyses could be more definitive with larger samples of stars that have more extreme metallicities than we present.

In Figure 10, right column, the stellar radii are plotted against the activity-determined, photometric rotation period, and the difference between the two. We see correlations in the two determinations of rotation periods that suggest a faster rotation period for larger stars. The more numerous solar-type stars and sparse number of larger stars makes the conclusion ambiguous.

In Figure 11 we plot only the difference panels from the previous figure, and we now include grade 2 (reliable, orange points) and grade 3 (highly reliable, blue points) rotation period labels. The differences between the activity-derived and photometric rotation periods are more pronounced for those that are deemed less reliably determined. This is likely explained by the lower-precision ground-based data, compared to Kepler data, that was used to generate the rotation-activity relations from Noyes et al. (1984) and Mamajek & Hillenbrand (2008).

3.3.3. Rossby Number and Chromosperic Activity

Recent work by David et al. (2022) used CKS-Gaia stellar properties and Kepler photometric rotation periods to reveal the Rossby Ridge, a clustering of stars in $T_{\rm eff}$ versus rotation period space that supports the theory of WMB. We use the CKS-HK rotation sample and our $\log(R'_{\rm HK})$ measurements to determine if chromospheric activity supports the presence of a Rossby Ridge. First we examine our $\log(R'_{\rm HK})$ values by comparing to the population of main-sequence stars used by Mamajek & Hillenbrand (2008).

The theoretical connection between chromospheric activity and stellar rotation is via the Rossby number, the ratio of the rotation period to the convective turnover time. By calculating

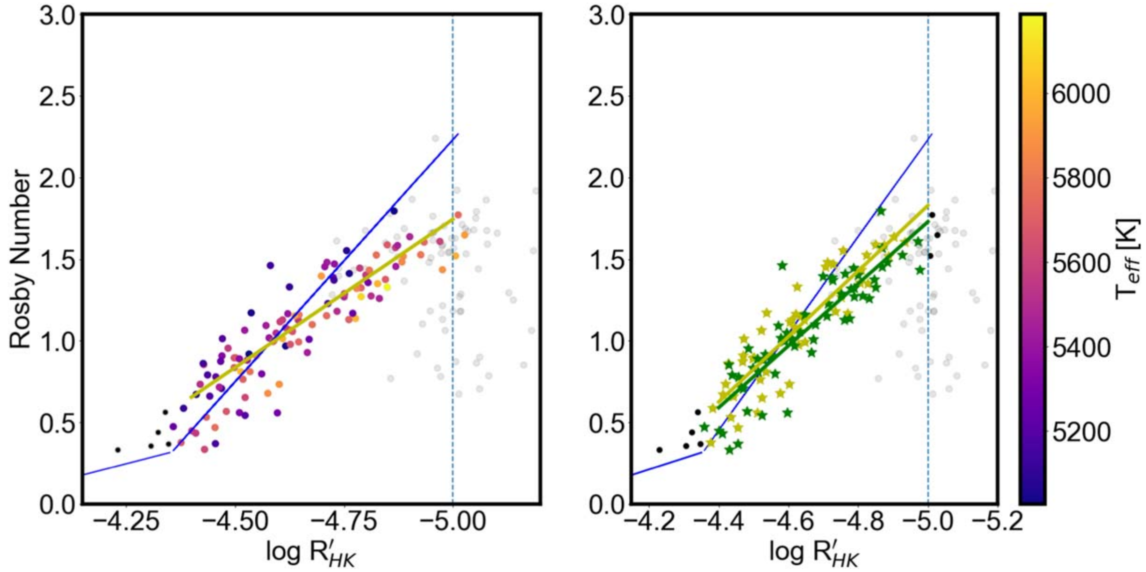

Figure 12. Left panel: the CKS-HK rotation sample is shown in relation to their $\log(R'_{\rm HK})$ values and Rossby numbers as determined by the Kepler rotation period divided by the convective turnover time as defined in Noyes et al. (1984), Equation (4). The best-fit from Mamajek & Hillenbrand (2008), Equation (5) is overplotted in blue. $T_{\rm eff}$ is less than 6250 K, and $\log(g)$ is required to be greater than 4.4, matching those cuts in that paper. The vertical line is the value of −5.0, shown to be the limit of the rotation-activity relations. The colors scale is stellar surface temperature. Right panel: the two colors represent [Fe/H] values divided at the median of the distribution, [Fe/H] = +0.09. The yellow and green fits to the lower and higher metallicity data are consistent with each other, showing that the impact of metallicity on this relation is weak in the range of [Fe/H]: [−0.3,+0.3]. The grayed-out data points are the CKS-HK stellar sample that have grade 0 or 1 stellar rotation periods and are not used in the fits.

the Rossby number using the Kepler rotation periods, we can compare $\log(R'_{\rm HK})$ and Rossby number (Mamajek & Hillenbrand 2008, their Figure 7). We focus our analysis in the active regime ($-5.0 \leqslant \log(R'_{\rm HK}) \leqslant -4.3$), since we lack a sufficient number of stars in the very-active regime ($\log(R'_{\rm HK}) \leqslant -4.3$). In Figure 12 we plot $\log(R'_{\rm HK})$ versus the Rossby number for our CKS-Gaia stellar sample, using 107 "very-reliable," photometric rotation periods (grade 3). The temperature range has been limited from 5000−6200 K, and the $\log(g)$ must be greater than 4.4, focusing on main-sequence stars and matching Mamajek & Hillenbrand (2008). Only data in the bounds of $\log(R'_{\rm HK})$ between −4.3 and −5.0 are used in the fit. The gray data are CKS-HK stars with unreliable, indistinct, or "reliable" rotation periods, flags of 0, 1, or 2 from David et al. (2021).

To assess subtleties in Figure 12, we split the sample in metallicity to reveal that [Fe/H] does not play a strong role in the relationship between Rossby number and $\log(R'_{\rm HK})$. We show the same data in both panels of Figure 12, with the best-fit from Mamajek & Hillenbrand (2008) in blue. The color bar describes the $T_{\rm eff}$ of the sample in the left panel. A vertical dotted line at $\log(R'_{\rm HK}) = -5.0$ identifies values where we expect a breakdown in the standard activity-rotation relations (Metcalfe & Egeland 2019). By fitting a line to the data in the left panel, we find a fit with a shallower, but similar slope compared to Mamajek & Hillenbrand (2008). The right panel shows a similar version with the stellar metallicity highlighted as two distinct colors divided at the median value of those plotted, +0.09. We find a very similar slope when fitting the lower-metallicity and higher-metallicity halves of the data separately, suggesting that metallicity does not play a strong role in this relationship, at least in the range of [−0.2 to +0.3].

Figure 12 reveals an upper limit of 1.75 on the Rossby number. Theoretical work suggests that the critical Rossby number is 2.0 or 2.16, higher than any of our target stars. This is explained by our restrictions on rotation period quality and the gravity cutoff of 4.4.

David et al. (2022) provided evidence in support of the van Saders et al. (2016) theory of WMB via the identification of the long-period pile-up in the temperature-rotation plane that results from magnetic braking. By using the CKS-Gaia sample and controlling for the quality of the rotation periods, the Rossby Ridge is identifiable. We rely on the same robust stellar properties from the CKS-Gaia sample and strictly vetted rotation periods to further confirm the theory of WMB.

We replicate the temperature versus rotation period plot from David et al. (2022) and add chromospheric activity data in the form of rotation periods derived from $\log(R'_{\rm HK})$ values (Figure 13). We color-code the stars for which the activity derived rotation period is larger than the photometric rotation period by more than 30%. With the standard uncertainty of the photometric rotation periods of 10% according to David et al. (2022), the choice of 30% corresponds to a 3σ discrepancy between rotation period determination methods. For all stars in the $T_{\rm eff}$ range of 5850–6250 K, the photometric rotation period is smaller than the activity derived period. We find that 79% of the stars in the trapezoid region have overpredicted rotation periods of more than 30%. This discrepancy points to the disconnect between the rotation period and magnetic field of a star, as stars reach a few gigayears old, as described by the theory of WMB. Masuda (2022) pointed out that the pile-up of stars in the $P_{\rm rot}$ versus $T_{\rm eff}$ plane is also affected by the decrease in the photometric amplitude of the rotation signal and that the pile-up may in fact be at longer periods but is currently below our detection limits.

To further explore the $T_{\rm eff}$ and rotation period plane, we change the color-code of $\log(R'_{\rm HK})$ values in Figure 14 and search for a connection between the $\log(R'_{\rm HK})$ values and the Rossby Ridge. By dividing the $\log(R'_{\rm HK})$ values at −4.8 and −5.1, we can identify stars that lie along the Rossby Ridge. There are 3/103 stars with $\log(R'_{\rm HK}) > -4.80$, 34/103 between

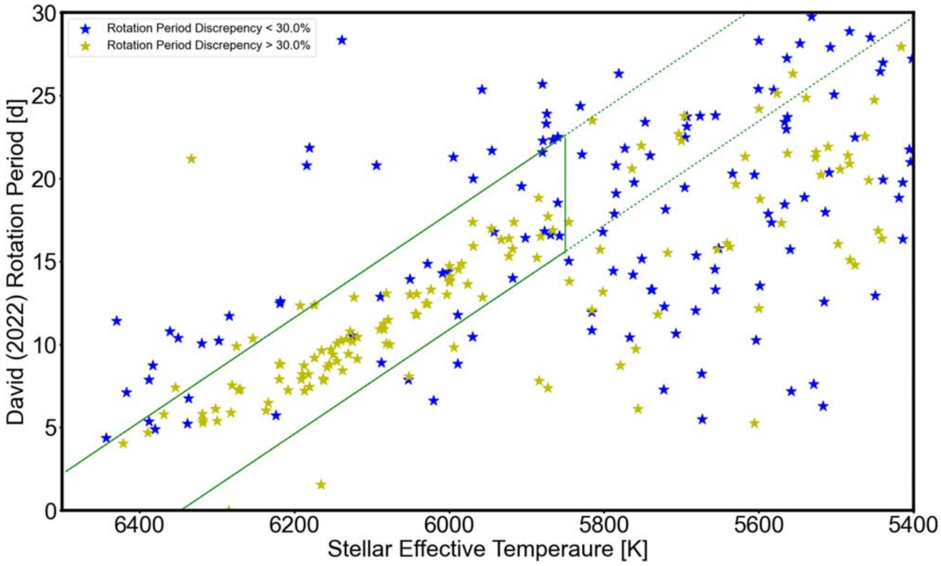

Figure 13. The temperature vs. rotation period plane similar to David et al. (2022, their Figure 4). Each symbol represents a star from the CKS-HK rotation period sample with grade 2 or 3 rotation period and $\log(g)> 4.0$. Blue symbols identify stars that show agreement between their photometric and activity derived rotation periods to better than 30%. Yellow data points show discrepancy larger than 30%. Large discrepancy points to a disassociation of the stellar spindown with age, consistent with the theory of weakened magnetic braking. We extend the trapezoid defined in David et al. (2022) to 5600 K, but find no evidence in the $\log(R'_{\rm HK})$ data that inform the breakdown of the Ridge into that range of $T_{\rm eff}$.

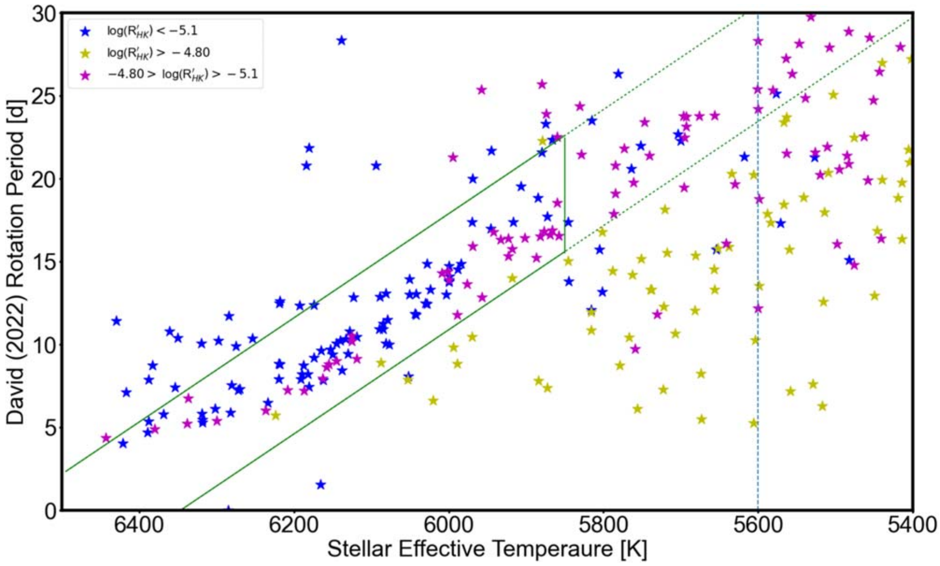

Figure 14. The $T_{\rm eff}$ vs. rotation period plane similar to David et al. (2022, their Figure 4). Each symbol represents a star from the CKS-HK rotation period sample with grade 2 or 3 rotation period and $\log(g) > 4.4$. Blue symbols are least active $\log(R'_{\rm HK}) < -5.1$, representing inactive stars. Yellow symbols have $\log(R'_{\rm HK}) > -4.80$, representing the active stars. Yellow symbols are within 0.15 of the critical value of $\log(R'_{\rm HK}) = -4.95$, where we expect the traditional spindown relations to break down in favor of the relations best described by weakened magnetic braking.

$\log(R'_{\rm HK})$ of -4.80 and -5.10 and 66 stars in the least active category of $\log(R'_{\rm HK})< -5.10$. We expect stars of a certain $T_{\rm eff}$, say 6000 K, to slowly spin down with age but to not change temperature while on the main sequence. If we had a population of more quickly rotating stars that populated the area below the trapezoid, we could likely see the most active stars with the fastest rotation periods, and stars with ever decreasing activity as they approach the Rossby Ridge. Our population of stars from 5850−6200 K has insufficient younger and more active stars to see the type of behavior that is seen in surveys with larger numbers of stars, such as McQuillan et al. (2014).

We extend the trapezoid defined in David et al. (2022) from 5850−5600 K and find tentative evidence in the log ($R'_{\rm HK}$) data that indicates Rossby Ridge projects into cooler ranges of $T_{\rm eff}$. These stars have thicker convective zones, spend longer on the main sequence, and take longer to spin down. These larger parameter spaces, and longer time spans in stellar evolution are a barrier to theoretical studies attempting to explain spindown for broader stellar populations. The conclusions by Masuda (2022) regarding the amplitudes of stellar rotation signals are even more relevant for this range of $T_{\rm eff}$ since these stars are inherently fainter,

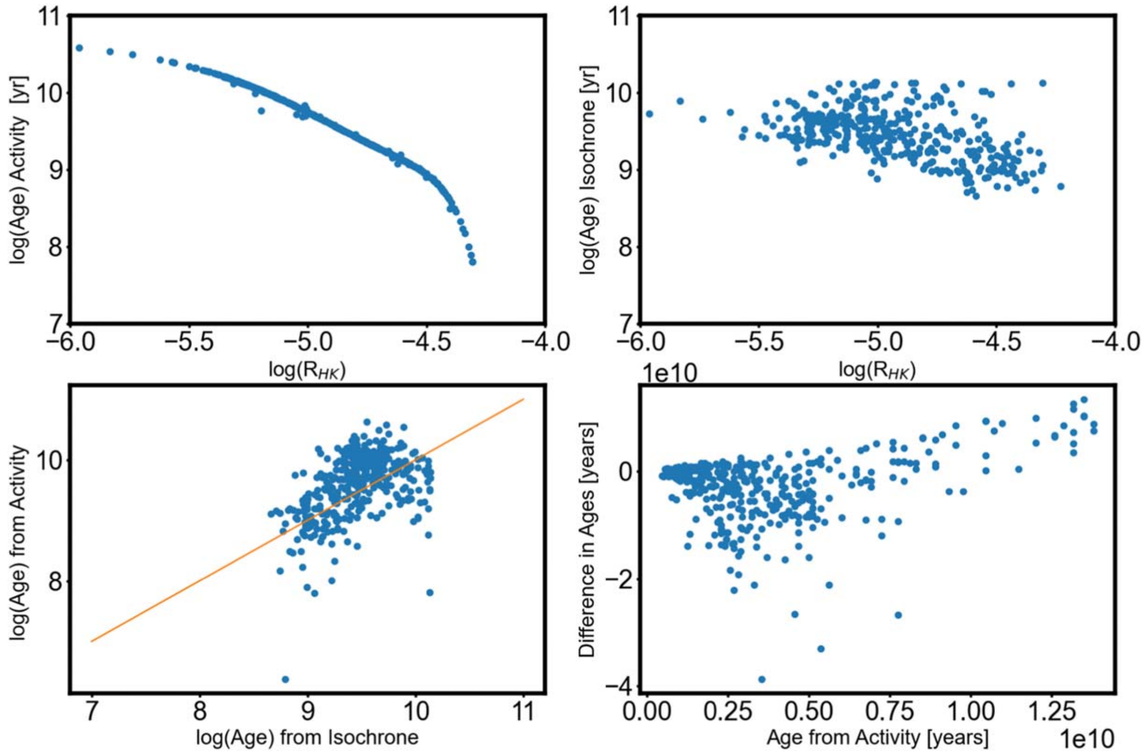

Figure 15. We explore the age vs. activity relationship with these four panels. Top left: the predicted rotation period determined the $\log(R'_{\rm HK})$ value of the star. Top right: the isochronal age from David et al. (2021) or CKS-Gaia as a function of the chromospheric activity. Bottom left: the isochronal age compared to the activity derived age and the one-to-one line overplotted. Bottom right: the difference between the two age determinations as a function of the isochronal age. Note this plot is in units of years, and the others are in log (age).

Table 2
Activity Metrics and Derived Values

Starname (KOI)	S-value	$\log(R'_{\rm HK})$	S/N per pixel	$P_{\rm Rot}$ Activity(d)	log(Age) Activity (yr)	Quality	Quality Flag	$P_{\rm Rot}$ Phot(d)	$P_{\rm Rot}$ Flag
K00001	0.145	−5.101	8	30.1	9.90	0	bad seeing	0.0	1
K00002	0.128	−5.247	11	6.9	10.09	1	ok	0.0	1
K00006	0.140	−5.103	19	8.5	9.91	1	ok	0.0	0
K00007	0.141	−5.136	27	30.9	9.95	1	ok	0.0	1
K00008	0.202	−4.779	14	16.6	9.40	1	ok	0.0	0
K00010	0.127	−5.270	19	16.8	10.12	1	ok	7.5	2
K00017	0.134	−5.202	10	41.8	10.04	1	ok	0.0	1
K00018	0.125	−5.289	19	10.9	10.14	1	ok	0.0	1
K00020	0.136	−5.178	21	27.3	10.00	1	ok	0.0	1
K00022	0.135	−5.190	17	29.5	10.02	1	ok	0.0	1

(This table is available in its entirety in machine-readable form.)

further clouding our ability to draw conclusions for these stars.

3.4. Ages and Chromospheric Activity

The works of van Saders et al. (2016), David et al. (2022), and Metcalfe & Egeland (2019) attempted to find a relationship between age, activity, and rotation, similar to Noyes et al. (1984), but with modern tools. Noyes et al. (1984) used rotation periods and a few assumptions about stellar structure. By examining two stars of similar $T_{\rm eff}$ and near the Kraft Break, Metcalfe & Egeland (2019) revealed the age−activity relation discontinuity, near $\log(R'_{\rm HK})$ of −4.95. For more active stars, the relationship between chromospheric ages and gyrochronology ages agree, but once stars' activity decreases beyond $\log(R'_{\rm HK})$ of −4.95, the age determinations diverge.

Figure 15 shows our two age metrics as function of $\log(R'_{\rm HK})$ in the two top panels. In the two bottom panels, the isochronal age is compared to the activity-derived age, and to the difference in the two age metrics for each star, in the left and right panels, respectively.

Broadly speaking, the chromospheric ages are overpredicted compared to the isochrone ages. Given our evidence in favor of WMB, we expect the activity-age determinations to perform poorly for stars older than 1 Gyr. However, the mismatch in ages between the youngest, most active, stars is unexpected. The S-values, $\log(R'_{\rm HK})$ values, rotation periods and activity derived ages for the CKS-HK star sample are collected in Table 2.

3.5. The Most Inactive Stars: Overview

Stars that mimic the activity of the Sun during its persistent minimum in the 17th century have been sought in an attempt to solidify the solar-stellar connection. Duncan et al. (1991) collected 18 yr of S-value time series with the Mt. Wilson H&K Activity project providing many examples of stars with solar-like stellar activity cycles (Baliunas et al. 1995), and several candidates for stars in low activity states. These stars were chosen as bright, Sun-like stars, but without the vigor of spectroscopic stellar classification that we have today. One method for identifying a star in Maunder minimum–like state (or magnetic minimum) is to look for a decrease in the S-values over time or a transition from a stellar cycle into a noncycling state. Several candidate Maunder minimum stars from the Mt. Wilson survey data alone were identified, though none has stood up to further scrutiny (Wright 2004) without additional data. Continued efforts to add modern data to the Mt. Wilson HK project's time-series data have identified several MM candidates.

With the addition of California Planet Search $\log(R'_{\rm HK})$ data, Shah et al. (2018) identified HD 4915 as a candidate for being in an activity minimum, but recent data showed the activity minimum is ending. Another analysis of the Mt. Wilson HK project plus CPS data (Wright et al. 2004; Isaacson & Fischer 2010) extended the observing baseline for 59 stars from two to five decades.

Baum et al. (2022) curated the various data sets and identified HD 166620 as a star that was in a previously cycling state and is now in a noncycling low-activity state. An extended effort has confirmed HD 166620 as a true MM star (Luhn et al. 2022) using photometry and critically timed S-value measurements. In that study, intraseasonal variability was considered a more useful diagnostic of an MM state than instantaneous measurements that are anomalously low.

Searching for MM stars by analyzing decades of time-series data is laborious and time consuming so other methods for identifying stars in activity minima have been explored. Surveys like the Hipparcos Mission (Perryman et al. 1997) made the identification of outliers more robust with precise measurements of parallax. The distance can be combined with spectral surveys that provide precise stellar surface gravities and metallicities (Wright 2004; Fulton & Petigura 2018; Rosenthal et al. 2021). Naturally, Gaia now provides precise parallax measurements for all stars down to $V\sim19$. The parallaxes can help to disentangle inactive main-sequence stars from evolved stars that are naturally inactive. The Gaia spectral measurements of the Calcium infrared triplet may enable statistical searches for inactive stars based on a small number of measurements for each star.

We can use the CKS-HK sample of stars to identify the least active stars and present candidates of stars in magnetic minima.

3.5.1. Identifying Stars in States of Magnetic Minima via Stellar Properties

The discussion on what constitutes an MM candidate has become more nuanced as our ability more precisely measure the fundamental stellar parameters of surface gravity, effective temperature, and metallicity have improved. We attempt to identify stars in an MM state, using a variety of methods including those of Wright et al. (2004) and Saar (2011). Henry et al. (1996) claimed that using a single $\log(R'_{\rm HK})$ value to identify quiet stars, for example, with a $\log(R'_{\rm HK})< -5.1$, is insufficient. Using $T_{\rm eff}$, $\log(g)$, and [Fe/H] is required (Saar 2011), and multiepoch spectroscopy is ideal (Baum et al. 2022). The CKS-Gaia stellar properties catalog enables a detailed study of activity, temperature, surface gravity, and metallicity in the search for the MM stars using single-epoch spectra.

The reliability of the metric $\log(R'_{\rm HK})$ depends on the inputs as defined in Noyes et al. (1984). Modern studies have created new variations on $\log(R'_{\rm HK})$, such as Hall et al. (2007), who prefer to use $F_{\rm HK}$ and delta $F_{\rm HK}$. This metric provides a different but related way for obtaining a minimum activity level. Improvements in the calculation or $\log(R'_{\rm HK})$ or of the bolometric corrections could be useful in identifying the least active stars. Mittag et al. (2013) created the log $(R^{+}_{\rm HK})$ metric, which separates the flux in the H&K lines into the basal, photospheric, and chromospheric components to create a metric at which the minimum activity level is 0 by definition. Saar (2011) required MM stars to have a minimum activity level, but did not assume it is based only on $T_{\rm eff}$, which was assumed by Noyes et al. (1984). This leads to a minimum level of activity that might indicate MM stars vary as a function of $V\sin(i)$, $\log(g)$, and [Fe/H] as well as $T_{\rm eff}$. Additionally, it requires knowing something about the longer-term variation, which can be variation of S-value over time (Saar 2011), or photometry (Hall et al. 2007) or X-rays (Judge & Saar 2007). Judge & Saar (2007) claimed that an MM star can only be confirmed if we know something about the X-ray flux, which can only be produced by a stellar dynamo.

We define the height above the main sequence using the Wright (2004) relation and search for stars that are both inactive, $\log(R'_{\rm HK})$ less than −5.1, and near or below the main sequence. To identify interesting candidates, we focus on the stellar temperature range of 4700−5500 K, where the main-sequence population and subgiant populations are well separated. Knowing that MM stars are rare, we are looking for outliers from the populations. In Figure 16, we identify no stars in the coolest bin that are MM candidates. In the 5500–6000 K bin, we see a set of stars, the most extreme of which may be an MM candidate. The best candidate in the 5500–6000 K bin is KOI-1531. There is a population of stars in the lower right quadrants for the temperatures 6000–6500 K. There are no outliers, but rather stars that naturally fall into the bottom-left box. We expect this because near the Kraft Break at $T_{\rm eff}$ of 6250 K, stars become fully radiative, and the sort of activity that we are probing is not viable through the same physical mechanisms as for cooler stars.

We highlight cool stars that lie far below the main sequence in a temperature−magnitude diagram (Figure 17). There are three stars that are more than 0.4 magnitude below the main sequence, as defined by Wright (2004) and are cooler than 6250 K, the Kraft Break. They are KOI-1531, KOI-4144, and KOI-5236. KOI-5236 has a planet with a period greater than 500d, and maybe false-positive planet candidate according to Community Follow-up Program (CFOP; Gautier et al. 2010). It has $T_{\rm eff} = 6100$ K, $\log(g) = 4.41$, and $\log(R'_{\rm HK}) = -5.365$. It is very inactive and has a $1\rlap{.}''9$ companion, but no detection of a secondary star in the spectrum. The nearby star makes the likelihood of the star being an MM star less certain. KOI-4144 has $T_{\rm eff}$ of 6000 K, $\log(g) = 4.49$, especially large RMS3 value from Kepler (Christiansen et al. 2012), distance of 860 pc. KOI-1531 is the furthest below the main sequence, and it has a

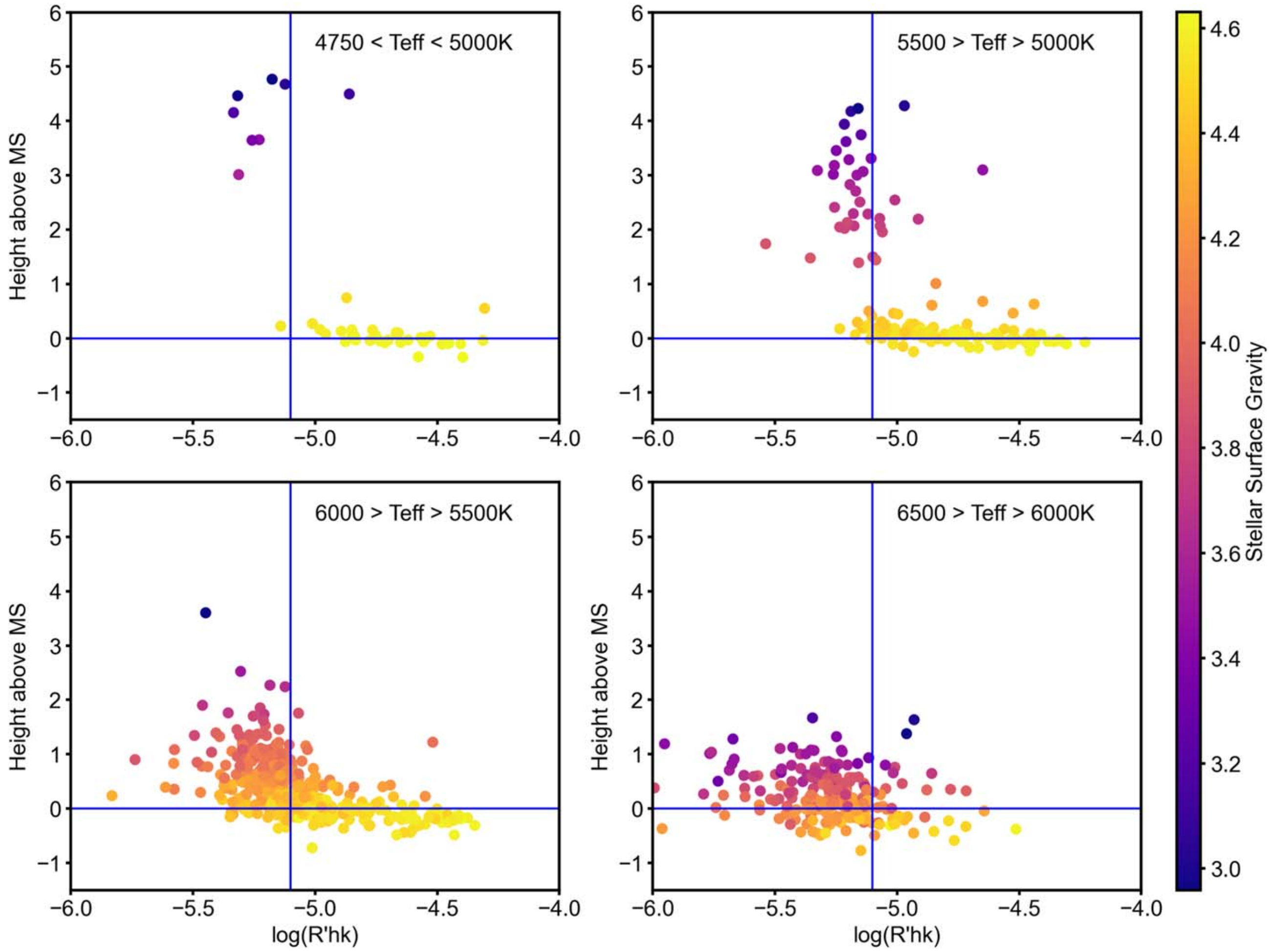

Figure 16. Examining delta magnitude above the main sequence (Wright 2004) vs. $\log(R'_{\mathrm{HK}})$, we expect stars that are experiencing magnetic activity minima to be in the bottom-left quadrant of these plots. Stars that populate the upper-left quadrant tend to be subgiants with large radii that are likely have their magnetic fields decoupled from their convective zones. The vertical line at $\log(R'_{\mathrm{HK}}) = -5.1$ is an arbitrary but reasonable division between active and inactive stars (Henry et al. 1996). Saar (2011) stated that it is not a good cutoff for MM star consideration because it was made before Hipparcos helped define the evolutionary state of a large sample of stars. We focus on main-sequence stars with $T_{\mathrm{eff}} < 5500$ K because we do not expect them to populate very inactive regime, except in extreme circumstances, such as Maunder minimum stars.

near Sun-like T_{eff}, and $\log(g)$ with $\log(R'_{\mathrm{HK}}) = -5.012$. It has a photometric rotation period from Angus et al. (2018) of 23 days and an activity rotation period of 34 days. This 30% discrepancy mismatch between the photometric and activity rotation periods is supportive of the theory of WMB. If this is the case, the star is old and inactive, but still has the rotation period of a younger star.

Henry et al. (1996) states that stars with $\log(R'_{\mathrm{HK}}) \leqslant -5.1$ are in MM states. Wright (2004) claims that without knowing $\log(g)$ or the height above the main sequence, it is easy to confuse subgiants with MM stars. This was problematic both because subgiants have inherently lower activity, so they can fall in the same parameter space as MM stars, and because the search for stars in states of magnetic minima is more compelling for Sun-like stars. If the conclusions from Wright (2004) are correct, we expect stars with $\log(R'_{\mathrm{HK}}) < -5.1$ to be evolved stars. The bottom row of Figure 6 shows stars with smaller radii are more active, populating the "Inactive" and "Active" bins. Our three best candidates above are distinctly not subgiants. We have an unusually large number of stars relative to the nearby star catalogs, with a full population of stars with $\log(R'_{\mathrm{HK}}) < -5.1$.

Hall et al. (2007) studied 18 solar-type stars and concluded that $\log(R'_{\mathrm{HK}})$ is not a good metric to identify stars in a magnetic minimum state. This is due to the unknown effects of metallicity and stellar surface gravity. They claimed that a better metric is delta F_{HK}, which is the measure of the flux caused by magnetic activity in the H and K lines. It is robust against high stellar rotation as well. This agrees with Saar (2006), who noted that the minimum activity of a star is dependent on metallicity. Specifically, metal-poor dwarfs have a higher minimum $\log(R'_{\mathrm{HK}})$ than dwarfs of solar metallicity.

X-rays play an important role in observing and assessing chromospheric activity and searching for MM stars because it is difficult to explain the creation of X-rays without the magnetic field processes associated with chromospheric activity detected in the optical. We defer the incorporation of X-ray data for future work.

Wright (2004) had precise parallaxes from Hipparcos but lacked precise metallicity and stellar surface gravity required to separate their relationship to stellar activity. We now have excellent metallicities, so we can check if stars that are below the main sequence are very metal-poor. Saar (2011) provided a

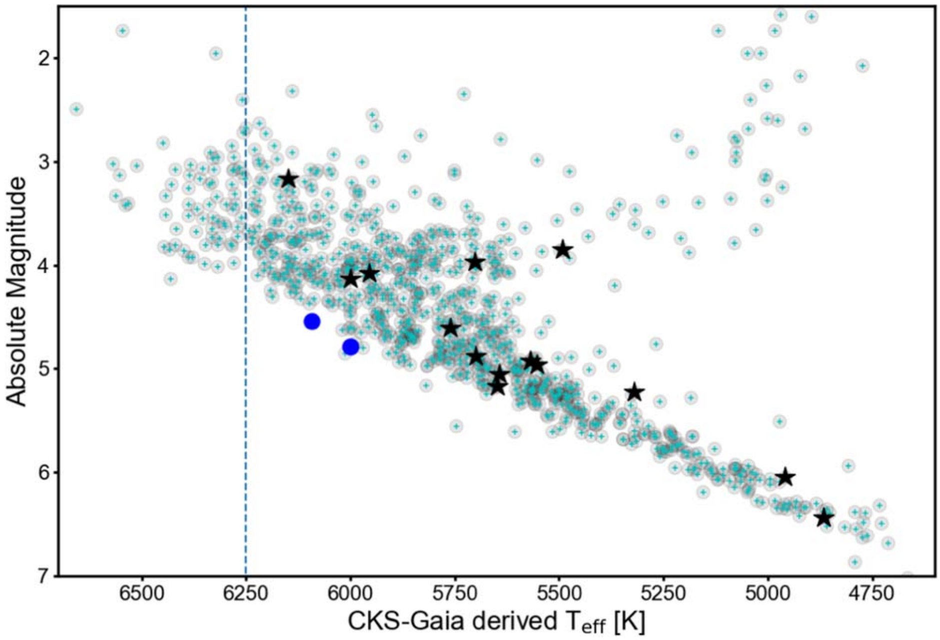

Figure 17. This color–magnitude diagram highlights several subcategories of stars and allows for identification of Maunder minimum candidate stars, following the logic of Wright (2004). We plot the CKS-HK stellar sample as the gray background of data points. Black star symbols highlight exceptionally metal-poor stars with [Fe/H] < -0.4. Blue circles represent stars that are 0.4 magnitudes below the main sequence and are "very inactive" with $\log(R'_{HK}) < -5.2$ as the threshold. Stars of very low stellar activity that fall below the main sequence are candidates for MM status. The vertical line denotes the temperature of the Kraft Break, above which we do not expect stars to have an active convective zone contributing to stellar activity. The two blue data points are KOI-4144 and KOI-5236. (KOI-1531 misses the $\log(R'_{HK}) < -5.2$ cutoff).

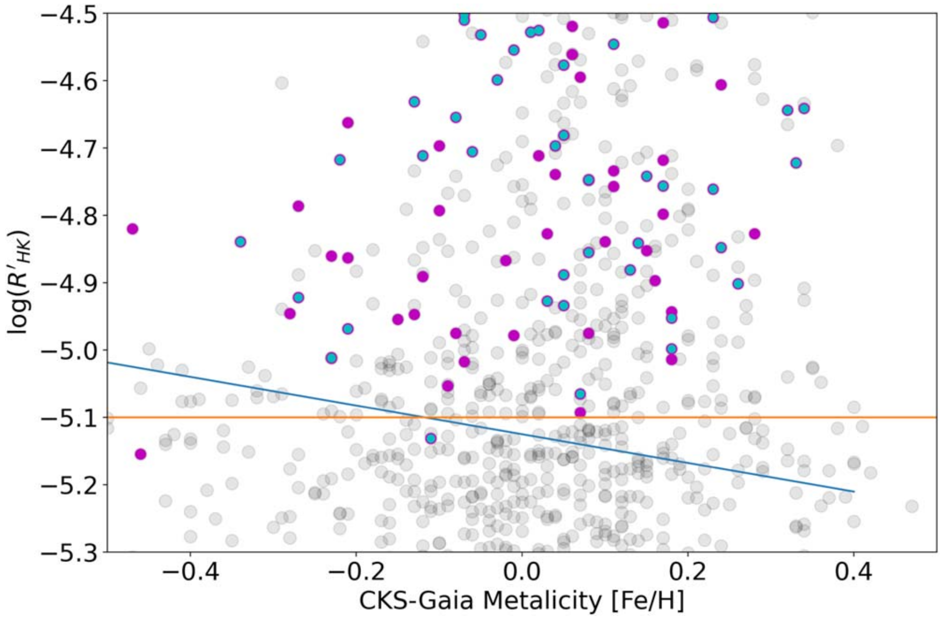

Figure 18. We search for the dependence of metallicity on the lowest level of activity for dwarf stars. Inspired by Saar (2011, their Figure 2), we examine metallicity vs. $\log(R'_{HK})$, with the blue diagonal line representing a minimum activity as a function of metallicity for dwarf stars. Our full set of 879 stars is shown in gray, with magenta stars representing stars with T_{eff} less than 5300 K and the cyan stars have delta magnitude above the main sequence of greater than 0.5. According to the criteria from Saar (2011), these are candidate MM stars, but knowing something about their long-term variability is also required. Since we do not have that with our sample, they must remain candidates. Contrary to Saar (2011), we do not see a dependence on metallicity for low-activity stars. Perhaps a sample of extremely low-metallicity stars would offer a stronger case for a correlation between activity and metallicity.

functional cutoff of in the plotting of $\log(R'_{HK})$ as a function of metallicity.

Using a similar analysis to Saar (2011), we can plot chromospheric activity as function of stellar metallicity, limit our search to dwarf stars, and identify the least active stars. Broadly speaking, we do not see the trend of minimum $\log(R'_{HK})$ that is noted by Saar (2011). Note that we lack many stars beyond $+/-$ 0.4 dex that give the most leverage in assessing effects of metallicity. Figure 18 shows no visible trend in metallicity for stars in the CKS-HK sample, although with limited parameter space. Specifically, we find that KOI-241 and KOI-2498 are the two least active stars, and confirm, by eye, that they have high-quality *S*-values. They are both quite cool stars compared to the solar temperature inactive stars that were previously discussed, with $T_{\rm eff}$ of 4960 and 5128 K, respectively. Their metallicities are −0.46 and −0.11. The David et al. (2021) rotation periods are 32.7 days and 15.2, respectively, but both are listed as ambiguous or lacking a clear cycle. An additional test would be to check the stars' variation over time. With only single-epoch measurements, we can only say these stars are currently in low activity states, but not necessarily in extended MM states.

3.5.2. Activity, Close-in Planets, and Toroidal Gas Rings

The work of Fossati et al. (2013) revealed that the star system hosting ultra-short-period hot-Jupiter planet WASP-12b shows evidence of a gas ring surrounding the star, which is due to excessively low flux in the Mg II H and K lines, located at 2586 Å. The Ca II H and K lines confirm this interpretation along with measurements of the strongly varying near-UV flux. We searched for similar occurrences of incredibly low $\log(R'_{\rm HK})$ values around similar-type planet hosting systems and find none as compelling as WASP-12, which has a $\log(R'_{\rm HK})$ value of −5.50 and $T_{\rm eff}$ 6250 K.

We searched our sample for stars with a $T_{\rm eff}$ between 5800 and 6250 K, planet orbital periods less than 1 day, and stellar surface gravity greater than 4.2, bracketing the properties of the WASP-12 system. Of the two systems that have planet radii larger than ten Earth-radii, both are eclipsing binaries from CFOP (Gautier et al. 2010). For planets with radii < 10 Earth-radii and the same stellar property limitations as previously listed, 10 systems remain, the largest with a planet radius of 3 Earth-radii. Three stars have $\log(R'_{\rm HK}) < -5.2$. KOI-2717 has a $\log(R'_{\rm HK})$ value = −5.226 and shows visible evidence of emission below the solar level, in a high-S/N spectrum. KOI-4072 ($\log(R'_{\rm HK}) = -5.241$) and KOI-4144 ($\log(R'_{\rm HK}) = -5.306$) show modest evidence of a very low flux, but the S/N makes visual confirmation difficult. Reobservation of these three stars at higher S/N could help confirm their activity level. Figure 19 shows WASP-12 Ca II H and K spectral features along with the three most inactive stars in our survey. We do not find convincing evidence of a toroidal gas ring, although our survey does not contain many hot Jupiters. Transit surveys such as TESS will detect many transiting bright stars enabling a larger survey of stars to search toroidal gas rings.

Kepler stars are more metal-rich than the solar neighborhood, so the paucity of hot Jupiters is not related to metallicity in a similar way to the hot-Jupiter occurrence in the solar neighborhood (Petigura et al. 2018). The bias of the Kepler sample also contains a large number of subgiants that have inherently lower chromospheric emission. Using a sample of Sun-like stars hosting hot Jupiters would provide a more complete search space than the CKS sample of transiting planet hosts. Using a large sample of hot-Jupiter host star spectra to search for such anomalous emission is more promising than using the CKS-HK data set.

Future work on this could include examination of the Rossiter McLaughlin sequences of inflated hot Jupiters to search for variations in the *S*-values over the course of the transit. Similarly, if a large sample of hot Jupiters were sampled such as those found by TESS, perhaps more stars similar to WASP-12 would be found.

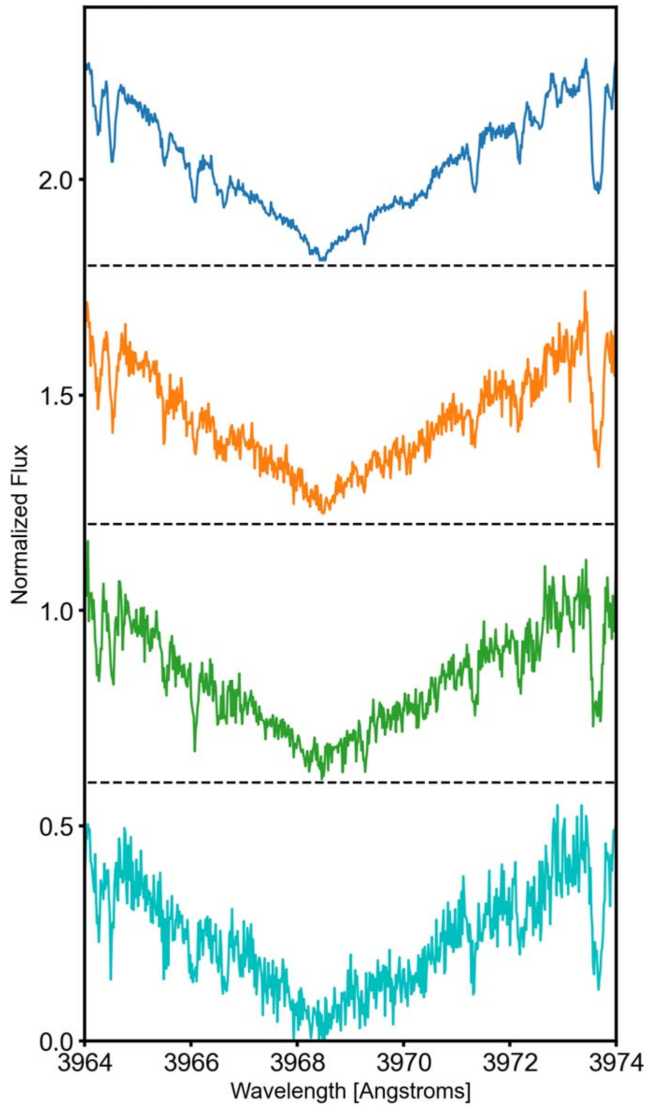

Figure 19. These four spectra represent the four most inactive stars in our survey. Each star is vertically offset with the dotted line representing zero flux. The top panel shows WASP-12 with exceptionally low activity and a spectrum with high S/N. The bottom three plots show that for stars with very little activity, it is difficult to visually distinguish between inactive and very inactive stars. Below WASP-12 are KOI-2786, KOI-2906, and KOI-2833. Their $\log(R'_{\rm HK})$ values are −6.122, −5.994, and −5.962, respectively.

3.6. Planet Radii and Chromospheric Activity

Identification of the small planet radius gap (Fulton gap) at roughly 1.8 $R_{\rm Earth}$ both theoretically and observationally has been of great interest to planet formation theory. Stellar insolation at the planets' average orbital distance is strongly correlated with planet radius on the small side of the radius gap receiving higher insolation and planets on the larger radius side receiving less. Stellar mass plays a critical role in shaping the exact radius at which the gap falls (Petigura et al. 2022) and predictions of the time frame over which the gap is sculpted range from < 1 Gyr (Berger et al. 2020a) to several gigayear timescales (David et al. 2022).

Acknowledging that stars become less active as they age, making age and activity degenerate, we examine the relationship between activity and planet radius directly with our CKS-

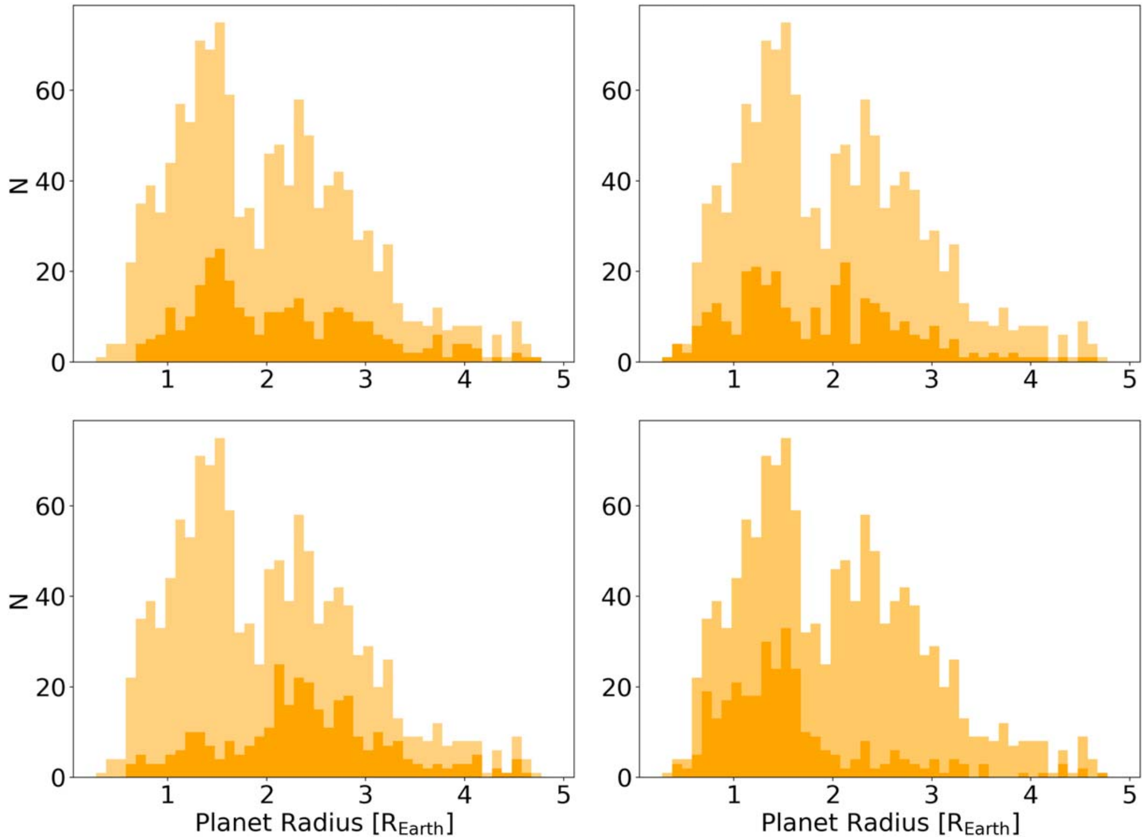

Figure 20. In the background of each plot, the CKS-HK planet population of 773 stars hosting 1243 small planets is plotted. In the two top panels, we examine the planet radius histogram to check how the super-Earth and mini-Neptune populations correspond to the most and least chromospherically active planet-host stars. Top left: with the dark color, we plot the top quartile of planets in the $\log(R'_{\rm HK})$ distribution. Top right: with the dark color, we plot the bottom quartile of planets in the $\log(R'_{\rm HK})$ distribution. We do not see an abundance of super-Earths in the active stars, nor an under-abundance in the sub-Neptunes as we might get if chromospheric activity was highly correlated with planet radius. The pattern present in the insolation plots is not reflected here. Bottom left: the quartile of stars with the lowest insolation is plotted in dark orange showing an overabundance of sub-Neptunes. Bottom right: the quartile of planets with the highest insolation is plotted, showing an overabundance of super-Earths. This is consistent with the results of Fulton et al. (2017).

HK planet sample. We plot histograms of the most active and least active stars and compare those planet populations to the planets with the most and least insolation flux. Figure 20 shows four histograms of the CKS-HK planet sample. Each panel shows the full sample histogram with a different subset overplotted. In the top two panels, we see the least active quartile overplotted (left) and the most active quartile (right). The bottom panels show the planets receiving the lowest quartile (left) and the highest quartile of insolation flux (right). Without absolute occurrence of planet in each bin, as was shown in Fulton & Petigura (2018), we can still identify the previously established trend of small mass planets receiving higher insolation. In the top panels, we see no obvious differences in the two quartiles that separate planet hosts in the most and least active quartiles. We expect the super-Earths to receive the most insolation and mini-Neptunes to receive less. If the present chromospheric activity of a star is correlated to the planet radius, we would expect a similar pattern in the top panels. Instead, we see a peak of super-Earths in the most chromospherically quiet stars. We also searched for trends and correlations in the $\log(R'_{\rm HK})$ versus orbital separation parameter space and found no significant trends.

The connection between planet size and chromospheric activity is degenerate with age, complicating the interpretation. We plot the chromospheric activity versus planet radius in Figure 21, subdividing the sample by both $T_{\rm eff}$ and [Fe/H]. For a full explanation of isochronal age dependence on the radius gap, see Berger et al. (2020a) and David et al. (2022).

4. Conclusion

We present chromospheric activity measurements of the well-studied CKS-Gaia sample of transiting planet host stars via the Ca II H and K spectral features that are known to track magnetic activity in solar-type stars. These novel measurements are used along with the fundamental stellar properties including temperature, surface gravity and metallicity, and photometric rotation periods to explore fundamental relationships in the age−rotation −activity regime of stellar astrophysics.

We have also used the chromospheric activity measurements to check for a dependency of metallicity on the rotation periods measured from photometry and the stars corresponding Rossby numbers. Using rotation periods determined from Kepler light curves, we have searched for stellar over-abundances among long and short rotation periods in the temperature−period plane. With our single-epoch spectra, we have identified very inactive stars, but we do not yet have the multiyear time series needed to verify stars in Maunder minimum (i.e., magnetic minimum)–like states.

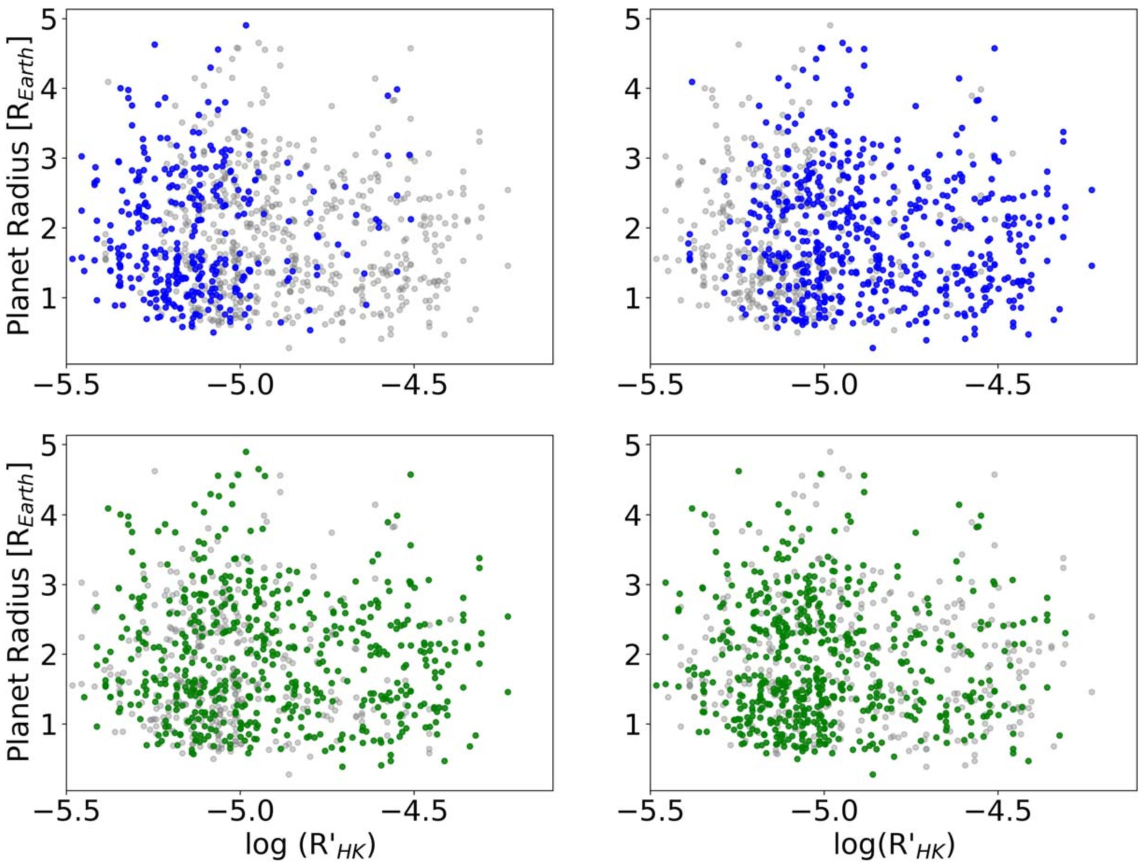

Figure 21. Planet radii as a function of chromospheric activity for Kepler's small planets. The top panels show stars hotter than the Sun ($T_{\rm eff} > 5770$ K, left) and those cooler than the Sun, right. The gray stars show the full sample of 912 planets that pass our quality criteria.. The bottom row shows the CKS-HK sample divided at the median metallicity of 0.05 with higher metallicity on the left and lower metallicity on the right.

From the large sample of precise stellar properties and activity results presented in this paper, we find no significant evidence for metallicity-dependent activity relations within the metallicity range of −0.2 to +0.3. Our results are supportive of the theory of WMB of stellar spindown in the form of discrepancies between activity determined and photometrically determined rotation periods. While 1 Gyr previously has been suggested as a critical age juncture, we find no significant evidence for a change in the activity−period relationship at this age using chromospherically derived ages. The activity−period relationship presented here, along with recently discovered nuances discovered in the temperature−period plane such as the Rossby Ridge and their relative independence from stellar metallicity, can all inform future theoretical studies of stellar rotation−activity relationships, and an understanding of the physics of the underlying stellar magnetic dynamos.

Acknowledgments

The authors extend thanks to Travis Metcalfe and Luke Bouma for helpful discussions on early versions of the paper. We also thank Ryan Rubenzahl, Sarah Blunt, and Aida Behmard for providing feedback during group discussions.

Some of the data presented herein were obtained at the W. M. Keck Observatory, which is operated as a scientific partnership among the California Institute of Technology, the University of California, and the National Aeronautics and Space Administration. The Observatory was made possible by the generous financial support of the W. M. Keck Foundation. This research has made use of NASA's Astrophysics Data System. L.M.W. acknowledges support from the NASA-Keck Key Strategic Mission Support program (grant No. 80NSSC19K1475) and the NASA Exoplanet Research Program (grant No. 80NSSC23K0269). Support was provided by the Simons Foundation grant "Planetary Context of Habitability and Exobiology".

The authors wish to recognize and acknowledge the very significant cultural role and reverence that the summit of Maunakea has always had within the indigenous Hawaiian community. We are most fortunate to have the opportunity to conduct observations from this mountain.

This project would not have been possible without major allocations of Keck telescope time from the University of California, California Institute of Technology, the University of Hawaii, and NASA. This work utilized the Exoplanet Archive, SIMBAD, the Community Follow-up Program, and data from NASA's Kepler Space Telescope.

Facility: Keck:I (HIRES), Kepler

Software: We made use of the following publicly available Python modules: astropy (Astropy Collaboration et al. 2013), matplotlib (Hunter 2007), numpy/scipy (van der Walt et al. 2011), and pandas (McKinney 2010). Interactive Data Language (IDL) was used to extract the spectral line information.

ORCID iDs

Howard Isaacson https://orcid.org/0000-0002-0531-1073
Stephen R. Kane https://orcid.org/0000-0002-7084-0529
Brad Carter https://orcid.org/0000-0002-7084-0529

Andrew W. Howard https://orcid.org/0000-0001-8638-0320
Lauren Weiss https://orcid.org/0000-0002-3725-3058
Erik A. Petigura https://orcid.org/0000-0003-0967-2893
Benjamin Fulton https://orcid.org/0000-0003-3504-5316

References

Aigrain, S., Pont, F., & Zucker, S. 2012, MNRAS, 419, 3147
Akana Murphy, J. M., Kosiarek, M. R., Batalha, N. M., et al. 2021, AJ, 162, 294
Amard, L., & Matt, S. P. 2020, ApJ, 889, 108
Angus, R., Morton, T., Aigrain, S., Foreman-Mackey, D., & Rajpaul, V. 2018, MNRAS, 474, 2094
Astropy Collaboration, Robitaille, Thomas P., Tollerud, Erik J., et al. 2013, A&A, 558, A33
Avallone, E. A., Tayar, J. N., van Saders, J. L., et al. 2022, ApJ, 930, 7
Baliunas, S. L., Donahue, R. A., Soon, W. H., et al. 1995, ApJ, 438, 269
Batalha, N. M., Borucki, W. J., Bryson, S. T., et al. 2011, ApJ, 729, 27
Batalha, N. M., Rowe, J. F., Bryson, S. T., et al. 2013, ApJS, 204, 24
Baum, A. C., Wright, J. T., Luhn, J. K., & Isaacson, H. 2022, AJ, 163, 183
Berger, T. A., Huber, D., Gaidos, E., van Saders, J. L., & Weiss, L. M. 2020a, AJ, 160, 108
Berger, T. A., Huber, D., van Saders, J. L., et al. 2020b, AJ, 159, 280
Blunt, S., Carvalho, A., David, T. J., et al. 2023, AJ, 166, 62
Borucki, W. J., Agol, E., Fressin, F., et al. 2013, Sci, 340, 587
Borucki, W. J., Koch, D. G., Basri, G., et al. 2011a, ApJ, 728, 117
Borucki, W. J., Koch, D. G., Basri, G., et al. 2011b, ApJ, 736, 19
Borucki, W. J., Koch, D. G., Brown, T. M., et al. 2010, ApJL, 713, L126
Brandenburg, A., Mathur, S., & Metcalfe, T. S. 2017, ApJ, 845, 79
Chen, H., & Rogers, L. A. 2016, ApJ, 831, 180
Christiansen, J. L., Jenkins, J. M., Caldwell, D. A., et al. 2012, PASP, 124, 1279
Curtis, J. L., Agüeros, M. A., Matt, S. P., et al. 2020, ApJ, 904, 140
Dai, F., Winn, J. N., Schlaufman, K., et al. 2020, AJ, 159, 247
David, T. J., Angus, R., Curtis, J. L., et al. 2022, ApJ, 933, 114
David, T. J., Contardo, G., Sandoval, A., et al. 2021, AJ, 161, 265
Duncan, D. K., Vaughan, A. H., Wilson, O. C., et al. 1991, ApJS, 76, 383
Eddy, J. A. 1976, Sci, 192, 1189
Fossati, L., Ayres, T. R., Haswell, C. A., et al. 2013, ApJL, 766, L20
Fulton, B. J., & Petigura, E. A. 2018, AJ, 156, 264
Fulton, B. J., Petigura, E. A., Howard, A. W., et al. 2017, AJ, 154, 109
Fulton, B. J., Weiss, L. M., Sinukoff, E., et al. 2015, ApJ, 805, 175
Gautier, T. N., Batalha, N. M., Borucki, W. J., et al. 2010, arXiv:1001.0352
Gomes da Silva, J., Santos, N. C., Adibekyan, V., et al. 2021, A&A, 646, A77
Hall, J. C., Lockwood, G. W., & Skiff, B. A. 2007, AJ, 133, 862
Hall, O. J., Davies, G. R., van Saders, J., et al. 2021, NatAs, 5, 707
Henry, T. J., Soderblom, D. R., Donahue, R. A., & Baliunas, S. L. 1996, AJ, 111, 439
Howard, A. W., Sanchis-Ojeda, R., Marcy, G. W., et al. 2013, Natur, 503, 381
Hsu, D. C., Ford, E. B., Ragozzine, D., & Ashby, K. 2019, AJ, 158, 109
Hunter, J. D. 2007, CSE, 9, 90
Isaacson, H., & Fischer, D. 2010, ApJ, 725, 875
Johnson, J. A., Petigura, E. A., Fulton, B. J., et al. 2017, AJ, 154, 108
Judge, P. G., & Saar, S. H. 2007, ApJ, 663, 643
Kolbl, R., Marcy, G. W., Isaacson, H., & Howard, A. W. 2015, AJ, 149, 18
Kosiarek, M. R., & Crossfield, I. J. M. 2020, AJ, 159, 271
Kraft, R. P. 1967, ApJ, 150, 551
Lissauer, J. J., Marcy, G. W., Bryson, S. T., et al. 2014, ApJ, 784, 44
Lopez, E. D., & Fortney, J. J. 2013, ApJ, 776, 2
Lubin, J., Robertson, P., Stefansson, G., et al. 2021, AJ, 162, 61
Luhn, J. K., Wright, J. T., Henry, G. W., Saar, S. H., & Baum, A. C. 2022, ApJL, 936, L23
Mamajek, E. E., & Hillenbrand, L. A. 2008, ApJ, 687, 1264
Masuda, K. 2022, ApJ, 933, 195
Mayor, M., & Queloz, D. 1995, Natur, 378, 355
Mazeh, T., Perets, H. B., McQuillan, A., & Goldstein, E. S. 2015, ApJ, 801, 3
McKinney, W. 2010, in Proc. of the 9th Python in Science Conf., ed. S. van der Walt & J. Millman, 56
McQuillan, A., Mazeh, T., & Aigrain, S. 2014, ApJS, 211, 24
Metcalfe, T. S., & Egeland, R. 2019, ApJ, 871, 39
Metcalfe, T. S., Egeland, R., & van Saders, J. 2016, ApJL, 826, L2
Mittag, M., Schmitt, J. H. M. M., & Schröder, K. P. 2013, A&A, 549, A117
Noyes, R. W., Hartmann, L. W., Baliunas, S. L., Duncan, D. K., & Vaughan, A. H. 1984, ApJ, 279, 763
Owen, J. E., & Wu, Y. 2013, ApJ, 775, 105
Pepe, F., Cameron, A. C., Latham, D. W., et al. 2013, Natur, 503, 377
Perryman, M. A. C., Lindegren, L., Kovalevsky, J., et al. 1997, A&A, 323, L49
Petigura, E. A. 2020, AJ, 160, 89
Petigura, E. A., Howard, A. W., Marcy, G. W., et al. 2017, AJ, 154, 107
Petigura, E. A., Marcy, G. W., Winn, J. N., et al. 2018, AJ, 155, 89
Petigura, E. A., Rogers, J. G., Isaacson, H., et al. 2022, AJ, 163, 179
Rosenthal, L. J., Fulton, B. J., Hirsch, L. A., et al. 2021, ApJS, 255, 8
Rowe, J. F., Bryson, S. T., Marcy, G. W., et al. 2014, ApJ, 784, 45
Saar, S. H. 2006, AAS/SPD Meeting, 37, 12.01
Saar, S. H. 2011, in ASP Conf. Ser. 448, 16th Cambridge Workshop on Cool Stars, Stellar Systems, and the Sun, ed. C. Johns-Krull, M. K. Browning, & A. A. West (San Francisco, CA: ASP), 1239
Sanchis-Ojeda, R., Rappaport, S., Winn, J. N., et al. 2014, ApJ, 787, 47
Santos, A. R. G., Breton, S. N., Mathur, S., & García, R. A. 2021, ApJS, 255, 17
Shah, S. P., Wright, J. T., Isaacson, H., Howard, A. W., & Curtis, J. L. 2018, ApJL, 863, L26
Skumanich, A. 1972, ApJ, 171, 565
Su, T., Zhang, L.-y., Long, L., et al. 2022, ApJS, 261, 26
Thompson, S. E., Coughlin, J. L., Hoffman, K., et al. 2018, ApJS, 235, 38
Valenti, J. A., & Fischer, D. A. 2005, ApJS, 159, 141
van der Walt, S., Colbert, S. C., & Varoquaux, G. 2011, CSE, 13, 22
Van Eylen, V., Agentoft, C., Lundkvist, M. S., et al. 2018, MNRAS, 479, 4786
van Saders, J. L., Ceillier, T., Metcalfe, T. S., et al. 2016, Natur, 529, 181
Vaughan, A. H., Preston, G. W., & Wilson, O. C. 1978, PASP, 90, 267
Walkowicz, L. M., & Basri, G. S. 2013, MNRAS, 436, 1883
Weiss, L. M., Marcy, G. W., Petigura, E. A., et al. 2018, AJ, 155, 48
Wright, J. T. 2004, AJ, 128, 1273
Wright, J. T., Marcy, G. W., Butler, R. P., et al. 2008, ApJL, 683, L63
Wright, J. T., Marcy, G. W., Butler, R. P., & Vogt, S. S. 2004, ApJS, 152, 261
Zhang, J., Bi, S., Li, Y., et al. 2020, ApJS, 247, 9

3.3 Links and implications

We have provided a catalog of stellar activity properties of planet host stars discovered by the *Kepler* spacecraft. They are homogeneously derived along with precise stellar parameters and can be used at the population level to establish trends between the properties of planet hosting stars and planet properties. The planet properties can include planet radius, planet mass and atmospheric composition. We explore stellar metallicity effects that have been linked to exoplanet properties such as the occurrence rate of Hot Jupiters (Fischer and Valenti 2005) and the impact of magnetic braking in F-type stars (Amard and Matt 2020; Amard et al. 2020). The level of precision in the activity measurements presented here is unparalleled. The population of stars with activity measurements has already been used in models that describe the underlying physics of magnetic fields in Sun-like stars. These survey properties allow for the identification of subtle astrophysics that can be lost in the diversity of exoplanet properties and the properties of their host stars. Stellar dynamos, rotation periods and stellar activity are deeply correlated and stellar surveys such as this can help to link the observations to theoretical models, so long as the observations are uniform and homogeneous.

CHAPTER 4: THE CALIFORNIA LEGACY SURVEY. V. CHROMOSPHERIC ACTIVITY CYCLES IN MAIN SEQUENCE STARS

4.1 Introduction

We will extract new value from the time-series dateset that was used to quantify the occurrence of Jovian planets in decades long orbits (Rosenthal et al. 2021; Fulton et al. 2021) to catalog the largest sample of activity cycles since the original Mount Wilson H & K Survey (Baliunas et al. 1995). Our catalog will consist of time-series measurements of high-resolution spectra of nearby stars, and our results will highlight the value of ground-based astronomical surveys, specifically those that provide consistent, reliable data over timescales of decades. With constantly changing technology and variations in scientific budgets, such consistency is increasingly difficult to find. The Keck Observatory leads the field in long-term strategic planning and execution of independently led scientific programs. In particular, the CLS data set that will be used to identify activity cycles was collected on the same detector from 2004–2024, with nightly optical alignment that results in rest-frame stability of one pixel. This is the level of precision required for the extraction of subtle flux values that are input to S-value time-series. After using the time-series to catalog activity cycles, we will use the precise stellar parameters, that are uniformly determined across the entire sample, to show that stellar effective temperature plays a critical role in determining the cycle period for stars between 1 and 4 Gyr.

4.2 Published paper

THE ASTROPHYSICAL JOURNAL SUPPLEMENT SERIES, 274:35 (22pp), 2024 October https://doi.org/10.3847/1538-4365/ad676c

The California Legacy Survey. V. Chromospheric Activity Cycles in Main-sequence Stars

Howard Isaacson[1,2], Andrew W. Howard[3], Benjamin Fulton[4], Erik A. Petigura[5], Lauren M. Weiss[6], Stephen R. Kane[2,7], Brad Carter[2], Corey Beard[8,20], Steven Giacalone[3,19], Judah Van Zandt[5], Joseph M. Akana Murphy[9,20], Fei Dai[3,10,19], Ashley Chontos[11,12,18], Alex S. Polanski[13], Malena Rice[14], Jack Lubin[5,8], Casey Brinkman[11], Ryan A. Rubenzahl[3,19,21], Sarah Blunt[15], Samuel W. Yee[12,18], Mason G. MacDougall[5], Paul A. Dalba[9,20], Dakotah Tyler[5], Aida Behmard[16], Isabel Angelo[5], Daria Pidhorodetska[7,20], Andrew W. Mayo[1,17], Rae Holcomb[8], Emma V. Turtelboom[1], Michelle L. Hill[7], Luke G. Bouma[3], Jingwen Zhang[11,20], Ian J. M. Crossfield[13], and Nicholas Saunders[11]

[1] 501 Campbell Hall, University of California at Berkeley, Berkeley, CA 94720, USA; hisaacson@berkeley.edu
[2] Centre for Astrophysics, University of Southern Queensland, Toowoomba, QLD, Australia
[3] Department of Astronomy, California Institute of Technology, Pasadena, CA 91125, USA
[4] NASA Exoplanet Science Institute/IPAC, California Institute of Technology, MC 314-6, 1200 E. California Blvd., Pasadena, CA 91125, USA
[5] Department of Physics & Astronomy, University of California Los Angeles, Los Angeles, CA 90095, USA
[6] Department of Physics and Astronomy, University of Notre Dame, Notre Dame, IN 46556, USA
[7] Department of Earth and Planetary Sciences, University of California, Riverside, CA 92521, USA
[8] Department of Physics & Astronomy, University of California Irvine, Irvine, CA 92697, USA
[9] Department of Astronomy and Astrophysics, University of California, Santa Cruz, CA 95064, USA
[10] Division of Geological and Planetary Sciences, California Institute of Technology, 1200 E. California Blvd., Pasadena, CA 91125, USA
[11] Institute for Astronomy, University of Hawai‘i, 2680 Woodlawn Dr., Honolulu, HI 96822, USA
[12] Department of Astrophysical Sciences, Princeton University, 4 Ivy Ln., Princeton, NJ 08544, USA
[13] Department of Physics & Astronomy, University of Kansas, 1082 Malott, 1251 Wescoe Hall Dr., Lawrence, KS 66045, USA
[14] Department of Astronomy, Yale University, New Haven, CT 06511, USA
[15] Center for Interdisciplinary Exploration and Research in Astrophysics (CIERA) and Department of Physics and Astronomy, Northwestern University, Evanston, IL 60208, USA
[16] Department of Astrophysics, American Museum of Natural History, 200 Central Park W., Manhattan, NY 10024, USA
[17] Centre for Star and Planet Formation, Natural History Museum of Denmark & Niels Bohr Institute, University of Copenhagen, Øster Voldgade 5-7, DK-1350 Copenhagen K., Denmark
Received 2024 May 12; revised 2024 June 25; accepted 2024 July 8; published 2024 September 30

Abstract

We present optical spectroscopy of 710 solar neighborhood stars collected over 20 years to catalog chromospheric activity and search for stellar activity cycles. The California Legacy Survey stars are amenable to exoplanet detection using precise radial velocities, and we present their Ca II H and K time series as a proxy for stellar and chromospheric activity. Using the High Resolution Echelle Spectrometer at Keck Observatory, we measured stellar flux in the cores of the Ca II H and K lines to determine *S*-values on the Mount Wilson scale and the $\log(R'_{\rm HK})$ metric, which is comparable across a wide range of spectral types. From the 710 stars, with 52,372 observations, 285 stars were sufficiently sampled to search for stellar activity cycles with periods of 2–25 yr, and 138 stars showed stellar cycles of varying length and amplitude. *S*-values can be used to mitigate stellar activity in the detection and characterization of exoplanets. We used them to probe stellar dynamos and to place the Sun's magnetic activity into context among solar neighborhood stars. Using precise stellar parameters and time-averaged activity measurements, we found tightly constrained cycle periods as a function of stellar temperature between $\log(R'_{\rm HK})$ of −4.7 and −4.9, a range of activity in which nearly every star has a periodic cycle. These observations present the largest sample of spectroscopically determined stellar activity cycles to date.

Unified Astronomy Thesaurus concepts: Stellar astronomy (1583); Main sequence stars (1000); Time series analysis (1916); Stellar chromospheres (230); Stellar activity (1580); Stellar evolution (1599); High resolution spectroscopy (2096); Optical telescopes (1174)

Materials only available in the online version of record: figure set, machine-readable tables

1. Introduction

Long-term, ground-based spectroscopic surveys are a pathway to understanding the Sun and its planets in the context of the solar neighborhood and to finding Earth-analog exoplanet systems. Such surveys can probe the depth of the convective zone, detect differential rotation, and track Sunlike stellar activity cycles. Chromospheric activity studies provide fascinating insights into the subsurface layers of stars that are not directly observable. Over the last two decades, these studies have been buoyed by radial velocity (RV) searches for exoplanets due to the collection of time cadence observations that include spectral information that can be used for both measuring precise RVs of stars and monitoring stellar chromospheric activity (Gomes da Silva et al. 2021; Rosenthal et al. 2021, hereafter CLS1).

[18] Henry Norris Russell Fellow.
[19] NSF Astronomy and Astrophysics Postdoctoral Fellow.
[20] NASA FINESST Fellow.
[21] NSF Graduate Research Fellow.

Nightly surveying of the chromospheric activity of nearby stars in the Mount Wilson Observatory HK Project began in 1966 (Wilson 1968) and continued for several decades (Vaughan et al. 1978). This survey detected variable stellar lines and identified the link between the Ca II H and K lines and the solar chromosphere (Eberhard & Schwarzschild 1913). After decades of data collection on F2–M2-type stars—an effort necessary to identify stellar activity cycles in some G0–K5 stars with activity periods similar to the Sun's 11 yr solar cycle—the results were summarized (Duncan et al. 1991) and the first catalog of stellar activity cycles was published (Baliunas et al. 1995). Out of 111 solar-type stars searched, 52 showed cycles, and 31 were flat or had linear trends. Another 29 stars had nonperiodic, variable activity. The conclusions put the Sun's activity cycle into the broader perspective of Sunlike stars in the solar neighborhood, showing that stellar activity cycles are common.

Several long-term ground-based surveys have contributed to our understanding of stellar magnetic activity. Identification of stellar activity cycles using Mount Wilson data combined with California Planet Search (CPS) data from the High Resolution Echelle Spectrometer (HIRES) at the W. M. Keck Observatory yielded baselines of 50 yr for 59 stars (Baum et al. 2022). Time-series spectroscopic observations of Sunlike stars include a survey of 800 Southern solar-type stars within 50 pc (Henry et al. 1996) and 143 Sunlike stars from 1996–2007 (Hall et al. 2007). These studies focused on measuring the average stellar variability, not stellar cycles. Fifty-three previously identified activity cycles were analyzed using S-values from the Mount Wilson Observatory HK Project and the High Accuracy Radial Velocity Planet Searcher (HARPS) telescope (Boro Saikia et al. 2018), but even the extended HARPS baseline was insufficient for identifying new stellar activity cycles that span years to decades. See Jeffers et al. (2023) for a comprehensive review of stellar activity cycles.

Stellar activity and planet searches that use the RV technique have contributed to our knowledge of Jupiter-mass planets with orbital periods of more than 10 yr and to the identification of solar-like stellar cycles (Wright et al. 2008; Fulton et al. 2021). Wright et al. (2004) and Isaacson & Fischer (2010) presented activity catalogs from Keck/HIRES and began to quantify the relationship between RV jitter and chromospheric activity. Luhn et al. (2020) examined 600 CPS stars to make RV jitter assessments that included dependence on stellar surface gravity. A summary of the ground-based spectroscopic survey of the AMBRE-HARPS sample (Gomes da Silva et al. 2021) resulted in an activity catalog of planet search stars in the Southern Hemisphere, with stellar activity time-series analysis forthcoming. Detecting Jupiter analogs requires forward-thinking surveys and understanding their dynamical impact in multiplanet systems will inform the study of solar-like planetary systems (Kane 2023).

In an analysis of Southern Hemisphere planet search stars similar to the Northern Hemisphere sample presented here, Lovis et al. (2011) analyzed seven years of HARPS S-values for 304 FGK-type stars and presented a catalog of 99 magnetic cycles and an analysis of the stellar activity impact on precise RVs. Using the Hα line as an activity metric Robertson et al. (2013) searched 93 K- and M-type stars using the High Resolution Spectrograph on the Hobby–Eberly Telescope at McDonald Observatory and identified examples of how activity cycles can mimic those of giant planets. These two catalogs provide examples of how planet search data has been used to study magnetic activity.

Only with long-term baselines of activity and RVs are the periodic signals of planets distinguished from quasiperiodic activity signals. In some cases, a stellar activity cycle is correlated with the RVs, making the planet interpretation ambiguous (Rosenthal et al. 2021). Kane et al. (2016) identified a stellar activity cycle in HD 99492, a planet-hosting system, while Dragomir et al. (2012) found a photometric activity cycle. Correlations between RVs and S-values over a single period of the planet's orbit or the stellar activity cycle are difficult to disentangle (Wright et al. 2008; Fulton et al. 2015). But if the baseline is extended sufficiently, the activity cycle may go out of phase, while a planet will maintain strict periodicity (Wright 2016). Stellar activity cycles have been probed by other spectral features that are sensitive to activity. The M dwarf GJ 328 has a confirmed planet along with a stellar activity cycle that was identified with Hα line measurements. The CARMENES planet search, which focuses on M dwarfs, has produced a catalog of $\log(R'_{\rm HK})$ measurements to assist in the interpretation of planet candidates (Perdelwitz et al. 2021).

Wide-field, space-based photometry is now available to search for transiting planets, measure stellar rotation periods, and monitor stellar activity. Such photometry is particularly useful for the determination of stellar rotation periods (McQuillan et al. 2014; Angus et al. 2018), and it has revolutionized rotation studies. Kepler data can be searched for stellar activity cycles, with thousands of cycle candidates (Shen et al. 2022), but the four-year duration of the Kepler mission makes it difficult for us to find solar-like cycles.

Long-term ground-based photometry can be used to find stellar activity cycles, but it is only sensitive to cycles for stars with large spot coverage such as M dwarfs. Irving et al. (2023) examined activity cycles for a collection of M dwarf stars. The coolest M dwarfs, M4 and later, require a different mechanism for magnetic field generation than solar-type stars since they lack a radiative–convective boundary. Spectral analyses of the Ca II H and K lines probe the chromosphere and the magnetic activity below the observable stellar surface, which are complementary to the results of photometric surveys. Photometric studies of activity cycles in M dwarfs have identified cycles in fully convective M dwarfs with masses as low as $0.12\,M_\odot$ (Savanov 2012; Suárez Mascareño et al. 2016, 2018; Wargelin et al. 2017).

Ground-based photometric surveys have been used to calibrate the age–activity–rotation relationship (Barnes 2007; Mamajek & Hillenbrand 2008) by correlating the stellar rotation periods of open clusters with well-determined ages. Time-averaged chromospheric flux measurements have been used to parameterize the physical mechanisms at work below the observable stellar photosphere. The Rossby number, the ratio of the rotation period to the convective turnover time (Noyes et al. 1984), is the standard metric for quantifying magnetic activity and its relationship to stellar rotation.

Observations of stellar rotation periods, combined with stellar activity cycles, are fleshing out the magnetic activity evolution of stars as their rotation periods decline over time through weakened magnetic braking (van Saders et al. 2016; David et al. 2022; Metcalfe et al. 2022). By combining Ca II H and K measurements with rotation periods, and direct measurements of the magnetic field through spectropolarimetry (Marsden et al. 2014; Metcalfe et al. 2024), more complete

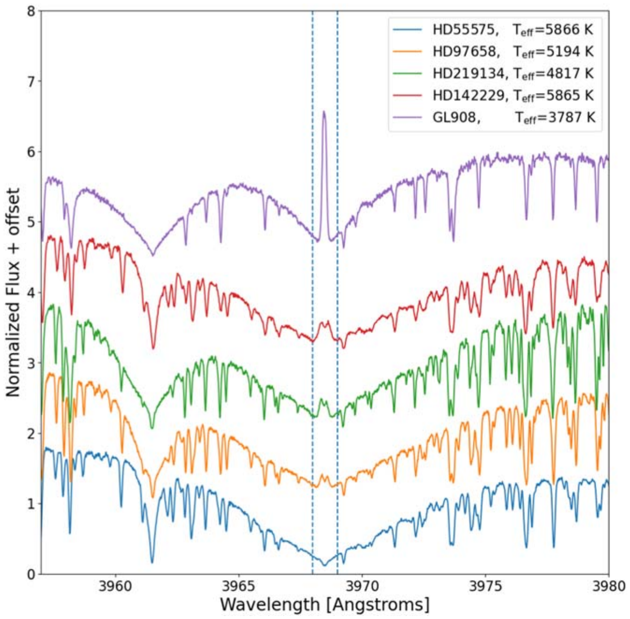

Figure 1. Ca H lines for a variety of effective temperatures from our survey, offset vertically for clarity. The dashed lines mark the center of the extracted flux region for the H line. From bottom to top: HD 55575 ($T_{\rm eff} = 5866$ K, S-value = 0.156), HD 97658 ($T_{\rm eff} = 5194$ K, S-value = 0.186), HD 219134 ($T_{\rm eff} = 4817$ K, S-value = 0.246), HD 142229 ($T_{\rm eff} = 5865$ K, S-value = 0.364), and GL 908 ($T_{\rm eff} = 3787$ K, S-value = 0.54).

explanations of the stellar dynamo are now coming into focus. We add to the observational evidence that can be used to understand main-sequence magnetic changes and potentially to explain weakened magnetic braking.

We present 20 years of stellar chromospheric activity time series for 710 nearby (median distance of 30 pc) main-sequence FGKM stars, analyze average activity in terms of fundamental stellar properties, and search for activity cycles like the Sun's 11 yr cycle. Section 2 discusses the observations and data quality. Section 3 discusses the CLS1 stellar sample and compares it to those of previously published works. Section 4 discusses our 285-star sample that is searched for cycles. Section 5 explores the activity cycles in terms of the stellar properties for 138 stars with detected cycles and Section 6 reveals the relationship between cycle period and $T_{\rm eff}$.

2. Observations

2.1. Data Source and Quality

The CLS1 paper provided RVs measured from data collected from the middle of three detectors (4976–6421 Å), and the S-values were simultaneously measured using data from the blue detector (3642–4797 Å). We used an updated raw reduction that converted 2D spectra to 1D spectra (Howard et al. 2010). This work improves the quality of the S-values as compared to CLS1 by using a restricted extraction width of eight pixels to reduce sky emission and scattered light contamination and by making additional quality controls. A sample of Ca H line profiles for properly reduced spectra in good seeing are shown in Figure 1.

HIRES spectra were collected with a variety of decker apertures. The primary science deckers for CPS are B5 ($0\farcs87 \times 5''$) and C2 ($0\farcs87 \times 14''$), which provide a resolution of 60,000. Two other deckers, B1 ($0\farcs5 \times 5''$) and B3 ($0\farcs5 \times 14''$), are used for templates and result in a resolution of 80,000. The C2 decker began operation in 2009 June, when the typical visual magnitude of RV targets changed from $V \sim 8$, for nearby-star surveys, to $V \sim 12$, for follow-up of Kepler planet-host stars. Sky contamination became a limiting factor in RV precision, requiring observations with the C2 decker (Marcy et al. 2014), at the occasional expense of useful S-value measurements. The B5 decker was used for stars brighter than $V \sim 10$, and C2 was used for fainter stars and for observations taken during twilight, when CLS1 stars were often observed.

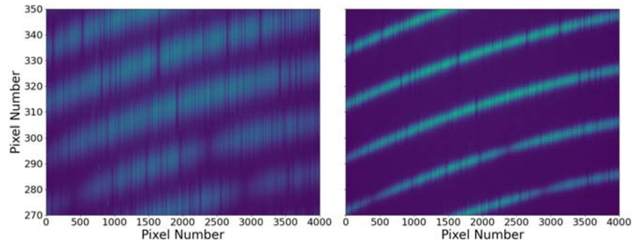

Figure 2. Two raw images of HD 141399 showing the Ca II H and K region. Left: seeing measured to be $2\farcs5$. Right: seeing measured to be $0\farcs9$. The extraction width in the cross-dispersion (vertical) direction is limited to eight pixels.

The height of the C2 and B3 deckers allows for simultaneous observations of sky pixels and causes order overlap on the middle CCD, and increasing overlap blueward. Echelle spectrographs with cross-dispersing gratings have blue orders closer together and red orders with larger separation, and the opposite is true for cross-dispersing prisms. The raw reduction has been tailored to account for this in the middle detector, resulting in equal RV precision for B5 and C2. For S-values, the additional overlap near the Ca II H and K lines is more problematic and causes degraded quality for observations taken in poor seeing conditions. By measuring the stellar profile in the spatial direction, we calculated the average seeing for each observation. Using chromospherically inactive stars, we identified the upper limit of $1\farcs6$ to be the critical seeing value required to avoid order-to-order contamination when observing with the C2 or B3 decker (Baum et al. 2022). We excluded S-values with seeing measurements beyond this value from our sample, removing 1549 S-values. The B5 and B1 deckers with their shorter height do not have order overlap and do not have this restriction. Figure 2 shows 2D echellegrams for the star HD 141399 taken in seeing conditions of $2\farcs5$ and $0\farcs9$, showing the order overlap that occurs during poor seeing conditions. In addition to the quality control described above, we visually examined exceptionally low S-values and excluded 98 observations with poor extractions.

2.2. S-value Error

We previously adopted the S-value error of 0.002, or 1% per individual observation, by assessing the S-value distribution of HD 10700 (τ Cet), a star with a well-established low level of activity (Isaacson & Fischer 2010). Our extended time baseline yields a dispersion of the HD 10700 S-values of 0.82% (0.00139/0.1675). We identified other stars with very low S-value variation, including HD 55575, our least active star that has a dispersion of $0.0007/0.156 = 0.45\%$. We adopted an S-value error of 0.001 for all observations, a value between the dispersions of HD 10700 and HD 55575. The HARPS-AMBRE survey found a dispersion of 0.83% for HD 10700,

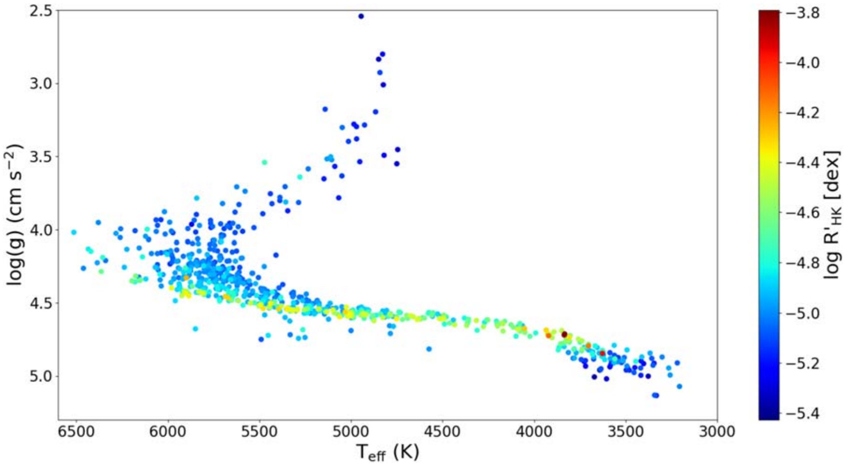

Figure 3. Stellar surface gravity as a function of effective temperature is plotted, with the median $\log(R'_{HK})$ value for each of the 710 stars in the California Legacy Survey activity sample represented on the color scale. Subgiants are visible at lower $\log(g)$ values, while the few very-low-metallicity subdwarfs in our sample fall below the main sequence. Most stars in our sample are slowly rotating FGKM stars on the main sequence.

showing that this precision level is achievable (Gomes da Silva et al. 2021). We discuss the least active stars in Section 5.6.

2.3. Sampling

The CLS1 survey required 10 RV observations over 8 yr (since 2005) on HIRES (Figure 2 in CLS1) to be included in their analysis. They supplemented their data set with pre-2005 HIRES RVs and Lick Observatory RVs (Fischer et al. 2014). We do not include the Lick Observatory *S*-values nor the pre-2005 HIRES *S*-values. We considered adding *S*-values from the Automated Planet Finder, but there is no additional baseline since the first observations were taken in 2014. Since CLS1 we have collected four additional years of *S*-values, improving the baseline for many stars.

We are primarily focused on finding stellar activity cycles with periods between 2 and 25 yr, so we require 45 observations since 2005. Stars with fewer, often sporadically timed, observations are insufficient for robustly detecting activity cycles. We include stars with as few as five measurements for the average activity analysis. Out of the 710 stars in our sample, we search 285 for cycles, and the 425 additional stars are included in the summary activity analysis.

2.4. Data Validation and Rejection

To ensure the highest-quality data set, we start by adding *S*-values for non-iodine observations that were omitted from CLS1 because they do not contribute to the RV time series. The spectral segments used to calculate the *S*-values are shifted and scaled to a high signal-to-noise ratio (SNR) template of that same star (Isaacson & Fischer 2010). For 11 stars, no such template exists, so we use a spectrum of Vesta, a reflective spectrum of the Sun, that is shifted to observatory wavelength solution. Vesta spectra have the benefit of having the same format and blaze function as all other HIRES spectra. Those stars are HD 114762, HD 120136, HIP 60633, HD 152391, HD 10853, HD 6101, HD 112914, HD 167042, HD 73344, HD 177153, and HD 8375. *S*-values for these stars have the same quality and uncertainties as the others.

We make the following requirements at the level of individual observations for quality control:

1. *S*-values less than 0.10 are rejected as nonastrophysical. Fifty-six *S*-values are removed, and 98 are identified by eye as having poor extractions.
2. The SNR must be greater than 7 at continuum near 4000 Å, removing 276 *S*-values. One star, GL 406, has no observations that meet this threshold and is omitted throughout our analysis. See Bowens-Rubin et al. (2023) for a detailed analysis of this star.
3. The seeing must be less than 1.″6 for C2 and B3 observations, excluding 1549 *S*-values from our sample.
4. Stars with $T_{eff} < 4000$ K are visually inspected and stars with Ca II H and K activity that extends beyond the 1.09 Å full width at half-maximum window that is used to calculate *S*-values are removed. Eight flare stars have flux emission in the H and K region that is not well modeled using *S*-values and are excluded. These stars also have a spectral helium line in emission that resides very near the H line, causing further ambiguity in the *S*-value measurement. The stars excluded are GL 83.1, GL 876, GL 905, HIP 112460, HIP 37766, HIP 5643, HIP 92403, and HD 75732B.
5. We retain 52,372 *S*-values from 2005 through 2023 October for 710 stars.

3. The 710-star Activity Sample

3.1. Overview

To assess the average activity of our sample we begin with the 710-star CLS1 sample that consists of slowly rotating FGK- and M-type stars that are amenable to RV measurements in search of exoplanets. Figure 3 presents our sample in the $\log(g)$ versus T_{eff} plane showing the average activity, ($\log R'_{HK}$), as a color scale. The sample is assembled to offer consistent sensitivity to long-period giant planets out to tens of astronomical units. The minimum baseline chosen of 8 yr, with 10 observations from HIRES and 20 total RVs, complements our search for stellar activity cycles, which tend to range from 2 to 25 yr (Baliunas et al. 1995; Baum et al. 2022). With many observations spanning the timescale of typical activity cycles, we present accurate measurements of the average activity for each star.

The California Legacy Survey (CLS) sample was originally selected to exclude stars that host known transiting planets and stars with known high metallicity. Samples of stars that focused on subgiants and young stars and those that had long-baseline observations due to the presence of hot Jupiters were also excluded. There are 178 known exoplanets or brown dwarfs around the stars in our sample.

3.2. Stellar Property Corrections

We amend the stellar property catalog from Rosenthal et al. (2021) by filling parameter values for five stars lacking $T_{\rm eff}$. For HD 134439 and HD 134440, chemically peculiar twin stars in a binary system with a long-period orbit, we use the $T_{\rm eff}$, $\log(g)$, [Fe/H], and $M_\star$ from Chen et al. (2014). For HD 201092 and HIP 106924, we add the $T_{\rm eff}$ from our SpecMatch-Synthetic analysis of HIRES spectra (Petigura et al. 2017). We obtain the extremely low metallicity value of −2.5 for HIP 106924 from Joyce & Chaboyer (2018). For GL 528 B, we apply the SpecMatch-Empirical code to a HIRES spectrum (Yee et al. 2017). These are important additions since we are interested in the dependence of activity on $T_{\rm eff}$.

3.3. Derived Properties

We calculate $\log(R'_{\rm HK})$ (Noyes et al. 1984) and stellar age (Mamajek & Hillenbrand 2008) to examine activity correlations with fundamental and derived stellar properties and to check for correlations with activity cycle properties. Cincunegui et al. (2007), Suárez Mascareño et al. (2015), Astudillo-Defru et al. (2017), Mittag et al. (2013), and Marvin et al. (2023) each extend the $\log(R'_{\rm HK})$ calibration to cool stars ($B - V = 1.6$) and $T_{\rm eff} = 2700$ K. We use the Noyes et al. (1984) method to enable cross-referencing with other works, rather than the Marvin et al. (2023) method, which overestimates the color correction factor resulting in the overestimation of $\log(R'_{\rm HK})$.

Since $B - V$ colors are used to calculate $\log(R'_{\rm HK})$, we derive $B - V$ using the Ramírez & Meléndez (2005) method, which uses both $T_{\rm eff}$ and [Fe/H] and is valid at $T_{\rm eff}$ of 7000–3870 K. For stars cooler than 3870 K, we use the CLS1 $B - V$ values. As a result, we use the Noyes et al. (1984) method for all of our analysis of $\log(R'_{\rm HK})$ and derived stellar parameters. The use of consistent $T_{\rm eff}$ values when converting to $\log(R'_{\rm HK})$ will be critical to our analysis of activity in relation to cycle period. With this choice, we urge caution when using $\log(R'_{\rm HK})$ values for stars cooler than 3870 K due to the uncertainty in $B - V$.

3.4. The 710 Stellar Activity Analysis

Our stellar sample is presented in temperature versus surface gravity space in Figure 3 with a color scale indicating the stellar activity, $\log(R'_{\rm HK})$. The prominently positioned subgiant stars that rise above the main sequence have the lowest stellar surface gravity values. Subgiant stars, with their larger stellar radii, typically have less stellar activity than main-sequence stars of the same $T_{\rm eff}$. As they evolve and expand, their rotation rate slows to conserve angular momentum, and the decrease in density produces a more subdued stellar dynamo.

The zero-age main sequence is visible as active stars with high $\log(R'_{\rm HK})$. Subdwarfs, with extremely low metallicities and old ages, fall below the zero-age main sequence. The coolest stars in our sample, below 4000 K, have a variety of activity values including the eight eruptive variables we exclude. This

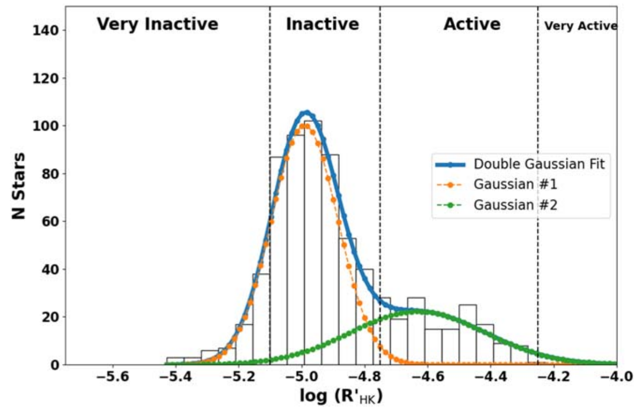

Figure 4. The distribution of our $\log(R'_{\rm HK})$ data is modeled with a double Gaussian model with peaks at −5.001 and −4.886. We find less structure than Gomes da Silva et al. (2021), perhaps due to the smaller number of stars in our survey compared to theirs. Activity qualifiers come from Wright et al. (2004). All 710 stars are included here.

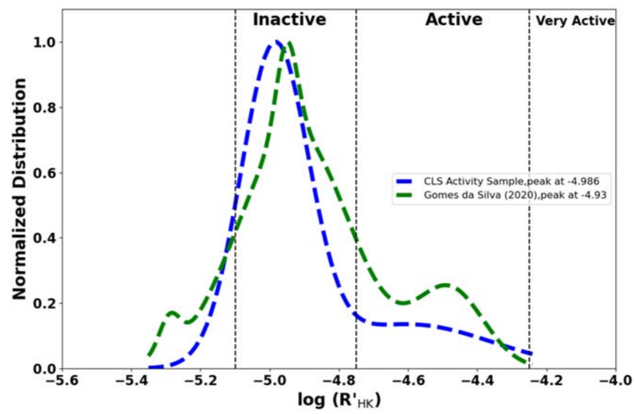

Figure 5. The distribution of our $\log(R'_{\rm HK})$ data is modeled with a double Gaussian model and compared with that of Gomes da Silva et al. (2021), which had a $T_{\rm eff}$ lower limit of 4500 K. Our sample extends to $T_{\rm eff}$ of 3000 K so we omit stars cooler than 4500 K from this plot to make the comparison more direct. We see the two main peaks show up in both our sample and that of Gomes da Silva et al. (2021). Our main peak is slightly offset in the direction of less activity. Gomes da Silva et al. (2021) modeled four Gaussians compared to our two Gaussians, potentially causing this offset. The amplitude of the offset is 0.10, or twice the calibration offset for *S*-values from different instruments (Mittag et al. 2013). The astrophysical explanation is that CLS gave lower priority to more active stars.

may be due to the $\log(R'_{\rm HK})$ metric being calibrated by Noyes et al. (1984) on Sunlike stars. Values of $\log(R'_{\rm HK})$ are also sensitive to the choice of conversion from $T_{\rm eff}$ to $B - V$. Using the average of the stellar activity time series makes for a robust measurement of the average activity of our sample. Each of the stars in our sample has at least five observations.

We compare our sample to the primary Southern-sky planet search survey, the AMBRE-HARPS survey (Gomes da Silva et al. 2021), by modeling our distribution of $\log(R'_{\rm HK})$ values as a sum of Gaussian contributions. Their catalog contains 1674 planet search stars, and they also focus on slowly rotating F-, G-, and K-type stars. Figure 4 shows our two-Gaussian fit to our 710-star sample and Figure 5 shows our sample compared to the AMBRE-HARPS sample. We normalize the *y*-axis and remove stars cooler than 4500 K in this plot to make as direct a comparison as possible. Their sample shows more structure than ours, and peaks at a slightly more active value. Their small peak near −5.3, attributed to giant stars, is not present in ours, due to our lack of giants. The additional structure for active stars may be due to their larger sample or is perhaps due to the CPS observing strategy of excluding active stars at early points in the survey. One possible systematic difference is the slit-fed versus fiber-fed spectrographs, HIRES and HARPS, respectively. However, we think this is sufficiently addressed in Section 2.1. The Gaussian properties representing our sample are available in Table 1.

We construct histograms for each of the FGK stars to compare the two samples as a function of spectral type (Figure 6). The smaller number of stars in our sample means that features in each distribution are not well defined, which leads to several degenerate model fits for each spectral type. Structurally the comparisons for each type of star are quite similar. The F stars have a broad distribution, represented by two Gaussians at $\log(R'_{\rm HK})$ of −5.018 and −4.934. The G-star distribution is dominated by a primary peak near −5.0 and a secondary peak of more active stars, at −4.50, which is broad and low-amplitude. Our distribution of $\log(R'_{\rm HK})$ for K stars is distinctly triple-peaked, similar to that in Gomes da Silva et al. (2021) but with a smaller peak at higher activity. Overall, we find the by-type comparison to be consistent with that found for planet search stars in the Southern Hemisphere.

3.5. Time-averaged Activity

We plot the S-value and $\log(R'_{\rm HK})$ of the 710-star sample against fundamental stellar properties, highlighting, with different colors, the extreme ends of each stellar property distribution (Figure 7). Maroon data points represent stars with $T_{\rm eff} < 4000$ K. Blue data points represent evolved stars, with $\log(g) < 4.0$. Low-metallicity stars with $[{\rm Fe/H}] < -0.5$ are represented in green. Cyan symbols identify those stars with cycles identified in Section 4.

In panel (A) $T_{\rm eff}$ versus S-values are plotted and the familiar flat floor of activity from 6500 to 5000 K is visible, followed by a steady increase from 5000 to 4000 K (Isaacson & Fischer 2010; Mittag et al. 2013). The slope of the activity floor inverts down to our lowest-$T_{\rm eff}$ stars. There is a lower density of stars from 6000 to 5000 K that is elevated above the primary distribution of very inactive stars. The low-metallicity stars and low-$\log(g)$ stars fall near the S-value floor, as expected for older stars and subgiants. Panel (B), with $\log(R'_{\rm HK})$ as a function of $T_{\rm eff}$, shows that most stars in our sample are between 5000 and 600 K. The more active stars that lie above −4.8 may have cycles but are too variable to be strictly periodic.

Panel (C) plots the median S-value as a function of stellar surface gravity showing the low-gravity stars that have started to evolve off of the main sequence are at the floor of the S-value distribution. The highlighted very-low-metallicity stars mostly fall in a unique parameter space at a $\log(g)$ of 4.6–4.7. Although our metallicity distribution is sparse at $[{\rm Fe/H}] < -0.5$ dex, the difference in S-value at that specific $\log(g)$ is distinct. The elevated population of stars at $T_{\rm eff}$ between 5000 and 6000 K in panel (A) is now compressed in panel (C) at a $\log(g)$ value of 4.5–4.7. This could be related to the age of these stars with younger stars being more active and having higher $\log(g)$. Panel (D) shows the most active stars have $\log(g)$ near 4.5, indicating that they are near the zero-age main sequence.

Panel (E) plots the median S-value for the 710 stars as a function of metallicity. At the bottom of the distribution, the subgiant population spans a wide range of [Fe/H]. Our sample is slightly overrepresented at [Fe/H] greater than solar (45/55%), but is sufficiently populated from ±0.4 such that we can draw conclusions about the presence of stellar activity cycles as a function of metallicity in Section 4.1. The Pearson correlation coefficients between the average S-value and metallicity and also between the S-value rms and metallicity are calculated and found to be less than 0.1 in each case. This suggests there is weak correlation between the spectroscopic activity metric S-value and metallicity, in contrast to photometric correlations to [Fe/H] such as noted in Kepler flare stars (See et al. 2023). Our findings are consistent with Lovis et al. (2011), in which the $B - V$ to temperature conversion accounts for metallicity.

3.6. Activity Variability

The long time baseline over which these observations are collected and the multiple observations for each star lead to robust measures of the average activity of our sample. We examine the variability of S-value as a function of $T_{\rm eff}$, $\log(g)$, and [Fe/H] in Figure 8. Stars below 4000 K are the most variable, with significant variation due to the stellar rotation period variations. These stars are more heavily spotted, confusing our search for sinusoidal stellar activity cycles with periods on timescales of years. We adopt the values of $T_{\rm eff}$, log (g), [Fe/H], $M_\star$, and $R_\star$ from Rosenthal et al. (2021), except where noted in Section 2.1. Table 2 contains the minimum, median, and maximum S-values, S-value rms value, standard deviation, $\log(R'_{\rm HK})$, $\log(R'_{\rm HK})$ rms, number of observations, and activity-derived stellar ages. The S-value time series are provided in Table 3.

4. The 285-star Sample to Search for Activity Cycles

We identify robust stellar activity cycles for use in analysis of stellar cycles as a function of stellar properties, including age. By requiring 45 observations, we define our stellar activity cycle sample of 285 stars. This choice helps to avoid a spurious detection of an activity cycle due to poor sampling.

4.1. Searching the 285-star Sample for Activity Cycles

The patterns of stellar activity can have complex structure on many different timescales, so we choose a simple sinusoidal model, with no eccentricity, to search for signals with periods between 2 and 25 yr. Cycles less than 2 yr are difficult to identify due to seasonal sampling, and ambiguity with rotation periods (Baliunas et al. 1995; Boro Saikia et al. 2018). We expect only the youngest (ages less than 1 Gyr) to have such short stellar activity cycles and the CPS RV planet surveys tend to exclude young stars in blind surveys. Notably, HD 115043 has a stellar activity cycle of 1.7 yr (Boro Saikia et al. 2018), but is not in our sample. HD 22049, ε Eri, has a multiple previously published cycle of 2.2 and 12 yr (Metcalfe et al. 2013) or perhaps a 3 yr, 11 yr, and 34 yr cycle (Fuhrmeister et al. 2023) when the calcium infrared triplet and X-ray measurements are analyzed. We have the sensitivity to detect these cycles with our data, but none of these periods pass our threshold. While the zero-eccentricity sinusoid model is sufficient for uniformly identifying activity cycles, a more complex model should be chosen for modeling young-star cycles and

Table 1
Gaussian Fit Parameters for the Activity Sample

Property Bin	Amplitude 1	Mean 1	Sigma 1	Amplitude 2	Mean 2	Sigma 2	Amplitude 3	Mean 3	Sigma 3	Chi-square	Reduced Chi-square
Full sample (710)	100.2	−4.990	0.1055	22.25	−4.632	0.2136	...	...	...	495	20.6
Comparison (564)	48.58	−4.985	0.097	6.81	−4.599	0.24	...	...	...	490	14.4
F-type stars (47)	7.757	−5.018	0.0508	2.764	−4.833	0.178	...	...	...	19.7	2.19
G-type stars (301)	35.98	−4.985	0.094	2.042	−4.483	0.272	...	...	...	280	11.7
K-type stars (171)	8.216	−4.950	0.068	4.617	−4.734	0.117	6.18	−4.443	0.044	190	6.13

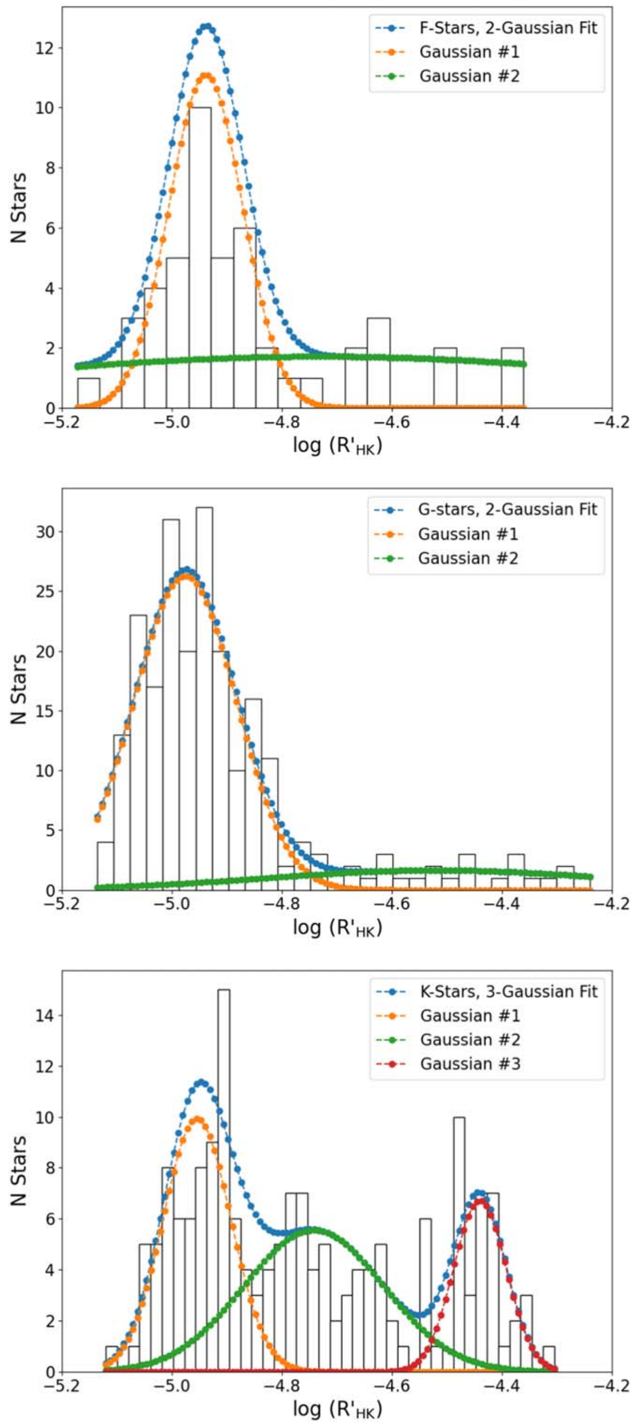

Figure 6. From top to bottom, the distributions of the $\log(R'_{\rm HK})$ for the CLS sample are shown for F stars, G stars, and K stars, with $\log(g) > 4.2$. We model each distribution with a series of Gaussians and compare it to that in Gomes da Silva et al. (2021). Structurally the sample agrees with the AMBRE-HARPS sample of planet search stars from the Southern Hemisphere.

those with complex signals such as the cycles of HD 18803, HD 219134, HD 201092, and HD 140538A.

We utilize the Lomb–Scargle periodogram routine in Astropy[22] and the "model normalization" option to identify peaks in the periodogram and fit a periodic function to the tallest peak. The "model-normalized" periodogram is a periodogram normalized around the residuals to the periodic model, rather than the constant model that is the default method of normalization. This normalization also accounts for the offset from zero typically expected from the generalized Lomb–Scargle periodogram. We limit the periodogram from 100 to 10,000 days (27.4 yr) and explore alternate limits such as 200–2000 days with no effect on recovered activity cycles. The strength of this method is the simplicity of the model, which is easy to parameterize and search. The weaknesses are that stellar activity cycles do not always stay in phase over many cycles, some cycles are better modeled by adding eccentricity, and stars with multiple cycles and different periods are difficult to identify.

We combine two quantitative metrics to identify stellar cycles. First, we calculate the difference between the standard deviation of the initial S-values and the standard deviation of the residuals, divided by the initial S-value standard deviation and the median S-value for that star (Equation (1)). Our threshold by this metric for detection is 1.20. We attempt to use chi-square as the best-fit metric but find the scatter in S-value over timescales of weeks and months makes this metric less useful. We determine the threshold value by ranking our stars with this metric and finding where the cycles become unreliable by eye.

$$\text{Threshold} = \frac{(\text{STD}_{\rm f} - \text{STD}_{\rm i})}{\text{STD}_{\rm i} * \text{Median } (S\text{–value})}. \tag{1}$$

As a secondary metric, we identify cycles through the Lomb–Scargle periodogram as those having a peak greater than 0.5. The maximum peak of any star is 14.0 (HD 192310) and the median peak value for all detected cycles is 2.01. The weakest signal in our data is from GL 699, with a peak value of 0.501. We also remove stars with candidate cycles if the second peak in the periodogram is more than 75% of the primary peak. Such peaks indicate that the identified period is not sufficiently unique for our purposes. Using the ratio of the first and second tallest peaks eliminates many stars that have very plausible cycles but have ambiguous periods. Many stars with cycles much longer than our observing baseline are removed in this quality cut. With the periodogram qualification, we recover 27 cycles that do not pass our threshold from Equation (1), including all of the detected cycles in stars below $T_{\rm eff}$ of 4400 K. By including our reliability metrics for all 285 stars, future studies can choose different thresholds to fit their analysis needs.

For three stars, we remove a linear trend and afterward detect an activity cycle. These trends are indicative of a second cycle, as has been studied most recently by Mittag et al. (2023). Those stars are HD 219134, HD 158633, and HD 82943. When a trend is removed for HD 23356 and HD 201092, they show candidate cycles but do not pass the quantitative thresholds. Generally, our search method is insensitive to cycles longer than our baseline of 20 yr and fails to robustly identify any previously unknown secondary cycles.

These combined metrics detect stars with incredibly small overall variations such as HD 126614 with a peak-to-peak S-value amplitude fit value of 0.0041. For comparison, HD 10700, considered an activity standard, has an S-value standard deviation of 0.0012 and a relative dispersion of 0.8%. The least active stars with and without cycles are discussed in

[22] https://docs.astropy.org/en/stable/timeseries/lombscargle.html, Astropy's Lomb–Scargle periodogram; see section on normalization = 'model'.

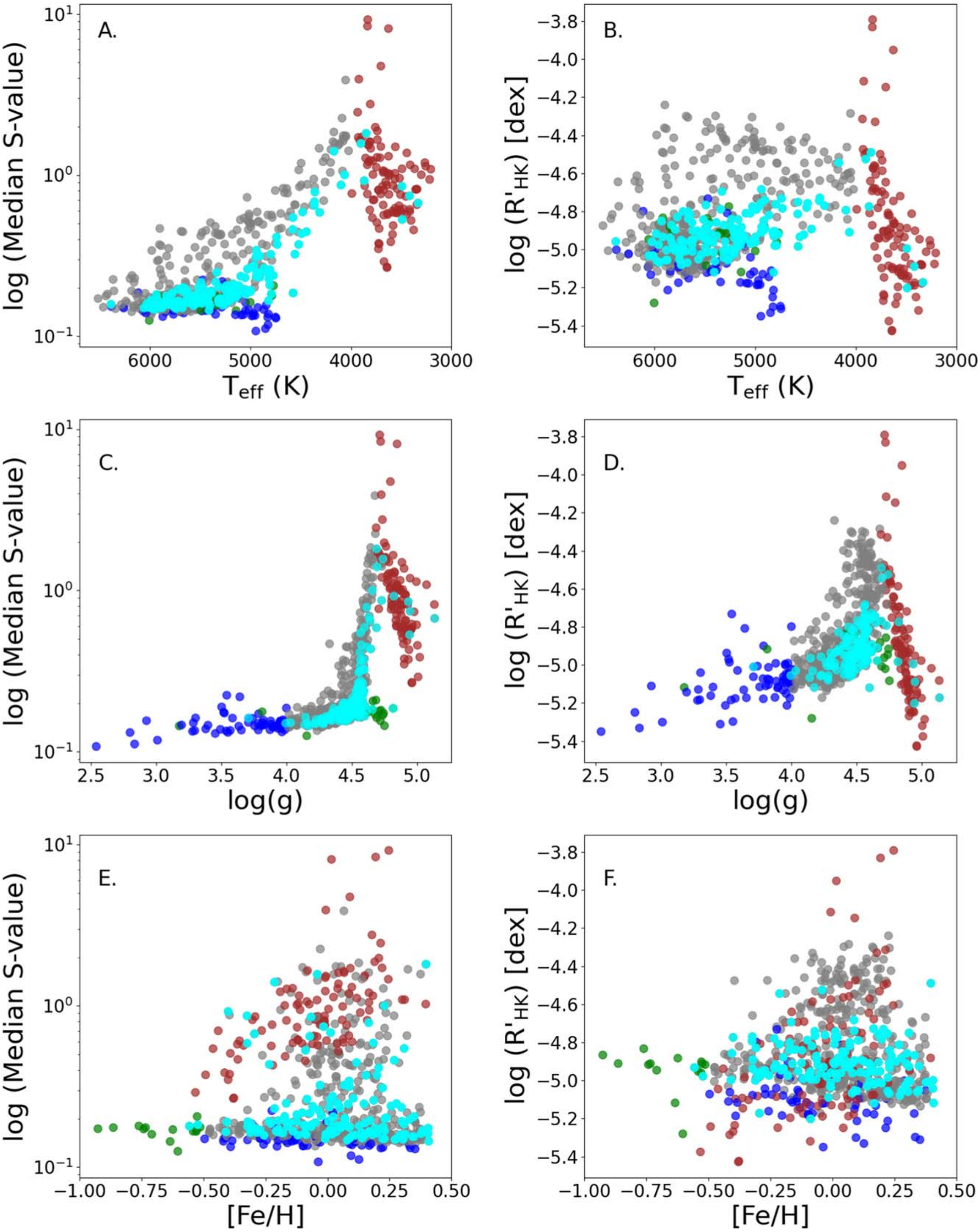

Figure 7. The values of T_{eff} (panels (A) and (B)), stellar surface gravity (panels (C) and (D)), and [Fe/H] (panels (E) and (F)) are plotted vs. the S-value and $\log(R'_{\mathrm{HK}})$ for the 710 stars. Maroon data points represent cool stars, with $T_{\mathrm{eff}} < 4000$ K. Blue data points are stars with $\log(g) < 4.0$, i.e., subgiants, and green data points represent stars with metallicity less than -0.5. Cyan symbols identify stars with cycles. The bottom two panels exclude 11 stars with [Fe/H] < -1. Gray data points represent stars not in the extremes of T_{eff}, $\log(g)$, and [Fe/H] and without cycles.

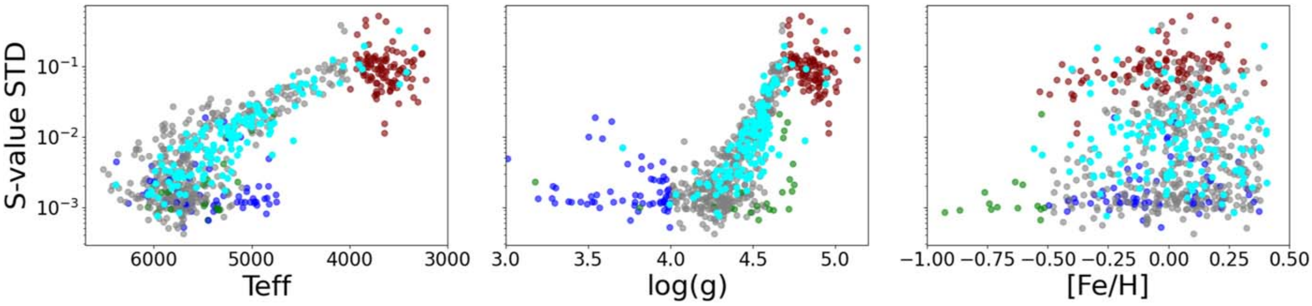

Figure 8. The S-value standard deviation is plotted as a function of $T_{\rm eff}$, log(g), and [Fe/H] for all 710 stars in our full sample. Stars with low log(g) are in blue, and stars with $T_{\rm eff} < 4000$ K are in maroon. The lowest-metallicity stars are shown in green. Eleven very-low-metallicity stars are taken off the plot. Cyan marks stars with detected cycles. The dichotomy of stars with low log(g) values is intriguing. We do not sample all of the parameter space equally, but the marked cycles still identify the area most likely to contain periodically cycling stars. The gray data points represent stars with $T_{\rm eff} > 4000$ K, log$g > 4.0$, and [Fe/H] > -0.5 and include stars above and below our threshold of 45 observations.

Table 2
Average Activity Values

Star	$S_{\rm min}$	$S_{\rm max}$	$S_{\rm med}$	$S_{\rm STD}$	$N_{\rm obs}$	$B-V$	Rphk_Noyes	Age (Gyr)
HD 10002	0.1585	0.1668	0.1598	0.00205	44	0.804	−5.041	6.45
HD 10008	0.3886	0.4526	0.4238	0.01347	37	0.768	−4.414	0.46
HD 100180	0.1615	0.1794	0.1679	0.00325	63	0.564	−4.916	4.12
HD 100623	0.1751	0.2165	0.1913	0.00930	82	0.763	−4.890	3.74
HD 101259	0.1392	0.1467	0.1443	0.00227	13	0.739	−5.118	8.37
HD 10145	0.1679	0.1769	0.1724	0.00150	27	0.660	−4.929	4.32
HD 101501	0.2769	0.3719	0.3135	0.02552	15	0.701	−4.526	0.99
HD 102158	0.1585	0.1601	0.1598	0.00050	12	0.557	−4.965	4.93
HD 103095	0.1910	0.2271	0.2087	0.00960	17	0.665	−4.774	2.44
HD 103432	0.2372	0.2716	0.2571	0.01037	9	0.645	−4.614	1.40

(This table is available in its entirety in machine-readable form in the online article.)

Table 3
Chromospheric Time Series

Star	Filename	BJD	S-value	SNR	Decker	Seeing (arcsec)
HD 185144	bj01.46	13237.736	0.2112	55	B5	1.0
HD 185144	bj01.47	13237.738	0.2120	34	B5	1.1
HD 185144	bj01.48	13237.739	0.2094	28	B5	1.1
HD 185144	bj01.49	13237.740	0.2118	30	B5	1.2
HD 185144	bj01.50	13237.740	0.2094	36	B5	1.0
HD 185144	bj01.51	13237.741	0.2112	43	B5	1.1
HD 185144	bj01.52	13237.742	0.2113	43	B5	1.0
HD 185144	bj01.53	13237.742	0.2114	48	B5	1.1
HD 185144	bj01.54	13237.743	0.2101	52	B5	1.0
HD 185144	bj01.55	13237.744	0.2115	49	B5	1.0

(This table is available in its entirety in machine-readable form in the online article.)

Section 5.6. From the 285 stars searched, we present 138 stellar activity cycles and next discuss our recovery of previously known cycling stars.

4.2. Cycle Comparison to Previous Studies

4.2.1. Mount Wilson Cycles

Most published activity cycles that were produced with S-values have been collected by the Mount Wilson Observatory HK Project. Baliunas et al. (1995) found that 52/111 main-sequence stars have cycles. The regularity of stellar cycles is dependent on age: young stars rarely display a smooth, cyclic variation; intermediate-age stars have occasional smooth cycles; and stars as old as the Sun have smooth cycles (Baliunas et al. 1995). Although our sample is vastly different, we find 138/284 stars have cycles. Our sinusoidal search is not sensitive to nonperiodic cycles of young stars such as HD 22049. Our search is most sensitive to the regular cycles of stars older than 1 Gyr. The largest sample of Mount Wilson stars compiled has 335 stars. From our 710-star sample, 173 stars overlap and we independently identify 44 cycles from those 173 stars. Since our sample contains a broader range of stellar types, we are exploring parameter space beyond Baliunas et al. (1995) allowing for the examination of correlations between cycle periods and stellar properties.

Summary analysis of the Mount Wilson cycles has claimed that the Sun is near the upper mass limit for cycling stars

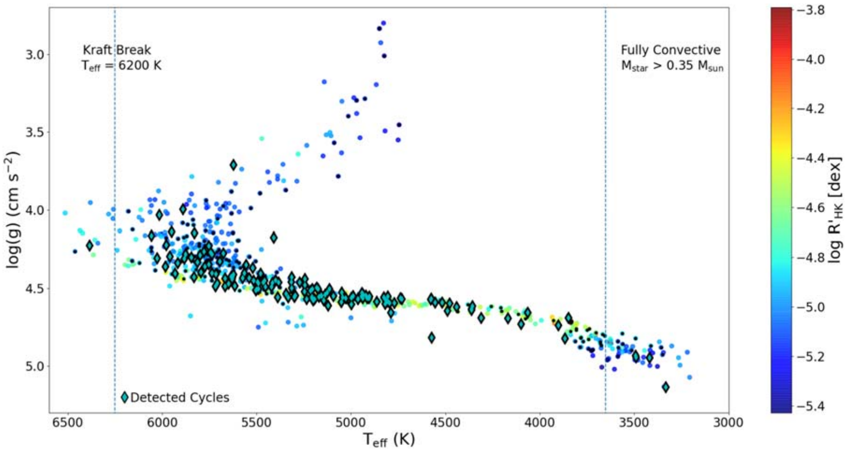

Figure 9. Effective temperature, stellar surface gravity, and median $\log(R'_{\rm HK})$ value for the 710 stars in our sample. Diamonds show detections of 138 stellar activity cycles. Circles identify the 285 stars with more than 45 observations that are searched for cycles, and the color scale represents $\log(R'_{\rm HK})$.

(Schröder et al. 2013), but the identification of many cycles down to 4400 K presented here and the handful of M dwarfs found here and by Irving et al. (2023) show that stars across the main sequence can be in cycling states.

4.2.2. Studies of Keck Data

We cross-check the 13 cycles from 59 stars examined in Baum et al. (2022), adding two years of HIRES data, and find 10 of the 13 cycles. Of those not detected, HD 166620 is in the well-studied minimum phase of its cycle (Luhn et al. 2022), while HD 101501 and HD 152391 have fewer than 45 observations. For the cycles that we expect to detect, our algorithm identifies them.

The CLS activity time series has been analyzed in relation to precise RVs. In CLS1, Table 7 mentions 43 false-positive planet signals that are attributed to stellar activity cycles, and 13 false positives due to rotation periods. We confirm 41 of the 43 as stellar activity cycles. Luhn et al. (2020) listed stars with possible stellar activity cycles, but the focus of that work was on average activity and its impacts on RV precision. For their stars that overlap with our sample, we quantify the intensity and period of those signals.

4.2.3. Johnson et al. (2016)

Johnson et al. (2016) used data collected from 295 spectra from the 2.7 m Harlan J. Smith Telescope at McDonald Observatory from 1998 to 2015 to monitor the RV of the HD 219134 system and also collected *S*-value measurements of stellar activity. They detected a stellar activity cycle of 11.7 yr with no linear trend. Our analysis finds a cycle period of 13.4 yr after removing a robust linear trend over the observation baseline of 20 yr. The discrepancy in the detection of a linear trend may be explained by differing measurement uncertainties and is worthy of further exploration.

4.2.4. Toledo-Padrón et al. (2019)

Toledo-Padrón et al. (2019) studied the stellar activity of GL 699, Barnard's star, and revealed an activity period of 8.8 yr in the Ca II H and K *S*-values. Our measured cycle of 8.5 yr is consistent with their value. Toledo-Padrón et al. (2019) also used photometry to determine the activity cycle finding a 10.5 yr cycle. Their conclusion that GL 699 is a very inactive star is consistent with our finding of the periodogram amplitude being just above the threshold of detection.

4.2.5. Mittag et al. (2023)

Mittag et al. (2023) listed 34 chromospherically detected activity cycles around FGK stars. For the 15 stars that overlap with our sample, and have more than 45 observations, we recover 14 of the cycles. HD 201092 has two cycles, but neither passes our thresholds. The 11 yr period is not detected due to our choice to fit only circular periodicity. Future studies that include the Mount Wilson and Keck/HIRES data sets can potentially confirm these complex cycles. Future analyses may require different levels of confidence in the cycle detection or will be conducted with a different model.

4.2.6. Studies of Fully Convective Stars

Photometric data from the ASAS-SN project identified 13 of 15 fully convective M dwarfs showing stellar cycles (Irving et al. 2023). Among overlapping stars in our sample with 45 observations HIP 80824 (GJ 628) and HIP 109388 (GJ 849) are not detected. GJ 317 has two cycles, but we detect neither. HIP 103039 (LP 816-60), HIP 57548 (GJ 447), GJ 285, GJ 54.1, GJ 234, and GL 406 all have fewer than 45 Keck/HIRES observations, falling below the inclusion threshold. The cycles with periods of a few years that Irving et al. (2023) detected with photometry must not have periodic signals amenable to detection with the Ca II H and K emission lines. The lack of chromospheric confirmation of the photometric cycles may be due to complex structures to which our simple sinusoid model is not sensitive. Indeed other studies have identified chromospheric cycles in M dwarfs (Suárez Mascareño et al. 2016; Wargelin et al. 2017).

From this point on we turn our focus to the 285 stars that have at least 45 Keck/HIRES *S*-values since 2005, eventually narrowing down the parameter space to show that nearly every star in that range has a periodic activity cycle.

5. Stars with Cycles

We examine the population of stars with identified cycles, starting within the context of fundamental stellar properties. Stars with cycles span a range of temperatures (6385 K $> T_{\rm eff} >$ 3332 K), stellar surface gravities ($5.13 > \log(g) > 3.71$), and metallicities ($-1.61 < [Fe/H] < 0.41$). The second lowest metallicity is -0.56. Figure 9, similar to Figure 3, identifies stars that are searched and those with stellar cycles in the T_{eff} versus $\log(g)$ parameter space. Most cycling stars are in the main sequence with temperatures from 4700 to 5900 K. Metallicity does not appear to hold a pivotal role in the presence of chromospherically detected activity cycles (see Section 5.4). Stars with detected cycles are listed in Table 4 along with their cycle properties.

In the following section, we divide stars below 4700 K from those with higher T_{eff}. This divide exists for two reasons. Near 4700 K, the models used to determine fundamental stellar parameters change due to the underlying physics inside stars. For example, stars below this divide use SpecMatch-Empirical (Yee et al. 2017) and stars above use SpecMatch-Synthetic (Petigura et al. 2017). The second reason is the historical division of stars at this T_{eff}, for which rotation periods and convective turnover times were devised (Noyes et al. 1984).

Figure 10 shows histograms of the fundamental stellar parameters T_{eff}, $\log(g)$, and [Fe/H] as well as the derived parameters $R_\star$, $M_\star$, and $\log(R'_{HK})$. Gray identifies the 710-star sample, yellow represents the 285-star sample that we search for cycles, and cyan represents detected cycles.

Figures 11 and 12 show the amplitudes and periods of the detected cycles as a function of both fundamental and derived stellar properties. In terms of amplitude, stellar cycles tend to increase as T_{eff} decreases and main-sequence stars have larger amplitudes than evolved stars, but some main-sequence star cycle amplitudes are comparable to those of subgiant stars. We find no correlation between metallicity and cycle amplitude or cycle period. A quantitative analysis is detailed in Section 5.4. We explore an intriguing correlation of cycle period to T_{eff} for the activity range within $\log(R'_{HK})$ of -4.7 to -4.9 in Section 6.

5.1. Solar-type Stars with Cycles

Previous surveys of chromospheric activity have focused on solar-like stars identified with similar $B - V$ colors and bolometric luminosities to the Sun (Baliunas et al. 1995; Henry et al. 1996), and we define our solar-similar sample to have $5600\ \mathrm{K} < T_{eff} < 5900\ \mathrm{K}$, with no metallicity or $\log(g)$ restrictions. Out of 70 solar-like stars, we find 29 stars with cycles having periods between 3.9 and 23 yr. This subsample is evenly distributed in metallicity (± 0.3 dex) and $\log(R'_{HK})$ (-4.8 to -5.08). When the average activity is used to derive the rotation period and age (Mamajek & Hillenbrand 2008), the solar-similar sample ranges from 14 to 34 days and from 2.7 to 7.4 Gyr, respectively. The range of cycle periods for this subsample offers insight into the decreasing activity and rotation as a function of age for solar-type stars. The cycle periods of solar-type stars and their dependencies on stellar properties are highlighted as yellow crosses in Figures 11 and 12.

5.2. Short-period Cycles

We identify 45 cycling stars with periods less than 7 yr. Baliunas et al. (1995) found that stars with cycles of periods shorter than 7 yr have a higher false-alarm probability, marking them as "fair" or "poor." We use numeric thresholds that can be used to mark the robustness of a detection but find the vastly different sampling can require judgment calls when defining thresholds. HD 218868 is an example of a convincing cycle with a period of just 4.8 yr. Since the Mount Wilson survey had

Table 4
Detected Stellar Cycles for 138 Stars

Star	$\mathrm{Amplitude_{fit}}$	$\mathrm{Period_{fit}}$	Threshold	Peak 1	Peak 2
HD 100180	0.1704	3.33	1.76	1.01	0.36
HD 100623	0.2070	8.03	2.57	2.88	0.70
HD 103932	0.5085	9.00	1.36	5.49	0.47
HD 104304	0.1643	10.00	2.63	1.96	0.44
HD 10476	0.1977	9.11	1.39	0.86	0.26
HD 107148	0.1607	5.69	2.20	1.32	0.57
HD 109358	0.1674	13.50	1.87	1.09	0.36
HD 110315	0.3774	11.81	1.96	6.39	0.64
HD 111031	0.1496	13.72	1.29	0.53	0.28
HD 114783	0.2055	9.10	2.25	2.01	0.29
HD 116442	0.1686	18.09	2.49	1.84	0.21
HD 116443	0.1880	14.24	2.57	2.25	0.25
HD 122064	0.2863	12.81	2.91	11.62	1.06
HD 122120	0.6042	20.86	0.66	1.71	0.52
HD 125455	0.1946	9.87	3.39	5.65	0.57
HD 126053	0.1660	17.53	1.82	1.04	0.34
HD 126614	0.1469	16.15	2.24	1.19	0.45
HD 127334	0.1521	16.08	1.52	0.68	0.42
HD 130992	0.3386	3.11	0.71	0.69	0.42
HD 136713	0.3320	6.85	1.10	1.30	0.36
HD 139323	0.2467	8.84	2.28	2.57	0.23
HD 140538A	0.2061	3.96	1.81	1.43	0.29
HD 14412	0.2032	6.15	2.51	2.68	0.63
HD 144287	0.1673	19.29	3.54	4.31	0.56
HD 145675	0.1883	11.20	3.49	4.24	0.21
HD 145958A	0.1916	7.63	2.27	1.75	0.59
HD 145958B	0.1868	8.30	1.79	1.15	0.75
HD 1461	0.1632	14.10	1.93	1.09	0.12
HD 146233	0.1735	6.27	3.30	3.87	0.97
HD 148467	0.7626	4.03	0.46	1.12	0.83
HD 149806	0.2244	6.71	2.08	1.99	0.95
HD 154088	0.1634	15.20	3.80	4.92	1.65
HD 154345	0.2320	6.95	2.82	5.58	0.40
HD 154363	0.5312	9.53	1.38	5.18	0.72
HD 155712	0.2296	9.33	3.15	5.12	0.85
HD 156279	0.1783	12.50	2.19	1.63	0.37
HD 156668	0.2462	11.38	1.95	2.37	0.19
HD 156985	0.3036	7.82	2.34	5.90	0.42
HD 158633	0.1780	11.83	2.13	1.51	0.90
HD 159062	0.1738	16.85	2.68	2.38	0.55
HD 16160	0.2371	12.43	2.31	3.40	0.48
HD 168009	0.1616	17.52	1.79	0.96	0.47
HD 170493	0.4691	8.75	1.26	3.33	0.98
HD 172051	0.1719	8.36	2.08	1.35	0.55
HD 17230	0.8034	15.20	0.24	0.53	0.13
HD 18143	0.1801	13.67	2.98	2.91	0.40
HD 182488	0.1704	11.54	2.79	2.34	0.35
HD 183263	0.1576	7.00	2.85	2.07	0.19
HD 185144	0.2179	5.93	1.94	1.78	0.20
HD 186408	0.1534	20.20	1.68	0.79	0.25
HD 18803	0.1894	5.04	2.20	1.75	0.31
HD 190406	0.1919	15.02	1.21	0.64	0.47
HD 191408	0.1978	16.77	2.56	2.56	0.76
HD 192310	0.2171	10.67	4.12	14.26	0.94
HD 19308	0.1627	22.28	3.11	2.86	0.40
HD 196761	0.1785	11.40	3.79	7.29	1.63
HD 197076	0.1886	5.31	3.17	4.27	2.33
HD 199305	1.6523	6.30	0.24	1.61	1.11
HD 201091	0.6256	7.17	0.68	1.75	0.38
HD 20165	0.2289	7.78	3.03	6.05	0.76
HD 202751	0.2474	12.49	3.03	6.29	0.52
HD 20619	0.2023	4.42	2.43	2.63	0.58
HD 208313	0.3012	5.96	1.80	2.57	0.68
HD 209458	0.1616	4.79	1.96	1.13	0.73
HD 210302	0.1609	5.85	1.65	0.83	0.55

Table 4
(Continued)

Star	$\text{Amplitude}_{\text{fit}}$	$\text{Period}_{\text{fit}}$	Threshold	Peak 1	Peak 2
HD 213042	0.4273	8.01	1.34	2.97	1.23
HD 215152	0.2642	8.04	1.71	2.03	0.62
HD 216259	0.1938	15.96	3.62	7.17	0.88
HD 216520	0.2015	19.19	2.25	2.11	0.48
HD 218566	0.2967	9.66	2.66	6.10	0.31
HD 218868	0.2133	4.84	2.43	2.78	0.40
HD 219134	0.2758	13.27	2.25	4.33	0.33
HD 219538	0.2516	7.09	1.88	2.24	1.26
HD 219834B	0.2059	9.70	3.61	6.77	0.77
HD 220339	0.2675	5.87	2.17	3.03	1.25
HD 221354	0.1599	18.84	1.51	0.71	0.19
HD 224619	0.1702	18.06	2.57	1.99	1.04
HD 239960	1.4673	15.78	0.32	0.88	0.49
HD 24496	0.2008	5.86	2.87	3.27	0.58
HD 25329	0.1952	6.01	2.36	2.16	0.33
HD 25665	0.3042	6.52	1.68	2.47	0.53
HD 26151	0.2061	16.35	3.24	5.25	0.40
HD 26161	0.1531	20.12	1.79	0.87	0.37
HD 26965	0.2060	9.11	2.13	1.92	0.42
HD 28005	0.1633	13.79	2.80	2.28	0.68
HD 28946	0.2443	5.90	2.38	3.29	1.49
HD 29883	0.1958	14.00	3.48	6.49	0.42
HD 31253	0.1526	13.08	1.48	0.66	0.43
HD 32147	0.2933	9.53	0.93	0.74	0.26
HD 34445	0.1665	23.01	1.69	0.91	0.23
HD 36003	0.4252	10.98	1.44	3.64	0.72
HD 36395	2.0485	2.30	0.21	1.63	1.22
HD 3651	0.1788	10.01	3.14	3.38	0.35
HD 37008	0.1821	21.27	1.37	0.76	0.27
HD 3765	0.2186	12.80	3.18	5.96	0.31
HD 38230	0.1642	23.15	2.32	1.54	0.81
HD 38529	0.1734	5.46	2.63	2.02	0.54
HD 4256	0.2639	9.66	1.73	1.93	0.32
HD 42618	0.1639	10.16	2.83	2.30	0.19
HD 43947	0.1586	12.88	2.12	1.26	0.52
HD 4628	0.2173	7.91	2.73	3.46	0.81
HD 4747	0.2676	4.90	1.43	1.41	0.65
HD 4915	0.2046	4.86	1.72	1.19	0.42
HD 49674	0.1977	4.05	1.12	0.62	0.36
HD 50499	0.1516	3.69	2.51	1.56	0.76
HD 51419	0.1948	23.43	2.09	1.67	0.23
HD 51866	0.3395	7.17	0.98	1.10	0.30
HD 52711	0.1602	13.96	2.91	2.42	0.49
HD 62613	0.2089	5.75	3.27	5.28	0.90
HD 65277	0.2543	12.19	2.66	6.53	0.51
HD 68988	0.1630	5.29	2.67	1.99	0.62
HD 69830	0.1734	10.83	1.84	1.12	0.60
HD 72673	0.1866	10.47	4.03	9.65	1.67
HD 73667	0.1717	19.00	2.33	1.64	0.59
HD 74156	0.1476	16.01	2.05	1.05	0.19
HD 75732	0.1973	11.02	3.79	6.74	0.27
HD 7924	0.2285	7.49	2.40	3.15	0.27
HD 80606	0.1566	16.27	1.96	1.06	0.34
HD 82943	0.1716	2.96	1.56	0.84	0.28
HD 8389	0.2158	10.67	3.24	4.31	0.42
HD 84035	0.5291	8.03	0.95	2.16	0.73
HD 87359	0.2047	4.40	1.91	1.64	0.82
HD 87883	0.2780	7.83	1.85	2.93	0.52
HD 89269	0.1698	16.95	2.84	2.63	0.37
HD 90875	0.7309	18.71	0.84	2.38	0.62
HD 9562	0.1509	15.39	1.57	0.71	0.29
HD 97658	0.2074	9.01	3.64	8.63	0.30
HD 98281	0.1801	15.51	2.53	2.33	0.94
HD 99491	0.2128	6.15	2.61	3.26	0.33
HD 99492	0.2820	9.81	1.97	2.81	0.19
HD 9986	0.1794	5.03	1.87	1.23	0.68
GL 239	1.0562	15.24	0.38	1.39	0.86
GL 273	0.8215	2.94	0.30	0.66	0.33
GL 699	0.8470	8.48	0.27	0.50	0.31
HIP 19165	0.7498	5.68	0.43	0.94	0.69
HIP 41689	0.9481	3.03	0.23	0.56	0.38
HIP 74995	0.5778	3.80	0.38	0.58	0.17
S130811	1.1601	13.58	0.45	2.27	0.43

(This table is available in machine-readable form in the online article.)

sufficient sampling and sensitivity for detecting short-period cycles, their sample selection is likely responsible for nondetections. Younger stars (ages less than 1 Gyr), such as HD 22046, have previously identified cycles, but we intriguingly find 15 stars near solar temperature with periods less than 7 yr (Section 6).

5.3. Studies of Fully Convective Stars

As with fully radiative stars, stars with masses below $0.35\,M_{\odot}$ become fully convective and lose their tachocline, requiring a different mechanism for generating magnetic fields compared to solar-type stars (Irving et al. 2023). Four fully convective (T_{eff} less than 3500 K) stars have periodic activity that passes our thresholds (Section 4.1): HD 239960, GL 273, GL 699, and HIP 74995. HD 239960 has observations during a flare that are much higher than the average activity value. We include flare stars—except those with helium emission that were omitted in Section 2.1—and less active stars that we can measure with traditional S-values.

HD 95735 has a candidate cycle showing a downward linear trend, indicating a period beyond our baseline of observations. For fully convective stars that are amenable to the S-value measurement, we find that the S-values are sometimes dominated by the rotation period, so our exclusion in our periodogram search below 100 days is useful. The cycles in fully convective stars are identified with the periodogram peak method, and are not typically identified with the threshold described by Equation (1).

The stellar activity of GL 699 was studied by Lubin et al. (2021), but that study focused on periods less than 1000 days. The peak value in the GL 699 periodogram is very close to our acceptable threshold, and combining multiple data sets would provide more confidence in the detection. A comparison between our results for GL 699 and those of Toledo-Padrón et al. (2019) is summarized in Section 4.2.4.

5.4. Metallicity of Stars with Cycles

We find no correlation between cycle period or amplitude and stellar metallicity. First, we divide the stars searched into those with supersolar and those with subsolar metallicity, and we find similar ratios of stars searched (45%/55%) to cycles found (44%/56%). The evidence for a correlation of the flare rate of Kepler stars with the metallicity found in Kepler stars (See et al. 2023) does not hold for our sample. Our sample

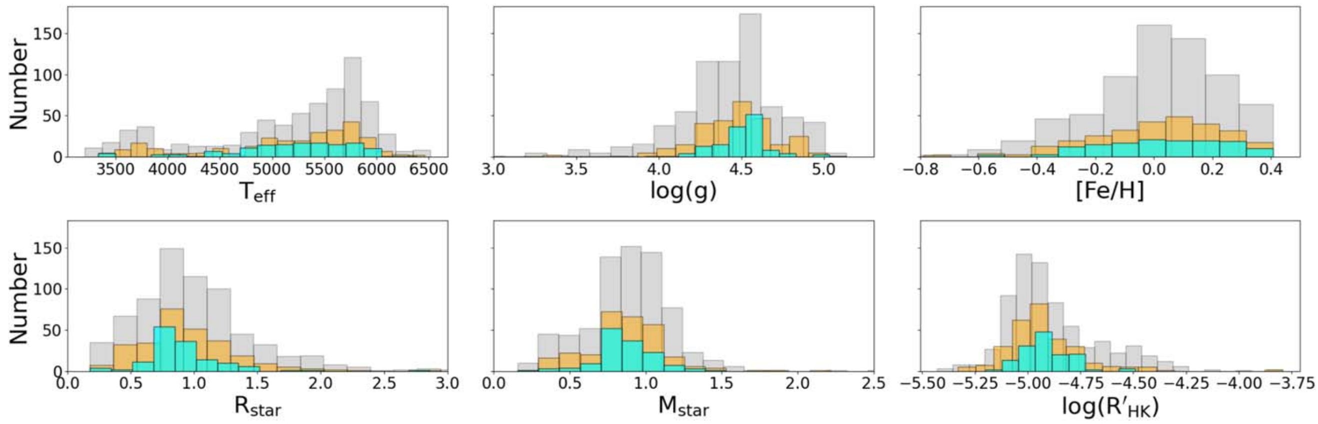

Figure 10. Distributions of $T_{\rm eff}$, $\log(g)$, [Fe/H], $R_\star$, $M_\star$, and $\log(R'_{\rm HK})$ for the 710 stars in our sample. The yellow areas show the 256 stars that have more than 45 observations, and cyan identifies the 138 stars with a cycle from this work. The stellar parameters of the stars that are searched and those that have cycles are representative of the entire sample, and are not strictly confined to particular stellar properties. Twenty-eight stars have radii larger than 2.5.

avoids stars with flares, which tend to be more active, making a direct comparison with studies of flare stars difficult.

The most metal-poor star with a detected cycle, HD 25329, has an [Fe/H] of −1.61. It has a smaller cycle amplitude compared to stars with a similar $T_{\rm eff}$ by a factor of 3. The extremely low metallicity is unusual in our sample, and the CLS1 stellar parameters list the Gaia parallax as an unlikely 12″, so the $T_{\rm eff}$ may not need to be revisited. It is also the outlier in panel (B) of Figure 11, raising suspicion.

To quantify the correlation between metallicity and activity, we calculate the Pearson and Spearman correlation coefficients for metallicity and a variety of activity indicators, finding no strong correlations. For correlations between [Fe/H] and cycle period and between [Fe/H] and cycle amplitude, we find coefficients below 0.10 indicating there is little or no correlation between metallicity and either cycle period or cycle amplitude.

5.5. Stars with Multiple Periodic Cycles

Our time baselines are sufficient to identify stars that have multiple simultaneous cycles, but our search method does not recover any of the known occurrences. HD 22049 (Metcalfe et al. 2013; 2.95 ± 0.03 yr and 12.7 ± 0.3 yr), HD 32147, HD 4915, HD 219234 (trend), HD 4628 (trend), and HD 45184 (5.14 yr; Flores et al. 2016) all show evidence of a second cycle. HD 100180 shows two possible periods in Oláh et al. (2016) but we only find one, and Baum et al. (2022) found none. HD 201091 and HD 201092 both have two cycles that will be apparent when combining the Mount Wilson data. HD 18803 has one strong cycle that changes significantly in amplitude over 20 yr. HD 219834B shows a linear trend on top of a cycle, indicative of a second cycle. The shorter of the cycles is typically not represented well by a sinusoid, so our nondetections are limited by our search method not our data quality.

5.6. The Least Active Stars

The search for stars in a Maunder minimum, or magnetic minimum state, attempts to connect the Sun's activity cycles to the cycles of other stars. HD 4915 is a candidate star in a Maunder minimum–like state (Shah et al. 2018), but our extended time baseline shows two cycles. One periodicity is at 4.9 yr, and the second is more than 40 yr, and the longer-period cycle is now turning higher. We detect the 4.9 yr period but cannot limit the period of the second cycle with Keck data alone. HD 166620 is the most convincing to have strong evidence in favor of being a Maunder minimum–like star (Baum et al. 2022; Luhn et al. 2022), and it continues to show very low variation in our extended time series.

In Isaacson & Fischer (2010), the 1% dispersion in the S-values of HD 10700 was used to gauge the systematic uncertainty of the S-values. Gomes da Silva et al. (2021) found a dispersion of 0.83%, which is comparable to our extended time baseline for HD 10700 S-values 0.75% (0.00125/0.1674). Our least active star with more than 45 observations is HD 55575 with a relative dispersion of $0.0007/0.1562 = 0.45\%$. Fifty stars have a smaller S-value standard deviation than HD 10700 and should be considered the least active well-sampled (45 observations or more) stars in our sample (Table 2). Differentiating inactivity due to stellar evolution, stellar viewing angle, and main-sequence spindown would be an interesting extension of this work.

5.7. Unexpectedly Cycling Stars

For stars with stellar surface gravity less than 4.0, we find that out of 28 stars only HD 38529 ($\log(g) = 3.93$) has a detectable cycle, and its period is 6.11 yr. Baliunas et al. (1995) stated that "the range of masses that can support solar-like magnetic activity is imprecisely known," and although we expect stars to lose their cycles as they age, spin down, and evolve, this cycle is an unexpected robust detection. HD 38529 has two substellar companions; the more massive of the two has an $M_{\sin i} = 13.2\ M_{\rm Jup}$, $P = 5.8$ yr, and eccentricity $= 0.35$. Our periodogram analysis shows that the peak in both the RV and the S-value periodogram is at 5.8 yr. This system is worthy of an analysis that explores the relationship between the planet and the activity cycle of this post-main-sequence star with stellar radius of $2.8\,R_\odot$ and a robust activity cycle. Gravitational interactions between exoplanets and stars have not been found to cause activity cycles (Obridko et al. 2022), but main-sequence stars (including our own) have been found to have activity cycles and planets with similar periods (Wright 2016).

Fully radiative stars, above the Kraft break (Kraft 1967), lack the radiative–convective boundary that is known to generate magnetic fields. Without a tachocline, it is not clear what

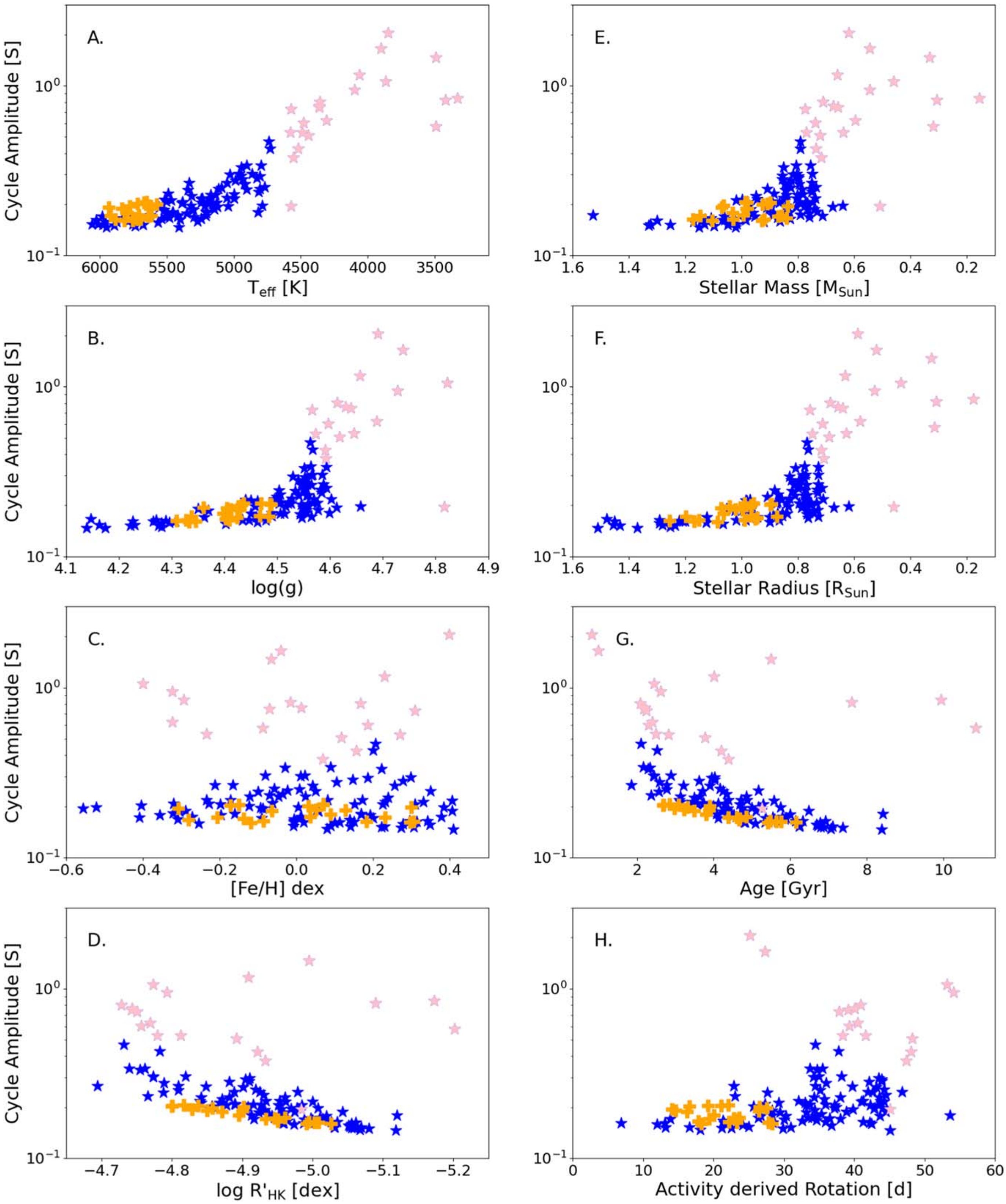

Figure 11. Stars with stellar activity cycles are plotted with their cycle amplitude as a function of fundamental stellar properties: T_{eff}, log(g), [Fe/H], and $\log(R'_{\mathrm{HK}})$ (panels (A), (B), (C), and (D), respectively). The derived parameters of $M_\star$, $R_\star$, chromospheric age, and activity-derived rotation period are plotted in panels (E), (F), (G), and (H), respectively. Age uncertainties are 60% (Mamajek & Hillenbrand 2008). Orange crosses highlight solar-type stars with 5600 K $< T_{\mathrm{eff}} <$ 5900 K. Pink stars have T_{eff} less than 4700 K. Note their distinct parameter space from the FGK stars. The ages and rotation periods for these cooler stars are not well calibrated with activity and are only shown for completeness. Cycle amplitudes are S-value peak amplitudes, not peak-to-peak. HD 38529 with a radius of 2.5 $R_\odot$ is not shown in panel (F).

mechanism would generate magnetic activity. We find one such star with a cycle, HD 210302 (5.7 yr, $T_{\mathrm{eff}} = 6385$ K). The S-value standard deviation is 0.0021 and the cycle amplitude is 0.160, placing the amplitude of this cycle near the limit of detection. Most stars with $T_{\mathrm{eff}} > 6000$ K have an S-value rms less than 0.002, the threshold below which we do not search for cycles.

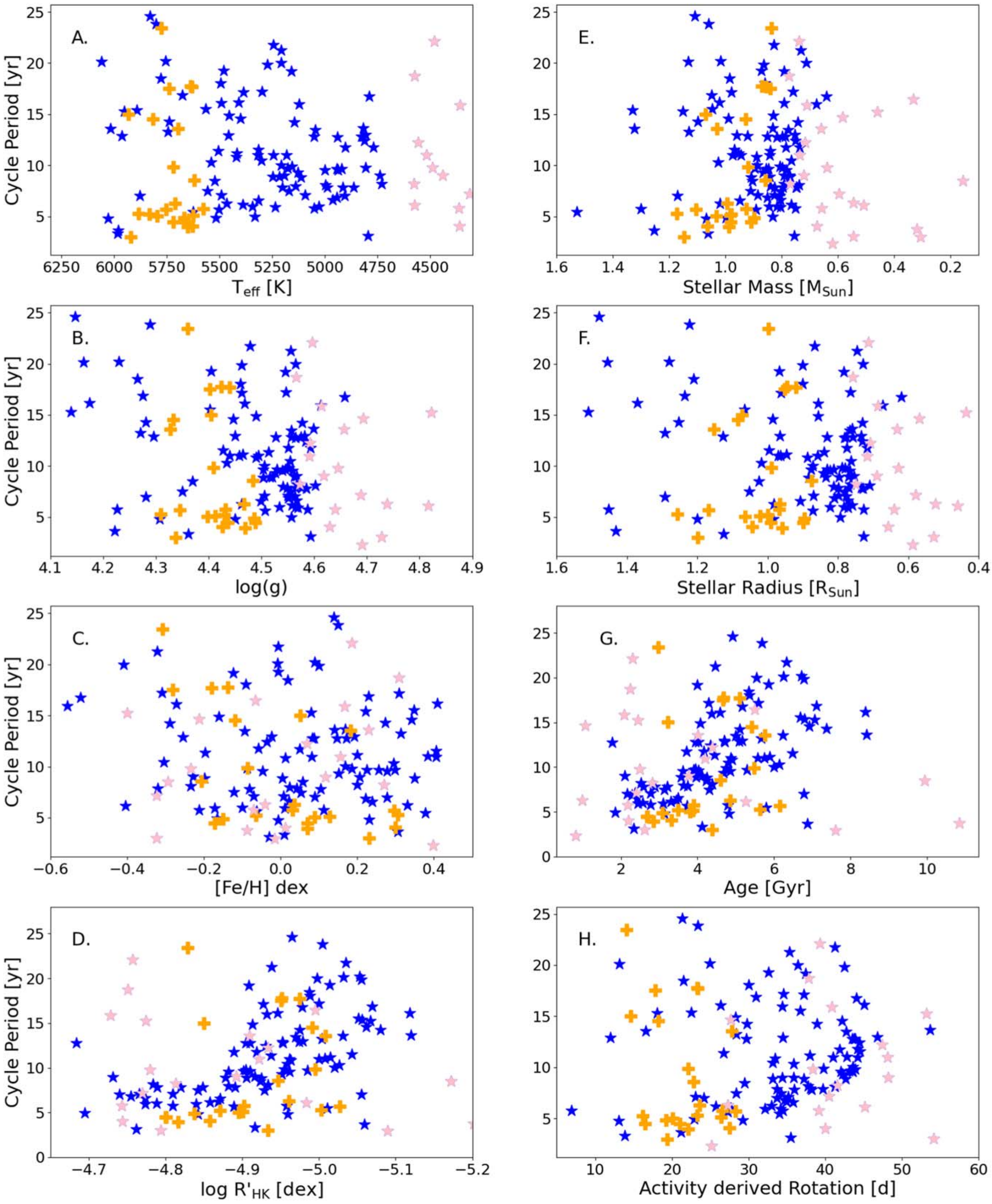

Figure 12. Stars with stellar activity cycles are plotted with their cycle period as a function of their fundamental stellar properties $T_{\rm eff}$, log(g), [Fe/H], and log($R'_{\rm HK}$) (panels (A), (B), (C), and (D), respectively) and derived parameters $M_\star$, $R_\star$, chromospheric age, and chromospheric rotation period (panels (E), (F), (G), and (H)). Orange crosses highlight solar-type stars with 5600 K < $T_{\rm eff}$ < 5900 K. Stars with $T_{\rm eff}$ < 4700 K are plotted in pink. Note their distinct parameter space from the FGK stars. The ages and rotation periods for these cooler stars are not well calibrated and are only shown for completeness.

5.8. Candidate Cycles

The choice of number of observations and the model selection drive our detection thresholds. While well-sampled stars with high-amplitude signals are straightforward to identify with numeric thresholds, those on the margin of detection, near the detection thresholds, or with poor sampling may not be considered cycling stars when additional observations are added or new detection methods are used such as the Fourier transform and the Choi–Williams distribution used in Oláh et al. (2016).

Some candidate cycles include HD 188015, which has a strong peak in the periodogram at 11 yr, but has only 38 observations. This shows that some of our declared cycles may not pass future thresholds, and others will be added to the cycling-star catalogs in the future. We do not identify linear trends, which are likely indications of cycles with periods beyond our baseline.

6. Discussion

6.1. Our Assessment

The changing nature of a star's cycle is impossible to observe over megayear to gigayear timescales. By collecting vignettes of hundreds of similar stars over several decades, we can piece together their long-term behavior. Observations of the solar cycle have been collected over hundreds of years, covering dozens of solar cycles. The nature of the solar cycle has been explored by observing solar-like stars' chromospheric activity on yearly and decades-long timescales. The dedicated long-term observing programs that have enabled the collection of data sets that cover 20, 30, and 40 yr have proven invaluable in revealing the evolution of stellar activity cycles.

High-resolution spectroscopy has contributed to these studies through time-series observations, primarily to find and characterize extrasolar planets. Ca II H and K time series are collected alongside RV measurements to decorrelate RVs from stellar activity (Mayor & Queloz 1995). The CLS provides 20 yr observing baselines for 285 stars (710 on shorter baselines) on a single instrument. Planet search spectroscopy also allows determination of precise stellar properties, which have been used effectively to search for subtle trends in exoplanet demographics (Fulton & Petigura 2018).

Using the activity time series and precise stellar properties we identify a range of stellar activity in which nearly every star is cycling. Refined $B-V$ values that are calculated from $T_{\rm eff}$ and [Fe/H] and are homogeneously determined are required for identifying the $\log(R'_{\rm HK})$ range on the main sequence for G- and K-type stars in which the period of the cycle is tightly correlated to the effective temperature. In the $T_{\rm eff}$ range of 4700–5900 K and the $\log(R'_{\rm HK})$ range between -4.7 and -4.9, we find the cycle period increases as $T_{\rm eff}$ decreases. And for stars less active than $\log(R'_{\rm HK}) = -4.9$, the correlation does not hold, and $T_{\rm eff}$ is no longer closely related to the cycle period.

As young, active stars with $\log(R'_{\rm HK})$ more than -4.7 spin down and expel their angular momentum, their cycles become detectable as they begin to have a more periodic nature. Prior to reaching the steady state of cycling these stars are likely categorized as "active/variable" in studies such as Baliunas et al. (1995) and Baum et al. (2022). Their stellar cycles may be present but they are less sinusoidal and their period is inconsistent from one cycle to the next. The activity level at which stars transition from irregular to regular cycle periods is different for different $T_{\rm eff}$. For Sunlike stars [5600, 5900] the cycles become regularly periodic around -4.80. For the next three bins of temperature, [5300, 5600], [5000, 5300], and [4700, 5000], the first periodic cycles are identified at -4.70, -4.76, and -4.7. The trends described in these temperature bins hold for the stars between [5900, 6300], but the bin has only 10 stars. The least active star with a cycle has a $\log(R'_{\rm HK}) = -4.85$.

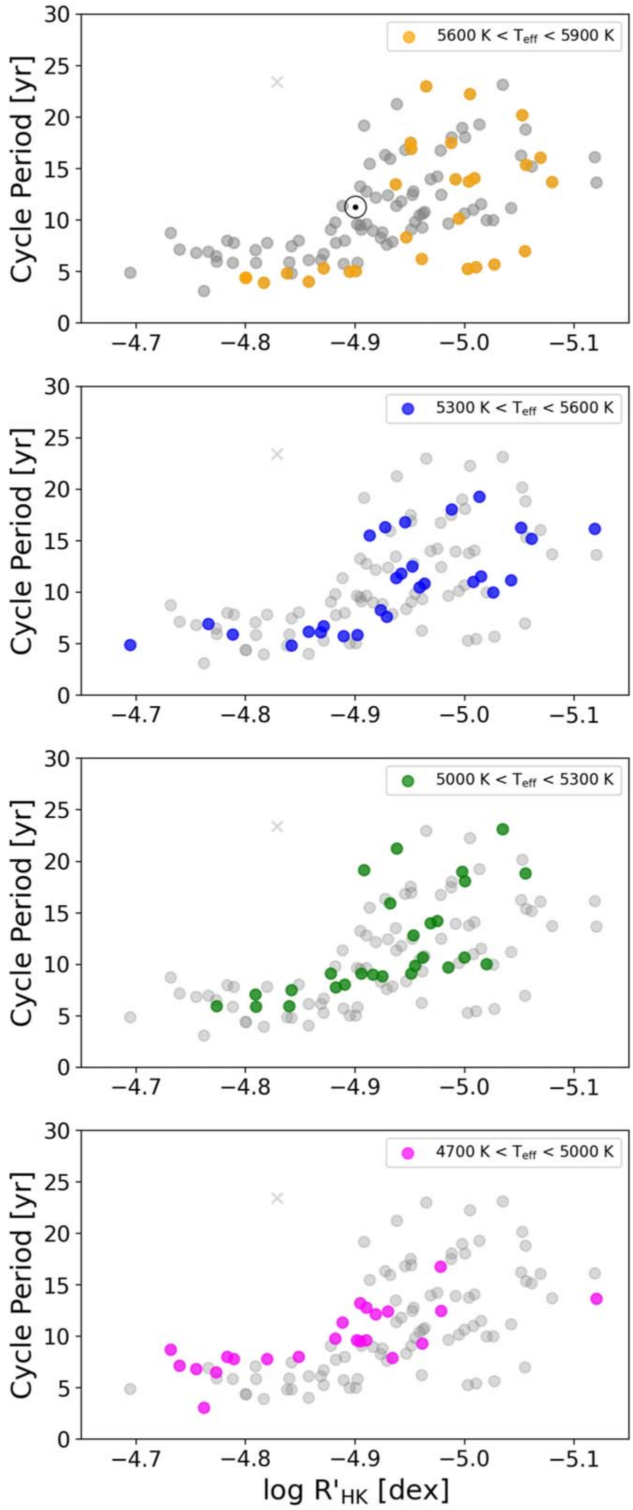

Figure 13. Stellar activity cycle period is presented as a function of chromospheric activity $\log(R'_{\rm HK})$ for different temperature ranges. The Sun is placed at $\log(R'_{\rm HK})$ of -4.9 and an 11 yr cycle period. The average cycle period increases at all activity levels for every temperature bin. In the range of $\log(R'_{\rm HK})$ between -4.7 and -4.9, 33/42 stars have cycles. In each specified range of $T_{\rm eff}$ and activity, the cycle period is tightly grouped. The gray data points represent all stars between [4700, 5900].

Figure 13 shows the relationship between $\log(R'_{\rm HK})$ and cycle periods for ranges of temperature in 300 K bins, revealing the transition of cycle period trends at a $\log(R'_{\rm HK})$ value near

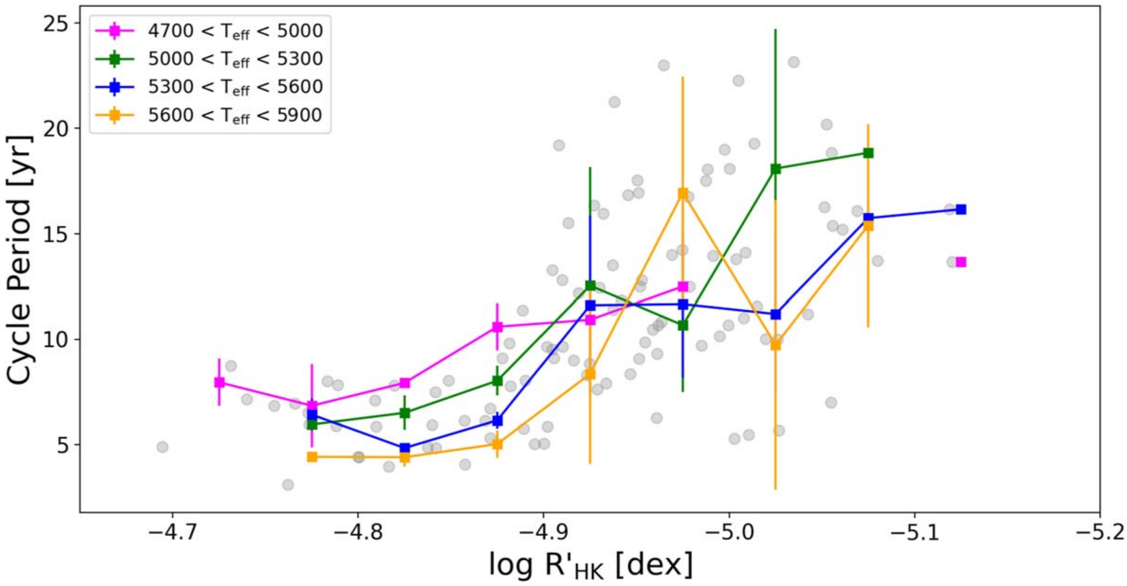

Figure 14. The average cycle period and the cycle period scatter increase for every temperature bin at $\log(R'_{\mathrm{HK}}) = -4.90$. For more active stars, cycle period and T_{eff} are tightly coupled. For less active stars, cycle period is not related to T_{eff}. The bin size is 0.05 and error bars represent the standard deviation in each temperature/activity bin.

−4.9. Divided at −4.9, more active stars have tightly grouped periods for each temperature range and the correlation disappears for less active stars. If we consider the stars more active than $\log(R'_{\mathrm{HK}})$ of −4.9, we find that in the solar temperature bin, cycles are 4.4 yr ± 0.5 yr. From 5300 to 5600 K cycles are 6.0 yr ± 0.7 yr. From 5000 to 5300 K cycles are 7.2 yr ± 1.1 yr. From 4700 to 5000 K cycles are 7.8 yr ± 2.0 yr.

For stars less active than $\log(R'_{\mathrm{HK}})$ of −4.9, activity and cycle period decorrelate and the deterministic nature of cycle period as a function of $\log(R'_{\mathrm{HK}})$ no longer holds. Cycle periods and standard deviation values are, from the hottest to the coolest bin, 13.7 ± 5.6 yr, 11.7 ± 3.6 yr, 12.8 ± 4.6 yr, and 12.2 ± 2.4 yr. In Figure 14, we average the cycle periods in bin sizes of 0.05 and plot the median with the standard deviation in each bin as an error bar, revealing a small scatter and tightly correlated cycle periods. The transition to longer periods as a function of activity occurs near $\log(R'_{\mathrm{HK}}) = -4.9$.

Of the 42 stars in this temperature–activity range, 33 stars have confirmed cycles. The remaining nine stars have candidate activity cycles with signals that do not meet our threshold requirement or periodogram peak power. Some of them do not have the periods we expect from this newly discovered correlation. We consider this tentative evidence that every star with T_{eff} between 4700 and 5900 K passes through a phase in which a strongly periodic signal exists within a narrow range of periods, and this period is a function of temperature. For this to be true, we must explain why there are no cycles in these nine exceptional stars.

The stars with T_{eff} between 4700 and 5900 K and $\log(R'_{\mathrm{HK}})$ between −4.7 and −4.9 that do not have cycles that pass our threshold are HD 159222, HD 185414, HD 176377, HD 68017, HD 37124, HD 51419, HD 212291, HD 23356, and HD 92719. HD 159222 ($T_{\mathrm{eff}} = 5876$ K) has a 3.1 yr candidate cycle that passes our threshold but has a secondary peak that strikes it from our final list of cycles. HD 185414 ($T_{\mathrm{eff}} = 5845$ K) has a candidate period at 10 yr, but its periodogram peak of 0.40 falls below our threshold of 0.5. HD 176377 ($T_{\mathrm{eff}} = 5804$ K) has a candidate cycle at 4.8 yr but its periodogram peak of 0.41 falls below our threshold. If future observations confirm this cycle, the cycle period would be consistent with our trend. HD 68017 ($T_{\mathrm{eff}} = 5712$ K) has a candidate cycle at 1.1 yr and is slightly less active in terms of both the median S-value and the S-value standard deviation. This star is potentially slightly more evolved than the others. A 1.1 yr cycle would not fit our trend. HD 37124 ($T_{\mathrm{eff}} = 5698$ K) has a potential cycle of 22.6 yr, but the cycle is not closed and the periodogram peak is ambiguous to higher periods, so we consider this a lower limit. It also has a slightly lower $\log(g)$ than the other stars discussed here. HD 51419 ($T_{\mathrm{eff}} = 5775$ K), marked with an X in Figure 13, is very similar to HD 37124 in that the cycle is not closed and the peak at 23.4 yr is not unique, providing only a lower limit on the period. Its $\log(g)$ value is 4.36. HD 212291 ($T_{\mathrm{eff}} = 5589$ K) has two strong peaks in the periodogram, at 4.9 and 5.6 yr, therefore the period is not uniquely determined. Further observations would likely confirm the period and it would fall into our expected trend. HD 23356 ($T_{\mathrm{eff}} = 4976$ K) has a candidate signal at 5.4 yr, but it is only identified after removing a linear trend, and even then it does not pass our periodogram peak threshold. If this cycle were confirmed, it would fit our trend. HD 92719 ($T_{\mathrm{eff}} = 5774$ K) has a cycle at 4.6 yr, but has an ambiguous period, with a second periodogram peak, removing it from our list.

For those stars in this exception list that do not have candidate cycles, which could be confirmed with more observations, possible explanations include an undervalued T_{eff}, which could shift the star into the $\log(R'_{\mathrm{HK}})$ range where we do not expect a cycle. This possibility is supported by the notion that the coolest star without an expected cycle has a T_{eff} of 5589 K, meaning every star below this value has a cycle within $\log(R'_{\mathrm{HK}})$ of −4.7 to −4.9. Another possibility is a pole-on orientation for these stars.

One star, HD 130992 ($T_{\mathrm{eff}} = 4796$ K), has a cycle of period 3.1 yr, going against our trend. We find the poor sampling of this star contributes to its potentially false detection, but it

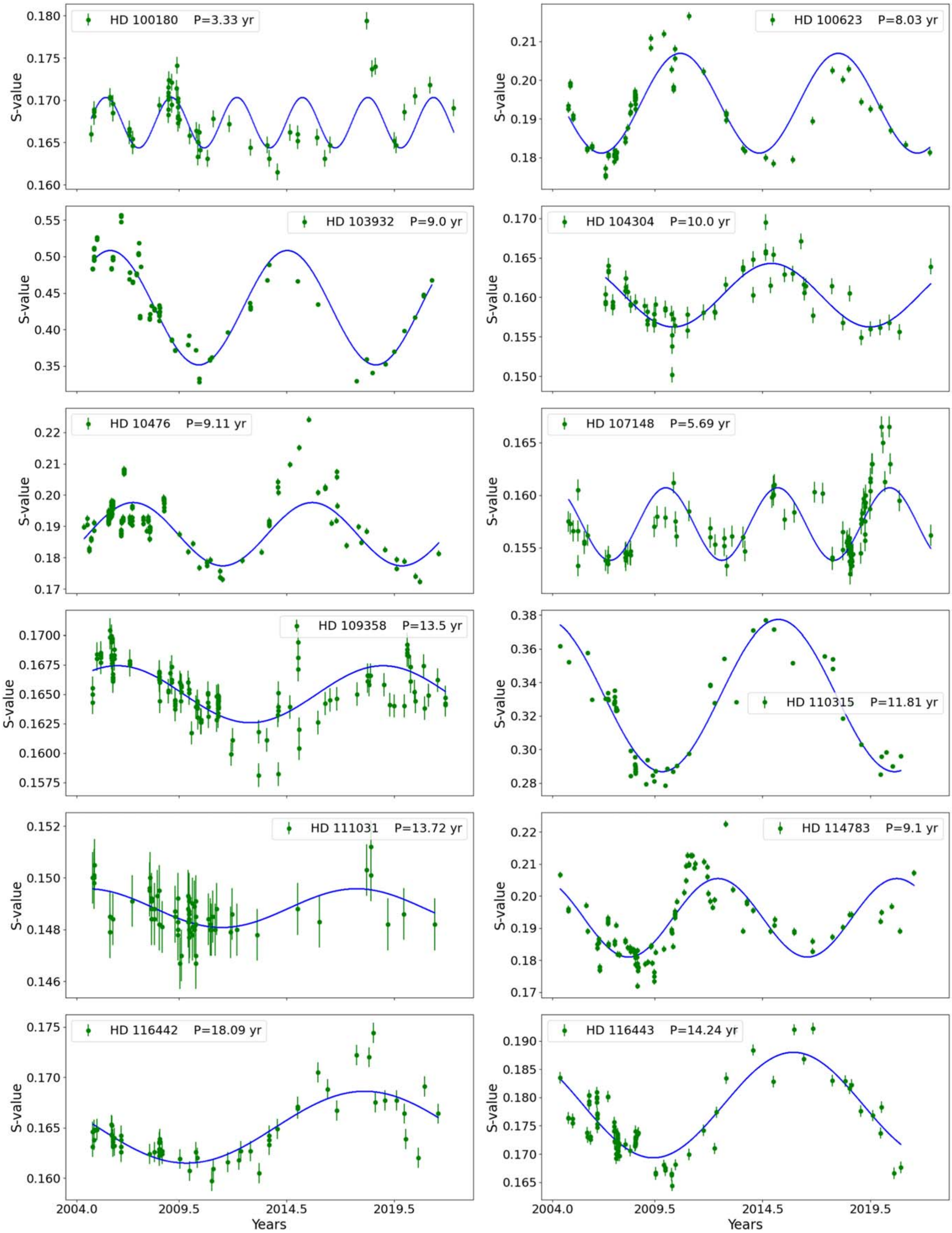

Figure 15. Cycles for stars HD 100180, HD 100623, HD 103932, HD 104304, HD 10476, HD 107148, HD 109358, HD 110315, HD 111031, HD 114783, HD 116442, and HD 116443. The complete figure set contains plots for all 710 stellar activity cycles in our sample.

(The complete figure set (60 images) is available in the online article.)

passes all of our numerical thresholds so we include it in our table.

With the possible explanations as to why these eight stars do not have cycles, we again pose the possibility that every star from $T_{\rm eff}$ 4700 to 5900 K and with $\log(R'_{\rm HK})$ between −4.7 and −4.9 has a regularly periodic activity cycle with a period correlated to $T_{\rm eff}$. Each of the 138 stars with cycles identified in this work is presented in Figure 15's figure set.

6.2. The Path Forward

Our collection of magnetic activity cycles, found via multi-decade ground-based monitoring of stars in the solar neighborhood, sets the stage for further studies of magnetic activity, rotation, and age.

When considering this specific temperature range, no restrictions are placed on $\log(g)$ or [Fe/H]. Stellar evolution becomes a factor only after activity values decrease beyond $\log(R'_{\rm HK})$ of −4.9, near the Sun's activity level, at which point the changes we observe in activity cycle period become a combination of main-sequence activity changes and evolution of stars off the main sequence. Spectropolarimetry of solar-type stars with different Rossby numbers (Metcalfe et al. 2023, 2024) is shown to support the theory of weakened magnetic braking. Adding the findings presented in this work may add to our understanding of the Sun's activity cycle relative to other solar-type stars.

Many stars have previously noted double periods and the ratio of these periods is a strong function of $T_{\rm eff}$. The Keck/HIRES time baseline of 20 yr is sensitive to cycles with a period of 25 yr, but identifying a second cycle per star will require a different method and threshold of detection. When analyzing stars with two cycles, most previous studies have relied on the Rossby number, the ratio of the rotation period to the convective turnover time (Mittag et al. 2023). In this work, we notably have identified this range of consistent, predictable stellar cycle periods without knowing the stellar rotation periods.

Perhaps the most intriguing question around stellar activity cycles and rotation periods is what happens to solar-type stars as their dynamo transitions from having a strong relationship between rotation, age, and activity. For old main-sequence stars, there is a breakdown between the rotation period and stellar age, but perhaps not between the overall chromospheric activity and the age of the star. The evolution of stars off the main sequence also clouds the interpretation of these relationships. The homogeneously determined stellar parameters from CLS1 have been used to disentangle such effects (David et al. 2022). The theory of weakened magnetic braking (van Saders et al. 2016; Metcalfe et al. 2022) is supported by the measurements of stellar rotation periods with Kepler photometry and independently with asteroseismically determined rotation periods. We present another independent data set that can be used to test weakened magnetic braking.

The examination of magnetic cycles as a function of age (Oláh et al. 2016) provides a path forward for future studies that can take advantage of large time series of Ca II H and K activity measurements. Figure 12 shows that the regularly cycling stars correspond to chromospheric ages between 2 and 4 Gyr. Using independently determined ages makes this conjecture more reliable. Adding measurements of rotational modulation and age to the data presented here will further elucidate the relationship between the magnetic activity of stars and their observable proxies. Examination of the ratio of rotation period to activity cycle for the Mount Wilson sample shows both consistency with previous studies and subtlety in the dependence on stellar temperature (Mittag et al. 2023). The larger sample of cycles presented here, with precise stellar properties, provides an opportunity to further study these relationships and their impact on stellar dynamos.

This new collection of stellar activity cycles, with its broad span in terms of stellar $T_{\rm eff}$ and $\log(g)$, can be used to broaden the connections between stellar cycle periods and theoretical understandings of the generation of magnetic fields in stars. We defer the analysis of ages, rotation periods, and Rossby numbers to future studies, noting specifically that the Rossby number is not required in our current analysis. We identify the trend between cycle period and $T_{\rm eff}$ and the transition from a strongly correlated period to a weak correlation with only activity time series.

7. Conclusion

We present the largest sample of spectroscopically determined stellar activity cycles to date, with optical spectroscopy of 710 solar neighborhood stars collected over two decades to catalog chromospheric activity, and search for stellar activity cycles. The CLS stars forming the basis of this survey may also aid exoplanet RV surveys. The Ca II H and K time-series data serves as a proxy for stellar and chromospheric activity, measurements that can be utilized in the detection and characterization of exoplanets.

From our Keck/HIRES Ca II H and K data set, a total of 285 stars are amenable to searches for stellar cycles with periods ranging from 2 to 25 yr, and 138 stars show stellar cycles of varying length and amplitude. These activity cycle observations in turn may be used to disentangle the effect of stellar magnetic activity when detecting and characterizing exoplanets.

The results presented may also find use in placing the Sun's stellar magnetic activity within the context of the activity of solar neighborhood stars, including an improved understanding of stellar activity through the star's main-sequence lifetime.

The collection of Ca II H and K measurements from the Mount Wilson Observatory HK Project helped to place the solar cycle into context in the solar neighborhood. The empirical identification of cycles and rotation periods, along with the theoretical underpinnings of convective turnover times and mixing lengths, has greatly improved the understanding of magnetic phenomena on and below the stellar surface. Folding stellar age into what we know about activity cycles and rotation may lead to deeper understanding of the changes in stars' chromospheric activity on gigayear timescales.

Finally, we provide tentative evidence that every G- and K-type star passes through a stage of stellar activity in which stellar activity cycles are present and their period is strongly correlated to the effective temperature.

Acknowledgments

We thank Daniel Huber, Simon Albrecht, Simon Murphy, and Aaron Householder for helpful comments, and Lee Rosenthal for his early work on CLS. And we thank the anonymous referee for constructive feedback during review.

This work was supported by NASA Keck PI Data Awards, administered by the NASA Exoplanet Science Institute. Some of the data presented herein were obtained at the W. M. Keck Observatory, which is operated as a scientific partnership among the California Institute of Technology, the University of California, and the National Aeronautics and Space Administration. The Observatory was made possible by the generous financial support of the W. M. Keck Foundation. This research made use of NASA's Astrophysics Data System.

This project would not have been possible without major allocations of Keck telescope time from the University of California, the California Institute of Technology, the University of Hawaii, and NASA. This work utilized the SIMBAD astronomical database.

Author contributions: H.I. conducted the analysis and wrote the paper. A.W.H. was an originator of the survey. B.F., E.A.P., and L.M.W. are original collaborators on CLS. S.R.K. and B.C. advised on the analysis. Authors C.B. to N.S. in the author list above provided comments on the paper and contributed to the observing effort in order of their appearance.

The data collected here, previously published and novel, was gathered on over 1500 individual nights by 152 unique observers. Without their contribution to astronomical data collection, this work would not be possible.

The authors wish to recognize and acknowledge the very significant cultural role and reverence that the summit of Maunakea has always had within the indigenous Hawaiian community. We are most fortunate to have the opportunity to conduct observations from this mountain.

Facility: Keck:I (HIRES)

Software: We made use of the following publicly available Python modules: Astropy (Astropy Collaboration et al. 2013, 2018, 2022), matplotlib (Hunter 2007), numpy (van der Walt et al. 2011), scipy (Virtanen et al. 2020), and pandas (McKinney 2010). IDL was used to extract the spectral line information (ENVI version 4.8; Exelis Visual Information Solutions, Boulder, Colorado).

ORCID iDs

Howard Isaacson https://orcid.org/0000-0002-0531-1073
Andrew W. Howard https://orcid.org/0000-0001-8638-0320
Benjamin Fulton https://orcid.org/0000-0003-3504-5316
Erik A. Petigura https://orcid.org/0000-0003-0967-2893
Lauren M. Weiss https://orcid.org/0000-0002-3725-3058
Stephen R. Kane https://orcid.org/0000-0002-7084-0529
Corey Beard https://orcid.org/0000-0001-7708-2364
Steven Giacalone https://orcid.org/0000-0002-8965-3969
Judah Van Zandt https://orcid.org/0000-0002-4290-6826
Joseph M. Akana Murphy https://orcid.org/0000-0001-8898-8284
Fei Dai https://orcid.org/0000-0002-8958-0683
Ashley Chontos https://orcid.org/0000-0003-1125-2564
Alex S. Polanski https://orcid.org/0000-0001-7047-8681
Malena Rice https://orcid.org/0000-0002-7670-670X
Jack Lubin https://orcid.org/0000-0001-8342-7736
Casey Brinkman https://orcid.org/0000-0002-4480-310X
Ryan A. Rubenzahl https://orcid.org/0000-0003-3856-3143
Sarah Blunt https://orcid.org/0000-0002-3199-2888
Samuel W. Yee https://orcid.org/0000-0001-7961-3907
Mason G. MacDougall https://orcid.org/0000-0003-2562-9043
Paul A. Dalba https://orcid.org/0000-0002-4297-5506
Dakotah Tyler https://orcid.org/0000-0003-0298-4667
Isabel Angelo https://orcid.org/0000-0002-9751-2664
Daria Pidhorodetska https://orcid.org/0000-0001-9771-7953
Andrew W. Mayo https://orcid.org/0000-0002-7216-2135
Rae Holcomb https://orcid.org/0000-0002-5034-9476
Emma V. Turtelboom https://orcid.org/0000-0002-1845-2617
Michelle L. Hill https://orcid.org/0000-0002-0139-4756
Luke G. Bouma https://orcid.org/0000-0002-0514-5538
Jingwen Zhang https://orcid.org/0000-0002-2696-2406
Nicholas Saunders https://orcid.org/0000-0003-2657-3889

References

Angus, R., Morton, T., Aigrain, S., Foreman-Mackey, D., & Rajpaul, V. 2018, MNRAS, 474, 2094
Astropy Collaboration, Price-Whelan, A. M., Lim, P. L., et al. 2022, ApJ, 935, 167
Astropy Collaboration, Price-Whelan, A. M., Sipőcz, B. M., et al. 2018, AJ, 156, 123
Astropy Collaboration, Robitaille, T. P., Tollerud, E. J., et al. 2013, A&A, 558, A33
Astudillo-Defru, N., Forveille, T., Bonfils, X., et al. 2017, A&A, 602, A88
Baliunas, S. L., Donahue, R. A., Soon, W. H., et al. 1995, ApJ, 438, 269
Barnes, S. A. 2007, ApJ, 669, 1167
Baum, A. C., Wright, J. T., Luhn, J. K., & Isaacson, H. 2022, AJ, 163, 183
Boro Saikia, S., Marvin, C. J., Jeffers, S. V., et al. 2018, A&A, 616, A108
Bowens-Rubin, R., Akana Murphy, J. M., Hinz, P. M., et al. 2023, AJ, 166, 260
Chen, Y., King, J. R., & Boesgaard, A. M. 2014, PASP, 126, 1010
Cincunegui, C., Díaz, R. F., & Mauas, P. J. D. 2007, A&A, 469, 309
David, T. J., Angus, R., Curtis, J. L., et al. 2022, ApJ, 933, 114
Dragomir, D., Kane, S. R., Henry, G. W., et al. 2012, ApJ, 754, 37
Duncan, D. K., Vaughan, A. H., Wilson, O. C., et al. 1991, ApJS, 76, 383
Eberhard, G., & Schwarzschild, K. 1913, ApJ, 38, 292
Fischer, D. A., Marcy, G. W., & Spronck, J. F. P. 2014, ApJS, 210, 5
Flores, M., González, J. F., Jaque Arancibia, M., Buccino, A., & Saffe, C. 2016, A&A, 589, A135
Fuhrmeister, B., Coffaro, M., Stelzer, B., et al. 2023, A&A, 672, A149
Fulton, B. J., & Petigura, E. A. 2018, AJ, 156, 264
Fulton, B. J., Rosenthal, L. J., Hirsch, L. A., et al. 2021, ApJS, 255, 14
Fulton, B. J., Weiss, L. M., Sinukoff, E., et al. 2015, ApJ, 805, 175
Gomes da Silva, J., Santos, N. C., Adibekyan, V., et al. 2021, A&A, 646, A77
Hall, J. C., Lockwood, G. W., & Skiff, B. A. 2007, AJ, 133, 862
Henry, T. J., Soderblom, D. R., Donahue, R. A., & Baliunas, S. L. 1996, AJ, 111, 439
Howard, A. W., Johnson, J. A., Marcy, G. W., et al. 2010, ApJ, 721, 1467
Hunter, J. D. 2007, CSE, 9, 90
Irving, Z. A., Saar, S. H., Wargelin, B. J., & do Nascimento, J.-D. 2023, ApJ, 949, 51
Isaacson, H., & Fischer, D. 2010, ApJ, 725, 875
Jeffers, S. V., Kiefer, R., & Metcalfe, T. S. 2023, SSRv, 219, 54
Johnson, M. C., Endl, M., Cochran, W. D., et al. 2016, ApJ, 821, 74
Joyce, M., & Chaboyer, B. 2018, ApJ, 856, 10
Kane, S. R. 2023, AJ, 166, 187
Kane, S. R., Thirumalachari, B., Henry, G. W., et al. 2016, ApJL, 820, L5
Kraft, R. P. 1967, ApJ, 150, 551
Lovis, C., Dumusque, X., Santos, N. C., et al. 2011, arXiv:1107.5325
Lubin, J., Robertson, P., Stefansson, G., et al. 2021, AJ, 162, 61
Luhn, J. K., Wright, J. T., Henry, G. W., Saar, S. H., & Baum, A. C. 2022, ApJL, 936, L23
Luhn, J. K., Wright, J. T., Howard, A. W., & Isaacson, H. 2020, AJ, 159, 235
Mamajek, E. E., & Hillenbrand, L. A. 2008, ApJ, 687, 1264
Marcy, G. W., Isaacson, H., Howard, A. W., et al. 2014, ApJS, 210, 20
Marsden, S. C., Petit, P., Jeffers, S. V., et al. 2014, MNRAS, 444, 3517
Marvin, C. J., Reiners, A., Anglada-Escudé, G., Jeffers, S. V., & Boro Saikia, S. 2023, A&A, 671, A162
Mayor, M., & Queloz, D. 1995, Natur, 378, 355
McKinney, W. 2010, in Proc. of the 9th Python in Science Conf., ed. W. Stéfan van der & M. Jarrod, 56
McQuillan, A., Mazeh, T., & Aigrain, S. 2014, ApJS, 211, 24
Metcalfe, T. S., Buccino, A. P., Brown, B. P., et al. 2013, ApJL, 763, L26
Metcalfe, T. S., Finley, A. J., Kochukhov, O., et al. 2022, ApJL, 933, L17
Metcalfe, T. S., Strassmeier, K. G., Ilyin, I. V., et al. 2023, ApJL, 948, L6
Metcalfe, T. S., Strassmeier, K. G., Ilyin, I. V., et al. 2024, ApJL, 960, L6

Mittag, M., Schmitt, J. H. M. M., & Schröder, K. P. 2013, A&A, 549, A117
Mittag, M., Schmitt, J. H. M. M., & Schröder, K. P. 2023, A&A, 674, A116
Noyes, R. W., Hartmann, L. W., Baliunas, S. L., Duncan, D. K., & Vaughan, A. H. 1984, ApJ, 279, 763
Obridko, V. N., Katsova, M. M., & Sokoloff, D. D. 2022, MNRAS, 516, 1251
Oláh, K., Kővári, Z., Petrovay, K., et al. 2016, A&A, 590, A133
Perdelwitz, V., Mittag, M., Tal-Or, L., et al. 2021, A&A, 652, A116
Petigura, E. A., Howard, A. W., Marcy, G. W., et al. 2017, AJ, 154, 107
Ramírez, I., & Meléndez, J. 2005, ApJ, 626, 465
Robertson, P., Endl, M., Cochran, W. D., MacQueen, P. J., & Boss, A. P. 2013, ApJ, 774, 147
Rosenthal, L. J., Fulton, B. J., Hirsch, L. A., et al. 2021, ApJS, 255, 8
Savanov, I. S. 2012, ARep, 56, 716
Schröder, K. P., Mittag, M., Hempelmann, A., González-Pérez, J. N., & Schmitt, J. H. M. M. 2013, A&A, 554, A50
See, V., Roquette, J., Amard, L., & Matt, S. 2023, MNRAS, 524, 5781
Shah, S. P., Wright, J. T., Isaacson, H., Howard, A. W., & Curtis, J. L. 2018, ApJL, 863, L26
Shen, Y.-F., Zhao, G., & Bird, S. A. 2022, Univ, 8, 488
Suárez Mascareño, A., Rebolo, R., González Hernández, J. I., & Esposito, M. 2015, MNRAS, 452, 2745
Suárez Mascareño, A., Rebolo, R., & González Hernández, J. I. 2016, A&A, 595, A12
Suárez Mascareño, A., Rebolo, R., González Hernández, J. I., et al. 2018, A&A, 612, A89
Toledo-Padrón, B., González Hernández, J. I., Rodríguez-López, C., et al. 2019, MNRAS, 488, 5145
van der Walt, S., Colbert, S. C., & Varoquaux, G. 2011, CSE, 13, 22
van Saders, J. L., Ceillier, T., Metcalfe, T. S., et al. 2016, Natur, 529, 181
Vaughan, A. H., Preston, G. W., & Wilson, O. C. 1978, PASP, 90, 267
Virtanen, P., Gommers, R., Oliphant, T. E., et al. 2020, NatMe, 17, 261
Wargelin, B. J., Saar, S. H., Pojmański, G., Drake, J. J., & Kashyap, V. L. 2017, MNRAS, 464, 3281
Wilson, O. C. 1968, ApJ, 153, 221
Wright, J. T. 2016, arXiv:1603.08384
Wright, J. T., Marcy, G. W., Butler, R. P., & Vogt, S. S. 2004, ApJS, 152, 261
Wright, J. T., Marcy, G. W., Butler, R. P., et al. 2008, ApJL, 683, L63
Yee, S. W., Petigura, E. A., & von Braun, K. 2017, ApJ, 836, 77

4.3 Links and implications

In Chapter 4 we extend the primary theme of stellar activity in main-sequence stars to catalog time-series activity for 710 stars, 138 of which have stellar activity cycles. Using the reliable Keck telescope and HIRES instrument, we present homogeneously collected S-value time-series over 20 years and present an empirical identification of the T_{eff} vs. stellar activity cycle period correlation. By including the precise determination of the fundamental stellar properties in our analysis, we can precisely identify connections and transitions in the phases as stellar chromospheric activity. Heterogeneous studies that attempt to pull as many observations as possible from published works must contend with systematic errors that can be difficult to identify and disentangle from astrophysical phenomena.

We present a decades-long survey that utilizes the same instrumental setup and procedure that is capable of producing 2 meters per second radial velocity variation measurements. We use simultaneous observations of the chromospheric-activity-sensitive Ca II H & K spectral lines to draw conclusions about the magnetic activity of main-sequence stars with ages between 1 and 4 Gyr. Such observations are only possible with dedicated ground-based observations and homogeneously determined stellar properties.

CHAPTER 5: THE CALIFORNIA LEGACY SURVEY VI - THE FATE OF STELLAR ACTIVITY CYCLES

5.1 Introduction

Drawing from our experience in exploring two astrophysical phenomena in Chapters 3 (stellar rotation) and 4 (stellar activity cycles), we will now focus on a narrow fraction of the CLS sample to analyze the late stages of main-sequence stellar activity. Our sample, chosen to be older than the age of the Sun at 4.5 Gyr, has weak rotational modulation, making it difficult to study compared to younger stars. We explore traditional activity metrics and time-series derived S-value variability to show that these old stars have a large range of activity variability at a mean activity level. We include precise and homogeneously derived stellar properties to show that variability only occurs for the oldest stars. While presenting evidence that stars can have varying cycle amplitudes over sequential cycles, we identify the least active stars as the likely end-state of stellar activity. The activity floor appears at the limit of our spectral measurements and is identified in stars with masses between 0.70 and 1.1 solar masses.

5.2 Submitted paper

Draft version January 22, 2025
Typeset using LaTeX twocolumn style in AASTeX631

The California Legacy Survey VI - The Fate of Activity Cycles in Sun-like Stars

Howard Isaacson [1,2] Stephen R. Kane [3,2] Brad Carter [2] and Andrew W. Howard [4]

[1] 501 Campbell Hall, University of California at Berkeley, Berkeley, CA 94720, USA
[2] Centre for Astrophysics, University of Southern Queensland, Toowoomba, QLD, Australia
[3] Department of Earth and Planetary Sciences, University of California, Riverside, CA 92521, USA
[4] California Institute of Technology, Pasadena, CA 91125, USA

ABSTRACT

We analyze the spectra of 91 solar-type G and K type main-sequence dwarfs in the solar neighborhood to assess activity trends with stellar properties. As a follow-on to our studies of the decoupling of rotation from age, we use chromospheric activity time series data to probe changes in stellar activity cycles as further evidence of differences in magnetic dynamos. We present evidence that the average chromospheric activity remains nearly constant while the variation in a star's activity decreases by an order of magnitude. Measurable changes to the stellar dynamo are suggested that are not strongly correlated with the average stellar activity, but instead correlated with the amplitude of activity variations for stars beyond the age of the Sun. In contrast, while the activity cycle period is strongly correlated with effective temperature for stars aged between 2 and 4 Gyr, we find no such correlation for stars older than the Sun or otherwise low activity stars beyond $\log(R'_{HK})$ = -4.90. By quantifying the Ca II H & K activity variation over the timescales of stellar cycles, we suggest that age dating of mature-age solar-type stars requires knowledge of activity variability in addition to the average activity.

Keywords: Chromospheric Activity, Stellar Activity Cycles, Stellar Astrophysics, Stellar Age

1. INTRODUCTION

From the earliest observations of Sun spots in the 1700s (Galileo's "Letters on SunSpots"), inhomogeneities on the solar surface have revealed the solar rotation period, and the stellar activity period (Schwabe 1843). Low-resolution spectra collected in the early 1900s connected the Calcium H and K lines to variability in the Sun, and later to the intensity of magnetic field strength (Eberhard & Schwarzschild 1913). Time series observations from the Mt. Wilson survey of nearby stars and their Ca II H and K line flux provided the first evidence of stellar activity cycles similar to the solar cycle (Baliunas et al. 1995). The observational effort to connect other stars to the Sun blossomed into the study of stellar activity, rotation and ages (Barnes 2007; Mamajek & Hillenbrand 2008).

Corresponding author: Howard Isaacson
hisaacson@berkeley.edu

Subtle deviations of classic spin down models, in which stars lose angular momentum to the stellar wind, have been informed by the Kepler Space Mission. *Kepler* provided precise photometry on months-long baselines that is capable of measuring stellar rotation periods for tens of thousands of stars (McQuillan et al. 2014) and precise stellar parameters for a subset of those stars via asteroseismology (Hall et al. 2021; Saunders et al. 2024; Bhalotia et al. 2024). Rotation period analysis in stellar clusters observed by Kepler revealed detailed correlations between rotation and temperature for stars at the same age (Curtis et al. 2020; Meibom et al. 2015).

The theory of Weakened Magnetic Braking (WMB) can provide an explanation for the observations that show some stars spin faster than they should for their age (van Saders et al. 2016), suggesting a disconnect between the rotation period and age of stars near the age of the Sun, 4 Gyr (Metcalfe & Egeland 2019). WMB describes a critical threshold of the Rossby number where a dramatic shift in the magnetic field occurs and is measurable in the rotation period and age relationship. Studies of Kepler planet host stars with measured rotation periods (David et al. 2022) are consistent with an overabundance of old stars with fast rotation. The stars that show this behavior most dramatically are F-stars with thin convective zones that evolve more quickly off the main-sequence than cooler stars.

Solar twins, similar in mass, temperature and composition, have been used to understand subtle changes in chromospheric activity. Lorenzo-Oliveira et al. (2018) studied solar twins observed with HARPS (High Accuracy Radial-velocity Planet Searcher) and argued for a continuous activity decrease in the age range 1–9 Gyr. They claimed that the non-uniform decreases in activity are due to an inadequate calculation of the log($\mathrm{R}'_{\mathrm{HK}}$) metric, specifically the underlying photospheric contribution to the S-value. As the most fundamental metric of chromospheric activity, the S-value is the ratio of the flux in the cores of the Ca II H and K lines normalized by the continuum on either side of the absorption features. Log($\mathrm{R}'_{\mathrm{HK}}$) is chromospheric activity metric that is valid across a range of main-sequence star temperatures (Noyes et al. 1984). Updates to log($\mathrm{R}'_{\mathrm{HK}}$) have provided a revised activity metric beyond solar twins that is comparable across all spectral types (Mittag et al. 2013, log $\mathrm{R}^{+}_{\mathrm{HK}}$). Using $B-V$ as the primary variable of the stellar type has been extremely useful due to vast number of stars that can analyzed.

Spectropolarimetry, measuring magnetic field orientations of stars with similar stellar properties but different activity levels, supports the conclusion of a rapid change in magnetic field topology near the age of the Sun (Brown et al. 2022; Metcalfe et al. 2022, 2024). These observations, along with WMB models are consistent in showing that stars with the same average chromospheric activity [log($\mathrm{R}'_{\mathrm{HK}}$)] can have very different magnetic field properties.

We examine a set of homogeneously determined stellar activity cycles, and inactive stars, with precisely determined stellar properties to probe the magnetic fields of G and K main-sequence stars with ages older than 4 Gyr (Section 2). We will introduce the standard deviation of the S-value time series (S-STD) as a critical variable in the evolution of stellar activity (Section 2.3), and will examine stellar activity changes in bins of stellar mass. We argue below that using the $\mathrm{T}_{\mathrm{eff}}$ rather $B-V$ to calculate log($\mathrm{R}'_{\mathrm{HK}}$) has several analytical benefits, but we use log($\mathrm{R}'_{\mathrm{HK}}$)-N1984 to perform our sample selection to offer continuity with past studies (Section 3).

Our primary analysis will examine the S-STD activity metric as a function of stellar properties (Section 3.4). We will also search for trends between the cycle period and the fundamental stellar properties of the star.

2. DATA AND SAMPLE

For our empirical analysis, we select 91 stars from the California Legacy Survey (CLS1; Rosenthal et al. 2021) sample of activity cycles, 58 of which are cycling (Isaacson et al. 2024). The CLS1 sample contains 719 stars of FGKM spectral types, including main-sequence stars and sub-giants. Of the 285 stars that were searched for activity cycles, our restricted sample for the present analysis must meet the following criteria:

1. The stellar mass range is between 0.7–1.1 $M_{\odot}$, binned by 0.10 $M_{\odot}$. Each increasing mass bin contains 18/24, 20/29, 15/24, 5/13 stars where the numbers correspond to those with cycles and the total number of stars in each bin. The next highest mass bin has only 7 stars and is omitted.

2. The log(g) values must be greater than 4.3. Changes to log(g) reflect changes in the stellar radius. We aim to identify changes to the magnetic dynamo that are independent of stellar evolution. Using a cutoff of 4.3 allows us to include more stars, especially in the higher mass bin, while limiting the effect of changes in the dynamo that are due to stellar evolution. Our resulting range of stellar masses and radii are 0.703 to 1.085 $M_{\odot}$ and 0.71 to 1.20 $R_{\odot}$, respectively. ADDED: *"The purpose of restricting the log(g) at 4.3 is to minimize the effects of stellar evolution in order to focus on stellar activity changes in stars that are on the main sequence. By using log(g) as a cutoff value, we are more likely to discard stars more massive than 1.0 $M_{\odot}$ and less likely to discard less massive stars. We have explored using the height above the main sequence as a threshold for including stars, but found this had a similar effect. "*

3. Metallicity has an important effect on our analysis, but we restrict [Fe/H] to be above -0.5, where our sample is more densely populated.

4. We remove HD 146362B due to the ambiguity in our data between it and its binary companion HD 146362A.

5. We categorize HD 45184 with the cycling stars, noting the cycle discovery in Flores et al. (2016).

6. We restrict the log($\mathrm{R}'_{\mathrm{HK}}$) values to be less than -4.90, the value at which log($\mathrm{R}'_{\mathrm{HK}}$) becomes less descriptive of a star's activity. We keep stars with and without activity cycles. This results in a minimum stellar chromospheric age of roughly 4 Gyr.

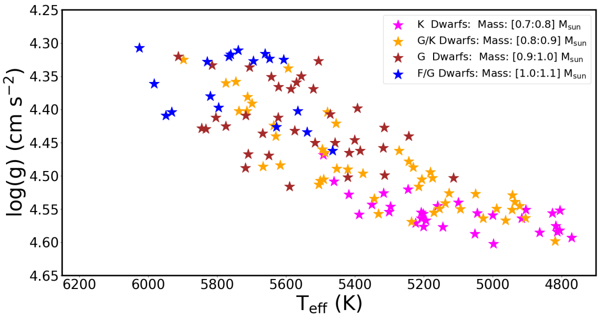

Figure 1. T_{eff}, $\log(g)$ and stellar mass are shown for our sample of stars. They have masses between 0.7–1.1 $M_{\odot}$. Stars with similar masses can have a range of T_{eff}. We narrow the $\log(g)$ range to assess magnetic field changes for stars while they are still on the main-sequence. Both the cycling stars and inactive stars are plotted.

7. Our sample has a minimum, median, and maximum number of observations of 47, 109, and 944.

8. Our resulting sample is shown in T_{eff}/$\log(g)$ space in Figure 1, highlighting the mass bins that we use in our analysis.

We motivate the choice to analyze stars less active than $\log(R'_{HK})$-4.90 with Figure 2 showing that as the median activity decreases, as expected, over time (time increases left to right), the S-STD changes by an order of magnitude at a constant median activity level. From top to bottom, we plot the average S-value, $\log(R'_{HK})$ from Noyes et al. (1984) and $\log(R'_{HK})$ from Lorenzo-Oliveira et al. (2018). For the least active stars, they have a very low median activity value and a very low standard deviation of the S-values (S-STD). We further divide the sample in the following sections and explore the different mass bins of stars based on their average activity and S-STD.

2.1. *Uncertainties*

We divide our sample into stellar mass bins with the goal of identifying activity evolution as a function of mass. Our mass uncertainties, taken from Rosenthal et al. (2021) range from 1–4.5%. Analysis of the uncertainties between stellar models and their limitations (Tayar et al. 2022) has shown that upper limits on stellar mass uncertainties are 5%. Even though differential mass measurements may be valid below this value, we find mass bins of 0.10 $M_{\odot}$ to be a reasonable bin size.

For the T_{eff}, $\log(g)$, and [Fe/H] values, we adopt the CLS1 uncertainties with median values of 80 K, 0.028, and 0.06, respectively. S-value uncertainties on individual measurements are 0.001, adopted from Isaacson et al. (2024). The extremely precise S-values and homogeneously determined stellar properties allow for an unprecedented examination of the main sequence stars older than the Sun.

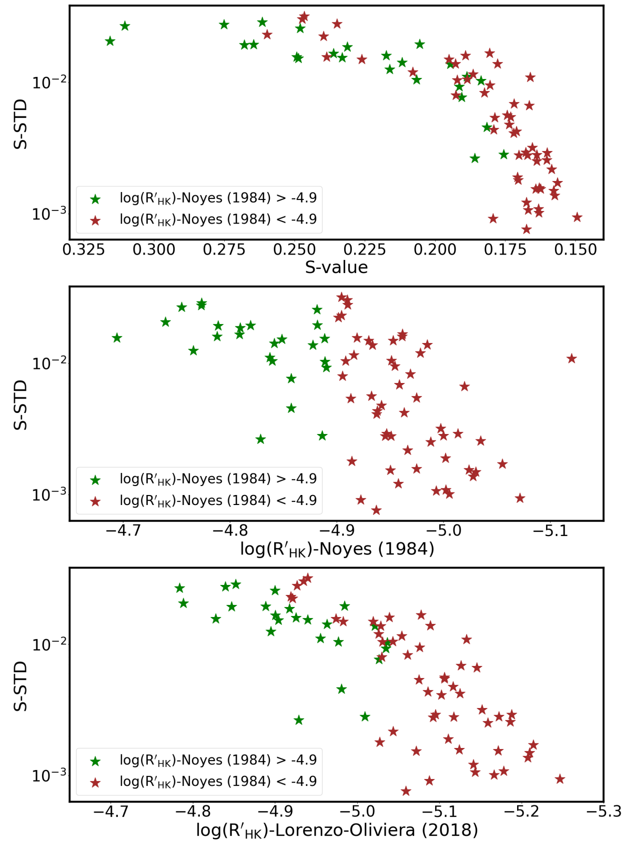

Figure 2. The standard deviation of the S-values (S-STD) is plotted as a function of median S-value, $\log(R'_{HK})$-N1984 and $\log(R'_{HK})$-L02018 for stars with masses between 0.7–1.1 $M_{\odot}$. The more active stars, with $\log(R'_{HK}) >$ -4.90 are in green, and the less active stars that compose our primary sample are in brown. The vertical stratification for any given value of the average activity displays the S-STD as a valuable metric for studying main-sequence magnetic field evolution.

2.2. *Dividing the sample*

Isaacson et al. (2024) found that by dividing the sample into temperature bins, the chromospheric activity cycle periods show strong correlation and low scatter for stars between 1–4 Gyr, corresponding to $\log(R'_{HK})$ from -4.70 to -4.90. The trend is consistent in showing that hotter stars have shorter cycles than cooler stars in this age/activity range as some dynamo models have shown (Kitchatinov 2022). At the transitional activity value of -4.90, near the activity level of the Sun, and near the onset of WMB, the gyrochronology-age relation breaks down (Metcalfe & Egeland (2019). We use this critical $\log(R'_{HK})$ value, which has been proposed to correspond to a critical Rossby number (van Saders et al. 2016), to define our sample, selecting stars less active than $\log(R'_{HK})$ of -4.90. We will show in Section 2.3 that for more active stars, the variability is similar for a given average value and for less active stars, the average activity of a star varies significantly. Figure 3 shows that the correlation in mass is not as strong as temperature bins for stars more active than -4.9, and more analysis is required to understand the less active stars. We present that analysis is Section 3.

2.3. *Metrics of Activity*

The $\log(R'_{HK})$ metric defined by Noyes et al. (1984) is an incredibly useful and widely adopted chromospheric activity metric. As a function of $B-V$ colors and S-value, the $\log(R'_{HK})$ metric can be used to compare activity levels across a wide range of spectral types, from F to K dwarfs. Using this metric, the solar value of $\log(R'_{HK}) = -4.95$ was identified as a transition point in the activity evolution of stars near the age of the Sun Metcalfe & Egeland (2019). At this average activity level, the age determinations from gyrochronology and chromospheric activity begin to diverge due to a change in the magnetic field structure (Metcalfe et al. 2022). For older, less active stars, the chromospheric ages disagree with gyrochronology ages. Overall, the $\log(R'_{HK})$ metric has been invaluable for chromospheric activity studies, and remains valid, especially when considering the activity ages and rotation of stars younger than the Sun. We conservatively choose -4.90 as our cutoff value.

Alternative formulations of the $\log(R'_{HK})$ metric have been created using updated stellar models and and T_{eff} instead of $B-V$. The PHOENIX models, catalog S-values, and $B-V$ photometry converted to T_{eff} were used to calculate an $\log(R'_{HK})$-like metric allowing comparison of giant, sub-giant, and main-sequence stars for a wide range of spectral types (Mittag et al. 2013). A later study of the HARPS sample used a metric, $\log(R_5)$ and log (σR_5) (Gomes da Silva et al. 2021), which are conceptually similar to the mean $\log(R'_{HK})$ and variation in $\log(R'_{HK})$. They also identified the importance of the activity variability using the log σ (R_5) metric. Separately, the color-correction factor that is used to calculate the photometric Ca II H and K flux was recalibrated, and the stellar effective temperature was used in place of $B-V$ to calculate the ages of solar twins (Lorenzo-Oliveira et al. 2018). Using $B-V$ value to calculate $\log(R'_{HK})$ is less precise than using T_{eff} because it conflates the temperature and metallicity (Lo-

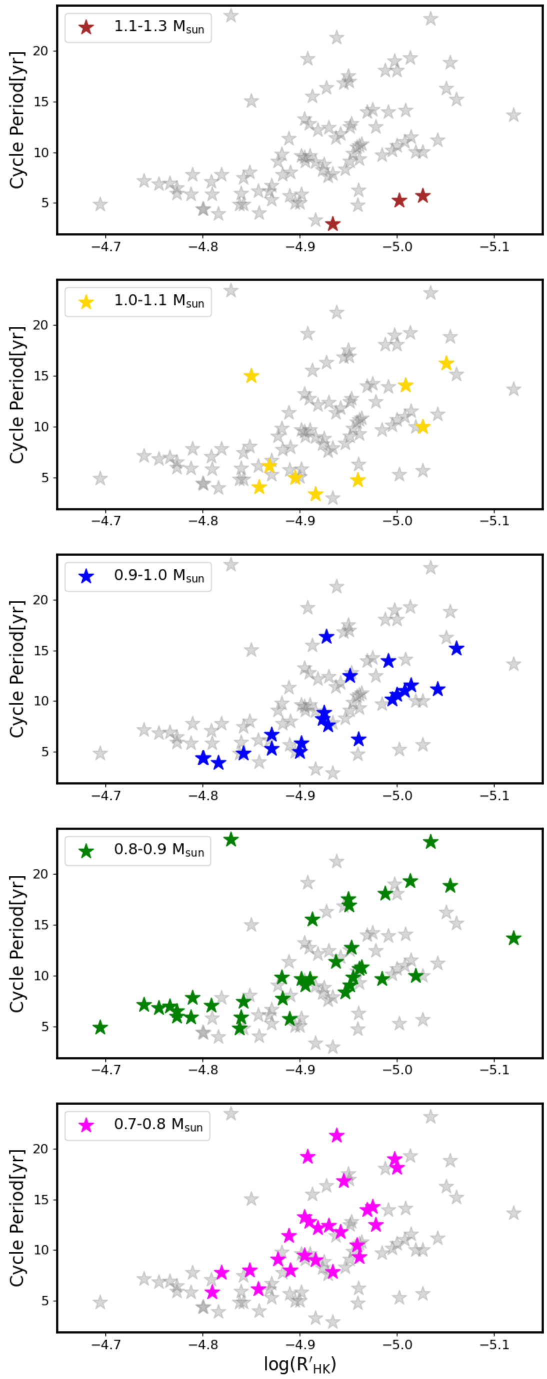

Figure 3. Stellar activity cycle period binned by stellar mass. We do not see the same tight correlation with temperature and cycle period for stars more active than $\log(R'_{HK})$ (Noyes-1984) of -4.90 compared to the tight correlation when binned by T_{eff} (Isaacson et al. 2024). The stars less active than -4.90 have large scatter in cycle period for a variety of time-averaged activity values. Gray data points represent all mass bins.

vis et al. 2011; Mittag et al. 2013; Isaacson et al. 2024). With the ability to calculate $T_{\rm eff}$, $\log(g)$, and [Fe/H] from the same spectra used to measure the S-values, the Lorenzo-Oliveira et al. (2018) version of $\log(R'_{HK})$ ($\log(R'_{HK})$-LO2018) can be used to search for correlations with metallicity that are otherwise conflated in the $\log(R'_{HK})$-N1984 calculation.

Our division of the sample by mass reduces the need for a spectral-type indifferent metric. We will assess the Lorenzo-Oliveira et al. (2018) and the Noyes et al. (1984) $\log(R'_{HK})$ values as activity metrics for stars older than the Sun and add the variation in activity levels and consider their use as a proxy for stellar age. Combining the fundamental stellar properties from CLS, and precise S-value time series, all of which are calculated from uniformly observed and analyzed spectra, we will use the S-value and standard deviation of the S-values (S-STD) to find subtle relationships between stellar activity and fundamental stellar properties. We will argue that S-value is more effective than using the $\log(R'_{HK})$-N1984 or $\log(R'_{HK})$-LO2018, or $\log(\sigma R_5)$ when stars are divided into bins by stellar mass.

3. RESULTS

3.1. *Setting the Stage*

Our analysis consists of examination of the best activity metrics to use, their strengths and weaknesses, and applying that knowledge to examining fundamental stellar property correlations to activity variability. We will argue that S-STD is an excellent choice for identifying exceptionally inactive stars, and that correlations between activity and stellar properties vary by stellar mass.

In Figure 4 we plot the S-STD as a function of median S-value, $\log(R'_{HK})$-N1984, and $\log(R'_{HK})$-LO2018 for four linearly-spaced mass bins in the range of 0.7–1.1 $M_\odot$. In each panel, average activity is higher on the left and decreases to the right. The vertical axis is S-STD, and indicates the level of variability in a star's S-value time-series.

By calculating the Pearson correlation coefficient (P-CC) for each panel, one value for the cycling stars and one for the cycling plus inactive stars, we see that the average S-value consistently tracks with the variability with higher correlation than the other metrics. These plots emphasize that $\log(R'_{HK})$-N1984 cannot distinguish between cycling and inactive stars below a value of -4.90 as well as the S-value. The stars with the lowest S-STD have a range of $\log(R'_{HK})$-N1984 values. The $\log(R'_{HK})$-LO2018 bins have similar P-CC values in the two lowest mass bins (0.92, 0.71) but shows weaker correlation for the two higher mass bins, (0.5, 0.5). We use yellow star symbols to indicate stars without detected activity cycles and find that they typically populate a unique parameter space, a smaller S-STD compared to the cycling stars in the same mass bins.

These correlations call for studies of theoretical dynamo models to utilize the variability of a star's activity-variability in addition to its average activity (Gomes da Silva et al. 2021; Brown et al. 2022; Luhn et al. 2022), and if only the average activity is available, the S-value plus the stellar mass is the best metric. One theory that could include activity variability is WMB which identifies an average value for activity for a star in $\log(R'_{HK})$-N1984 and converts that into a Rossby number using a theoretical prediction for the convective turnover time (Noyes et al. 1984; Corsaro et al. 2021). This is sufficient treatment for stars more active than the -4.90 threshold, where the average activity value tracks with the S-STD (Figure 2). Using the P-CC values, our sample shows that using an average value of $\log(R'_{HK})$-N1984 (low P-CC values) does not fully inform the state of a star's activity as measured by S-STD. Using the S-value is a better solution for every mass bin because they have the highest P-CC values, although $\log(R'_{HK})$-LO2018 will perform comparably for the lowest mass bin.

3.2. *The Least Active Stars*

We identify the least active stars in Figure 4 (yellow star symbols) as those having the smallest S-STD values and no identified activity cycle (Isaacson et al. 2024). The average chromospheric activity metrics are insufficient to distinguish these inactive stars from those that are still cycling. Time-series data is required to identify the absence of a cycle and to show that such stars are much less active than the cycling stars with similar average activity.

In the 0.70–0.80 $M_\odot$ mass bin of Figure 4, HD 166620 is identified as one of the five least active stars (magenta symbol), consistent with the identification of its Maunder Minimum Baum et al. (2022); Luhn et al. (2022). Tau Ceti (green symbol), a well-studied stellar activity standard star, is known to have a pole-on inclination (Korolik et al. 2023) that precludes us from identifying its chromospheric activity cycle or rotational modulation via S-value time-series. HD 190067 (brown symbol) has no identified cycle in a parameter space where we expect one. We assess this outlier as likely have an unidentified cycle due to poor time sampling. *ADDED: The lack of visible activity cycle is an observational assessment of Tau Ceti S-values. Possible explanations of why we do not see activity cycle changes include the decrease in spot intensity as they migrate from the equator*

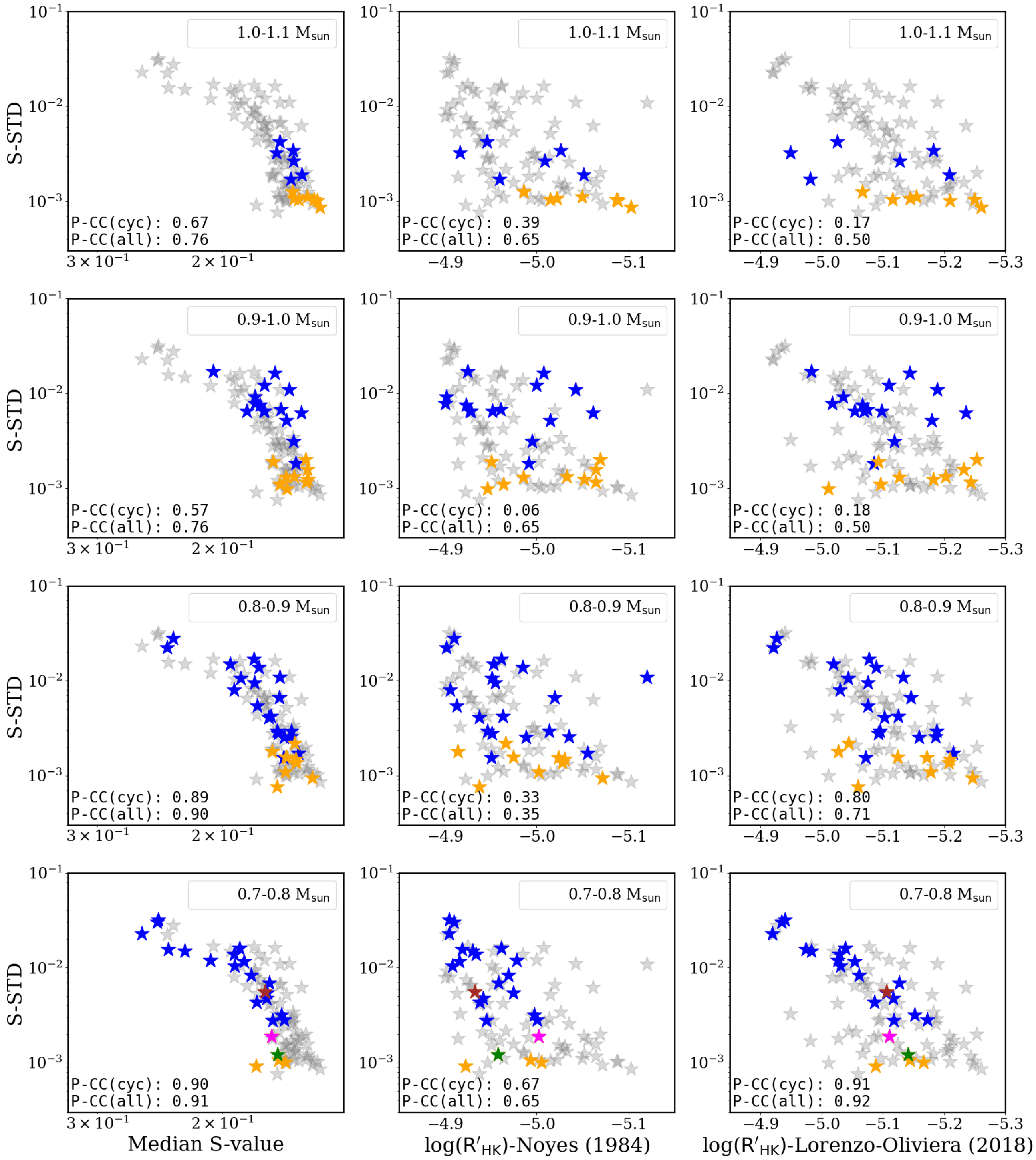

Figure 4. Average activity data vs S-STD is plotted for four equally spaced mass bins that decrease from top to bottom. The left, middle and right columns show the median S-value, the log(R'_{HK})-N1984 value and the log(R'_{HK})-LO2018 metric on the x-axis. For each panel, the Pearson correlation coefficient (P-CC) is calculated separately for the cycling stars (blue symbols) and all stars in each mass bin. We find the correlations between activity variation and each activity metric vary by mass bin, with S-value showing the strongest correlation on average. From the inactive stars (gold symbols) we single out HD 166620 (magenta) Tau Ceti (green) and HD 190067 (brown). Gray data points represent stars from all mass bins.

to the pole, diminished differences between spot and non-spot coverage due to limb darkening, and the effect of pole-on viewing angle on plages. It is possible for other stars to have this scenario but it is statistically unlikely.

In the 0.80–0.90 $M_\odot$ bin of Figure 4, the inactive and cycling stars overlap. The non-cycling stars have no *identified* cycles but have similar S-STD to cycling stars. The two stars with cycles that overlap the inactive stars are robustly detected cycles but have extremely small amplitudes. These stars are HD 126053 and HD 221354 with S-value cycle semi-amplitudes of 0.0018 and 0.0035. The single measurement S-value uncertainty of 0.001. For a very small amplitude cycle to be detected, perhaps these stars have near edge-on inclinations.

In the 0.90–1.00 $M_\odot$ bin of Figure 4 two populations are vertically differentiated, one near S-STD of 0.01 and one near 0.001. The two stars that are cycling but near the inactive cluster, are HD 52711 and HD 42618. Again, if these stars are edge on, we are more likely to detect their small amplitude cycles. The pile-up of stars near an S-STD value of 0.01 that is not present in any other mass bin, may reveal a change in the stellar dynamo in this mass bin that happens over astrophysically short timescales. Or if stars move between cycling and inactive phases, perhaps a stochastic mechanism requires a bimodal distribution of S-STD.

In the 1.00-1.10 $M_\star$ bin of Figure 4, the inactive stars are vertically clustered indicating the floor of activity, and perhaps the lower limit of our measurements. The inactive stars in this bin represent very old stars that have low amplitude activity cycles that either fall below our measurement threshold or have periods longer than our observing baseline, or both. Continued monitoring could reveal a star exiting its inactive state, or only its permanent inactivity.

There is no metric of average activity that uniquely identifies inactive stars. For stars with chromospheric ages older than the Sun, the stars without cycles are the least active in time-averaged activity, for every mass bin, although in some bins the populations overlap. As stars decrease in S-STD the regular periodic cycles tend to become less complex, their amplitude lower (Oláh et al. 2016). Next, we search for correlations the S-STD values and fundamental stellar parameters.

3.3. *Stellar Properties and Activity Variability*

In Figure 5 we examine the relationship between stellar properties determined from high-resolution spectra from Keck/HIRES and the CLS survey to determine whether any of these properties can differentiate the cycling stars from inactive stars that may have aged out of their cycles. We also search for correlations between S-STD and $T_{\rm eff}$, log(g) and [Fe/H] such as the temperature-period relationship for 2–4 Gyr stars empirically identified in Isaacson et al. (2024).

3.3.1. *S-STD and Stellar Surface Temperature*

In the left column of Figure 5 the $T_{\rm eff}$ is plotted against S-STD for the same 0.7–1.1 $M_\odot$ stellar mass bins as in Figure 4. For the sub-solar mass bins, the negative P-CC values (-0.70 – -0.79) reveal that the cooler stars have higher variability compared to hotter stars at the same mass, but both cycling an inactive stars can have the same $T_{\rm eff}$. The coolest inactive star is HD 166620 ($T_{\rm eff}$ = 5099 K). In the 0.9–1.0 $M_\odot$ mass bin a gap in S-STD vertically separates the cycling and inactive stars (with two exceptions) and is suggestive of a rapid (on stellar timescales) transition from a cycling state to an inactive state. With our knowledge of the Sun's magnetic minima phases, we have evidence that these transitions can occur quickly, on order of years. The two cycling stars that are near the inactive cluster may have a favorable inclination that allows us to measure the very small amplitudes of their cycles or may be undergoing a transition from cycling to inactive.

The mechanisms that cause a star to enter and exit a magnetic minimum requires a stochastic process that is poorly understood. We do have one example in HD 166620 and we know that inclination angle also plays a role in cycle detection. Since the S-STD tracks with the amplitude of the stellar cycle, the 0.8–0.9 $M_\odot$ mass bin is the most suggestive of a gradual decline in cycle amplitude as the star decreases in $T_{\rm eff}$, before the cycle amplitudes fall below our detection limit.

3.4. *S-STD and Stellar Surface Gravity*

While stellar evolution, including the increase in stellar radius that accompanies a departure from main-sequence, causes its own magnetic field morphology, changes to magnetic field without evolutionary changes must be considered (Metcalfe et al. 2023, 2024). By choosing a narrow range of log(g) values we can identify magnetic field changes of stars while they are still on the main-sequence. In the super-solar mass bin, the inactive stars populate a very narrow parameter space, but not one unique in log(g). There are both cycling stars and inactive stars at the edge of the log(g) distribution. In the three highest mass bins, the inactive stars skew toward low log(g) but it would be more accurate to say that the highest log(g) stars tend to be cycling, but the lowest log(g) stars can be cycling or inactive. Given the median log(g) uncertainty of 0.28, these can be viewed as tendencies rather than definitive correlations.

The 0.7–0.8 $M_\odot$ bin is the most straightforward to interpret because the variation in S-STD that we measure

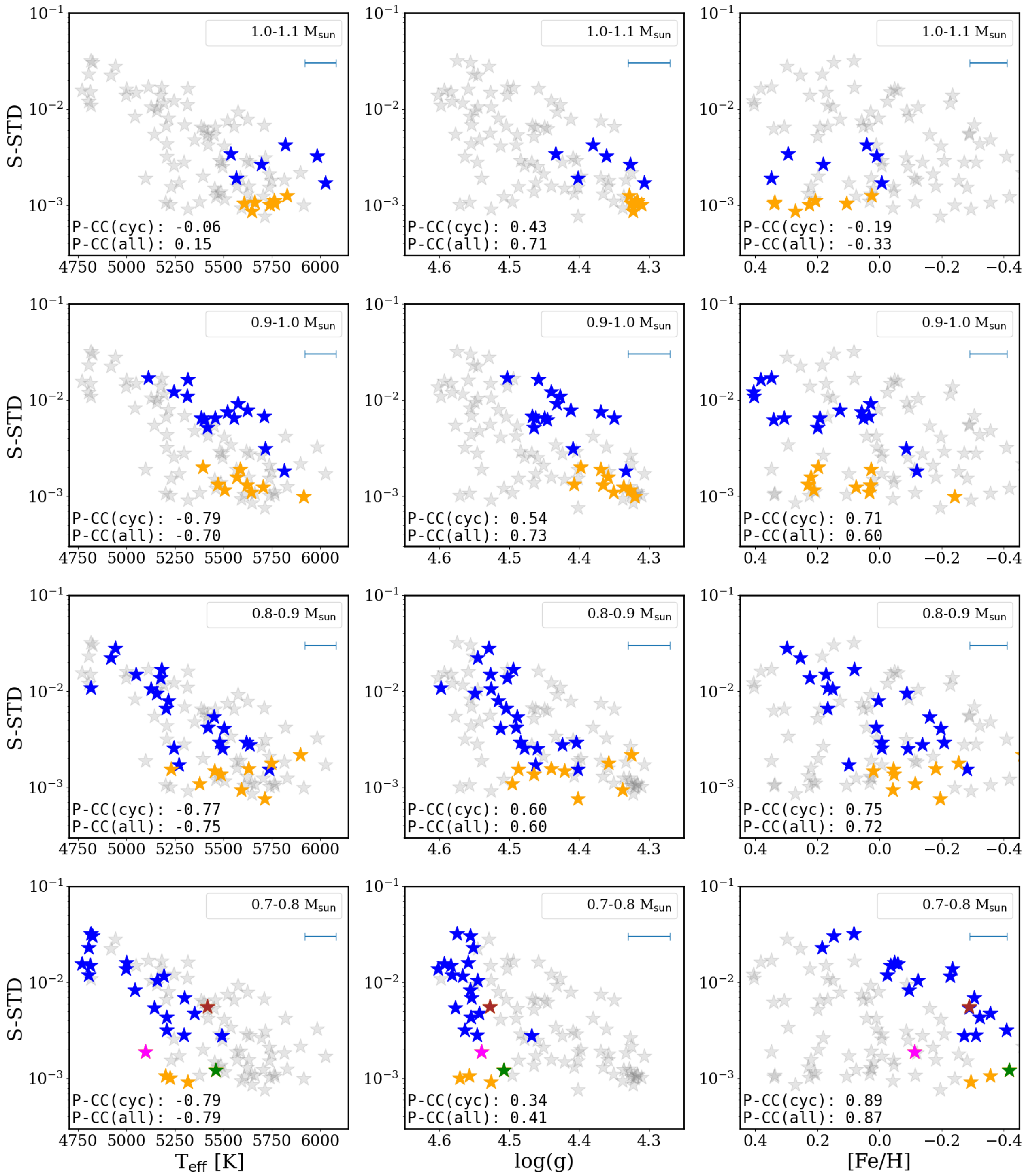

Figure 5. Fundamental stellar properties vs S-STD are plotted for four equally spaced mass bins that decrease from top to bottom. The left, middle and right columns plot the $T_{\rm eff}$, $\log(g)$, and [Fe/H] vs S-STD, respectively. Gray data points represent stars from all mass bins. We find the sub-solar mass bins have more consistent P-CC values than the super-solar mass bin for all three stellar properties. The inactive stars behave similarly to the cycling stars, but at lower S-STD values, suggesting the inactive stars represent a stage of activity that stars reach after their cycling amplitudes are no longer detectable. A representative error bar is shown for the x-axis values. From the inactive stars (gold symbols) we single out HD 166620 (magenta) Tau Ceti (green) and HD 190067 (brown).

occurs without any corresponding changes to the stellar surface gravity (within errors). The variation in S-STD for this mass bin occurs on the main-sequence. The observed inactivity corresponds to an insufficient amount of contrast on the stellar surface to measure cycle modulation, confirming that stars can reach magnetically inactive states while still on main-sequence.

3.5. *S-STD and [Fe/H]*

The right column of Figure 5 shows how S-STD and [Fe/H] are related as a function of mass. The super-solar mass bin has a low correlation between S-STD and metallicity (P-CC = -0.33). The three low-mass bins show strong correlation (P-CC = 0.6, 0.7, 0.9). Stars with the smallest S-STD tend be more metal-poor and the correlation grows stronger as mass decreases.

Similar to the $T_{\rm eff}$ correlations, there is a population of high-metallicity stars that contains no inactive stars. While we do not see inactive stars populating unique parameter space in metallicity, they skew metal-poor. Metallicity effects on stellar rotation have been shown to be important, especially in stars with thin convective zones (Amard & Matt 2020). We present new evidence showing that metal-poor stars in our sample can either be cycling or be inactive. Conversely, we show that metal rich stars can be in cycling or inactive states. A broader sample of inactive, metal-poor, stars would further solidify our conclusion, as our [Fe/H] range is limited to 0.4 to -0.4.

The P-CC values for the $T_{\rm eff}$ and [Fe/H] columns of sub-solar mass stars are nearly identical, leading to a degeneracy between the fundamental stellar parameters in the context of activity variability. For each mass bin, cooler stars tend to be more metal rich, making it difficult to isolate the primary factor. Broadly speaking, hotter, metal-poor stars for a given mass are less active with smaller cycle amplitude and tend toward inactivity.

3.6. *Cycle period-amplitude relationship.*

The simplest explanation between the stellar cycle amplitude would be a direct correlation where the amplitude and period steadily decrease as the star sheds angular momentum over time, but we find a more complicated scenario. Theoretical studies that model the stellar cycle found the period to be strongly correlated with the temperature (Kitchatinov 2022) and observational studies confirm this (Isaacson et al. 2024). For stars older than the Sun, the cycle period - $T_{\rm eff}$ becomes stochastic. Figure 6 shows that for a given period, the cycle amplitudes have a large scatter, especially for sub-solar masses.

The highest amplitude cycles tend to have a period of 10 years, except for the super-solar mass bin, which

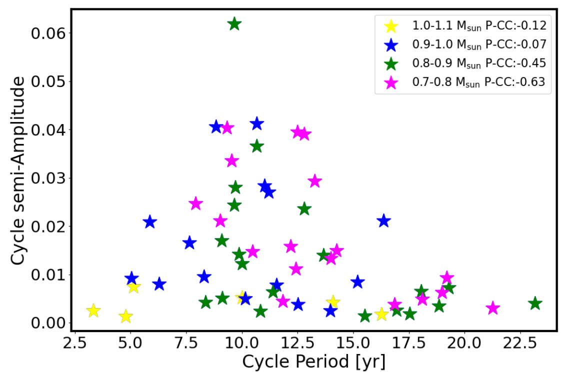

Figure 6. The cycle period vs cycle amplitude for stars with masses between 0.7-1.1 $M_{\odot}$. Across sub-solar mass bins, the primary feature is a maximum in the amplitude distribution at a period of 10 years. The correlation coefficients are strongest in the two lowest mass bins, and nearly zero in the near-solar mass bins. The secondary feature is that cycle periods longer than 15 years have consistently low amplitudes. Perhaps passing the 15 year threshold is the point of no return and cycles only tend toward longer and smaller amplitude cycles.

has only small amplitude cycles. But small amplitude cycles exist at cycle periods from 2–23 years across mass bins. We can use the P-CC to assess how strongly the period and amplitude are coupled and we find it to vary as a function of stellar mass. From the lowest to highest mass bin, we find P-CC values of -0.12, -0.07, -0.45 and -0.63. The two lowest mass bins have cycle periods that range from 7 to 23 years, but the two higher mass bins range from 2.5 to 16 years.

Some stars have observed cycles with varying amplitudes, further complicating our interpretation. HD 18803, with a 5-year period, increases its semi-amplitude by a factor of two in only 20 years (Isaacson et al. 2024). A second example is HD 4915, a one-time magnetic minimum candidate that had a steadily decreasing amplitude (Shah et al. 2018), before turning over with an increasing amplitude. The highest amplitude of the four, five-year cycles was an S-value of 0.22 and the lowest was 0.19 two cycles later.

The most prominent feature in Figure 6 is the extremely small semi-amplitudes for stellar cycles longer than 15 years for all mass bins. This may indicate that a star's cycle period and intensity may vary, but it will eventually end up in a long-period, low amplitude cycle before the amplitude falls below our measurement precision (Metcalfe & van Saders 2017).

3.7. *Cycle Period and Activity Variability*

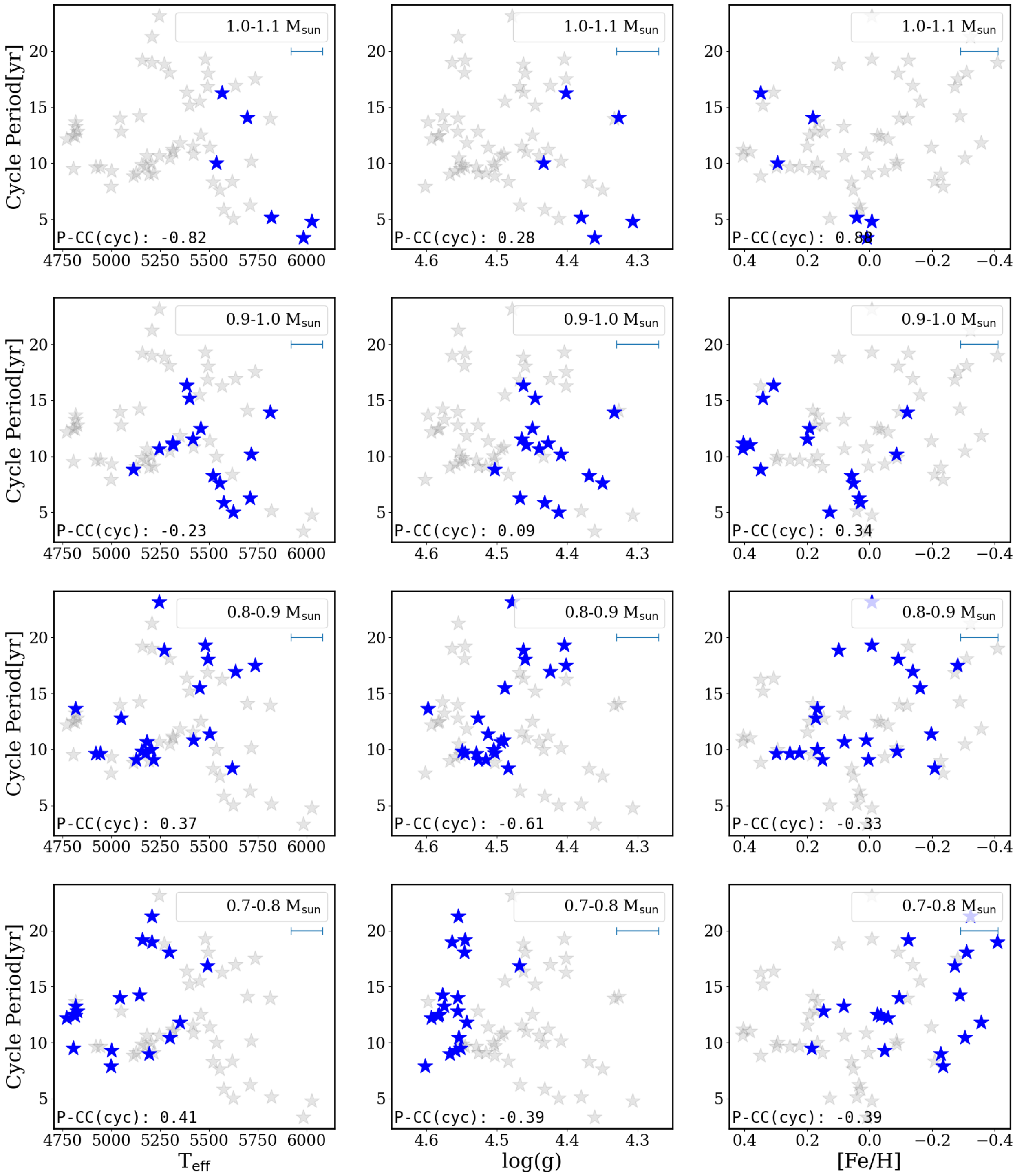

Figure 7. Fundamental stellar properties vs stellar cycle periods are plotted for four mass bins. The equally spaced mass bins decrease from top to bottom. The left, middle and right columns plot the $T_{\rm eff}$, $\log(g)$, and [Fe/H] vs cycle period, respectively. Gray data points represent stars from all mass bins. If one of the parameters was critical in determining the cycle period, we would see a strong P-CC for all mass bins, but no property shows such consistency.

We examine the activity cycle periods as a function of stellar parameters in Figure 7 concluding that there are no strong correlations with any one parameter across mass bins. While the $T_{\rm eff}$ and [Fe/H] correlations showing consistency for sub-solar mass bins in Figure 5, we find a nearly random set of correlation coefficients when breaking down the cycle period correlations with fundamental properties by stellar mass. Previous studies have shown that the oldest stars have more regular cycles, (Oláh et al. 2016), with diminishing amplitude, we find a more complex scenario that must be governed by a stochastic process.

3.8. *Observational Biases*

The observational expense of collecting S-values over the duration of stellar cycles has lead to the use of the average $\log(R'_{\rm HK})$ value to study magnetic dynamos. Rotational modulation and cycle modulation lead to inaccurate values of the averages unless sampling spans rotation period and activity cycle timescales. Single epoch $\log(R'_{\rm HK})$ observations, which are even more limited, should be used with caution when drawing conclusions about population trends (Isaacson et al. 2024). With many observations across their sample, Lovis et al. (2011) claimed mean activity was a good indicator of magnetic variability, but multi-epoch observations from the BCOOL survey Brown et al. (2022) showed that for a given level of average activity, the activity variability can vary by an order of magnitude. Many of their stars had fewer than twenty observations and included stars much younger and more active than our sample. Yet they reached the valuable conclusion that S-value variability is important in choosing targets for precise RV surveys. Longer-baseline observations of the AMBRE-HARPS exoplanet survey (Gomes da Silva et al. 2021) identify similar trends in the least active stars as presented here, and noted that activity variability is an important consideration in addition to mean activity level.

Studies that use models of stellar spin down (van Saders et al. 2016; Saunders et al. 2024) require observed values of the rotation period for comparison to theoretical models. We present data spanning 20 years, ensuring robust measurements in chromospheric variability, and do not require a periodic cycle for interpretation. S-STD can be used to inform dynamo evolution models of main-sequence stars that typically require Rossby numbers calculated using average activity values, when stellar rotation periods are below the threshold of observational detection.

For the lowest amplitude cycles, we heed the work of Masuda (2022) understanding that we may be limited by our ability to measure the flux in the cores of the Ca II H and K lines based strictly on signal to noise. We are able to differentiate cycling stars from inactive stars with relatively little overlap between the populations. By focusing on a narrow range of chromospheric activity with precise long-term averages, and using $T_{\rm eff}$, $\log(g)$, [Fe/H], that are homogeneously determined, we have attempted to mitigate the observational biases of this survey.

3.9. *Impact on Radial Velocity surveys*

The S-STD metric provides a valuable tool for selecting targets for precise radial velocity observations of exoplanets. While potential targets cannot be vetted with a single observation, ground-based radial velocity (RV) surveys of FGK stars in the solar neighborhood already have the time baseline necessary to calculate S-STD over the timescales of stellar activity cycles (Isaacson et al. 2024; Gomes da Silva et al. 2021).

The value in choosing RV targets with low S-STD is two-fold. The contribution to the radial velocity jitter that comes from a spotted stellar surface is dramatically reduced and the interpretation of the radial velocity signal is simplified. For example, Rosenthal et al. (2021) listed 103 false positives in their radial velocity analysis. Forty-two are attributed to a stellar activity correlation with radial velocities and sixteen are likely from activity induced rotation signals. Stars at the bottom of the S-STD distribution do not need to be decorrelated from RVs because they have no S-value variation down to the limit of the measurements, making them excellent candidates for extremely precise RVs.

We cross reference the CLS sample with the NASA ExEP imaging list (Mamajek & Stapelfeldt 2024) to recommend the stars that are the least active. These stars have $\log(R'_{\rm HK})$ of less active than $\log(R'_{\rm HK})$ of -4.90 and listed without cycles in Isaacson et al. (2024). They are HD 10700 (Tau Ceti), HD 110897, HD 115617, HD 136352, HD 166620, HD 38858, HD 4614, HD 86728, and HD 95128.

4. DISCUSSION

In contrast with the $T_{\rm eff}$ to cycle period relationship ($\pm$1.0 yr) for stars with $\log(R'_{\rm HK})$-N1984 between -4.70 and -4.90 (Isaacson et al. 2024), we find no strong relationships between stellar cycle period and fundamental stellar parameters for stars less active that $\log(R'_{\rm HK})$-N1984 $<$ -4.90. Mass-binned stars reside on the same evolutionary tracks and represent a consistent picture of activity through time, and the lack of identified trends represents the presence of a stochastic dynamo process that governs the magnetic fields of these stars.

Our choice of $\log(R'_{\rm HK})$-N1984 = -4.90 is consistent with the time at which the relationship between rotation and stellar age breaks down (Metcalfe & van Saders 2017), a phenomenon described by the theory of weakened magnetic braking (van Saders et al. 2016). We choose our sample to exclude stars that have evolved off of the main-sequence. By using the standard deviation of the S-value time series, S-STD, we have identified the magnetic transition without the typically required knowledge of the rotation period of the star. We find that as stars decrease in activity beyond $\log(R'_{HK})$-N1984 of -4.90, their average chromospheric activity value changes relatively little, but the variability decreases by an order of magnitude.

With the breakdown of the gyrochronology relationship for stars around the age of the Sun, we provide the S-STD metric that may be useful in calculating the ages of stars older than 4 Gyr. An independent determination of the ages for these stars is required for such a calibration, such as from stellar isochrones, or asteroseismology. Since the determination of the Rossby number, the ratio of the convective turnover time to the rotation period, is typically calculated using the average activity of a star (Noyes et al. 1984; van Saders et al. 2016; Corsaro et al. 2021), the Rossby number needs to include a time-variable activity metric will be needed to fully explain the magnetic activity of stars older than the Sun.

We find the S-value, with knowledge of the stellar mass to be the best activity metric and that stars with the least average activity AND the smallest deviations of S-value are the least active stars. We find the one Maunder Minimum star, HD 166620 has extremely low variability, as expected, and that stellar inclination is important to consider in interpreting S-STD. Whether or not stars reach an inactive level that is inescapable or if they can begin cycling again will require addition observations of these already well-observed stars.

5. SUMMARY AND CONCLUSION

We present a detailed analysis of main-sequence FGK stars older than the Sun, searching for a deterministic relationship between fundamental stellar parameters and the periods of their stellar activity cycles. With the observed sample covering several decades, we obtain long-term averages and standard deviations of the S-value. Using the age of the Sun as the lower age limit of our sample and using mass bins, we find a wide array of correlations.

We find that the S-STD is correlated with $T_{\rm eff}$, but not for stars more massive than the Sun. The S-STD is modestly correlated with $\log(g)$ for three out of four mass bins, with the smallest mass bin having the weakest correlation. The metallicity correlation with S-STD is near zero for super-solar masses and consistently strong for three sub-solar mass bins. We find that for the inactive stars, those without a detected cycle are identified with the S-STD activity metric, but average activity metrics of S-value, $\log(R'_{HK})$-N1984, nor the revised $\log(R'_{HK})$ metric from Lorenzo-Oliveira et al. (2018) are not able to identify them. More so than these two types of $\log(R'_{HK})$, the S-value itself, best correlates with S-value variability. In contrast to dividing the cycling stars by $T_{\rm eff}$ and finding the small scatter in cycle period for stars between $\log(R'_{HK})$-N1984 of -4.70 and -4.90, we find sporadic correlations between cycle period and stellar properties for stars less active than -4.90. Searching $T_{\rm eff}$, $\log(g)$ and [Fe/H], the primary stellar parameters obtained from high-resolution spectroscopy, we find inconsistent correlations between them and the cycle period.

The activity cycle and stellar variability analysis presented here poses new questions for stellar dynamo theorists to contemplate, for stars older than the Sun. The sporadic nature of the correlations, a departure from the well-behaved activity cycles for stars with ages between 2-4 Gyr, will require the inclusion of chromospheric variability as well as average chromospheric activity when calculating dynamo variables such as Rossby number and convective turnover time.

In conclusion, we find measurable changes in the dynamos of main-sequence solar-type stars older than the Sun that are correlated with the amplitude of their activity variations. In contrast, while the activity cycle period is strongly correlated with effective temperature for main sequence stars 2 to 4 Gyr, no such correlation is apparent for stars older than the Sun, or otherwise low activity stars. We suggest that knowledge of activity variations over the timescale of stellar cycles and not just average activity levels is important in age dating stars older than the Sun.

Finally, with the detailed analysis of the oldest G and K dwarfs in the solar neighborhood, we have a more complete picture of the activity over the lifetime of a star. When stars are very young (less than 100 Myr), they show chaotic activity, without cycles or periodicity. As they spin-down they are capable of having irregular cycles that vary from cycle to cycle, for example Eps Eri (Metcalfe et al. 2016). Next they settle into cycles with regular periodic structure, sometimes with a short period cycle of a few years and a longer cycle of several decades (Oláh et al. 2016). Between 2–4 Gyr, essentially all FGK stars have regular period cycles and their temperature determines the period. At the age of the Sun, 4.5 Gyr, stars maintain a constant average activity but decrease their variability, and eventually extend

their cycle period beyond our ability to measure either
their amplitude or period.

6. ACKNOWLEDGMENTS

Much of the data presented herein were obtained at Keck Observatory, which is a private 501(c)3 non-profit organization operated as a scientific partnership among the California Institute of Technology, the University of California, and the National Aeronautics and Space Administration. The Observatory was made possible by the generous financial support of the W. M. Keck Foundation. This research has made use of NASA's Astrophysics Data System.

This project would not have been possible without major allocations of Keck telescope time from the University of California, California Institute of Technology, the University of Hawaii and NASA. This work utilized the Exoplanet Archive and SIMBAD.

Author Contributions: H.I Conducted the analysis and wrote the paper. AWH was an originator of the survey. S.K. and B.C. advised on the analysis. All authors provided comments.

The authors wish to recognize and acknowledge the very significant cultural role and reverence that the summit of Maunakea has always had within the indigenous Hawaiian community. We are most fortunate to have the opportunity to conduct observations from this mountain.

Facilities: Keck:I (HIRES)

Software: We made use of the following publicly available Python modules: Astropy (**?**), matplotlib (Hunter 2007), numpy (van der Walt et al. 2011), scipy (Virtanen et al. 2020) and pandas (Wes McKinney 2010).

REFERENCES

Amard, L., & Matt, S. P. 2020, ApJ, 889, 108, doi: 10.3847/1538-4357/ab6173

Baliunas, S. L., Donahue, R. A., Soon, W. H., et al. 1995, ApJ, 438, 269, doi: 10.1086/175072

Barnes, S. A. 2007, ApJ, 669, 1167, doi: 10.1086/519295

Baum, A. C., Wright, J. T., Luhn, J. K., & Isaacson, H. 2022, AJ, 163, 183, doi: 10.3847/1538-3881/ac5683

Bhalotia, V., Huber, D., van Saders, J. L., et al. 2024, ApJ, 970, 166, doi: 10.3847/1538-4357/ad4eb1

Brown, E. L., Jeffers, S. V., Marsden, S. C., et al. 2022, MNRAS, 514, 4300, doi: 10.1093/mnras/stac1291

Corsaro, E., Bonanno, A., Mathur, S., et al. 2021, A&A, 652, L2, doi: 10.1051/0004-6361/202141395

Curtis, J. L., Agüeros, M. A., Matt, S. P., et al. 2020, ApJ, 904, 140, doi: 10.3847/1538-4357/abbf58

David, T. J., Angus, R., Curtis, J. L., et al. 2022, ApJ, 933, 114, doi: 10.3847/1538-4357/ac6dd3

Eberhard, G., & Schwarzschild, K. 1913, ApJ, 38, 292, doi: 10.1086/142037

Flores, M., González, J. F., Jaque Arancibia, M., Buccino, A., & Saffe, C. 2016, A&A, 589, A135, doi: 10.1051/0004-6361/201628145

Gomes da Silva, J., Santos, N. C., Adibekyan, V., et al. 2021, A&A, 646, A77, doi: 10.1051/0004-6361/202039765

Hall, O. J., Davies, G. R., van Saders, J., et al. 2021, Nature Astronomy, 5, 707, doi: 10.1038/s41550-021-01335-x

Hunter, J. D. 2007, Computing in Science and Engineering, 9, 90, doi: 10.1109/MCSE.2007.55

Isaacson, H., Howard, A. W., Fulton, B., et al. 2024, arXiv e-prints, arXiv:2406.17332, doi: 10.48550/arXiv.2406.17332

Kitchatinov, L. 2022, Research in Astronomy and Astrophysics, 22, 125006, doi: 10.1088/1674-4527/ac9780

Korolik, M., Roettenbacher, R. M., Fischer, D. A., et al. 2023, AJ, 166, 123, doi: 10.3847/1538-3881/ace906

Lorenzo-Oliveira, D., Freitas, F. C., Meléndez, J., et al. 2018, A&A, 619, A73, doi: 10.1051/0004-6361/201629294

Lovis, C., Dumusque, X., Santos, N. C., et al. 2011, arXiv e-prints, arXiv:1107.5325, doi: 10.48550/arXiv.1107.5325

Luhn, J. K., Wright, J. T., Henry, G. W., Saar, S. H., & Baum, A. C. 2022, ApJL, 936, L23, doi: 10.3847/2041-8213/ac8b13

Mamajek, E., & Stapelfeldt, K. 2024, arXiv e-prints, arXiv:2402.12414, doi: 10.48550/arXiv.2402.12414

Mamajek, E. E., & Hillenbrand, L. A. 2008, ApJ, 687, 1264, doi: 10.1086/591785

Masuda, K. 2022, ApJ, 937, 94, doi: 10.3847/1538-4357/ac8d58

McQuillan, A., Mazeh, T., & Aigrain, S. 2014, ApJS, 211, 24, doi: 10.1088/0067-0049/211/2/24

Meibom, S., Barnes, S. A., Platais, I., et al. 2015, Nature, 517, 589, doi: 10.1038/nature14118

Metcalfe, T. S., & Egeland, R. 2019, ApJ, 871, 39, doi: 10.3847/1538-4357/aaf575

Metcalfe, T. S., Egeland, R., & van Saders, J. 2016, ApJL, 826, L2, doi: 10.3847/2041-8205/826/1/L2

Metcalfe, T. S., & van Saders, J. 2017, SoPh, 292, 126, doi: 10.1007/s11207-017-1157-5

5.3 Links and implications

In Chapter 5 we extended our analysis of chromospheric activity time-series to identify the changing activity levels of stars older than the Sun. With the dataset from Chapter 4 in hand, we used the robust chromospheric activity averages that we collected on timescales of stellar activity cycles. By focusing on stars without rotation modulation that is measurable in the S-values, we strictly analyze the activity cycle contribution of the S-value. The primary activity metric, log(R'_{HK}), is a sensitive function of the stellar temperature, especially for exceptionally old stars. We take advantage of the exceptionally precise nature of our activity measurements, along with the homogeneously determined T_{eff} values to probe this poorly understand period of a star's magnetic life. Consistent with our reliance on time-series activity measurements and robust stellar properties, we are able to show that our understanding of magnetic field properties of the oldest stars is missing a critical component, the decreasing time variation of activity at constant average activity. This final thread ties together the primary research presented here: stellar rotation, stellar activity cycles, and the ultimate state of magnetic activity in main-sequence stars.

CHAPTER 6: DISCUSSION AND CONCLUSIONS

6.1 The California-Kepler Activity Survey

In Chapter 3 we presented the eleventh installment of CKS, expanding the analysis of this extensive ground-based observing program. Building primarily on the catalog of precise stellar properties that were compiled from the analysis of Keck/HIRES spectroscopy (Petigura et al. 2017; Johnson et al. 2017), the chromospheric activity catalog represents an extension of the CKS catalog that can be used in a wide variety of exoplanet studies.

6.1.1 A chromospheric activity catalog for Kepler *planet hosts*

Using the CKS chromospheric activity catalog, we place the *Kepler* planet-host stellar sample into context with samples of solar-neighborhood stars. The Mount Wilson Survey, the CPS survey for exoplanets (Wright et al. 2004; Isaacson and Fischer 2010), the AMBRE-HARPS sample of stars (Gomes da Silva et al. 2021), and a survey of southern hemisphere solar-type stars (Henry et al. 1996) offer insights into the activity distribution of nearby stars. Although each survey has its own selection function, the *Kepler* sample, which is primary located beyond 300 pc, has been shown to include a majority of stars less active than the Sun (Gilliland et al. 2011). The CKS sample included only stars with transiting planets. Stars that are not amenable to planet transit detection due to their high activity levels are not included in CKS. This resulted in a sample that is mostly older than 1 Gyr, (Petigura et al. 2022; Berger et al. 2020). Rather than the rapidly rotating stars that were also found in *Kepler* rotation analyses McQuillan et al. (2014), this selection function led to the use of the CKS catalog in stellar rotation analysis and hypothesis testing for the theory of WMB in David et al. (2022) and Chapter 3.

The CKS activity catalog will provide an important activity metric for future studies of individual systems that can be used as a component in planet atmosphere studies and planet formation theories. The catalog will offer chromospheric measurements that can be used to study planet-star interaction, determine whether a star is amenable to precise radial velocities, and assess a star's spin-down and rotation. These last properties are especially complementary to the *Kepler* photometric data. The various timescales of variability that *Kepler* measured include the 12-hour precision used as a metric for that ability to find Earth-sized planets, the timescales of rotational variability (McQuillan et al. 2014) and photometric variation on long timescales (Zhang et al. 2020). The activity measurements presented in Chapter 3 are highly complementary to these variability measurements since the Ca II H & K lines are sensitive to the chromosphere and a proxy for magnetic field strength, measurements beyond what the *Kepler* broadband photometry can offer.

6.1.2 Support for WMB from CKS

Chapter 3 focuses on stars withe ages older than 1 Gyr when astrophysical theories such as WMB become relevant, specifically near the age of the Sun at 4.5 Gyr. *Kepler* rotation rates from McQuillan et al. (2014) have been used to great effect to test WMB descriptions of stellar spin-down (van Saders et al. 2016). David et al. (2022) combined the precise stellar properties of the CKS sample with rotation rates to identify ”Rossby Ridge” feature where stars pile-up in $T_{\rm eff}$ and rotation period space. We use the CKS-HK catalog to show that the activity level of stars on the Rossby Ridge is at the critical level of -4.90 identified in studies of field stars (Metcalfe and Egeland 2019). Using additional data to compound the observational evidence in support of theoretical astrophysical explanations is a fundamental strength of the work presented here.

6.1.3 Extending of single epoch measurements of activity

During the CKS-HK analysis, the analysis was limited by the single epoch measurements of the CKS catalog. As star spots on the stellar surface change due to rotational modulation, spots move in and out of our view. Multi-epoch observations can use S-value variations to identify the rotation period and draw correlations between rotation and activity. We relied on previously determined activity-rotation relationships, when comparing activity derived rotation periods to photometric rotation periods. An extension of Chapter 3 could use time-series S-values to measure the rotation period with a chromospheric diagnostic to complement the photometric rotation periods from *Kepler*. X-ray observations, another metric used to measure magnetic activity, could be observed, extending our understanding of stellar activity to higher energy levels.

6.1.4 Connections between planet radii and chromospheric activity

The CKS dataset, containing roughly 1,000 planet host stars, is ideally suited to study the distribution of planet radii. The most dramatic discovery is the planet radius gap, and theoretical studies have been able to explain the differentiation of super-Earths and sub-Neptunes with photoevaporation that largely occurs in the first 100 Myr of planet formation (Owen and Wu 2017). The theory of core-powered mass loss can explain rocky vs gaseous planet differentiation (Gupta and Schlichting 2019). The definitive explanation of planet formation for super-Earths and sub-Neptunes is still open for debate. Using updated stellar parameters for the full *Kepler* catalog and utilizing Gaia DR2 data of more than 200,000 stars, differences were identified between stars older than 1 Gyr compared to older stars. In particular, the fraction of super-Earths to sub-Neptunes at young ages increases from 0.61 ± 0.61 to 1.00 ± 0.10 at old ages (Berger et al. 2020).

Our work in Chapter 3 was limited to stars older than 1 Gyr, and we showed that stellar insolation is a more important factor than average chromospheric activity when considering photoevaporation in the context of planet formation. This holds true for F, G and K-type dwarf stars, but studies have indicated that high energy flux in M-dwarfs may play a critical role in planetary atmospheric erosion in these stars (O'Malley-James and Kaltenegger 2019). The role of high-energy flux in planetary atmospheres of M-dwarfs is of high interest due to the large number of M-dwarfs available for study and the observational advantages they have over solar type stars. These small cool stars have habitable zones that are closer in distance compared to solar-type stars, making the high-energy flux important in quantifying planetary atmospheric escape.

6.1.5 CKS as a foundation for theoretical studies

The interplay between theory and observation plays a fundamental role in astronomy. In the context of planet formation, theoretical formation models have been challenged by observation in the last 30 years. After the discovery of Hot-Jupiter planets, dynamical evolution models were developed to migrate Jupiter-mass planets from the volatile-rich areas beyond the snow-line to close-in orbits (Dawson et al. 2015). Such models were needed since in situ formation was difficult to explain. The discovery of the common occurrence of small, close-in planets from the *Kepler* mission (Howard et al. 2010b) caused another overhaul of planet formation models (Ida and Lin 2005, 2010) that had previously excluded the possibility of super-Earths and sub-Neptunes in orbits shorter than 50 days.

Publication of the first CKS papers coincided with the theoretical explanation of the radius gap by photoevaporation, yet challenges remain. When considering the formation of the solar system, the terrestrial planets and the lack of super-Earth or sub-Neptunes remains difficult to explain (Morbidelli and Raymond 2016). Jupiter's role in forming the solar system, particularly in understanding volatile delivery to the inner system is relevant to understanding the same process in exoplanet systems. The median eccentricity of Jupiter analogs is 0.23 (Kane and Wittenmyer 2024), higher than that of Jupiter and Saturn. This may lead observers to follow-up exoplanet systems with known eccentric Jovians, and their higher volatile inventory, that could lead to a higher occurrence of terrestrial planets. The CKS activity catalog could be used in studies of exoplanet atmospheres. Recent studies identifying helium escaping from exoplanet atmospheres (Gully-Santiago et al. 2024) will require a thorough understanding of the magnetic activity profile of host stars Fig 6.1.

6.1.6 CKS will stand the test of time

The CKS dataset, now with a chromospheric activity catalog to complement the precise stellar and planet parameters, offers an observational foundation for use in future theoretical studies and a benchmark for future observational surveys. The value of consistent, uniform, high-quality, ground-based data was used to add scientific depth to an already impressive Discovery class NASA mission. These fundamental spectroscopic stellar parameters have been used for primary science of planet demographics and can be used as starting points for stellar isochrone analysis (Huber 2017). While the population level information has been revolutionary, single system parameters can be used in follow-up observations with HST, JWST, and beyond. A similar catalog that observes TESS-identified planet hosts that matches the consistency and quality of CKS should be undertaken, but the most impactful exoplanet discoveries from CKS will not be surpassed soon.

With the ongoing collection of stellar activity data to understand magnetic dynamos in solar type stars, we offer a uniform catalog that can be extended by collecting future observations. A new survey that studies the fundamental relationships in the age-rotation-activity regime of stellar astrophysics would continue to gain value with longer baselines.

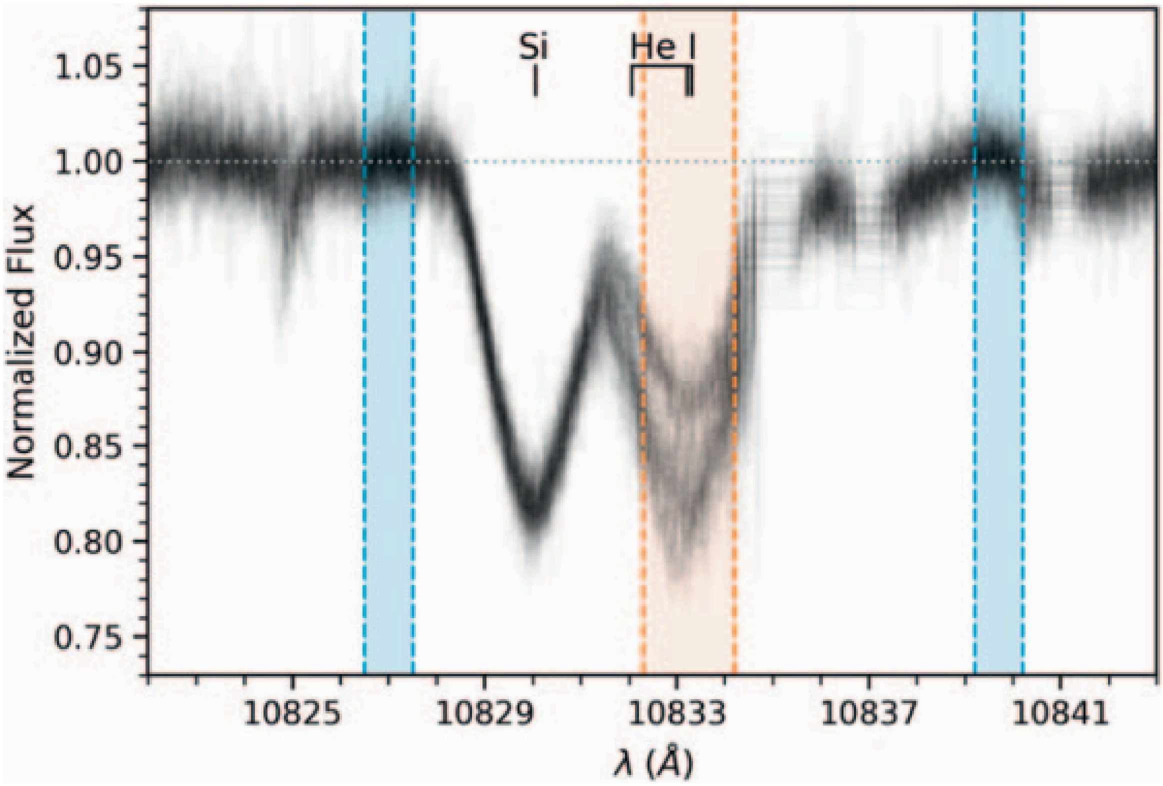

Figure 6.1: From Gully-Santiago et al. (2024), figure 7: ”Overlay of all 152 individual Habitable Planet Finder exposures of HAT-P-67, spanning 2020–2022. Variability is seen in the He I 10833 Angstrom triplet near the vertical orange shaded band but not in the adjacent Si line. These snapshot spectra were barycentric corrected and continuum flattened with a linear fit to the regions in the blue vertical bands. Sharp telluric absorption lines have been masked in regions near 10835 and 10837.5 Angstroms.” Our ability to measure changes in individual spectral features at high-resolution enables exoplanet science and fundamental stellar astrophysics. Differentiating between changes due to a planet’s atmosphere versus changes due to variations in a star’s magnetic field will be critical in correctly interpreting results from JWST and future space-based missions.

Studies of stellar rotation, Rossby number, WMB and late-stage stellar spin-down can utilize the CKS activity data to better understand individual systems that are already well-studied by *Kepler*. The search for stars in magnetic states that resemble the Sun's Maunder Minimum will remain a quest and will influence and inspire future observational studies of the magnetic fields of solar-type stars. Age estimates from new sources can be compared with activity ages to identify new aspects of main-sequence magnetic dynamo evolution.

The connection between measured rotation periods of *Kepler* stars and their activity is an active area of research. Current age-activity-rotation relations are well established across a range of ages using young clusters (Mamajek and Hillenbrand 2008; Curtis et al. 2020), and will be expanded as wide-field high-cadence observational surveys such as Rubin Observatory see first light. Documented detections of star-planet interactions are uncommon, but new instruments and telescopes have identified candidates in the radio (Ortiz Ceballos et al. 2024). Knowing the stellar chromospheric activity properties of candidate system will be vital inputs into fully understanding these systems.

6.2 The California Legacy Survey

6.2.1 The value of long time-baseline observations

The CLS Survey, the *Kepler* photometric dataset and Mount Wilson H & K survey set the standard for high-quality time-series datasets. The Mount Wilson H & K dataset has been the standard bearer in stellar activity analysis since its publication because it consists of homogeneously determined data that was quality controlled and vetted for outliers. It consists of a simple metric that is straightforward to interpret and can easily be brought to bear on important astrophysical questions. The value in the time-baseline is from the *Kepler* photometry baseline of four years. That time span allows for robust measurements of planet occurrence out to 50 days (Howard et al. 2010b; Fressin et al. 2013) and can be extended to 300 days with careful consideration of quarterly offsets in the *Kepler* data (Petigura et al. 2013; Burke et al. 2015).

The CLS dataset, with precise RVs dating from as far back as 1989, from Lick Observatory, to the present, from Keck Observatory, is unique in that it can probe the occurrence of Jovian-mass planets in Jupiter-like orbits (Rosenthal et al. 2021; Fulton et al. 2021). While offsets exist between different detectors and different instruments (Fischer et al. 2014), the consistency across the entire baseline is sufficient for occurrence rate calculations out to 100 au (Figure 6.2). Long-term stability of instruments and consistent observing procedures can ensure that calibration errors are small, enabling comparison of activity indices across multiple instruments (Baum et al. 2022). We utilized data from Keck Observatory and the CLS that was collected on a single detector since 2005, to present the largest stellar activity time series catalog since Baliunas et al. (1995), along with identification of stellar activity cycles.

6.2.2 The value of precise stellar parameters

The determination of stellar properties plays a critical role in exoplanet analysis, and high-resolution spectroscopy is an essential component. While photometry is capable of surveying and a cataloging massive num-

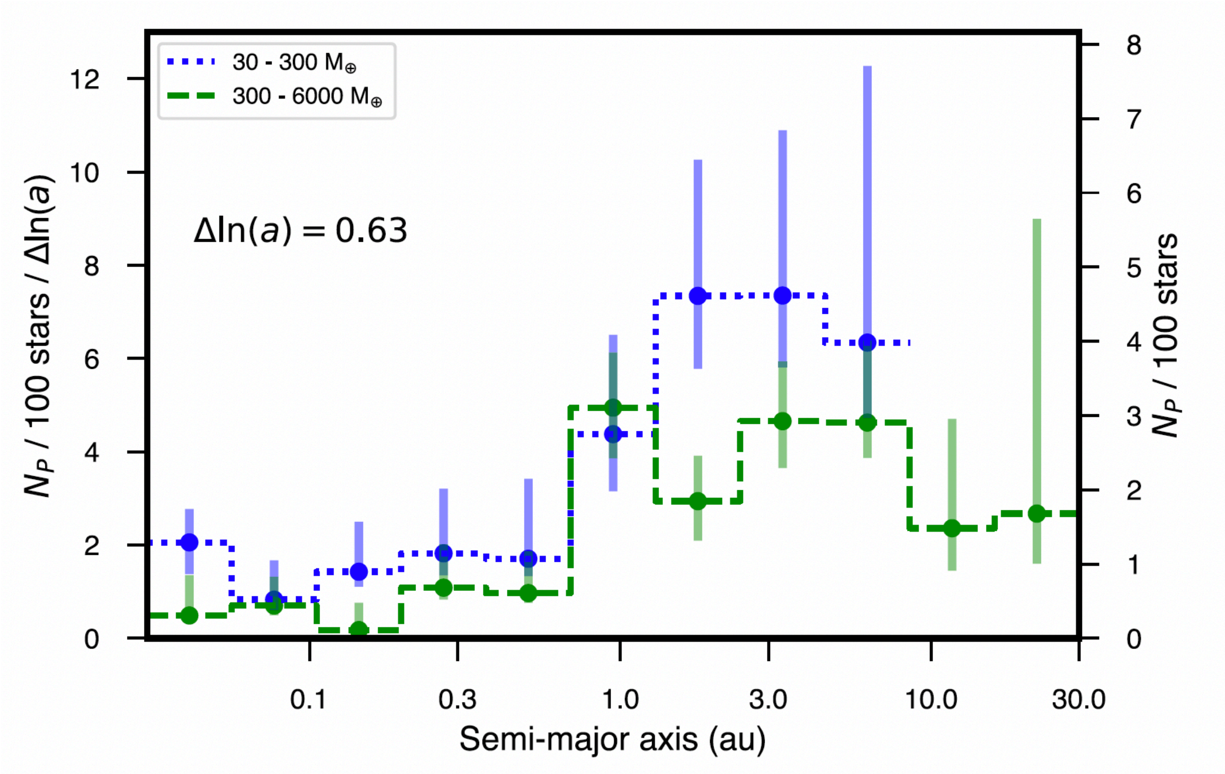

Figure 6.2: From Fulton et al. (2021), figure 5: "Comparison between sub- and super-Jovian occurrence. Steps and dots show maximum posterior values, and vertical lines show 15.9%–84.1% confidence intervals. The sub-Jovians are consistently more common than the super-Jovians, and both populations are enhanced beyond 1 au. Combining these two populations produces the same trends seen when we assume uniform occurrence across all masses." Knowing the occurrence rates of Jovian planets provides a starting point for exploring a variety of exoplanet studies. Those topics include studying planetary systems with the same architecture as our own and studying the formation of systems that consist of a Jovian and inner rocky planets. When interpreting signals in RVs with periods similar to Jupiter, the presence of stellar activity cycles must be taken into consideration.

bers of stars (for example *Kepler*) the resulting stellar radii, critical for determining the planet radii, are only accurate to roughly 30% using photometry (Brown et al. 2011). High-resolution spectroscopy, observed traditionally a single star at a time, and in some cases a few dozen at a time with multiplexing technology, can provide fundamental stellar properties such as stellar temperature, surface gravity and metallicity (Valenti and Piskunov 1996; Buchhave et al. 2012; Gilliland et al. 2013; Petigura et al. 2017; Johnson et al. 2017). For transiting exoplanets, the spectroscopy results can be combined with photometry catalogs such as the Kepler Input Catalog to determine the stellar mass and radius to a precision of 10%, a significant improvement over photometry alone (Petigura et al. 2017; Johnson et al. 2017).

The addition of Gaia data is influential in the stellar properties realm because of the improved parallax and distance measurements that improve the fundamental stellar parameters for billions of stars (Luri et al. 2018). The combination of stellar distances from Gaia and stellar spectroscopy can lead to stellar radius, and therefore planet radius uncertainties of less than five percent (Fulton and Petigura 2018). Determining precise planetary radii relies directly on determining stellar radii precisely. Asteroseismology proves to be even more capable than spectroscopy alone with its ability to measure stellar pulsations and determine the stellar mass and radius with uncertainties near 2% (Huber et al. 2013b). Precise stellar radii lead to precise planet radii, but limitations of stellar models should be kept in mind (Tayar et al. 2022). Asteroseismology existed before *Kepler* but it has not been the same since. The quality of *Kepler* photometry is unprecedented, allowing for the determination of stellar obliquity using photometric oscillations (Chaplin et al. 2013; Huber et al. 2013a). The combination of Gaia data with high-resolution spectroscopy has allowed for discoveries that would not be possible independently.

6.2.3 Extending CLS

Extending the CLS survey would be a valuable contribution to exoplanet and stellar activity studies. With the transition from the HIRES to KPF instruments on Keck, an instrumental offset will now be required to connect the two datasets. The Automated Planet Finder telescope and Levy spectrograph provide a better opportunity. With less speed and sensitivity, the entire CLS sample could not be observed, but the Mount Wilson sample represents a valuable subset that would benefit greatly from expanded observations.

The use of the Mount Wilson H & K survey data to explore the relationship between rotation period and activity cycles has been incredibly fruitful. From observations that multiple dynamos exist in stars (Böhm-Vitense 2007) to the use of the observational catalog in dynamo modeling (Oláh et al. 2016; Mittag et al. 2023), the dataset has been invaluable. With the CLS Activity Survey, we add to the legacy of Mount Wilson by identifying new activity cycles and confirming previously published cycles, and hope that the primary sample of stars that overlap Mt. Wilson and CLS could be observed.

6.3 Late stage main-sequence magnetic dynamo evolution

In Chapter 5 we focus on stars older than the Sun. These stars have no rotational modulation, and some have diminished cycle amplitudes below our detection limit. But the final magnetic state of these stars is still unknown. We know of one star in a magnetic minimum, HD 166620 and other stars with varying cycle amplitudes such as HD 4915 (Shah et al. 2018). For these oldest stars, it appears stochastic processes dominate their magnetic activity variability. Future work on dynamo modeling can use the variability of the activity metrics to further inform the spin-down modeling, and activity cycle decline.

The activity cycle period and cycle amplitude relationship is not simplistic in stars older than the Sun. As additional observing resources are brought to bear on these old stars, such as spectropolarimetry (Metcalfe et al. 2023, 2024), we will continue to unravel the secrets hidden in the magnetic fields of these stars.

6.4 Stellar activity mitigation and finding Earth-mass planets

Over the next decade, one of the most fascinating and important tasks for astronomers will be searching for biosignatures in the atmospheres of Earth-sized exoplanets. For decades, the state of the art in exoplanet atmospheric studies used Hubble Space Telescope (HST) data (Crossfield et al. 2012; Crossfield and Kreidberg 2017; Kreidberg et al. 2018). Many Jupiter sized exoplanets have had their had their atmospheres measured, and planets similar in size to Neptune have pushed the limit of current instruments (Benneke et al. 2019; Tsiaras et al. 2019). The *Spitzer* spacecraft provided valuable information about planet temperatures in the infrared spectrum (Knutson et al. 2009; Fraine et al. 2013). Small sample sizes and several measurements showing flat spectra have stymied clear interpretations for the smallest planets, but the path forward shows promise (Gressier et al. 2022).

NASA's TESS mission (Ricker et al. 2015) is surveying 85% of the sky in search of the nearest and brightest transiting exoplanets for transit spectroscopy using the HST and the James Webb Space Telescope (Bean et al. 2018, JWST). Of the promising targets for atmospheric detection the TRAPPIST-1 planets have already been observed in search of reflected light from their likely rocky surfaces (Greene et al. 2023). The next generation of space telescopes will search for definitive evidence of biosignatures on planets as small and cool as the Earth. The HWO (Kopparapu et al. 2018), will potentially be capable of measuring biosignatures in transmission spectra, and/or directly imaging the reflected light Earth-sized exoplanets. Until these next great observatories are ready for launch space missions such as PLATO (Matuszewski et al. 2023; Rauer et al. 2024) and ARIEL (Bocchieri et al. 2023) will provide exciting opportunities in exoplanet science.

The Decadal plan for detecting biosignatures involves the discovery and detailed characterization of Earth-like planets (National Academies of Sciences and Medicine 2021). High precision RV spectrometers such as Keck/HIRES (Vogt 1992) and Automated Planet Finder/Levy spectrograph (Radovan et al. 2010, APF), KPF (Gibson et al. 2018) , Habitable Planet Finder (Ninan et al. 2019, HPF), EXtreme PREcision Spectrometer (Brewer et al. 2020, EXPRES), Echelle SPectrograph for Rocky Exoplanets and Stable Spectroscopic Observations (Pepe et al. 2021, ESPRESSO) and NEID (Robertson et al. 2019) will play a critical role in measuring the masses of these planets. With instrumental precision below 1.0 meters per second, the largest contribution to the error budget will be stellar jitter, making mitigation of astrophysical noise the largest obstacle to measuring the mass of an Earth-sized planet (Robertson et al. 2014; Kosiarek et al. 2019; Aigrain and Foreman-Mackey 2023). Intricate knowledge of stellar spectroscopy will be critical toward the interpretation of future discoveries of biosignatures in the atmospheres of exoplanets, and 5-sigma mass measurements are needed to break model atmosphere degeneracies (Batalha et al. 2019).

Since the type of planetary system, rather than the stellar properties, often dominates the interest level of intriguing exoplanet systems, the most amenable stars for RV analysis may not be ideal for RV analysis. With transit surveys such as TESS searching for the planets that will provide the best targets for atmospheric studies, it is not certain that these will be RV quiet stars. Precise mass measurements for these planets will require both the next generation of RV facilities (NEID, KPF, HPF, etc.) as well as the analysis that will disentangle stellar noise from planet-induced signals such as Gaussian Processes (Grunblatt et al. 2015; Lubin et al. 2021; Beard et al. 2022). Even when the next generation of stabilized spectrographs are fully operational, activity decorrelation, modeling, and mitigation will play a critical role in measuring precise exoplanet masses. Chromospheric activity catalogs such as those presented here will be increasingly valuable and needed to improve RV performance.

6.4.1 Reaching 10 cm/s RV precision, in the search for Earth-analogs

By examining stars with publicly available RVs from the NEID spectrograph such as HD 166620 (RV scatter = 0.74 meters per second) and HD 217107 (RV scatter of 4.0 m/s residuals to the planet fit), we find the former to be amenable to identification of extremely small RV amplitudes. The larger RMS-residual value for HD 217107, a solar-type star, suggests that additional planets may be waiting to be identified. Our work in Chapter 5 showed that the extremely low S-value variation will simplify the interpretation of the low-amplitude signals yet to be identified. These RV standard deviation values are possible without advanced techniques that decorrelate stellar activity from RV signals. The instrumentation technology is now capable of extremely small instrumental uncertainties on quiet stars. KPF has an instrumental uncertainty goal of 30 centimeters per second (Gibson et al. 2024). Our understanding of stellar activity and development of stellar activity techniques must match the instrumental capability.

K-dwarfs have long been thought to be the best RV targets due to their low RMS of standard stars (i.e. HD 10700 and HD 166620). In the case of RV jitter due to spots this makes sense. A handful of stars have been shown to have minimal impact from spots. It is also possible that other types of noise such as pressure-mode oscillations have commonly been covered by the slightly fainter K-dwarfs and their longer exposure times, and now that we have predictions for pressure-mode oscillations as from asteroseismology (Chaplin et al. 2019), we can increase exposure times (or collect sequential exposures) on G-dwarfs to reduce RV pressure-mode noise. If the impact of RV jitter from spot modulation can be reduced by choosing stars with extremely low stellar activity, ever smaller RV-amplitude planets can be found.

Stellar activity can be mitigated and modeled post-observation and has been to great effect. Analyses such as line-by-line analysis to determine RVs (Dumusque 2018; Siegel et al. 2022) or Gaussian Processes to decorrelate RV signals from stellar activity (Aigrain and Foreman-Mackey 2023) are among the many examples of methods that can maximize precision in extracting RVs and decorrelating stellar noise either through photometry or contemporaneous S-values.

The CLS stellar sample was primary selected for an exoplanet survey and focused on nearby stars that were amenable to precise radial velocities, specifically targeting slowly rotating F, G and K-type stars. The average log(R'_{HK}) (Noyes et al. 1984a) value was useful to identify stars that were RV quiet at the 10 m/s level. Typically stars more active than log(R'_{HK}) of -4.70 were omitted as too active (Howard et al. 2010b) but extreme RV precision of nearby stars will require focusing on the least active stars, as identified by their S-value scatter (Chapter 5).

6.5 Concluding remarks

The research presented represents the work of a collaboration of astronomers dedicated to collecting ground-based observations to further our understanding of astrophysical phenomena. With access to the Keck Observatory telescopes and suite of instruments, we have been able to propose for telescope time through all of the Keck partners: University of California, California Institute of Technology, the National Aeronautics and Space Administration (NASA), and the University of Hawai'i. Dozens of individual investigators have written telescope proposals focusing on a wide variety science topics and in support of NASA space missions. The ability to pool telescope time to access an increased number of individual nights has been a foundational part of our research.

The time-domain nature of the chromospheric activity data presented in

Chapter 5 is the most valuable publicly available data that we offer. In the great tradition of ground-based astronomy, the Mount Wilson H & K Project provided a consistently high-quality, homogeneous stellar activity catalog covering 35 years. We present, for use in the astronomy community, 52372 measurements of 710 nearby stars that were collected on 1760 individual nights, the equivalent of 4.8 complete years over a twenty year span.

Without access to the Keck Observatory, which sits on the summit of Maunakea in Hawai'i, USA, this research would not be possible. I wish to recognize and acknowledge the very significant cultural role and reverence that the summit of Maunakea has always had within the Native Hawaiian community. We are most fortunate to have the opportunity to conduct observations from this mountain.

REFERENCES

Note that the references presented here are for Chapters 1, 2 and 6, as well as the introductory and concluding sections of the remaining chapters. References for the papers included in Chapters 3 – 5 are included in the references sections of the papers.

E. R. Adams, D. R. Ciardi, A. K. Dupree, III Gautier, T. N., C. Kulesa, and D. McCarthy. Adaptive Optics Images of Kepler Objects of Interest. *AJ*, 144(2):42, August 2012. doi: 10.1088/0004-6256/144/2/42.

Suzanne Aigrain and Daniel Foreman-Mackey. Gaussian Process Regression for Astronomical Time Series. , 61:329–371, August 2023. doi: 10.1146/annurev-astro-052920-103508.

Louis Amard and Sean P. Matt. The Impact of Metallicity on the Evolution of the Rotation and Magnetic Activity of Sun-like Stars. *ApJ*, 889(2):108, February 2020. doi: 10.3847/1538-4357/ab6173.

Louis Amard, Julia Roquette, and Sean P. Matt. Evidence for metallicity-dependent spin evolution in the Kepler field. *MNRAS*, 499(3):3481–3493, December 2020. doi: 10.1093/mnras/staa3038.

Ruth Angus, Timothy Morton, Suzanne Aigrain, Daniel Foreman-Mackey, and Vinesh Rajpaul. Inferring probabilistic stellar rotation periods using Gaussian processes. *MNRAS*, 474(2):2094–2108, Feb 2018. doi: 10.1093/mnras/stx2109.

Anthony S. Atkinson, David Alexander, and Alison O. Farrish. Exploring the Effects of Stellar Magnetism on the Potential Habitability of Exoplanets. *ApJ*, 969(2):147, July 2024. doi: 10.3847/1538-4357/ad4605.

G. Bakos, R. W. Noyes, G. Kovács, K. Z. Stanek, D. D. Sasselov, and I. Domsa. Wide-Field Millimagnitude Photometry with the HAT: A Tool for Extrasolar Planet Detection. , 116(817):266–277, March 2004. doi: 10.1086/382735.

S. L. Baliunas, R. A. Donahue, W. H. Soon, J. H. Horne, J. Frazer, L. Woodard-Eklund, M. Bradford, L. M. Rao, O. C. Wilson, Q. Zhang, W. Bennett, J. Briggs, S. M. Carroll, D. K. Duncan, D. Figueroa, H. H. Lanning, T. Misch, J. Mueller, R. W. Noyes, D. Poppe, A. C. Porter, C. R. Robinson, J. Russell, J. C. Shelton, T. Soyumer, A. H. Vaughan, and J. H. Whitney. Chromospheric Variations in Main-Sequence Stars. II. *ApJ*, 438:269, Jan 1995. doi: 10.1086/175072.

Thomas Barclay, Christopher J. Burke, Steve B. Howell, Jason F. Rowe, Daniel Huber, Howard Isaacson, Jon M. Jenkins, Rea Kolbl, Geoffrey W. Marcy, Elisa V. Quintana, Martin Still, Joseph D. Twicken, Stephen T. Bryson, William J. Borucki, Douglas A. Caldwell, David Ciardi, Bruce D. Clarke, Jessie L. Christiansen, Jeffrey L. Coughlin, Debra A. Fischer, Jie Li, Michael R. Haas, Roger Hunter, Jack J. Lissauer, Fergal Mullally, Anima Sabale, Shawn E. Seader, Jeffrey C. Smith, Peter Tenenbaum, A. K. M. Kamal Uddin, and Susan E. Thompson. A Super-Earth-sized Planet Orbiting in or Near the Habitable Zone around a Sun-like Star. *ApJ*, 768(2):101, May 2013a. doi: 10.1088/0004-637X/768/2/101.

Thomas Barclay, Jason F. Rowe, Jack J. Lissauer, Daniel Huber, François Fressin, Steve B. Howell, Stephen T. Bryson, William J. Chaplin, Jean-Michel Désert, Eric D. Lopez, Geoffrey W. Marcy, Fergal Mullally, Darin Ragozzine, Guillermo Torres, Elisabeth R. Adams, Eric Agol, David Barrado, Sarbani Basu, Timothy R. Bedding, Lars A. Buchhave, David Charbonneau, Jessie L. Christiansen, Jørgen Christensen-Dalsgaard, David Ciardi, William D. Cochran, Andrea K. Dupree, Yvonne

Elsworth, Mark Everett, Debra A. Fischer, Eric B. Ford, Jonathan J. Fortney, John C. Geary, Michael R. Haas, Rasmus Handberg, Saskia Hekker, Christopher E. Henze, Elliott Horch, Andrew W. Howard, Roger C. Hunter, Howard Isaacson, Jon M. Jenkins, Christoffer Karoff, Steven D. Kawaler, Hans Kjeldsen, Todd C. Klaus, David W. Latham, Jie Li, Jorge Lillo-Box, Mikkel N. Lund, Mia Lundkvist, Travis S. Metcalfe, Andrea Miglio, Robert L. Morris, Elisa V. Quintana, Dennis Stello, Jeffrey C. Smith, Martin Still, and Susan E. Thompson. A sub-Mercury-sized exoplanet. *Nature*, 494(7438):452–454, February 2013b. doi: 10.1038/nature11914.

Sydney A. Barnes. Ages for Illustrative Field Stars Using Gyrochronology: Viability, Limitations, and Errors. *ApJ*, 669(2):1167–1189, Nov 2007. doi: 10.1086/519295.

Gibor Basri and Hieu T. Nguyen. Double Dipping: A New Relation between Stellar Rotation and Starspot Activity. *ApJ*, 863(2):190, Aug 2018. doi: 10.3847/1538-4357/aad3b6.

Fabienne A. Bastien, Keivan G. Stassun, Gibor Basri, and Joshua Pepper. A Granulation "Flicker"-based Measure of Stellar Surface Gravity. *ApJ*, 818(1):43, Feb 2016. doi: 10.3847/0004-637X/818/1/43.

Natalie M. Batalha, William J. Borucki, Stephen T. Bryson, Lars A. Buchhave, Douglas A. Caldwell, Jørgen Christensen-Dalsgaard, David Ciardi, Edward W. Dunham, Francois Fressin, III Gautier, Thomas N., Ronald L. Gilliland, Michael R. Haas, Steve B. Howell, Jon M. Jenkins, Hans Kjeldsen, David G. Koch, David W. Latham, Jack J. Lissauer, Geoffrey W. Marcy, Jason F. Rowe, Dimitar D. Sasselov, Sara Seager, Jason H. Steffen, Guillermo Torres, Gibor S. Basri, Timothy M. Brown, David Charbonneau, Jessie Christiansen, Bruce Clarke, William D. Cochran, Andrea Dupree, Daniel C. Fabrycky, Debra Fischer, Eric B. Ford, Jonathan Fortney, Forrest R. Girouard, Matthew J. Holman, John Johnson, Howard Isaacson, Todd C. Klaus, Pavel Machalek, Althea V. Moorehead, Robert C. Morehead, Darin Ragozzine, Peter

Tenenbaum, Joseph Twicken, Samuel Quinn, Jeffrey VanCleve, Lucianne M. Walkowicz, William F. Welsh, Edna Devore, and Alan Gould. Kepler's First Rocky Planet: Kepler-10b. *ApJ*, 729(1):27, March 2011. doi: 10.1088/0004-637X/729/1/27.

Natalie M. Batalha, Jason F. Rowe, Stephen T. Bryson, Thomas Barclay, Christopher J. Burke, Douglas A. Caldwell, Jessie L. Christiansen, Fergal Mullally, Susan E. Thompson, Timothy M. Brown, Andrea K. Dupree, Daniel C. Fabrycky, Eric B. Ford, Jonathan J. Fortney, Ronald L. Gilliland, Howard Isaacson, David W. Latham, Geoffrey W. Marcy, Samuel N. Quinn, Darin Ragozzine, Avi Shporer, William J. Borucki, David R. Ciardi, III Gautier, Thomas N., Michael R. Haas, Jon M. Jenkins, David G. Koch, Jack J. Lissauer, William Rapin, Gibor S. Basri, Alan P. Boss, Lars A. Buchhave, Joshua A. Carter, David Charbonneau, Joergen Christensen-Dalsgaard, Bruce D. Clarke, William D. Cochran, Brice-Olivier Demory, Jean-Michel Desert, Edna Devore, Laurance R. Doyle, Gilbert A. Esquerdo, Mark Everett, Francois Fressin, John C. Geary, Forrest R. Girouard, Alan Gould, Jennifer R. Hall, Matthew J. Holman, Andrew W. Howard, Steve B. Howell, Khadeejah A. Ibrahim, Karen Kinemuchi, Hans Kjeldsen, Todd C. Klaus, Jie Li, Philip W. Lucas, Søren Meibom, Robert L. Morris, Andrej Prša, Elisa Quintana, Dwight T. Sanderfer, Dimitar Sasselov, Shawn E. Seader, Jeffrey C. Smith, Jason H. Steffen, Martin Still, Martin C. Stumpe, Jill C. Tarter, Peter Tenenbaum, Guillermo Torres, Joseph D. Twicken, Kamal Uddin, Jeffrey Van Cleve, Lucianne Walkowicz, and William F. Welsh. Planetary Candidates Observed by Kepler. III. Analysis of the First 16 Months of Data. *ApJS*, 204(2):24, Feb 2013. doi: 10.1088/0067-0049/204/2/24.

Natasha E. Batalha, Taylor Lewis, Jonathan J. Fortney, Natalie M. Batalha, Eliza Kempton, Nikole K. Lewis, and Michael R. Line. The Precision of Mass Measurements Required for Robust Atmospheric Characterization of Transiting Exoplanets. *ApJL*, 885(1):L25, November 2019. doi: 10.3847/2041-8213/ab4909.

Anna C. Baum, Jason T. Wright, Jacob K. Luhn, and Howard Isaacson. Five Decades of Chromospheric Activity in 59 Sun-like Stars and New Maunder Minimum Candidate HD 166620. *AJ*, 163(4):183, April 2022. doi: 10.3847/1538-3881/ac5683.

Jacob L. Bean, Kevin B. Stevenson, Natalie M. Batalha, Zachory Berta-Thompson, Laura Kreidberg, Nicolas Crouzet, Björn Benneke, Michael R. Line, David K. Sing, Hannah R. Wakeford, Heather A. Knutson, Eliza M. R. Kempton, Jean-Michel Désert, Ian Crossfield, Natasha E. Batalha, Julien de Wit, Vivien Parmentier, Joseph Harrington, Julianne I. Moses, Mercedes Lopez-Morales, Munazza K. Alam, Jasmina Blecic, Giovanni Bruno, Aarynn L. Carter, John W. Chapman, Leen Decin, Diana Dragomir, Thomas M. Evans, Jonathan J. Fortney, Jonathan D. Fraine, Peter Gao, Antonio García Muñoz, Neale P. Gibson, Jayesh M. Goyal, Kevin Heng, Renyu Hu, Sarah Kendrew, Brian M. Kilpatrick, Jessica Krick, Pierre-Olivier Lagage, Monika Lendl, Tom Louden, Nikku Madhusudhan, Avi M. Mandell, Megan Mansfield, Erin M. May, Giuseppe Morello, Caroline V. Morley, Nikolay Nikolov, Seth Redfield, Jessica E. Roberts, Everett Schlawin, Jessica J. Spake, Kamen O. Todorov, Angelos Tsiaras, Olivia Venot, William C. Waalkes, Peter J. Wheatley, Robert T. Zellem, Daniel Angerhausen, David Barrado, Ludmila Carone, Sarah L. Casewell, Patricio E. Cubillos, Mario Damiano, Miguel de Val-Borro, Benjamin Drummond, Billy Edwards, Michael Endl, Nestor Espinoza, Kevin France, John E. Gizis, Thomas P. Greene, Thomas K. Henning, Yucian Hong, James G. Ingalls, Nicolas Iro, Patrick G. J. Irwin, Tiffany Kataria, Fred Lahuis, Jérémy Leconte, Jorge Lillo-Box, Stefan Lines, Joshua D. Lothringer, Luigi Mancini, Franck Marchis, Nathan Mayne, Enric Palle, Emily Rauscher, Gaël Roudier, Evgenya L. Shkolnik, John Southworth, Mark R. Swain, Jake Taylor, Johanna Teske, Giovanna Tinetti, Pascal Tremblin, Gregory S. Tucker, Roy van Boekel, Ingo P. Waldmann, Ian C. Weaver, and Tiziano Zingales. The Transiting Exoplanet Community Early Release Science Program for JWST. *PASP*, 130(993):114402, Nov 2018. doi: 10.1088/1538-3873/aadbf3.

Corey Beard, Paul Robertson, Shubham Kanodia, Jack Lubin, Caleb I. Cañas, Arvind F. Gupta, Rae Holcomb, Sinclaire Jones, Jessica E. Libby-Roberts, Andrea S. J. Lin, Suvrath Mahadevan, Guđmundur Stefánsson, Chad F. Bender, Cullen H. Blake, William D. Cochran, Michael Endl, Mark Everett, Eric B. Ford, Connor Fredrick, Samuel Halverson, Leslie Hebb, Dan Li, Sarah E. Logsdon, Jacob Luhn, Michael W. McElwain, Andrew J. Metcalf, Joe P. Ninan, Jayadev Rajagopal, Arpita Roy, Maria Schutte, Christian Schwab, Ryan C. Terrien, John Wisniewski, and Jason T. Wright. GJ 3929: High-precision Photometric and Doppler Characterization of an Exo-Venus and Its Hot, Mini-Neptune-mass Companion. , 936(1):55, September 2022. doi: 10.3847/1538-4357/ac8480.

G. Belvedere. Solar and Stellar Activity - the Theoretical Approach. *Solar Physics*, 100:363, October 1985. doi: 10.1007/BF00158436.

Björn Benneke, Ian Wong, Caroline Piaulet, Heather A. Knutson, Joshua Lothringer, Caroline V. Morley, Ian J. M. Crossfield, Peter Gao, Thomas P. Greene, Courtney Dressing, Diana Dragomir, Andrew W. Howard, Peter R. McCullough, Eliza M. R. Kempton, Jonathan J. Fortney, and Jonathan Fraine. Water Vapor and Clouds on the Habitable-zone Sub-Neptune Exoplanet K2-18b. , 887(1):L14, December 2019. doi: 10.3847/2041-8213/ab59dc.

Travis A. Berger, Daniel Huber, Eric Gaidos, Jennifer L. van Saders, and Lauren M. Weiss. The Gaia-Kepler Stellar Properties Catalog. II. Planet Radius Demographics as a Function of Stellar Mass and Age. *AJ*, 160 (3):108, September 2020. doi: 10.3847/1538-3881/aba18a.

Vanshree Bhalotia, Daniel Huber, Jennifer L. van Saders, Travis S. Metcalfe, Keivan G. Stassun, Timothy R. White, Víctor Aguirre Børsen-Koch, Warrick H. Ball, Sarbani Basu, Aldo M. Serenelli, Erica Sawczynec, Joyce A. Guzik, Andrew W. Howard, and Howard Isaacson. A New Asteroseismic Kepler Benchmark Constrains the Onset of Weakened Magnetic Braking in Mature Sun-like Stars. *ApJ*, 970(2):166, August 2024. doi: 10.3847/1538-4357/ad4eb1.

Andrea Bocchieri, Lorenzo V. Mugnai, Enzo Pascale, Quentin Changeat, and Giovanna Tinetti. Detecting molecules in Ariel low resolution transmission spectra. *Experimental Astronomy*, 56(2-3):605–644, September 2023. doi: 10.1007/s10686-023-09911-x.

Erika Böhm-Vitense. Chromospheric Activity in G and K Main-Sequence Stars, and What It Tells Us about Stellar Dynamos. *ApJ*, 657(1):486–493, March 2007. doi: 10.1086/510482.

W. J. Borucki, E. W. Dunham, D. G. Koch, W. D. Cochran, J. D. Rose, D. K. Cullers, A. Granados, and J. M. Jenkins. FRESIP: A Mission to Determine the Character and Frequency of Extra-Solar Planets Around Solar-Like Stars. , 241(1):111–134, March 1996. doi: 10.1007/BF00644220.

William J. Borucki, David Koch, Gibor Basri, Natalie Batalha, Timothy Brown, Douglas Caldwell, John Caldwell, Jørgen Christensen-Dalsgaard, William D. Cochran, Edna DeVore, Edward W. Dunham, Andrea K. Dupree, Thomas N. Gautier, John C. Geary, Ronald Gilliland, Alan Gould, Steve B. Howell, Jon M. Jenkins, Yoji Kondo, David W. Latham, Geoffrey W. Marcy, Søren Meibom, Hans Kjeldsen, Jack J. Lissauer, David G. Monet, David Morrison, Dimitar Sasselov, Jill Tarter, Alan Boss, Don Brownlee, Toby Owen, Derek Buzasi, David Charbonneau, Laurance Doyle, Jonathan Fortney, Eric B. Ford, Matthew J. Holman, Sara Seager, Jason H. Steffen, William F. Welsh, Jason Rowe, Howard Anderson, Lars Buchhave, David Ciardi, Lucianne Walkowicz, William Sherry, Elliott Horch, Howard Isaacson, Mark E. Everett, Debra Fischer, Guillermo Torres, John Asher Johnson, Michael Endl, Phillip MacQueen, Stephen T. Bryson, Jessie Dotson, Michael Haas, Jeffrey Kolodziejczak, Jeffrey Van Cleve, Hema Chandrasekaran, Joseph D. Twicken, Elisa V. Quintana, Bruce D. Clarke, Christopher Allen, Jie Li, Haley Wu, Peter Tenenbaum, Ekaterina Verner, Frederick Bruhweiler, Jason Barnes, and Andrej Prsa. Kepler Planet-Detection Mission: Introduction and First Results. *Science*, 327(5968):977, Feb 2010. doi: 10.1126/science.1185402.

William J. Borucki, David G. Koch, Gibor Basri, Natalie Batalha, Timothy M. Brown, Stephen T. Bryson, Douglas Caldwell, Jørgen Christensen-Dalsgaard, William D. Cochran, Edna DeVore, Edward W. Dunham, III Gautier, Thomas N., John C. Geary, Ronald Gilliland, Alan Gould, Steve B. Howell, Jon M. Jenkins, David W. Latham, Jack J. Lissauer, Geoffrey W. Marcy, Jason Rowe, Dimitar Sasselov, Alan Boss, David Charbonneau, David Ciardi, Laurance Doyle, Andrea K. Dupree, Eric B. Ford, Jonathan Fortney, Matthew J. Holman, Sara Seager, Jason H. Steffen, Jill Tarter, William F. Welsh, Christopher Allen, Lars A. Buchhave, Jessie L. Christiansen, Bruce D. Clarke, Santanu Das, Jean-Michel Désert, Michael Endl, Daniel Fabrycky, Francois Fressin, Michael Haas, Elliott Horch, Andrew Howard, Howard Isaacson, Hans Kjeldsen, Jeffery Kolodziejczak, Craig Kulesa, Jie Li, Philip W. Lucas, Pavel Machalek, Donald McCarthy, Phillip MacQueen, Søren Meibom, Thibaut Miquel, Andrej Prsa, Samuel N. Quinn, Elisa V. Quintana, Darin Ragozzine, William Sherry, Avi Shporer, Peter Tenenbaum, Guillermo Torres, Joseph D. Twicken, Jeffrey Van Cleve, Lucianne Walkowicz, Fred C. Witteborn, and Martin Still. Characteristics of Planetary Candidates Observed by Kepler. II. Analysis of the First Four Months of Data. *ApJ*, 736(1):19, Jul 2011. doi: 10.1088/0004-637X/736/1/19.

Axel Brandenburg, Steven H. Saar, and Christen R. Turpin. Time Evolution of the Magnetic Activity Cycle Period. *ApJL*, 498(1):L51–L54, May 1998. doi: 10.1086/311297.

Axel Brandenburg, Savita Mathur, and Travis S. Metcalfe. Evolution of Co-existing Long and Short Period Stellar Activity Cycles. *ApJ*, 845(1): 79, August 2017. doi: 10.3847/1538-4357/aa7cfa.

John M. Brewer, Debra A. Fischer, Ryan T. Blackman, Samuel H. C. Cabot, Allen B. Davis, Gregory Laughlin, Christopher Leet, J. M. Joel

Ong, Ryan R. Petersburg, Andrew E. Szymkowiak, Lily L. Zhao, Gregory W. Henry, and Joe Llama. EXPRES. I. HD 3651 as an Ideal RV Benchmark. *AJ*, 160(2):67, August 2020. doi: 10.3847/1538-3881/ab99c9.

E. L. Brown, S. V. Jeffers, S. C. Marsden, J. Morin, S. Boro Saikia, P. Petit, M. M. Jardine, V. See, A. A. Vidotto, M. W. Mengel, M. N. Dahlkemper, and the BCool Collaboration. Linking chromospheric activity and magnetic field properties for late-type dwarf stars. *MNRAS*, 514(3):4300–4319, August 2022. doi: 10.1093/mnras/stac1291.

Timothy M. Brown, David W. Latham, Mark E. Everett, and Gilbert A. Esquerdo. Kepler Input Catalog: Photometric Calibration and Stellar Classification. *AJ*, 142(4):112, Oct 2011. doi: 10.1088/0004-6256/142/4/112.

A. S. Brun, R. A. García, G. Houdek, D. Nandy, and M. Pinsonneault. The Solar-Stellar Connection. In M. J. Thompson, A. S. Brun, J. L. Culhane, L. Gizon, M. Roth, and T. Sekii, editors, *Helioseismology and Dynamics of the Solar Interior*, volume 48, pages 309–362. 2017. doi: 10.1007/978-94-024-1034-1_13.

S. Bryson, J. Coughlin, N. M. Batalha, T. Berger, D. Huber, C. Burke, J. Dotson, and S. E. Mullally. A Probabilistic Approach to Kepler Completeness and Reliability for Exoplanet Occurrence Rates. , 159(6):279, June 2020. doi: 10.3847/1538-3881/ab8a30.

Lars A. Buchhave, David W. Latham, Anders Johansen, Martin Bizzarro, Guillermo Torres, Jason F. Rowe, Natalie M. Batalha, William J. Borucki, Erik Brugamyer, Caroline Caldwell, Stephen T. Bryson, David R. Ciardi, William D. Cochran, Michael Endl, Gilbert A. Esquerdo, Eric B. Ford, John C. Geary, Ronald L. Gilliland, Terese Hansen, Howard Isaacson, John B. Laird, Philip W. Lucas, Geoffrey W. Marcy, Jon A. Morse, Paul Robertson, Avi Shporer, Robert P. Stefanik, Martin Still, and Samuel N. Quinn. An abundance of small exoplanets around stars with a wide range of metallicities. *Nature*, 486(7403):375–377, Jun 2012. doi: 10.1038/nature11121.

Christopher J. Burke, Jessie L. Christiansen, F. Mullally, Shawn Seader, Daniel Huber, Jason F. Rowe, Jeffrey L. Coughlin, Susan E. Thompson, Joseph Catanzarite, Bruce D. Clarke, Timothy D. Morton, Douglas A. Caldwell, Stephen T. Bryson, Michael R. Haas, Natalie M. Batalha, Jon M. Jenkins, Peter Tenenbaum, Joseph D. Twicken, Jie Li, Elisa Quintana, Thomas Barclay, Christopher E. Henze, William J. Borucki, Steve B. Howell, and Martin Still. Terrestrial Planet Occurrence Rates for the Kepler GK Dwarf Sample. *ApJ*, 809(1):8, Aug 2015. doi: 10.1088/0004-637X/809/1/8.

R. P. Butler, G. W. Marcy, E. Williams, C. McCarthy, P. Dosanjh, and S. S. Vogt. Attaining Doppler Precision of 3 M s-1. *PASP*, 108:500, Jun 1996. doi: 10.1086/133755.

Douglas A. Caldwell, Jeffery J. Kolodziejczak, Jeffrey E. Van Cleve, Jon M. Jenkins, Paul R. Gazis, Vic S. Argabright, Eric E. Bachtell, Edward W. Dunham, John C. Geary, Ronald L. Gilliland, Hema Chandrasekaran, Jie Li, Peter Tenenbaum, Hayley Wu, William J. Borucki, Stephen T. Bryson, Jessie L. Dotson, Michael R. Haas, and David G. Koch. Instrument Performance in Kepler's First Months. *ApJL*, 713(2):L92–L96, April 2010. doi: 10.1088/2041-8205/713/2/L92.

W. J. Chaplin, T. Appourchaux, Y. Elsworth, R. A. García, G. Houdek, C. Karoff, T. S. Metcalfe, J. Molenda-Żakowicz, M. J. P. F. G. Monteiro, M. J. Thompson, T. M. Brown, J. Christensen-Dalsgaard, R. L. Gilliland, H. Kjeldsen, W. J. Borucki, D. Koch, J. M. Jenkins, J. Ballot, S. Basu, M. Bazot, T. R. Bedding, O. Benomar, A. Bonanno, I. M. Brandão, H. Bruntt, T. L. Campante, O. L. Creevey, M. P. Di Mauro, G. Doğan, S. Dreizler, P. Eggenberger, L. Esch, S. T. Fletcher, S. Frandsen, N. Gai, P. Gaulme, R. Handberg, S. Hekker, R. Howe, D. Huber, S. G. Korzennik, J. C. Lebrun, S. Leccia, M. Martic, S. Mathur, B. Mosser, R. New, P. O. Quirion, C. Régulo, I. W. Roxburgh, D. Salabert, J. Schou, S. G. Sousa,

D. Stello, G. A. Verner, T. Arentoft, C. Barban, K. Belkacem, S. Benatti, K. Biazzo, P. Boumier, P. A. Bradley, A. M. Broomhall, D. L. Buzasi, R. U. Claudi, M. S. Cunha, F. D'Antona, S. Deheuvels, A. Derekas, A. García Hernández, M. S. Giampapa, M. J. Goupil, M. Gruberbauer, J. A. Guzik, S. J. Hale, M. J. Ireland, L. L. Kiss, I. N. Kitiashvili, K. Kolenberg, H. Korhonen, A. G. Kosovichev, F. Kupka, Y. Lebreton, B. Leroy, H. G. Ludwig, S. Mathis, E. Michel, A. Miglio, J. Montalbán, A. Moya, A. Noels, R. W. Noyes, P. L. Pallé, L. Piau, H. L. Preston, T. Roca Cortés, M. Roth, K. H. Sato, J. Schmitt, A. M. Serenelli, V. Silva Aguirre, I. R. Stevens, J. C. Suárez, M. D. Suran, R. Trampedach, S. Turck-Chièze, K. Uytterhoeven, R. Ventura, and P. A. Wilson. The Asteroseismic Potential of Kepler: First Results for Solar-Type Stars. *ApJL*, 713(2):L169–L175, April 2010. doi: 10.1088/2041-8205/713/2/L169.

W. J. Chaplin, R. Sanchis-Ojeda, T. L. Campante, R. Hand berg, D. Stello, J. N. Winn, S. Basu, J. Christensen-Dalsgaard, G. R. Davies, T. S. Metcalfe, L. A. Buchhave, D. A. Fischer, T. R. Bedding, W. D. Cochran, Y. Elsworth, R. L. Gilliland, S. Hekker, D. Huber, H. Isaacson, C. Karoff, S. D. Kawaler, H. Kjeldsen, D. W. Latham, M. N. Lund, M. Lundkvist, G. W. Marcy, A. Miglio, T. Barclay, and J. J. Lissauer. Asteroseismic Determination of Obliquities of the Exoplanet Systems Kepler-50 and Kepler-65. *ApJ*, 766(2):101, Apr 2013. doi: 10.1088/0004-637X/766/2/101.

W. J. Chaplin, H. M. Cegla, C. A. Watson, G. R. Davies, and W. H. Ball. Filtering Solar-Like Oscillations for Exoplanet Detection in Radial Velocity Observations. *AJ*, 157(4):163, April 2019. doi: 10.3847/1538-3881/ab0c01.

David Charbonneau, Timothy M. Brown, David W. Latham, and Michel Mayor. Detection of Planetary Transits Across a Sun-like Star. *ApJl*, 529(1):L45–L48, Jan 2000. doi: 10.1086/312457.

David Charbonneau, Zachory K. Berta, Jonathan Irwin, Christopher J. Burke, Philip Nutzman, Lars A. Buchhave, Christophe Lovis, Xavier Bonfils, David W. Latham, Stéphane Udry, Ruth A. Murray-Clay, Matthew J. Holman, Emilio E. Falco, Joshua N. Winn, Didier Queloz, Francesco Pepe, Michel Mayor, Xavier Delfosse, and Thierry Forveille. A super-Earth transiting a nearby low-mass star. *Nature*, 462(7275):891–894, December 2009. doi: 10.1038/nature08679.

E. Corsaro, A. Bonanno, S. Mathur, R. A. García, A. R. G. Santos, S. N. Breton, and A. Khalatyan. A calibration of the Rossby number from asteroseismology. *A&A*, 652:L2, August 2021. doi: 10.1051/0004-6361/202141395.

Ian J. M. Crossfield and Laura Kreidberg. Trends in Atmospheric Properties of Neptune-size Exoplanets. *AJ*, 154(6):261, Dec 2017. doi: 10.3847/1538-3881/aa9279.

Ian J. M. Crossfield, Travis Barman, Brad M. S. Hansen, Ichi Tanaka, and Tadayuki Kodama. Re-evaluating WASP-12b: Strong Emission at 2.315 □m, Deeper Occultations, and an Isothermal Atmosphere. *ApJ*, 760(2):140, Dec 2012. doi: 10.1088/0004-637X/760/2/140.

Jason Lee Curtis, Marcel A. Agüeros, Sean P. Matt, Kevin R. Covey, Stephanie T. Douglas, Ruth Angus, Steven H. Saar, Ann Marie Cody, Andrew Vanderburg, Nicholas M. Law, Adam L. Kraus, David W. Latham, Christoph Baranec, Reed Riddle, Carl Ziegler, Mikkel N. Lund, Guillermo Torres, Søren Meibom, Victor Silva Aguirre, and Jason T. Wright. When Do Stalled Stars Resume Spinning Down? Advancing Gyrochronology with Ruprecht 147. *ApJ*, 904(2):140, December 2020. doi: 10.3847/1538-4357/abbf58.

Daniel Czech, Howard Isaacson, Logan Pearce, Tyler Cox, Sofia Z. Sheikh, Bryan Brzycki, Sarah Buchner, Steve Croft, David DeBoer, Julia DeMarines, Jamie Drew, Vishal Gajjar, Brian C. Lacki, Matt Lebofsky, David H. E. MacMahon, Cherry Ng, Imke de Pater, Danny C. Price, Andrew P. V. Siemion, Ruby Van Rooyen, and S. Pete Worden. The Breakthrough Listen Search for Intelligent Life: MeerKAT Target Selection. *PASP*, 133(1024):064502, June 2021. doi: 10.1088/1538-3873/abf329.

Trevor J. David, Ruth Angus, Jason L. Curtis, Jennifer L. van Saders, Isabel L. Colman, Gabriella Contardo, Yuxi Lu, and Joel C. Zinn. Further Evidence of Modified Spin-down in Sun-like Stars: Pileups in the Temperature-Period Distribution. *ApJ*, 933(1):114, July 2022. doi: 10.3847/1538-4357/ac6dd3.

Rebekah I. Dawson, Ruth A. Murray-Clay, and John Asher Johnson. The Photoeccentric Effect and Proto-hot Jupiters. III. A Paucity of Proto-hot Jupiters on Super-eccentric Orbits. *ApJ*, 798(2):66, January 2015. doi: 10.1088/0004-637X/798/2/66.

X. Delfosse, T. Forveille, M. Mayor, C. Perrier, D. Naef, and D. Queloz. The closest extrasolar planet. A giant planet around the M4 dwarf GL 876. *A&A*, 338:L67–L70, October 1998. doi: 10.48550/arXiv.astro-ph/9808026.

Courtney D. Dressing and David Charbonneau. The Occurrence of Potentially Habitable Planets Orbiting M Dwarfs Estimated from the Full Kepler Dataset and an Empirical Measurement of the Detection Sensitivity. *ApJ*, 807(1):45, Jul 2015. doi: 10.1088/0004-637X/807/1/45.

X. Dumusque. Measuring precise radial velocities on individual spectral lines. I. Validation of the method and application to mitigate stellar activity. *A&A*, 620:A47, Nov 2018. doi: 10.1051/0004-6361/201833795.

Douglas K. Duncan, Arthur H. Vaughan, Olin C. Wilson, George W. Preston, James Frazer, Howard Lanning, Anthony Misch, Jean Mueller, David Soyumer, L. Woodard, Sallie L. Baliunas, Robert W. Noyes, Lee W. Hartmann, Alain Porter, Cornelis Zwaan, Frans Middelkoop, Rene G. M. Rutten, and Dimitri Mihalas. CA II H and K Measurements Made at Mount Wilson Observatory, 1966–1983. *ApJS*, 76:383, May 1991. doi: 10.1086/191572.

G. Eberhard and K. Schwarzschild. On the reversal of the calcium lines H and K in stellar spectra. *ApJ*, 38:292–295, October 1913. doi: 10.1086/142037.

T. D. Fay, Jr., W. L. Stein, and W. H. Warren, Jr. Scanner Observations of Selected Cool Stars. , 86(513):772, October 1974. doi: 10.1086/129673.

Debra A. Fischer and Jeff Valenti. The Planet-Metallicity Correlation. , 622(2):1102–1117, April 2005. doi: 10.1086/428383.

Debra A. Fischer, Geoffrey W. Marcy, and Julien F. P. Spronck. The Twenty-five Year Lick Planet Search. *ApJS*, 210(1):5, January 2014. doi: 10.1088/0067-0049/210/1/5.

M. Flores, J. F. González, M. Jaque Arancibia, A. Buccino, and C. Saffe. Discovery of an activity cycle in the solar analog HD 45184. Exploring Balmer and metallic lines as activity proxy candidates. *A&A*, 589:A135, May 2016. doi: 10.1051/0004-6361/201628145.

Eric B. Ford, Jason F. Rowe, Daniel C. Fabrycky, Joshua A. Carter, Matthew J. Holman, Jack J. Lissauer, Darin Ragozzine, Jason H. Steffen, Natalie M. Batalha, William J. Borucki, Steve Bryson, Douglas A. Caldwell, Edward W. Dunham, III Gautier, Thomas N., Jon M. Jenkins, David G. Koch, Jie Li, Philip Lucas, Geoffrey W. Marcy, Sean McCauliff, Fergal R. Mullally, Elisa Quintana, Martin Still, Peter Tenenbaum, Susan E. Thompson, and Joseph D. Twicken. Transit Timing Observations from Kepler. I. Statistical Analysis of the First Four Months. *ApJS*, 197 (1):2, November 2011. doi: 10.1088/0067-0049/197/1/2.

Jonathan D. Fraine, Drake Deming, Michaël Gillon, Emmanuël Jehin, Brice-Olivier Demory, Bjoern Benneke, Sara Seager, Nikole K. Lewis, Heather Knutson, and Jean-Michel Désert. Spitzer Transits of the Super-Earth GJ1214b and Implications for its Atmosphere. *ApJ*, 765(2):127, Mar 2013. doi: 10.1088/0004-637X/765/2/127.

François Fressin, Guillermo Torres, David Charbonneau, Stephen T. Bryson, Jessie Christiansen, Courtney D. Dressing, Jon M. Jenkins, Lucianne M. Walkowicz, and Natalie M. Batalha. The False Positive Rate of Kepler and the Occurrence of Planets. *ApJ*, 766(2):81, Apr 2013. doi: 10.1088/0004-637X/766/2/81.

Benjamin J. Fulton and Erik A. Petigura. The California-Kepler Survey. VII. Precise Planet Radii Leveraging Gaia DR2 Reveal the Stellar Mass Dependence of the Planet Radius Gap. *AJ*, 156(6):264, Dec 2018. doi: 10.3847/1538-3881/aae828.

Benjamin J. Fulton, Lauren M. Weiss, Evan Sinukoff, Howard Isaacson, Andrew W. Howard, Geoffrey W. Marcy, Gregory W. Henry, Bradford P. Holden, and Robert I. Kibrick. Three Super-Earths Orbiting HD 7924. *ApJ*, 805(2):175, Jun 2015. doi: 10.1088/0004-637X/805/2/175.

Benjamin J. Fulton, Erik A. Petigura, Andrew W. Howard, Howard Isaacson, Geoffrey W. Marcy, Phillip A. Cargile, Leslie Hebb, Lauren M. Weiss, John Asher Johnson, Timothy D. Morton, Evan Sinukoff, Ian J. M. Crossfield, and Lea A. Hirsch. The California-Kepler Survey. III. A Gap in the Radius Distribution of Small Planets. *AJ*, 154(3):109, September 2017. doi: 10.3847/1538-3881/aa80eb.

Benjamin J. Fulton, Lee J. Rosenthal, Lea A. Hirsch, Howard Isaacson, Andrew W. Howard, Cayla M. Dedrick, Ilya A. Sherstyuk, Sarah C. Blunt, Erik A. Petigura, Heather A. Knutson, Aida Behmard, Ashley Chontos, Justin R. Crepp, Ian J. M. Crossfield, Paul A. Dalba, Debra A. Fischer, Gregory W. Henry, Stephen R. Kane, Molly Kosiarek, Geoffrey W. Marcy, Ryan A. Rubenzahl, Lauren M. Weiss, and Jason T. Wright. California Legacy Survey. II. Occurrence of Giant Planets beyond the Ice Line. *ApJS*, 255(1):14, July 2021. doi: 10.3847/1538-4365/abfcc1.

III Gautier, Thomas N., Natalie M. Batalha, William J. Borucki, William D. Cochran, Edward W. Dunham, Steve B. Howell, David G. Koch, David W. Latham, Geo? W. Marcy, Lars A. Buchhave, David R. Ciardi, Michael

Endl, Gabor Furesz, Howard Isaacson, Phillip MacQueen, Georgi Mandushev, and Lucianne Walkowicz. The Kepler Follow-up Observation Program. *arXiv e-prints*, art. arXiv:1001.0352, January 2010. doi: 10.48550/arXiv.1001.0352.

Sara Gettel, David Charbonneau, Courtney D. Dressing, Lars A. Buchhave, Xavier Dumusque, Andrew Vanderburg, Aldo S. Bonomo, Luca Malavolta, Francesco Pepe, Andrew Collier Cameron, David W. Latham, Stéphane Udry, Geoffrey W. Marcy, Howard Isaacson, Andrew W. Howard, Guy R. Davies, Victor Silva Aguirre, Hans Kjeldsen, Timothy R. Bedding, Eric Lopez, Laura Affer, Rosario Cosentino, Pedro Figueira, Aldo F. M. Fiorenzano, Avet Harutyunyan, John Asher Johnson, Mercedes Lopez-Morales, Christophe Lovis, Michel Mayor, Giusi Micela, Emilio Molinari, Fatemeh Motalebi, David F. Phillips, Giampaolo Piotto, Didier Queloz, Ken Rice, Dimitar Sasselov, Damien Ségransan, Alessandro Sozzetti, Chris Watson, Sarbani Basu, Tiago L. Campante, Jørgen Christensen-Dalsgaard, Steven D. Kawaler, Travis S. Metcalfe, Rasmus Handberg, Mikkel N. Lund, Mia S. Lundkvist, Daniel Huber, and William J. Chaplin. The Kepler-454 System: A Small, Not-rocky Inner Planet, a Jovian World, and a Distant Companion. *ApJ*, 816(2):95, January 2016. doi: 10.3847/0004-637X/816/2/95.

Steven R. Gibson, Andrew W. Howard, Arpita Roy, Christopher Smith, Sam Halverson, Jerry Edelstein, Marc Kassis, Edward H. Wishnow, Michael Raffanti, Steve Allen, Jason Chin, David Coutts, David Cowley, Jim Curtis, William Deich, Tobias Feger, Daniel Finstad, Yulia Gurevich, Yuzo Ishikawa, Ean James, Elisha Jhoti, Kyle Lanclos, Scott Lilley, Tim Miller, Steve Milner, Tom Payne, Kodi Rider, Constance Rockosi, Dale Sandford, Christian Schwab, Andreas Seifahrt, Martin M. Sirk, Roger Smith, Julian Stuermer, Marie Weisfeiler, Mavourneen Wilcox, Adam Vandenberg, and Peter Wizinowich. Keck Planet Finder: preliminary design. In *Proc. SPIE*, volume 10702 of *Society of Photo-Optical Instrumentation Engineers (SPIE) Conference Series*, page 107025X, Jul 2018. doi: 10.1117/12.2311565.

Steven R. Gibson, Andrew W. Howard, Kodi Rider, Samuel Halverson, Arpita Roy, Ashley D. Baker, Jerry Edelstein, Christopher Smith, Benjamin J. Fulton, Josh Walawender, Max Brodheim, Matthew Brown, Dwight Chan, Fei Dai, William Deich, Colby Gottschalk, Jason Grillo, David Hale, Grant Hill, Bradford Holden, Aaron Householder, Howard Isaacson, Yuzo Ishikawa, Sharon Jelinsky, Marc Kassis, Stephen Kaye, Russ Laher, Kyle Lanclos, Chien-Hsiu Lee, Scott Lilley, Benjamin McCarney, Timothy N. Miller, Joel Payne, Erik Petigura, Claire Poppett, Michael P. Raffanti, Ryan Rubenzahl, Dale Sandford, Christian Schwab, Abby P. Shaum, Martin M. Sirk, Roger Smith, Jim Thorne, John Valliant, Adam Vandenberg, Shin-Ywan Wang, Edward H. Wishnow, Truman Wold, Sherry Yeh, Steve Baca, Charles Beichman, Bruce Berriman, Thomas Brown, Kelleen Casey, Jason Chin, James Chong, David Cowley, Mark Devenot, Hamza Elwir, Daniel Finstad, Matthew Fraysse, Ean James, Elisha Jhoti, Joe Killian, Obie Levine, Adela Chenyang Li, Eduardo Marin, Steven Milner, Craig Nance, Timothy J. O'Hanlon, Daniel Orr, Roberto Ortiz-Soto, Tom Payne, Jacob Pember, Gert Raskin, Maureen Savage, Andreas Seifahrt, Brett Smith, Rob Storesund, Julian Stürmer, Nick Suominen, Jerez Tehero, Tod Von Boeckmann, Keith Wages, Marie Weisfeiler, Mavourneen Wilcox, Peter Wizinowich, and Anna Wolfenberger. System design of the Keck Planet Finder. In Julia J. Bryant, Kentaro Motohara, and Joël R. D. Vernet, editors, *Ground-based and Airborne Instrumentation for Astronomy X*, volume 13096, page 1309609. International Society for Optics and Photonics, SPIE, 2024. doi: 10.1117/12.3017841. URL https://doi.org/10.1117/12.3017841.

Ronald L. Gilliland and Sallie L. Baliunas. Objective Characterization of Stellar Activity Cycles. I. Methods and Solar Cycle Analyses. *ApJ*, 314: 766, March 1987. doi: 10.1086/165103.

Ronald L. Gilliland, Timothy M. Brown, Jørgen Christensen-Dalsgaard, Hans Kjeldsen, Conny Aerts, Thierry Appourchaux, Sarbani Basu, Timothy R. Bedding, William J. Chaplin, Margarida S. Cunha, Peter De Cat, Joris De Ridder, Joyce A. Guzik, Gerald Handler, Steven Kawaler, László Kiss, Katrien Kolenberg, Donald W. Kurtz, Travis S. Metcalfe, Mario J. P. F. G. Monteiro, Robert Szabó, Torben Arentoft, Luis Balona, Jonas Debosscher, Yvonne P. Elsworth, Pierre-Olivier Quirion, Dennis Stello, Juan Carlos Suárez, William J. Borucki, Jon M. Jenkins, David Koch, Yoji Kondo, David W. Latham, Jason F. Rowe, and Jason H. Steffen. Kepler Asteroseismology Program: Introduction and First Results. *PASP*, 122 (888):131, Feb 2010. doi: 10.1086/650399.

Ronald L. Gilliland, William J. Chaplin, Edward W. Dunham, Vic S. Argabright, William J. Borucki, Gibor Basri, Stephen T. Bryson, Derek L. Buzasi, Douglas A. Caldwell, Yvonne P. Elsworth, Jon M. Jenkins, David G. Koch, Jeffrey Kolodziejczak, Andrea Miglio, Jeffrey van Cleve, Lucianne M. Walkowicz, and William F. Welsh. Kepler Mission Stellar and Instrument Noise Properties. *ApJS*, 197(1):6, November 2011. doi: 10.1088/0067-0049/197/1/6.

Ronald L. Gilliland, Geoffrey W. Marcy, Jason F. Rowe, Leslie Rogers, Guillermo Torres, Francois Fressin, Eric D. Lopez, Lars A. Buchhave, Jørgen Christensen-Dalsgaard, Jean-Michel Désert, Christopher E. Henze, Howard Isaacson, Jon M. Jenkins, Jack J. Lissauer, William J. Chaplin, Sarbani Basu, Travis S. Metcalfe, Yvonne Elsworth, Rasmus Handberg, Saskia Hekker, Daniel Huber, Christoffer Karoff, Hans Kjeldsen, Mikkel N. Lund, Mia Lundkvist, Andrea Miglio, David Charbonneau, Eric B. Ford, Jonathan J. Fortney, Michael R. Haas, Andrew W. Howard, Steve B. Howell, Darin Ragozzine, and Susan E. Thompson. Kepler-68: Three Planets, One with a Density between that of Earth and Ice Giants. *ApJ*, 766(1):40, Mar 2013. doi: 10.1088/0004-637X/766/1/40.

J. Gomes da Silva, N. C. Santos, V. Adibekyan, S. G. Sousa, T. L. Campante, P. Figueira, D. Bossini, E. Delgado-Mena, M. J. P. F. G. Monteiro, P. de Laverny, A. Recio-Blanco, and C. Lovis. Stellar chromospheric activity of 1674 FGK stars from the AMBRE-HARPS sample. I. A catalogue of homogeneous chromospheric activity. *A&A*, 646:A77, February 2021. doi: 10.1051/0004-6361/202039765.

Thomas P. Greene, Taylor J. Bell, Elsa Ducrot, Achrène Dyrek, Pierre-Olivier Lagage, and Jonathan J. Fortney. Thermal emission from the Earth-sized exoplanet TRAPPIST-1 b using JWST. *Nature*, 618(7963): 39–42, June 2023. doi: 10.1038/s41586-023-05951-7.

A. Gressier, M. Mori, Q. Changeat, B. Edwards, J. P. Beaulieu, E. Marcq, and B. Charnay. Near-infrared transmission spectrum of TRAPPIST-1 h using Hubble WFC3 G141 observations. *A&A*, 658:A133, February 2022. doi: 10.1051/0004-6361/202142140.

Samuel K. Grunblatt, Andrew W. Howard, and Raphaëlle D. Haywood. Determining the Mass of Kepler-78b with Nonparametric Gaussian Process Estimation. *ApJ*, 808(2):127, Aug 2015. doi: 10.1088/0004-637X/808/2/127.

Michael Gully-Santiago, Caroline V. Morley, Jessica Luna, Morgan MacLeod, Antonija Oklopčić, Aishwarya Ganesh, Quang H. Tran, Zhoujian Zhang, Brendan P. Bowler, William D. Cochran, Daniel M. Krolikowski, Suvrath Mahadevan, Joe P. Ninan, Guđmundur Stefánsson, Andrew Vanderburg, Joseph A. Zalesky, and Gregory R. Zeimann. A Large and Variable Leading Tail of Helium in a Hot Saturn Undergoing Runaway Inflation. *AJ*, 167(4):142, April 2024. doi: 10.3847/1538-3881/ad1ee8.

Akash Gupta and Hilke E. Schlichting. Sculpting the valley in the radius distribution of small exoplanets as a by-product of planet formation: the core-powered mass-loss mechanism. , 487(1):24–33, July 2019. doi: 10.1093/mnras/stz1230.

George E. Hale. On the Probable Existence of a Magnetic Field in Sun-Spots. *ApJ*, 28:315, November 1908. doi: 10.1086/141602.

Jeffrey C. Hall, G. W. Lockwood, and Brian A. Skiff. The Activity and Variability of the Sun and Sun-like Stars. I. Synoptic Ca II H and K Observations. *AJ*, 133(3):862–881, March 2007. doi: 10.1086/510356.

Oliver J. Hall, Guy R. Davies, Jennifer van Saders, Martin B. Nielsen, Mikkel N. Lund, William J. Chaplin, Rafael A. García, Louis Amard, Angela A. Breimann, Saniya Khan, Victor See, and Jamie Tayar. Weakened magnetic braking supported by asteroseismic rotation rates of Kepler dwarfs. *Nature Astronomy*, 5:707–714, July 2021. doi: 10.1038/s41550-021-01335-x.

L. Hartmann, D. R. Soderblom, R. W. Noyes, N. Burnham, and A. H. Vaughan. An analysis of the Vaughan-Preston survey of chromospheric emission. , 276:254–265, January 1984. doi: 10.1086/161609.

Gregory W. Henry, Geoffrey W. Marcy, R. Paul Butler, and Steven S. Vogt. A Transiting “51 Peg-like” Planet. *ApJl*, 529(1):L41–L44, Jan 2000. doi: 10.1086/312458.

Todd J. Henry, David R. Soderblom, Robert A. Donahue, and Sallie L. Baliunas. A Survey of Ca II H and K Chromospheric Emission in Southern Solar-Type Stars. *AJ*, 111:439, January 1996. doi: 10.1086/117796.

Matthew J. Holman, Daniel C. Fabrycky, Darin Ragozzine, Eric B. Ford, Jason H. Steffen, William F. Welsh, Jack J. Lissauer, David W. Latham, Geoffrey W. Marcy, Lucianne M. Walkowicz, Natalie M. Batalha, Jon M. Jenkins, Jason F. Rowe, William D. Cochran, Francois Fressin, Guillermo Torres, Lars A. Buchhave, Dimitar D. Sasselov, William J. Borucki, David G. Koch, Gibor Basri, Timothy M. Brown, Douglas A. Caldwell, David Charbonneau, Edward W. Dunham, Thomas N. Gautier, John C. Geary, Ronald L. Gilliland, Michael R. Haas, Steve B. Howell, David R. Ciardi, Michael Endl, Debra Fischer, Gábor Fűrész, Joel D. Hartman, Howard Isaacson, John A. Johnson, Phillip J. MacQueen, Althea V. Moorhead, Robert C. Morehead, and Jerome A. Orosz. Kepler-9: A System of Multiple Planets Transiting a Sun-Like Star, Confirmed by Timing Variations. *Science*, 330(6000):51, October 2010. doi: 10.1126/science.1195778.

Andrew W. Howard, John Asher Johnson, Geoffrey W. Marcy, Debra A. Fischer, Jason T. Wright, David Bernat, Gregory W. Henry, Kathryn M. G. Peek, Howard Isaacson, Kevin Apps, Michael Endl, William D. Cochran, Jeff A. Valenti, Jay Anderson, and Nikolai E. Piskunov. The California Planet Survey. I. Four New Giant Exoplanets. *ApJ*, 721(2):1467–1481, October 2010a. doi: 10.1088/0004-637X/721/2/1467.

Andrew W. Howard, Geoffrey W. Marcy, John Asher Johnson, Debra A. Fischer, Jason T. Wright, Howard Isaacson, Jeff A. Valenti, Jay Anderson, Doug N. C. Lin, and Shigeru Ida. The Occurrence and Mass Distribution of Close-in Super-Earths, Neptunes, and Jupiters. *Science*, 330(6004): 653, Oct 2010b. doi: 10.1126/science.1194854.

Andrew W. Howard, Roberto Sanchis-Ojeda, Geoffrey W. Marcy, John Asher Johnson, Joshua N. Winn, Howard Isaacson, Debra A. Fischer, Benjamin J. Fulton, Evan Sinukoff, and Jonathan J. Fortney. A rocky composition for an Earth-sized exoplanet. *Nature*, 503(7476):381–384, Nov 2013. doi: 10.1038/nature12767.

Danley C. Hsu, Eric B. Ford, Darin Ragozzine, and Keir Ashby. Occurrence Rates of Planets Orbiting FGK Stars: Combining Kepler DR25, Gaia DR2, and Bayesian Inference. , 158(3):109, September 2019. doi: 10.3847/1538-3881/ab31ab.

Daniel Huber. isoclassify: v1.2, May 2017.

Daniel Huber, Joshua A. Carter, Mauro Barbieri, Andrea Miglio, Katherine M. Deck, Daniel C. Fabrycky, Benjamin T. Montet, Lars A. Buchhave, William J. Chaplin, Saskia Hekker, Josefina Montalbán, Roberto Sanchis-Ojeda, Sarbani Basu, Timothy R. Bedding, Tiago L. Campante, Jørgen Christensen-Dalsgaard, Yvonne P. Elsworth, Dennis Stello, Torben Arentoft, Eric B. Ford, Ronald L. Gilliland , Rasmus Handberg, Andrew W. Howard, Howard Isaacson, John Asher Johnson, Christoffer Karoff, Steven D. Kawaler, Hans Kjeldsen, David W. Latham, Mikkel N. Lund, Mia Lundkvist, Geoffrey W. Marcy, Travis S. Metcalfe, Victor

Silva Aguirre, and Joshua N. Winn. Stellar Spin-Orbit Misalignment in a Multiplanet System. *Science*, 342(6156):331–334, Oct 2013a. doi: 10.1126/science.1242066.

Daniel Huber, William J. Chaplin, Jørgen Christensen-Dalsgaard, Ronald L. Gilliland, Hans Kjeldsen, Lars A. Buchhave, Debra A. Fischer, Jack J. Lissauer, Jason F. Rowe, Roberto Sanchis-Ojeda, Sarbani Basu, Rasmus Handberg, Saskia Hekker, Andrew W. Howard, Howard Isaacson, Christoffer Karoff, David W. Latham, Mikkel N. Lund, Mia Lundkvist, Geoffrey W. Marcy, Andrea Miglio, Victor Silva Aguirre, Dennis Stello, Torben Arentoft, Thomas Barclay, Timothy R. Bedding, Christopher J. Burke, Jessie L. Christiansen, Yvonne P. Elsworth, Michael R. Haas, Steven D. Kawaler, Travis S. Metcalfe, Fergal Mullally, and Susan E. Thompson. Fundamental Properties of Kepler Planet-candidate Host Stars using Asteroseismology. *ApJ*, 767(2):127, Apr 2013b. doi: 10.1088/0004-637X/767/2/127.

S. Ida and D. N. C. Lin. Toward a Deterministic Model of Planetary Formation. III. Mass Distribution of Short-Period Planets around Stars of Various Masses. *ApJ*, 626(2):1045–1060, June 2005. doi: 10.1086/429953.

S. Ida and D. N. C. Lin. Toward a Deterministic Model of Planetary Formation. VI. Dynamical Interaction and Coagulation of Multiple Rocky Embryos and Super-Earth Systems around Solar-type Stars. *ApJ*, 719(1): 810–830, Aug 2010. doi: 10.1088/0004-637X/719/1/810.

Howard Isaacson and Debra Fischer. Chromospheric Activity and Jitter Measurements for 2630 Stars on the California Planet Search. *ApJ*, 725 (1):875–885, Dec 2010. doi: 10.1088/0004-637X/725/1/875.

Howard Isaacson, Andrew P. V. Siemion, Geoffrey W. Marcy, Matt Lebofsky, Danny C. Price, David MacMahon, Steve Croft, David DeBoer, Jack Hickish, Dan Werthimer, Sofia Sheikh, Greg Hellbourg, and J. Emilio Enriquez. The Breakthrough Listen Search for Intelligent Life: Target Selection of Nearby Stars and Galaxies. *PASP*, 129(975):054501, May 2017. doi: 10.1088/1538-3873/aa5800.

Jon M. Jenkins, William J. Borucki, David G. Koch, Geoffrey W. Marcy, William D. Cochran, William F. Welsh, Gibor Basri, Natalie M. Batalha, Lars A. Buchhave, Timothy M. Brown, Douglas A. Caldwell, Edward W. Dunham, Michael Endl, Debra A. Fischer, III Gautier, Thomas N., John C. Geary, Ronald L. Gilliland, Steve B. Howell, Howard Isaacson, John Asher Johnson, David W. Latham, Jack J. Lissauer, David G. Monet, Jason F. Rowe, Dimitar D. Sasselov, Andrew W. Howard, Phillip MacQueen, Jerome A. Orosz, Hema Chandrasekaran, Joseph D. Twicken, Stephen T. Bryson, Elisa V. Quintana, Bruce D. Clarke, Jie Li, Christopher Allen, Peter Tenenbaum, Hayley Wu, Søren Meibom, Todd C. Klaus, Christopher K. Middour, Miles T. Cote, Sean McCauliff, Forrest R. Girouard, Jay P. Gunter, Bill Wohler, Jennifer R. Hall, Khadeejah Ibrahim, AKM Kamal Uddin, Michael S. Wu, Paresh A. Bhavsar, Jeffrey Van Cleve, David L. Pletcher, Jessie L. Dotson, and Michael R. Haas. Discovery and Rossiter-Mclaughlin Effect of Exoplanet Kepler-8b. *ApJ*, 724(2):1108–1119, December 2010a. doi: 10.1088/0004-637X/724/2/1108.

Jon M. Jenkins, Douglas A. Caldwell, Hema Chandrasekaran, Joseph D. Twicken, Stephen T. Bryson, Elisa V. Quintana, Bruce D. Clarke, Jie Li, Christopher Allen, Peter Tenenbaum, Hayley Wu, Todd C. Klaus, Jeffrey Van Cleve, Jessie A. Dotson, Michael R. Haas, Ronald L. Gilliland, David G. Koch, and William J. Borucki. Initial Characteristics of Kepler Long Cadence Data for Detecting Transiting Planets. *ApJL*, 713 (2):L120–L125, April 2010b. doi: 10.1088/2041-8205/713/2/L120.

John Asher Johnson, Erik A. Petigura, Benjamin J. Fulton, Geoffrey W. Marcy, Andrew W. Howard, Howard Isaacson, Leslie Hebb, Phillip A. Cargile, Timothy D. Morton, Lauren M. Weiss, Joshua N. Winn, Leslie A. Rogers, Evan Sinukoff, and Lea A. Hirsch. The California-Kepler Survey.

II. Precise Physical Properties of 2025 Kepler Planets and Their Host Stars. *AJ*, 154(3):108, Sep 2017. doi: 10.3847/1538-3881/aa80e7.

Stephen R. Kane and Robert A. Wittenmyer. Eccentricity Distribution beyond the Snow Line and Implications for Planetary Habitability. *ApJL*, 962(1):L21, February 2024. doi: 10.3847/2041-8213/ad2463.

Stephen R. Kane, Diana Dragomir, David R. Ciardi, Jae-Woo Lee, Gaspare Lo Curto, Christophe Lovis, Dominique Naef, Suvrath Mahadevan, Genady Pilyavsky, Stephane Udry, Xuesong Wang, and Jason Wright. Stellar Variability of the Exoplanet Hosting Star HD 63454. *ApJ*, 737(2): 58, August 2011. doi: 10.1088/0004-637X/737/2/58.

Heather A. Knutson, David Charbonneau, Nicolas B. Cowan, Jonathan J. Fortney, Adam P. Showman, Eric Agol, Gregory W. Henry, Mark E. Everett, and Lori E. Allen. Multiwavelength Constraints on the Day-Night Circulation Patterns of HD 189733b. *ApJ*, 690(1):822–836, Jan 2009. doi: 10.1088/0004-637X/690/1/822.

David Koch, William Borucki, Kent Cullers, Edward Dunham, Larry Webster, Tom Miers, and Harold Reitsema. System design of a mission to detect Earth-sized planets in the inner orbits of solar-like stars. , 101 (E4):9297–9302, April 1996. doi: 10.1029/96JE00468.

Ravi Kumar Kopparapu, Eric Hébrard, Rus Belikov, Natalie M. Batalha, Gijs D. Mulders, Chris Stark, Dillon Teal, Shawn Domagal-Goldman, and Avi Mandell. Exoplanet Classification and Yield Estimates for Direct Imaging Missions. *ApJ*, 856(2):122, Apr 2018. doi: 10.3847/1538-4357/aab205.

Molly R. Kosiarek, Sarah Blunt, Mercedes López-Morales, Ian J. M. Crossfield, Evan Sinukoff, Erik A. Petigura, Erica J. Gonzales, Ennio Poretti, Luca Malavolta, Andrew W. Howard, Howard Isaacson, Raphaëlle D. Haywood, David R. Ciardi, Makennah Bristow, Andrew Collier Cameron, David Charbonneau, Courtney D. Dressing, Pedro Figueira, Benjamin J. Fulton, Bronwen J. Hardee, Lea A. Hirsch, David W. Latham, Annelies Mortier, Chantanelle Nava, Joshua E. Schlieder, Andrew Vanderburg, Lauren Weiss, Aldo S. Bonomo, François Bouchy, Lars A. Buchhave, Adrien Coffinet, Mario Damasso, Xavier Dumusque, Christophe Lovis, Michel Mayor, Giusi Micela, Emilio Molinari, Francesco Pepe, David Phillips, Giampaolo Piotto, Ken Rice, Dimitar Sasselov, Damien Ségransan, Alessandro Sozzetti, Stéphane Udry, and Chris Watson. K2-291b: A Rocky Super-Earth in a 2.2 day Orbit. *AJ*, 157 (3):116, Mar 2019. doi: 10.3847/1538-3881/aafe83.

Laura Kreidberg, Michael R. Line, Daniel Thorngren, Caroline V. Morley, and Kevin B. Stevenson. Water, High-altitude Condensates, and Possible Methane Depletion in the Atmosphere of the Warm Super-Neptune WASP-107b. *ApJl*, 858(1):L6, May 2018. doi: 10.3847/2041-8213/aabfce.

Michelle Kunimoto and Jaymie M. Matthews. Searching the Entirety of Kepler Data. II. Occurrence Rate Estimates for FGK Stars. , 159(6):248, June 2020. doi: 10.3847/1538-3881/ab88b0.

David W. Latham, Jason F. Rowe, Samuel N. Quinn, Natalie M. Batalha, William J. Borucki, Timothy M. Brown, Stephen T. Bryson, Lars A. Buchhave, Douglas A. Caldwell, Joshua A. Carter, Jessie L. Christiansen, David R. Ciardi, William D. Cochran, Edward W. Dunham, Daniel C. Fabrycky, Eric B. Ford, III Gautier, Thomas N., Ronald L. Gilliland, Matthew J. Holman, Steve B. Howell, Khadeejah A. Ibrahim, Howard Isaacson, Jon M. Jenkins, David G. Koch, Jack J. Lissauer, Geoffrey W. Marcy, Elisa V. Quintana, Darin Ragozzine, Dimitar Sasselov, Avi Shporer, Jason H. Steffen, William F. Welsh, and Bill Wohler. A First Comparison of Kepler Planet Candidates in Single and Multiple Systems. *ApJL*, 732(2): L24, May 2011. doi: 10.1088/2041-8205/732/2/L24.

A. Léger, D. Rouan, J. Schneider, P. Barge, M. Fridlund, B. Samuel, M. Ollivier, E. Guenther, M. Deleuil, H. J. Deeg, M. Auvergne, R. Alonso, S. Aigrain, A. Alapini, J. M. Almenara, A. Baglin, M. Barbieri, H. Bruntt, P. Bordé, F. Bouchy, J. Cabrera, C. Catala, L. Carone, S. Carpano, Sz.

Csizmadia, R. Dvorak, A. Erikson, S. Ferraz-Mello, B. Foing, F. Fressin, D. Gandolfi, M. Gillon, Ph. Gondoin, O. Grasset, T. Guillot, A. Hatzes, G. Hébrard, L. Jorda, H. Lammer, A. Llebaria, B. Loeillet, M. Mayor, T. Mazeh, C. Moutou, M. Pätzold, F. Pont, D. Queloz, H. Rauer, S. Renner, R. Samadi, A. Shporer, Ch. Sotin, B. Tingley, G. Wuchterl, M. Adda, P. Agogu, T. Appourchaux, H. Ballans, P. Baron, T. Beaufort, R. Bellenger, R. Berlin, P. Bernardi, D. Blouin, F. Baudin, P. Bodin, L. Boisnard, L. Boit, F. Bonneau, S. Borzeix, R. Briet, J. T. Buey, B. Butler, D. Cailleau, R. Cautain, P. Y. Chabaud, S. Chaintreuil, F. Chiavassa, V. Costes, V. Cuna Parrho, F. de Oliveira Fialho, M. Decaudin, J. M. Defise, S. Djalal, G. Epstein, G. E. Exil, C. Fauré, T. Fenouillet, A. Gaboriaud, A. Gallic, P. Gamet, P. Gavalda, E. Grolleau, R. Gruneisen, L. Gueguen, V. Guis, V. Guivarc'h, P. Guterman, D. Hallouard, J. Hasiba, F. Heuripeau, G. Huntzinger, H. Hustaix, C. Imad, C. Imbert, B. Johlander, M. Jouret, P. Journoud, F. Karioty, L. Kerjean, V. Lafaille, L. Lafond, T. Lam-Trong, P. Landiech, V. Lapeyrere, T. Larqué, P. Laudet, N. Lautier, H. Lecann, L. Lefevre, B. Leruyet, P. Levacher, A. Magnan, E. Mazy, F. Mertens, J. M. Mesnager, J. C. Meunier, J. P. Michel, W. Monjoin, D. Naudet, K. Nguyen-Kim, J. L. Orcesi, H. Ottacher, R. Perez, G. Peter, P. Plasson, J. Y. Plesseria, B. Pontet, A. Pradines, C. Quentin, J. L. Reynaud, G. Rolland, F. Rollenhagen, R. Romagnan, N. Russ, R. Schmidt, N. Schwartz, I. Sebbag, G. Sedes, H. Smit, M. B. Steller, W. Sunter, C. Surace, M. Tello, D. Tiphène, P. Toulouse, B. Ulmer, O. Vandermarcq, E. Vergnault, A. Vuillemin, and P. Zanatta. Transiting exoplanets from the CoRoT space mission. VIII. CoRoT-7b: the first super-Earth with measured radius. *A&A*, 506(1):287–302, October 2009. doi: 10.1051/0004-6361/200911933.

Jack J. Lissauer, Daniel C. Fabrycky, Eric B. Ford, William J. Borucki, Francois Fressin, Geoffrey W. Marcy, Jerome A. Orosz, Jason F. Rowe, Guillermo Torres, William F. Welsh, Natalie M. Batalha, Stephen T. Bryson, Lars A. Buchhave, Douglas A. Caldwell, Joshua A. Carter, David Charbonneau, Jessie L. Christiansen, William D. Cochran, Jean-Michel

Desert, Edward W. Dunham, Michael N. Fanelli, Jonathan J. Fortney, III Gautier, Thomas N., John C. Geary, Ronald L. Gilliland, Michael R. Haas, Jennifer R. Hall, Matthew J. Holman, David G. Koch, David W. Latham, Eric Lopez, Sean McCauliff, Neil Miller, Robert C. Morehead, Elisa V. Quintana, Darin Ragozzine, Dimitar Sasselov, Donald R. Short, and Jason H. Steffen. A closely packed system of low-mass, low-density planets transiting Kepler-11. *Nature*, 470(7332):53–58, February 2011. doi: 10.1038/nature09760.

Eric D. Lopez and Jonathan J. Fortney. Understanding the Mass-Radius Relation for Sub-neptunes: Radius as a Proxy for Composition. *ApJ*, 792 (1):1, Sep 2014. doi: 10.1088/0004-637X/792/1/1.

Diego Lorenzo-Oliveira, Fabrício C. Freitas, Jorge Meléndez, Megan Bedell, Iván Ramírez, Jacob L. Bean, Martin Asplund, Lorenzo Spina, Stefan Dreizler, Alan Alves-Brito, and Luca Casagrande. The Solar Twin Planet Search. The age-chromospheric activity relation. *A&A*, 619:A73, November 2018. doi: 10.1051/0004-6361/201629294.

C. Lovis, X. Dumusque, N. C. Santos, F. Bouchy, M. Mayor, F. Pepe, D. Queloz, D. Ségransan, and S. Udry. The HARPS search for southern extra-solar planets. XXXI. Magnetic activity cycles in solar-type stars: statistics and impact on precise radial velocities. *arXiv e-prints*, art. arXiv:1107.5325, July 2011. doi: 10.48550/arXiv.1107.5325.

Jack Lubin, Paul Robertson, Gudmundur Stefansson, Joe Ninan, Suvrath Mahadevan, Michael Endl, Eric Ford, Jason T. Wright, Corey Beard, Chad Bender, William D. Cochran, Scott A. Diddams, Connor Fredrick, Samuel Halverson, Shubham Kanodia, Andrew J. Metcalf, Lawrence Ramsey, Arpita Roy, Christian Schwab, and Ryan Terrien. Stellar Activity Manifesting at a One-year Alias Explains Barnard b as a False Positive. *AJ*, 162(2):61, August 2021. doi: 10.3847/1538-3881/ac0057.

X. Luri, A. G. A. Brown, L. M. Sarro, F. Arenou, C. A. L. Bailer-Jones, A. Castro-Ginard, J. de Bruijne, T. Prusti, C. Babusiaux, and H. E. Delgado. Gaia Data Release 2. Using Gaia parallaxes. *A&A*, 616:A9, Aug 2018. doi: 10.1051/0004-6361/201832964.

Eric E. Mamajek and Lynne A. Hillenbrand. Improved Age Estimation for Solar-Type Dwarfs Using Activity-Rotation Diagnostics. *ApJ*, 687(2): 1264–1293, Nov 2008. doi: 10.1086/591785.

G. W. Marcy. A technique for measuring magnetic fields on solar-type stars. *PASP*, 94:989–996, December 1982. doi: 10.1086/131097.

Geoffrey W. Marcy and R. Paul Butler. A Planetary Companion to 70 Virginis. *ApJl*, 464:L147, Jun 1996. doi: 10.1086/310096.

Geoffrey W. Marcy, R. Paul Butler, Steven S. Vogt, Debra Fischer, and Jack J. Lissauer. A Planetary Companion to a Nearby M4 Dwarf, Gliese 876. *ApJL*, 505(2):L147–L149, October 1998. doi: 10.1086/311623.

Geoffrey W. Marcy, Howard Isaacson, Andrew W. Howard, Jason F. Rowe, Jon M. Jenkins, Stephen T. Bryson, David W. Latham, Steve B. Howell, III Gautier, Thomas N., Natalie M. Batalha, Leslie Rogers, David Ciardi, Debra A. Fischer, Ronald L. Gilliland, Hans Kjeldsen, Jørgen Christensen-Dalsgaard, Daniel Huber, William J. Chaplin, Sarbani Basu, Lars A. Buchhave, Samuel N. Quinn, William J. Borucki, David G. Koch, Roger Hunter, Douglas A. Caldwell, Jeffrey Van Cleve, Rea Kolbl, Lauren M. Weiss, Erik Petigura, Sara Seager, Timothy Morton, John Asher Johnson, Sarah Ballard, Chris Burke, William D. Cochran, Michael Endl, Phillip MacQueen, Mark E. Everett, Jack J. Lissauer, Eric B. Ford, Guillermo Torres, Francois Fressin, Timothy M. Brown, Jason H. Steffen, David Charbonneau, Gibor S. Basri, Dimitar D. Sasselov, Joshua Winn, Roberto Sanchis-Ojeda, Jessie Christiansen, Elisabeth Adams, Christopher Henze, Andrea Dupree, Daniel C. Fabrycky, Jonathan J. Fortney, Jill Tarter, Matthew J. Holman, Peter Tenenbaum, Avi Shporer, Philip W. Lucas, William F. Welsh, Jerome A. Orosz, T. R. Bedding, T. L. Campante, G. R. Davies, Y. Elsworth, R. Handberg, S. Hekker, C. Karoff, S. D. Kawaler, M. N. Lund, M. Lundkvist, T. S. Metcalfe, A. Miglio, V. Silva Aguirre, D. Stello, T. R. White, Alan Boss, Edna Devore, Alan Gould, Andrej Prsa, Eric Agol, Thomas Barclay, Jeff Coughlin, Erik Brugamyer, Fergal Mullally, Elisa V. Quintana, Martin Still, Susan E. Thompson, David Morrison, Joseph D. Twicken, Jean-Michel Désert, Josh Carter, Justin R. Crepp, Guillaume Hébrard, Alexandre Santerne, Claire Moutou, Charlie Sobeck, Douglas Hudgins, Michael R. Haas, Paul Robertson, Jorge Lillo-Box, and David Barrado. Masses, Radii, and Orbits of Small Kepler Planets: The Transition from Gaseous to Rocky Planets. *ApJS*, 210(2):20, Feb 2014. doi: 10.1088/0067-0049/210/2/20.

C. J. Marvin, A. Reiners, G. Anglada-Escudé, S. V. Jeffers, and S. Boro Saikia. Absolute Ca II H & K and H-alpha flux measurements of low-mass stars: Extending R'$_{HK}$ to M dwarfs. *A&A*, 671:A162, March 2023. doi: 10.1051/0004-6361/201937306.

F. Matuszewski, N. Nettelmann, J. Cabrera, A. Börner, and H. Rauer. Estimating the number of planets that PLATO can detect. *A&A*, 677: A133, September 2023. doi: 10.1051/0004-6361/202245287.

E. Walter Maunder. The Prolonged Sunspot Minimum, 1645-1715. *Journal of the British Astronomical Association*, 32:140–145, February 1922.

M. Mayor, M. Marmier, C. Lovis, S. Udry, D. Ségransan, F. Pepe, W. Benz, J. L. Bertaux, F. Bouchy, X. Dumusque, G. Lo Curto, C. Mordasini, D. Queloz, and N. C. Santos. The HARPS search for southern extra-solar planets XXXIV. Occurrence, mass distribution and orbital properties of super-Earths and Neptune-mass planets. *arXiv e-prints*, art. arXiv:1109.2497, Sep 2011.

Michel Mayor and Didier Queloz. A Jupiter-mass companion to a solar-type star. *Nature*, 378(6555):355–359, Nov 1995. doi: 10.1038/378355a0.

A. McQuillan, T. Mazeh, and S. Aigrain. Rotation Periods of 34,030 Kepler Main-sequence Stars: The Full Autocorrelation Sample. *ApjS*, 211 (2):24, Apr 2014. doi: 10.1088/0067-0049/211/2/24.

Søren Meibom, Sydney A. Barnes, David W. Latham, Natalie Batalha, William J. Borucki, David G. Koch, Gibor Basri, Lucianne M. Walkowicz, Kenneth A. Janes, Jon Jenkins, Jeffrey Van Cleve, Michael R. Haas, Stephen T. Bryson, Andrea K. Dupree, Gabor Furesz, Andrew H. Szentgyorgyi, Lars A. Buchhave, Bruce D. Clarke, Joseph D. Twicken, and Elisa V. Quintana. The Kepler Cluster Study: Stellar Rotation in NGC 6811. *ApJL*, 733(1):L9, May 2011. doi: 10.1088/2041-8205/733/1/L9.

Travis S. Metcalfe and Ricky Egeland. Understanding the Limitations of Gyrochronology for Old Field Stars. *ApJ*, 871(1):39, January 2019. doi: 10.3847/1538-4357/aaf575.

Travis S. Metcalfe, Klaus G. Strassmeier, Ilya V. Ilyin, Jennifer L. van Saders, Thomas R. Ayres, Adam J. Finley, Oleg Kochukhov, Pascal Petit, Victor See, Keivan G. Stassun, Sandra V. Jeffers, Stephen C. Marsden, Julien Morin, and Aline A. Vidotto. Constraints on Magnetic Braking from the G8 Dwarf Stars 61 UMa and τ Cet. *ApJL*, 948(1):L6, May 2023. doi: 10.3847/2041-8213/acce38.

Travis S. Metcalfe, Klaus G. Strassmeier, Ilya V. Ilyin, Derek Buzasi, Oleg Kochukhov, Thomas R. Ayres, Sarbani Basu, Ashley Chontos, Adam J. Finley, Victor See, Keivan G. Stassun, Jennifer L. van Saders, Aldo G. Sepulveda, and George R. Ricker. Weakened Magnetic Braking in the Exoplanet Host Star 51 Peg. *ApJL*, 960(1):L6, January 2024. doi: 10.3847/2041-8213/ad0a95.

Sean M. Mills, Andrew W. Howard, Erik A. Petigura, Benjamin J. Fulton, Howard Isaacson, and Lauren M. Weiss. The California-Kepler Survey. VIII. Eccentricities of Kepler Planets and Tentative Evidence of a High-metallicity Preference for Small Eccentric Planets. *AJ*, 157(5):198, May 2019. doi: 10.3847/1538-3881/ab1009.

M. Mittag, J. H. M. M. Schmitt, and K. P. Schröder. Ca II H+K fluxes from S-indices of large samples: a reliable and consistent conversion based on PHOENIX model atmospheres. *A&A*, 549:A117, January 2013. doi: 10.1051/0004-6361/201219868.

M. Mittag, J. H. M. M. Schmitt, and K. P. Schröder. Revisiting the connection between magnetic activity, rotation period, and convective turnover time for main-sequence stars. *AaP*, 618:A48, October 2018. doi: 10.1051/0004-6361/201833498.

M. Mittag, J. H. M. M. Schmitt, and K. P. Schröder. Revisiting the cycle-rotation connection for late-type stars. *A&A*, 674:A116, June 2023. doi: 10.1051/0004-6361/202245060.

Alessandro Morbidelli and Sean N. Raymond. Challenges in planet formation. *Journal of Geophysical Research (Planets)*, 121(10):1962–1980, October 2016. doi: 10.1002/2016JE005088.

Engineering National Academies of Sciences and Medicine. *Pathways to Discovery in Astronomy and Astrophysics for the 2020s*. x, 2021. doi: 10.17226/26141.

Joe P. Ninan, Gudmundur Stefansson, Suvrath Mahadevan, Chad Bender, Paul Robertson, Lawrence Ramsey, Ryan Terrien, Jason Wright, Scott A. Diddams, Shubham Kanodia, William Cochran, Michael Endl, Eric B. Ford, Connor Fredrick, Samuel Halverson, Fred Hearty, Jeff Jennings, Kyle Kaplan, Emily Lubar, Andrew J. Metcalf, Andrew Monson, Colin Nitroy, Arpita Roy, and Christian Schwab. Detection of He I 10830 Å~absorption during the transit of a warm Neptune around the M-dwarf GJ 3470 with the Habitable-zone Planet Finder. *arXiv e-prints*, art. arXiv:1910.02070, Oct 2019.

R. W. Noyes, L. W. Hartmann, S. L. Baliunas, D. K. Duncan, and A. H. Vaughan. Rotation, convection, and magnetic activity in lower main-sequence stars. *ApJ*, 279:763–777, Apr 1984a. doi: 10.1086/161945.

R. W. Noyes, N. O. Weiss, and A. H. Vaughan. The relation between stellar rotation rate and activity cycle periods. *ApJ*, 287:769–773, December 1984b. doi: 10.1086/162735.

R. W. O'Connell. Absolute spectral energy distribution of common stellar types. , 78:1074–1092, December 1973. doi: 10.1086/111510.

K. Oláh, Zs. Kővári, K. Petrovay, W. Soon, S. Baliunas, Z. Kolláth, and K. Vida. Magnetic cycles at different ages of stars. *A&A*, 590:A133, June 2016. doi: 10.1051/0004-6361/201628479.

Jack T. O'Malley-James and L. Kaltenegger. Lessons from early Earth: UV surface radiation should not limit the habitability of active M star systems. *MNRAS*, 485(4):5598–5603, June 2019. doi: 10.1093/mnras/stz724.

Kevin N. Ortiz Ceballos, Yvette Cendes, Edo Berger, and Peter K. G. Williams. A Volume-limited Radio Search for Magnetic Activity in 140 Exoplanets with the Very Large Array. *AJ*, 168(3):127, September 2024. doi: 10.3847/1538-3881/ad58be.

James E. Owen and Yanqin Wu. The Evaporation Valley in the Kepler Planets. *ApJ*, 847(1):29, September 2017. doi: 10.3847/1538-4357/aa890a.

G. Pace. Chromospheric activity as age indicator. An L-shaped chromospheric-activity versus age diagram. *A&A*, 551:L8, Mar 2013. doi: 10.1051/0004-6361/201220364.

F. Pepe, S. Cristiani, R. Rebolo, N. C. Santos, H. Dekker, A. Cabral, P. Di Marcantonio, P. Figueira, G. Lo Curto, C. Lovis, M. Mayor, D. Mégevand, P. Molaro, M. Riva, M. R. Zapatero Osorio, M. Amate, A. Manescau, L. Pasquini, F. M. Zerbi, V. Adibekyan, M. Abreu, M. Affolter, Y. Alibert, M. Aliverti, R. Allart, C. Allende Prieto, D. Álvarez, D. Alves, G. Avila, V. Baldini, T. Bandy, S. C. C. Barros, W. Benz, A. Bianco, F. Borsa, V. Bourrier, F. Bouchy, C. Broeg, G. Calderone, R. Cirami, J. Coelho,

P. Conconi, I. Coretti, C. Cumani, G. Cupani, V. D'Odorico, M. Damasso, S. Deiries, B. Delabre, O. D. S. Demangeon, X. Dumusque, D. Ehrenreich, J. P. Faria, A. Fragoso, L. Genolet, M. Genoni, R. Génova Santos, J. I. González Hernández, I. Hughes, O. Iwert, F. Kerber, J. Knudstrup, M. Landoni, B. Lavie, J. Lillo-Box, J. L. Lizon, C. Maire, C. J. A. P. Martins, A. Mehner, G. Micela, A. Modigliani, M. A. Monteiro, M. J. P. F. G. Monteiro, M. Moschetti, M. T. Murphy, N. Nunes, L. Oggioni, A. Oliveira, M. Oshagh, E. Pallé, G. Pariani, E. Poretti, J. L. Rasilla, J. Rebordão, E. M. Redaelli, S. Santana Tschudi, P. Santin, P. Santos, D. Ségransan, T. M. Schmidt, A. Segovia, D. Sosnowska, A. Sozzetti, S. G. Sousa, P. Spanò, A. Suárez Mascareño, H. Tabernero, F. Tenegi, S. Udry, and A. Zanutta. ESPRESSO at VLT. On-sky performance and first results. *A&A*, 645:A96, January 2021. doi: 10.1051/0004-6361/202038306.

Francesco Pepe, Andrew Collier Cameron, David W. Latham, Emilio Molinari, Stéphane Udry, Aldo S. Bonomo, Lars A. Buchhave, David Charbonneau, Rosario Cosentino, Courtney D. Dressing, Xavier Dumusque, Pedro Figueira, Aldo F. M. Fiorenzano, Sara Gettel, Avet Harutyunyan, Raphaëlle D. Haywood, Keith Horne, Mercedes Lopez-Morales, Christophe Lovis, Luca Malavolta, Michel Mayor, Giusi Micela, Fatemeh Motalebi, Valerio Nascimbeni, David Phillips, Giampaolo Piotto, Don Pollacco, Didier Queloz, Ken Rice, Dimitar Sasselov, Damien Ségransan, Alessandro Sozzetti, Andrew Szentgyorgyi, and Christopher A. Watson. An Earth-sized planet with an Earth-like density. *Nature*, 503(7476):377–380, November 2013. doi: 10.1038/nature12768.

Joshua Pepper, Richard W. Pogge, D. L. DePoy, J. L. Marshall, K. Z. Stanek, Amelia M. Stutz, Shawn Poindexter, Robert Siverd, Thomas P. O'Brien, Mark Trueblood, and Patricia Trueblood. The Kilodegree Extremely Little Telescope (KELT): A Small Robotic Telescope for Large-Area Synoptic Surveys. , 119(858):923–935, August 2007. doi: 10.1086/521836.

Erik A. Petigura. Two Views of the Radius Gap and the Role of Light

Curve Fitting. *AJ*, 160(2):89, August 2020. doi: 10.3847/1538-3881/ab9fff.

Erik A. Petigura, Andrew W. Howard, and Geoffrey W. Marcy. Prevalence of Earth-size planets orbiting Sun-like stars. *Proceedings of the National Academy of Science*, 110(48):19273–19278, Nov 2013. doi: 10.1073/pnas.1319909110.

Erik A. Petigura, Andrew W. Howard, Geoffrey W. Marcy, John Asher Johnson, Howard Isaacson, Phillip A. Cargile, Leslie Hebb, Benjamin J. Fulton, Lauren M. Weiss, Timothy D. Morton, Joshua N. Winn, Leslie A. Rogers, Evan Sinukoff, Lea A. Hirsch, and Ian J. M. Crossfield. The California-Kepler Survey. I. High-resolution Spectroscopy of 1305 Stars Hosting Kepler Transiting Planets. *AJ*, 154(3):107, Sep 2017. doi: 10.3847/1538-3881/aa80de.

Erik A. Petigura, Geoffrey W. Marcy, Joshua N. Winn, Lauren M. Weiss, Benjamin J. Fulton, Andrew W. Howard, Evan Sinukoff, Howard Isaacson, Timothy D. Morton, and John Asher Johnson. The California-Kepler Survey. IV. Metal-rich Stars Host a Greater Diversity of Planets. *AJ*, 155(2):89, Feb 2018. doi: 10.3847/1538-3881/aaa54c.

Erik A. Petigura, James G. Rogers, Howard Isaacson, James E. Owen, Adam L. Kraus, Joshua N. Winn, Mason G. MacDougall, Andrew W. Howard, Benjamin Fulton, Molly R. Kosiarek, Lauren M. Weiss, Aida Behmard, and Sarah Blunt. The California-Kepler Survey. X. The Radius Gap as a Function of Stellar Mass, Metallicity, and Age. *AJ*, 163(4):179, April 2022. doi: 10.3847/1538-3881/ac51e3.

D. L. Pollacco, I. Skillen, A. Collier Cameron, D. J. Christian, C. Hellier, J. Irwin, T. A. Lister, R. A. Street, R. G. West, D. R. Anderson, W. I. Clarkson, H. Deeg, B. Enoch, A. Evans, A. Fitzsimmons, C. A. Haswell, S. Hodgkin, K. Horne, S. R. Kane, F. P. Keenan, P. F. L. Maxted, A. J. Norton, J. Osborne, N. R. Parley, R. S. I. Ryans, B. Smalley, P. J. Wheatley, and D. M. Wilson. The WASP Project and the SuperWASP Cameras. , 118(848):1407–1418, October 2006. doi: 10.1086/508556.

Matthew V. Radovan, Gerald F. Cabak, Lee H. Laiterman, Christopher T. Lockwood, and Steven S. Vogt. A radial velocity spectrometer for the Automated Planet Finder Telescope at Lick Observatory. In , volume 7735 of *Society of Photo-Optical Instrumentation Engineers (SPIE) Conference Series*, page 77354K, Jul 2010. doi: 10.1117/12.857726.

Iván Ramírez and Jorge Meléndez. The Effective Temperature Scale of FGK Stars. II. T_{eff}:Color:[Fe/H] Calibrations. *ApJ*, 626(1):465–485, June 2005. doi: 10.1086/430102.

Heike Rauer, Conny Aerts, Juan Cabrera, Magali Deleuil, Anders Erikson, Laurent Gizon, Mariejo Goupil, Ana Heras, Jose Lorenzo-Alvarez, Filippo Marliani, César Martin-Garcia, J. Miguel Mas-Hesse, Laurence O'Rourke, Hugh Osborn, Isabella Pagano, Giampaolo Piotto, Don Pollacco, Roberto Ragazzoni, Gavin Ramsay, Stéphane Udry, Thierry Appourchaux, Willy Benz, Alexis Brandeker, Manuel Güdel, Eduardo Janot-Pacheco, Petr Kabath, Hans Kjeldsen, Michiel Min, Nuno Santos, Alan Smith, Juan-Carlos Suarez, Stephanie C. Werner, Alessio Aboudan, Manuel Abreu, Lorena Acu a, Moritz Adams, Vardan Adibekyan, Laura Affer, François Agneray, Craig Agnor, Victor Aguirre Børsen-Koch, Saad Ahmed, Suzanne Aigrain, Ashraf Al-Bahlawan, M de los Angeles Alcacera Gil, Eleonora Alei, Silvia Alencar, Richard Alexander, Julia Alfonso-Garzón, Yann Alibert, Carlos Allende Prieto, Leonardo Almeida, Roi Alonso Sobrino, Giuseppe Altavilla, Christian Althaus, Luis Alonso Alvarez Trujillo, Anish Amarsi, Matthias Ammler-von Eiff, Eduardo Amôres, Laerte Andrade, Alexandros Antoniadis-Karnavas, Carlos António, Beatriz Aparicio del Moral, Matteo Appolloni, Claudio Arena, David Armstrong, Jose Aroca Aliaga, Martin Asplund, Jeroen Audenaert, Natalia Auricchio, Pedro Avelino, Ann Baeke, Kevin Baillié, Ana Balado, Pau Ballber Balagueró, Andrea Balestra, Warrick Ball, Herve Ballans, Jerome Ballot, Caroline Barban, Gaële Barbary, Mauro Barbieri, Sebasti Barceló Forteza, Adrian Barker, Paul Barklem, Sydney Barnes, David Barrado Navascues, Oscar Barragan, Clément Baruteau, Sarbani Basu, Frederic Baudin, Philipp Baumeister, Daniel Bayliss, Michael Bazot, Paul G. Beck, Tim Bedding, Kevin Belkacem, Earl Bellinger, Serena Benatti, Othman Benomar, Diane Bérard, Maria Bergemann, Maria Bergomi, Pierre Bernardo, Katia Biazzo, Andrea Bignamini, Lionel Bigot, Nicolas Billot, Martin Binet, David Biondi, Federico Biondi, Aaron C. Birch, Bertram Bitsch, Paz Victoria Bluhm Ceballos, Attila Bódi, Zsófia Bognár, Isabelle Boisse, Emeline Bolmont, Alfio Bonanno, Mariangela Bonavita, Andrea Bonfanti, Xavier Bonfils, Rosaria Bonito, Aldo Stefano Bonomo, Anko Börner, Sudeshna Boro Saikia, Elisa Borreguero Martín, Francesco Borsa, Luca Borsato, Diego Bossini, Francois Bouchy, Gwenaël Boué, Rodrigo Boufleur, Patrick Boumier, Vincent Bourrier, Dominic M. Bowman, Enrico Bozzo, Louisa Bradley, John Bray, Alessandro Bressan, Sylvain Breton, Daniele Brienza, Ana Brito, Matteo Brogi, Beverly Brown, David J. A. Brown, Allan Sacha Brun, Giovanni Bruno, Michael Bruns, Lars A. Buchhave, Lisa Bugnet, Gaël Buldgen, Patrick Burgess, Andrea Busatta, Giorgia Busso, Derek Buzasi, José A. Caballero, Alexandre Cabral, Juan-Francisco Cabrero Gomez, Flavia Calderone, Robert Cameron, Andrew Cameron, Tiago Campante, Néstor Campos Gestal, Bruno Leonardo Canto Martins, Christophe Cara, Ludmila Carone, Josep Manel Carrasco, Luca Casagrande, Sarah L. Casewell, Santi Cassisi, Marco Castellani, Matthieu Castro, Claude Catala, Irene Catalán Fernández, Márcio Catelan, Heather Cegla, Chiara Cerruti, Virginie Cessa, Merieme Chadid, William Chaplin, Stephane Charpinet, Cristina Chiappini, Simone Chiarucci, Andrea Chiavassa, Simonetta Chinellato, Giovanni Chirulli, Jørgen Christensen-Dalsgaard, Ross Church, Antonio Claret, Cathie Clarke, Riccardo Claudi, Lionel Clermont, Hugo Coelho, Joao Coelho, Fabrizio Cogato, Josep Colomé, Mathieu Condamin, Fernando Conde García, and Simon Conseil. The PLATO Mission. *arXiv e-prints*, art. arXiv:2406.05447, June 2024. doi: 10.48550/arXiv.2406.05447.

Timo Reinhold and Laurent Gizon. Rotation, differential rotation, and gyrochronology of active Kepler stars. *A&A*, 583:A65, Nov 2015. doi: 10.1051/0004-6361/201526216.

George R. Ricker, Joshua N. Winn, Roland Vanderspek, David W. Latham, Gáspár Á. Bakos, Jacob L. Bean, Zachory K. Berta-Thompson, Timothy M. Brown, Lars Buchhave, Nathaniel R. Butler, R. Paul Butler, William J. Chaplin, David Charbonneau, Jørgen Christensen-Dalsgaard, Mark Clampin, Drake Deming, John Doty, Nathan De Lee, Courtney Dressing, Edward W. Dunham, Michael Endl, Francois Fressin, Jian Ge, Thomas Henning, Matthew J. Holman, Andrew W. Howard, Shigeru Ida, Jon M. Jenkins, Garrett Jernigan, John Asher Johnson, Lisa Kaltenegger, Nobuyuki Kawai, Hans Kjeldsen, Gregory Laughlin, Alan M. Levine, Douglas Lin, Jack J. Lissauer, Phillip MacQueen, Geoffrey Marcy, Peter R. McCullough, Timothy D. Morton, Norio Narita, Martin Paegert, Enric Palle, Francesco Pepe, Joshua Pepper, Andreas Quirrenbach, Stephen A. Rinehart, Dimitar Sasselov, Bun'ei Sato, Sara Seager, Alessandro Sozzetti, Keivan G. Stassun, Peter Sullivan, Andrew Szentgyorgyi, Guillermo Torres, Stephane Udry, and Joel Villasenor. Transiting Exoplanet Survey Satellite (TESS). *Journal of Astronomical Telescopes, Instruments, and Systems*, 1:014003, Jan 2015. doi: 10.1117/1.JATIS.1.1.014003.

Paul Robertson, Suvrath Mahadevan, Michael Endl, and Arpita Roy. Stellar activity masquerading as planets in the habitable zone of the M dwarf Gliese 581. *Science*, 345(6195):440–444, Jul 2014. doi: 10.1126/science.1253253.

Paul Robertson, Tyler Anderson, Gudmundur Stefansson, Frederick R. Hearty, Andrew Monson, Suvrath Mahadevan, Scott Blakeslee, Chad Bender, Joe P. Ninan, David Conran, Eric Levi, Emily Lubar, Amanda Cole, Adam Dykhouse, Shubham Kanodia, Colin Nitroy, Joseph Smolsky, Demetrius Tuggle, Basil Blank, Matthew Nelson, Cullen Blake, Samuel Halverson, Chuck Henderson, Kyle F. Kaplan, Dan Li, Sarah E.

Logsdon, Michael W. McElwain, Jayadev Rajagopal, Lawrence W. Ramsey, Arpita Roy, Christian Schwab, Ryan Terrien, and Jason T. Wright. Ultrastable environment control for the NEID spectrometer: design and performance demonstration. *Journal of Astronomical Telescopes, Instruments, and Systems*, 5:015003, Jan 2019. doi: 10.1117/1.JATIS.5.1.015003.

Leslie A. Rogers. Most 1.6 Earth-radius Planets are Not Rocky. *ApJ*, 801(1):41, Mar 2015. doi: 10.1088/0004-637X/801/1/41.

Lee J. Rosenthal, Benjamin J. Fulton, Lea A. Hirsch, Howard T. Isaacson, Andrew W. Howard, Cayla M. Dedrick, Ilya A. Sherstyuk, Sarah C. Blunt, Erik A. Petigura, Heather A. Knutson, Aida Behmard, Ashley Chontos, Justin R. Crepp, Ian J. M. Crossfield, Paul A. Dalba, Debra A. Fischer, Gregory W. Henry, Stephen R. Kane, Molly Kosiarek, Geoffrey W. Marcy, Ryan A. Rubenzahl, Lauren M. Weiss, and Jason T. Wright. The California Legacy Survey. I. A Catalog of 178 Planets from Precision Radial Velocity Monitoring of 719 Nearby Stars over Three Decades. *ApJS*, 255(1):8, July 2021. doi: 10.3847/1538-4365/abe23c.

Jason F. Rowe, Stephen T. Bryson, Geoffrey W. Marcy, Jack J. Lissauer, Daniel Jontof-Hutter, Fergal Mullally, Ronald L. Gilliland, Howard Issacson, Eric Ford, Steve B. Howell, William J. Borucki, Michael Haas, Daniel Huber, Jason H. Steffen, Susan E. Thompson, Elisa Quintana, Thomas Barclay, Martin Still, Jonathan Fortney, III Gautier, T. N., Roger Hunter, Douglas A. Caldwell, David R. Ciardi, Edna Devore, William Cochran, Jon Jenkins, Eric Agol, Joshua A. Carter, and John Geary. Validation of Kepler's Multiple Planet Candidates. III. Light Curve Analysis and Announcement of Hundreds of New Multi-planet Systems. *ApJ*, 784(1):45, March 2014. doi: 10.1088/0004-637X/784/1/45.

Steven H. Saar. Maunder Minimum Dwarfs: Defined Out Of Existence? In *AAS/Solar Physics Division Meeting #37*, volume 37 of *AAS/Solar Physics Division Meeting*, page 12.01, June 2006.

A. R. G. Santos, S. N. Breton, S. Mathur, and R. A. García. Surface Rotation and Photometric Activity for Kepler Targets. II. G and F Main-sequence Stars and Cool Subgiant Stars. *ApJS*, 255(1):17, July 2021. doi: 10.3847/1538-4365/ac033f.

N. C. Santos, M. Mayor, D. Naef, F. Pepe, D. Queloz, S. Udry, and A. Blecha. The CORALIE survey for Southern extra-solar planets. IV. Intrinsic stellar limitations to planet searches with radial-velocity techniques. *AAP*, 361:265–272, September 2000.

N. C. Santos, J. Gomes da Silva, C. Lovis, and C. Melo. Do stellar magnetic cycles influence the measurement of precise radial velocities? *A&A*, 511:A54, February 2010. doi: 10.1051/0004-6361/200913433.

Nicholas Saunders, Jennifer L. van Saders, Alexander J. Lyttle, Travis S. Metcalfe, Tanda Li, Guy R. Davies, Oliver J. Hall, Warrick H. Ball, Richard Townsend, Orlagh Creevey, and Curt Dodds. Stellar Cruise Control: Weakened Magnetic Braking Leads to Sustained Rapid Rotation of Old Stars. *ApJ*, 962(2):138, February 2024. doi: 10.3847/1538-4357/ad1516.

B. Schwarzschild. First of the twin 10-meter Keck telescopes starts doing astronomy. *Physics Today*, 46(10):17–18, January 1993. doi: 10.1063/1.2809059.

Victor See, Yuxi (Lucy) Lu, Louis Amard, and Julia Roquette. The impact of stellar metallicity on rotation and activity evolution in the Kepler field using gyro-kinematic ages. *MNRAS*, 533(2):1290–1299, September 2024. doi: 10.1093/mnras/stae1828.

Shivani P. Shah, Jason T. Wright, Howard Isaacson, Andrew W. Howard, and Jason L. Curtis. HD 4915: A Maunder Minimum Candidate. *ApJL*, 863(2):L26, August 2018. doi: 10.3847/2041-8213/aad40c.

Jared C. Siegel, Ryan A. Rubenzahl, Samuel Halverson, and Andrew W. Howard. Into the Depths: A New Activity Metric for High-precision Radial

Velocity Measurements Based on Line Depth Variations. *AJ*, 163(6):260, June 2022. doi: 10.3847/1538-3881/ac609a.

A. Skumanich. Time Scales for Ca II Emission Decay, Rotational Braking, and Lithium Depletion. *ApJ*, 171:565, February 1972. doi: 10.1086/151310.

D. Staab, C. A. Haswell, J. R. Barnes, G. Anglada-Escudé, L. Fossati, J. P. J. Doherty, J. Cooper, J. S. Jenkins, M. R. Díaz, and M. G. Soto. A compact multi-planet system around a bright nearby star from the Dispersed Matter Planet Project. *Nature Astronomy*, 4:399–407, January 2020. doi: 10.1038/s41550-019-0974-x.

Jason H. Steffen, Daniel C. Fabrycky, Eric B. Ford, Joshua A. Carter, Jean-Michel Désert, Francois Fressin, Matthew J. Holman, Jack J. Lissauer, Althea V. Moorhead, Jason F. Rowe, Darin Ragozzine, William F. Welsh, Natalie M. Batalha, William J. Borucki, Lars A. Buchhave, Steve Bryson, Douglas A. Caldwell, David Charbonneau, David R. Ciardi, William D. Cochran, Michael Endl, Mark E. Everett, Thomas N. Gautier, Ron L. Gilliland, Forrest R. Girouard, Jon M. Jenkins, Elliott Horch, Steve B. Howell, Howard Isaacson, Todd C. Klaus, David G. Koch, David W. Latham, Jie Li, Philip Lucas, Phillip J. MacQueen, Geoffrey W. Marcy, Sean McCauliff, Christopher K. Middour, Robert L. Morris, Fergal R. Mullally, Samuel N. Quinn, Elisa V. Quintana, Avi Shporer, Martin Still, Peter Tenenbaum, Susan E. Thompson, Joseph D. Twicken, and Jeffery Van Cleve. Transit timing observations from Kepler - III. Confirmation of four multiple planet systems by a Fourier-domain study of anticorrelated transit timing variations. *MNRAS*, 421(3):2342–2354, April 2012. doi: 10.1111/j.1365-2966.2012.20467.x.

Jamie Tayar, Zachary R. Claytor, Daniel Huber, and Jennifer van Saders. A Guide to Realistic Uncertainties on the Fundamental Properties of Solar-type Exoplanet Host Stars. *ApJ*, 927(1):31, March 2022. doi: 10.3847/1538-4357/ac4bbc.

Angelos Tsiaras, Ingo P. Waldmann, Giovanna Tinetti, Jonathan Tennyson, and Sergey N. Yurchenko. Water vapour in the atmosphere of the habitable-zone eight-Earth-mass planet K2-18 b. *Nature Astronomy*, page 451, Sep 2019. doi: 10.1038/s41550-019-0878-9.

Joseph D. Twicken, Jon M. Jenkins, Shawn E. Seader, Peter Tenenbaum, Jeffrey C. Smith, Lee S. Brownston, Christopher J. Burke, Joseph H. Catanzarite, Bruce D. Clarke, Miles T. Cote, Forrest R. Girouard, Todd C. Klaus, Jie Li, Sean D. McCauliff, Robert L. Morris, Bill Wohler, Jennifer R. Campbell, Akm Kamal Uddin, Khadeejah A. Zamudio, Anima Sabale, Steven T. Bryson, Douglas A. Caldwell, Jessie L. Christiansen, Jeffrey L. Coughlin, Michael R. Haas, Christopher E. Henze, Dwight T. Sanderfer, and Susan E. Thompson. Detection of Potential Transit Signals in 17 Quarters of Kepler Data: Results of the Final Kepler Mission Transiting Planet Search (DR25). *AJ*, 152(6):158, December 2016. doi: 10.3847/0004-6256/152/6/158.

J. A. Valenti and N. Piskunov. Spectroscopy made easy: A new tool for fitting observations with synthetic spectra. *A&AS*, 118:595–603, Sep 1996.

Jennifer L. van Saders, Tugdual Ceillier, Travis S. Metcalfe, Victor Silva Aguirre, Marc H. Pinsonneault, Rafael A. García, Savita Mathur, and Guy R. Davies. Weakened magnetic braking as the origin of anomalously rapid rotation in old field stars. *Nature*, 529(7585):181–184, January 2016. doi: 10.1038/nature16168.

A. H. Vaughan, G. W. Preston, and O. C. Wilson. Flux measurements of Ca II and K emission. *PASP*, 90:267–274, June 1978. doi: 10.1086/130324.

S. S. Vogt. HIRES - a High Resolution Echelle Spectrometer for the Keck Ten-Meter Telescope. In *European Southern Observatory Conference and Workshop Proceedings*, volume 40, page 223, Jun 1992.

Lauren M. Weiss and Geoffrey W. Marcy. The Mass-Radius Relation for 65 Exoplanets Smaller than 4 Earth Radii. *ApJl*, 783(1):L6, Mar 2014. doi: 10.1088/2041-8205/783/1/L6.

Lauren M. Weiss, Geoffrey W. Marcy, Jason F. Rowe, Andrew W. Howard, Howard Isaacson, Jonathan J. Fortney, Neil Miller, Brice-Olivier Demory, Debra A. Fischer, Elisabeth R. Adams, Andrea K. Dupree, Steve B. Howell, Rea Kolbl, John Asher Johnson, Elliott P. Horch, Mark E. Everett, Daniel C. Fabrycky, and Sara Seager. The Mass of KOI-94d and a Relation for Planet Radius, Mass, and Incident Flux. *ApJ*, 768(1):14, May 2013. doi: 10.1088/0004-637X/768/1/14.

Lauren M. Weiss, Geoffrey W. Marcy, Erik A. Petigura, Benjamin J. Fulton, Andrew W. Howard, Joshua N. Winn, Howard T. Isaacson, Timothy D. Morton, Lea A. Hirsch, Evan J. Sinukoff, Andrew Cumming, Leslie Hebb, and Phillip A. Cargile. The California-Kepler Survey. V. Peas in a Pod: Planets in a Kepler Multi-planet System Are Similar in Size and Regularly Spaced. *AJ*, 155(1):48, Jan 2018a. doi: 10.3847/1538-3881/aa9ff6.

Lauren M. Weiss, Geoffrey W. Marcy, Erik A. Petigura, Benjamin J. Fulton, Andrew W. Howard, Joshua N. Winn, Howard T. Isaacson, Timothy D. Morton, Lea A. Hirsch, Evan J. Sinukoff, Andrew Cumming, Leslie Hebb, and Phillip A. Cargile. The California-Kepler Survey. V. Peas in a Pod: Planets in a Kepler Multi-planet System Are Similar in Size and Regularly Spaced. *AJ*, 155(1):48, Jan 2018b. doi: 10.3847/1538-3881/aa9ff6.

Lauren M. Weiss, Howard Isaacson, Andrew W. Howard, Benjamin J. Fulton, Erik A. Petigura, Daniel Fabrycky, Daniel Jontof-Hutter, Jason H. Steffen, Hilke E. Schlichting, Jason T. Wright, Corey Beard, Casey L. Brinkman, Ashley Chontos, Steven Giacalone, Michelle L. Hill, Molly R. Kosiarek, Mason G. MacDougall, Teo Močnik, Alex S. Polanski, Emma V. Turtelboom, Dakotah Tyler, and Judah Van Zandt. The Kepler Giant Planet Search. I. A Decade of Kepler Planet-host Radial Velocities from W. M. Keck Observatory. *ApJS*, 270(1):8, January 2024. doi: 10.3847/1538-4365/ad0cab.

O. C. Wilson. Flux Measurements at the Centers of Stellar H- and K-Lines. *ApJ*, 153:221, Jul 1968. doi: 10.1086/149652.

A. Wolszczan and D. A. Frail. A planetary system around the millisecond pulsar PSR1257 + 12. , 355(6356):145–147, January 1992. doi: 10.1038/355145a0.

J. T. Wright, G. W. Marcy, R. Paul Butler, and S. S. Vogt. Chromospheric Ca II Emission in Nearby F, G, K, and M Stars. *ApJS*, 152(2):261–295, Jun 2004. doi: 10.1086/386283.

J. T. Wright, G. W. Marcy, R. P. Butler, S. S. Vogt, G. W. Henry, H. Isaacson, and A. W. Howard. The Jupiter Twin HD 154345b. *ApJL*, 683(1): L63, August 2008. doi: 10.1086/587461.

J. T. Wright, G. W. Marcy, A. W. Howard, John Asher Johnson, T. D. Morton, and D. A. Fischer. The Frequency of Hot Jupiters Orbiting nearby Solar-type Stars. *ApJ*, 753(2):160, July 2012. doi: 10.1088/0004-637X/753/2/160.

Jinghua Zhang, Shaolan Bi, Yaguang Li, Jie Jiang, Tanda Li, Han He, Jie Yu, Shourya Khanna, Zhishuai Ge, Kang Liu, Zhijia Tian, Yaqian Wu, and Xianfei Zhang. Magnetic Activity of F-, G-, and K-type Stars in the LAMOST-Kepler Field. *ApJS*, 247(1):9, March 2020. doi: 10.3847/1538-4365/ab6165.